Tissue substitutes for particulate radiations and their use in radiation dosimetry and radiotherapy

Constantinou, Christodoulos

TISSUE SUBSTITUTES FOR PARTICULATE RADIATIONS

AND THEIR USE IN

RADIATION DOSIMETRY AND RADIOTHERAPY

CHRISTODOULOS CONSTANTINOU, M.Sc

A THESIS SUBMITTED TO THE UNIVERSITY OF LONDON

FOR THE DEGREE OF DOCTOR OF PHILOSOPHY

1978

Physics Department
The Medical College of
St. Bartholomew's Hospital
London EC1

ABSTRACT

Most of the tissue substitute materials currently used in clinical radiation dosimetry are designed to simulate muscle or bone when irradiated with photons. A few materials have been developed for neutron dosimetry, but substitutes specifically designed for beams of high energy charged particles are not to be found in the literature.

This thesis deals with the formulation and manufacture of tissue substitutes for particulate radiations and the subsequent application of these substitutes in electron, pion, proton and neutron dosimetry. The method of "elemental equivalence" was used and over 80 solid, gel and liquid substitutes have been produced, which simulate the most important tissues (adipose, blood, bone, muscle, etc), body organs (brain, lung, etc) and tissue components (fat, protein, water). Most of these materials are "tissue equivalent" and are useful for all types of radiations.

The compilation of selected chemical compounds (compound library) used for the formulation, and the computer programs written for the theoretical evaluation of the new materials are described and discussed. The experimental comparison of some selected substitutes with the corresponding real tissues, using fast neutrons, high energy protons, cobalt-60 gamma rays and 120 kVp X-rays, verified the high precision of the simulation procedures. The results of depth dose measurements in various tissue substitutes, as well as water, using 7.5 MeV neutrons 150 MeV protons, 70 MeV negative pions, 10 MeV electrons and cobalt-60 gamma rays are presented. The effect of tissue heterogeneities on the dose distributions from these radiations was

investigated. Isodose shift factors for air, lung, fat and bone were derived for all the above radiation modalities and detailed lung correction factors were measured for 7.5 MeV neutrons and cobalt-60 gamma rays.

In view of the proposed use of the 160 MeV proton beam of the Atomic Energy Research Establishment (Harwell, U.K) for patient treatment, a complete series of pre-therapeutic measurements was performed with this proton beam facility using the new materials, and the results are presented and discussed in detail.

Finally, the applications of the new substitutes in other practical clinical aspects are described and some examples of such applications given.

ACKNOWLEDGEMENTS

I would like to express my gratitude to Dr N.F..Kember for acting as my supervisor and for his continued support and advice during this study.

My employers, St Bartholomew's Hospital, London, are acknowledged for permitting me to perform this research on a part-time basis. The help and encouragement of numerous colleagues at the hospital and the Medical College of St Bartholomew's Hospital is appreciated. Special thanks are due to Dr D.R. White for his continued advice, help and encouragement, to Dr W.E. Liversage for his helpful discussions throughout this study and for his comments on the thesis, and to Professor J. Rotblat for his advice at the beginning of the study.

The advice by Dr F.A. Smith and Dr S. Lovell and the help of the latter during the measurements on the linear accelerator of the Medical College of St Bartholomew's Hospital are gratefully acknowledged. The help of Mr. P. Browne on the computing involved in this work as well as the technical assistance of Messrs P. Taylor, R. Darlison, A. Rickwood and J.R. Spratley is also gratefully acknowledged.

I would also like to thank the following for permitting me to use the equipment in their departments and for the comments of each one of them on the results of the experimental work carried out in their establishments:

- Dr R. Palmer, City University, London, for the measurements with alpha particles.

- Dr D.K. Bewley, Dr J. Parnell and Mr B. Page, for the work on the Medical Research Council cyclotron, Hammersmith Hospital, London.

- Dr D.H. Reading, Mr M. Hynes and Mr W. Spinks, Rutherford Laboratory, U.K., for the work on the pion beam of the NIMROD synchrotron.

- Dr S. Klevenhagen and Mr D. Putney, the London Hospital, for the work on the electron beam of the MEL SL75 linear accelerator.

- Dr C. Whitehead and Mr G. Huxtable, Harwell, for the measurements on the proton beam of the A.E.R.E. synchrocyclotron (Harwell, U.K.).

Thanks are due to the Medical Research Council for financing the pre-therapeutic measurements on the A.E.R.E. proton beam, and to the Central Research Fund Committee of the University of London, for the grant with which the equipment needed for the manufacture of the new tissue substitutes was purchased.

Last, but not the least, I would like to thank my family and in particular my wife Nafsika whose unfailing support and encouragement during the three years of this study was invaluable.

C. CONSTANTINOU
Radiation Physics Department
St Bartholomew's Hospital

CONTENTS

CHAPTER 2 cont....

CHAPTER 1

AN INTRODUCTION TO THE THESIS

The distribution of absorbed dose in the body of a patient undergoing radiotherapy can be obtained either by calculation or by measurement in tissue substitute materials under simulated irradiation conditions. If it were possible to design materials with elemental composition and density identical to that of various human tissues, then "body phantoms" could be manufactured which would absorb and scatter radiation in the same way as the human body. Such body phantoms would be useful not only for photons and electrons but also for heavy particles such as protons, neutrons, pions and alpha particles. Many of the so-called "TISSUE EQUIVALENT" materials used in dosimetric studies with X-rays, gamma rays and electrons in the past, give poor simulation of the corresponding real tissues.

This thesis deals with the general problem of tissue simulation for particulate radiations used in radiotherapy. The method of 'elemental equivalence' is employed to formulate a family of new tissue substitutes which simulate the important tissues and body organs, in the liquid, gel and solid states. Most of these systems have the same elemental composition and density as that of the corresponding real tissues. Consequently they are useful for all types of radiations.

The formulation and manufacture of the new tissue substitutes is described in Chapters 2 and 3 and the theoretical and experimental verification of their 'tissue equivalence' is presented in Chapter 4. Some of these materials were selected and used in dosimetric studies with protons, negative pions, electrons, fast neutrons as well as

cobalt-60 gamma rays. The effect of tissue heterogeneities such as lung, fat and bone on the dose distributions of the above types of radiations was investigated and the results are discussed in Chapters 5 and 6. Some applications of the new tissue substitutes are given in Chapter 7.

1.1 THE MEANING OF "EQUIVALENCE" AND THE NEED FOR TISSUE SUBSTITUTES SUITABLE FOR PARTICULATE RADIATIONS

With the use of neutrons and charged particles such as electrons, protons, negative pions and heavy ions in radiotherapy, it is becoming increasingly important to establish depth dose and beam profile data acceptable for radiotherapy, and to understand the influence of tissue heterogeneities on the dose distributions obtained when these radiation modalities are used. In order to facilitate these investigations "TISSUE EQUIVALENT" materials are needed for the construction of both radiation detectors and realistic body phantoms.

The term "TISSUE EQUIVALENT" is often misused and materials which have acceptable physical density but unknown composition are frequently referred to as tissue equivalent. A typical example is the use of pressdwood as tissue equivalent material. Reports of measurements using cork to represent lung tissue and aluminium to represent bone, continue to be published, even to the present day (e.g. SONTAG and CUNNINGHAM, 1977). Several authors have indicated that such materials should not be called "TISSUE EQUIVALENT", but often no attention has been paid to the advice given. (ROSSI and FAILLA, 1956; SHONKA et al., 1958; FRIGERIO et al., 1972).

In his detailed study WHITE (1974), stressed this point further and suggested that for materials that approximate tissue in their absorption of energy, from all or some of the directly and indirectly ionising radiations, the term "TISSUE SUBSTITUTE" should be used. In this respect, he produced phantom materials which simulate the corresponding tissues very accurately for photons of energies from 10 keV to 100 MeV and for low energy electrons. These materials, however, have no resemblance to tissue as far as elemental composition is concerned and could give large errors if used in neutron and high energy charged particle dosimetry. This is also the case for most of the phantom materials used in the past; most of them were designed for photons and very few for neutron interactions. Materials designed specifically for heavy charged particle dosimetry are not to be found in the literature.

1.1 (i) CRITERIA FOR TISSUE EQUIVALENCE

A material is said to simulate accurately another material, if the two absorb and scatter radiation in exactly the same way.

The following quantities must be identical for the phantom material and the tissue that it simulates, if the two are to absorb and scatter any type of radiation in the same way:

(i) Photon mass attenuation and mass energy absorption coefficient.

(ii) Electron mass stopping power and mass angular scattering power.

(iii) Mass stopping power and mass angular scattering power for heavy charged particles and heavy ions.

(iv) Neutron interaction cross sections or kerma factors.

(v) If equal masses of two materials are to have the same volume, then the mass densities of the two must also be the same.

It is obvious that the above can only be achieved if the material is made to have the same elemental constituents and in the same proportion by weight as the real tissue; it is only for such materials that the term "TISSUE EQUIVALENT" should be used.

The new substitutes developed during this study were formulated so that, wherever possible, their elemental composition and relative density is exactly the same as that of the tissue which they were designed to simulate. This was easier to achieve with liquid substitutes and water-based gels than with solids, especially when epoxy resins and polymers were used, due to the fact that these materials are very rich in carbon and poor in oxygen.

1.1 (ii) SOME GENERAL PROBLEMS - CRITICAL TISSUE ELEMENTS

It was realised, at an early stage of this work, that partial replacement of oxygen by carbon had to be accepted in the case of solid substitutes and the mechanisms with which various particulate radiations interact with matter were considered, in order to find which of the elements present in various tissues are the most critical for each type of radiation. As fast neutrons are already used in radiotherapy on a routine basis, their interactions with matter are of great interest.

Neutrons interact primarily with nuclei and tissue equivalence in a phantom requires the right nuclei to be present in the right proportions; the achievement of the correct effective atomic number,

an adequate criterion for X-ray phantoms, is not adequate for neutron phantoms.

Since the interactions of fast neutrons with hydrogen account for 70-90% of the total dose in soft tissue (JONES, 1974), the prime consideration is to have the right proportion of hydrogen; for slow neutrons both the hydrogen and nitrogen content are important, due to the absorption reactions $^{1}H(n,\gamma)^{2}H$ and $^{14}N(n,p)^{14}C$. Hydrogen is also the most critical element for the interactions of heavy charged, particles with matter; these will be discussed in a following section.

The relative proportion of carbon and oxygen in tissue was found to be less critical and the replacement of part of oxygen by carbon in most of the solid epoxy resin-based substitutes was found not to affect the neutron attenuation significantly. Trace elements were also found, both by experiment and by calculation, to play no significant role in the absorption of fast neutrons, high energy protons or negative pions.

For those substitutes in which all elements are correct except for carbon (C) and oxygen (O), but with the sum (C + O) the same as that of the real tissue, the term "QUÁSI-EQUIVALENT" could be used. The term "TISSUE SUBSTITUTE" will be generally used to cover both those materials which are tissue equivalent and those materials which are claimed to approximate a tissue in their response to radiation. It should be mentioned here that the elemental composition of many biological tissues is either not precisely known or it varies with age and this makes the task of simulation more difficult. If the composition is known to vary over a given range, then a family of substitutes should be formulated to cover this range.

Another problem arises from the fact that physical phase effects and differences in molecular binding between solids and liquids or vapours of the same chemical composition, may affect the stopping powers of the substitutes for the various charged particles through which energy is deposited in tissue. There is fragmentary and, at times, conflicting evidence for such phase effects in organic materials. TWAITES and WATT (1978) reviewed the available data and concluded that there is a definite phase effect in the stopping of low energy charged particles, decreasing their stopping power in condensed state media as compared to their corresponding gases or vapours (e.g. polyethylene-ethylene), but lack of extensive data makes the evaluation of the errors involved difficult.

Frequently the 'Bragg additivity rule' (BRAGG and KLEEMAN, 1905) is used to derive the radiation characteristics of a compound or a mixture from those of its components. BOURLAND and POWERS (1971), and more recently PALMER (1973), experimented with alpha particles of energies up to 8 MeV and they found no major differences in molecular stopping powers due to chemical binding; they also showed that the 'Bragg rule is obeyed in gases for all molecules, except those containing a triple bond. According to BICHSEL (1977), the application of the Bragg rule in the calculation of stopping powers for protons, '... is valid only with an uncertainty which could exceed 3% ...'

It is conceivable that the molecular binding in real tissues is much more complex than in the liquids, resins, polymers and inorganic compounds used to manufacture the tissue substitutes and it can be argued that it is futile to simulate to better than $\pm$ 2% a tissue whose composition varies considerably from one set of published tissue data to another.

Nearly 80 different formulations had been published before 1974 which were claimed to simulate muscle, lung, fat and bone. All too frequently these materials gave large errors in the energy ranges for which they were designed. However, the family of substitutes for photon interactions recently produced by WHITE (1974), were found to give errors smaller than 4-5% for all photon energies from 10 keV up to 100 MeV.

Few liquid substitutes were developed specifically for neutron dosimetry in the past. In 1956 ROSSI and FAILLA introduced their liquid system comprising a mixture of water/glycerol/urea/ sucrose, which represented elementally an approximate formula for soft tissue $C_5H_{40}O_{11}N$. This was later improved by GOODMAN (1969) who removed sucrose. More recently FRIGERIO, et al., (1972), produced liquid systems closely simulating the formula of muscle given by ICRU (NBS, 1964).

Solids developed for neutron studies include the conducting plastics of SHONKÁ, et al., (1958), and an epoxy resin substitute (WILSON and WHITE, 1974). The components and elemental composition of the most important substitutes developed in the past are given in Appendix 4.

Figures 1.1 and 1.2 show the central axis depth dose curves of 5 different radiation modalities, namely, 7.5 MeV neutrons, 150 MeV protons, 10 MeV electrons, 70 MeV negative pions and cobalt-60 gamma rays, measured during the course of this study in water and in muscle equivalent liquid (MS/L1). (For coding see next section). Although it is claimed that with respect to dose composition in the BRAGG peak there are no great differences between water and soft tissue (DUTRANOIS et al., 1972), Figures 1.1 and 1.2 show that

the depth of the Bragg peak is not the same and this is important in precision radiotherapy. Bearing in mind, however, that the choice of substitute for a particular investigation is frequently governed by finance and availability and looking at the poor characteristics of some of the existing substitutes, it is fortunate that water had remained the most popular substitute in the past. In the case of 7.5 MeV neutrons, the depth doses that were measured in water, were found to be closer to those measured in the muscle equivalent liquid MS/L1 than are the data in unit density muscle reported in B.J.R. Supplement 11, for the same neutron beam. Obviously, the higher hydrogen content of water almost compensates for the higher density of muscle.

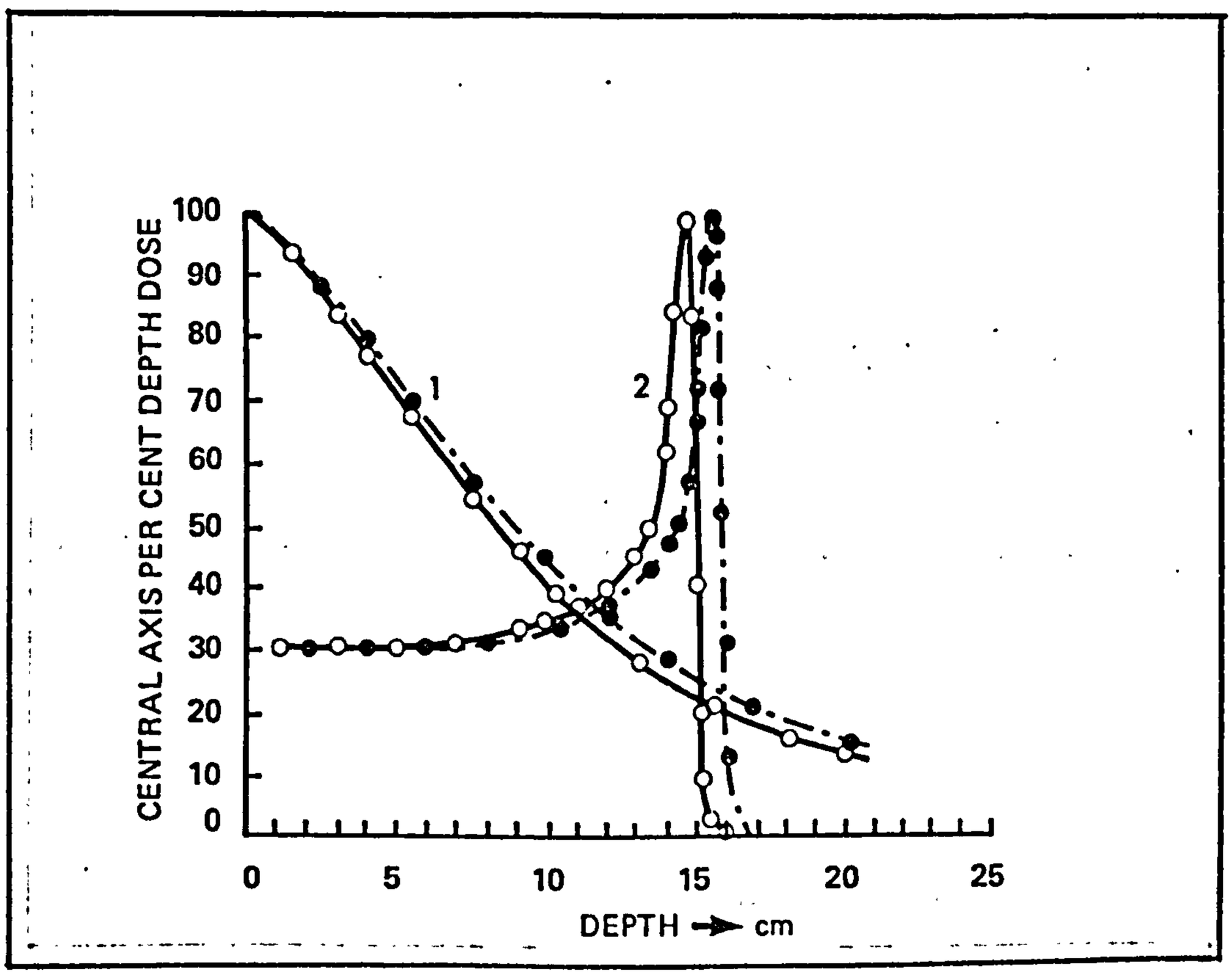

Figure 1.1 DEPTH DOSES IN MUSCLE (○) AND IN WATER (●)

1. 7.5 MeV Neutrons
2. 150 MeV Protons

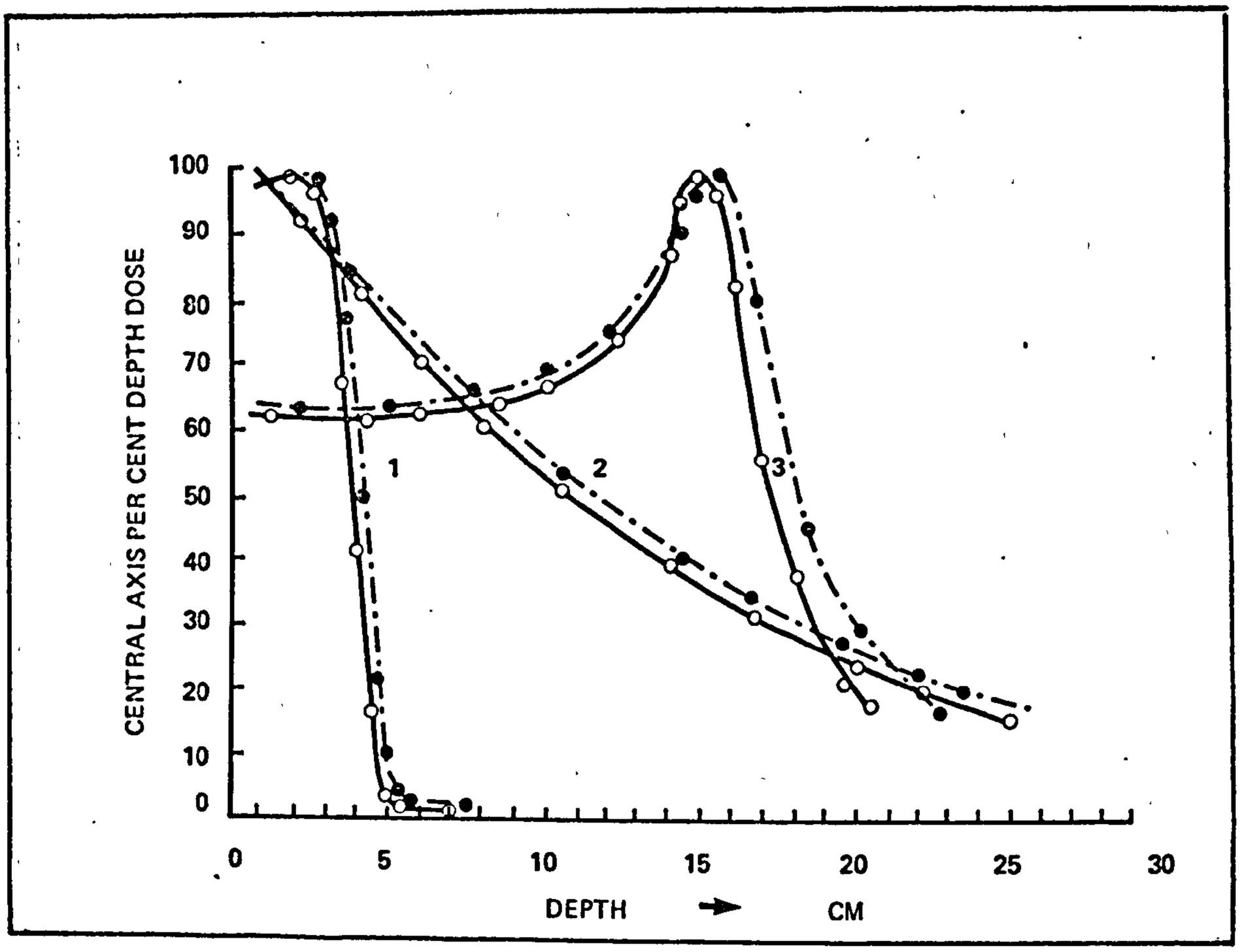

Figure 1.2 DEPTH DOSES IN MUSCLE (○) AND IN WATER (●)

1. 10 MeV Electrons
2. Cobalt - 60 gamma rays
3. 70 MeV pions

1.1 (iii) TERMINOLOGY

The symbols and nomenclature referred to in this thesis are summarised in Appendix 1.

The term "SUBSTITUTE" will be used to describe any material which has been or could be used to simulate a tissue.

The word "COEFFICIENT" will be used in a general sense to describe both the total and partial photon interactions. Similarly, the term "POWER" will be taken to generally mean collision and radiation stopping powers and mass angular scattering powers of a material for charged particles.

The new substitutes will be coded and numbered for easy reference and their phase will be indicated: /SR = solid rigid,

/SF = solid flexible, /G = Gel and /L = liquid. MS/SR1, for example, means the muscle substitute number 1 which is solid rigid. BRN/L6 is the brain substitute number 6 which is liquid. The following terms will also be used and their definition will be given in the text: Linear Energy Transfer (LET), Relative Biological Effectiveness (RBE), Oxygen Enhancement Ratio (OER), Therapeutic Ratio (TR), KERMA (K), KERMA FACTOR (KF), etc.

1.2 PHYSICAL ASPECTS

In order to design tissue substitutes for particulate radiations it is important to understand the interaction mechanisms followed when these radiations interact with matter. Obviously, these mechanisms differ between charged particles and neutrons. For this reason a brief review of the theory of interaction of charged particles and neutrons with matter will follow. Protons are treated as representative of heavy charged particles and electrons as light ones.

The type of interaction that takes place when a medium is irradiated, depends on the type and energy of the radiation and on the composition of the medium. Energies up to 1000 MeV will be considered for protons, up to 100 MeV for electrons and up to 30 MeV for neutrons.

1.2(i) INTERACTIONS OF CHARGED PARTICLES WITH MATTER

At very low energies (below 0.1 MeV for protons and below a few eV for electrons), the incident particle interacts with the atom as a whole, in contrast to the situation at higher energies where the transfer of energy is not affected appreciably by the coupling between the atomic electrons and the nucleus.

In the Intermediate energy region (up to the rest mass energy Mc^2 of the particle, i.e. for proton kinetic energies below about 1000 MeV and for electron kinetic energies below 0.5 MeV), the principal interaction is between the incident particle and the atomic electrons of the stopping medium. Unlike protons which are deflected through very small angles and lose only a small fraction of their energy in each such interaction, incident electrons can lose a large fraction of their energy in a single event and can be deflected through large angles.

As the energy of the particles increases, interactions with the nuclei of the target become more and more important; for protons of 1000 MeV, only a fraction of less than 1% would reach the end of their range without having a nuclear interaction.

In the case of electrons, interactions with the nuclei of the stopping medium lead to radiative loss of energy (Bremsstrahlung), which becomes important at higher energies; a critical energy T_c can be defined, at which the energy loss due to collisions with atomic electrons is equal to the radiative loss:

$$T_c \simeq \left[\frac{700}{Z + 1.2} \right] \text{ MeV} \qquad (1.1)$$

where Z is the atomic number of the stopping medium. For human tissue, T_c is about 85 MeV.

With protons, Bremsstrahlung becomes important at energies well above their rest mass energy ($T > Mc^2$). At these high energies, the bulk properties of the medium (dielectric constant etc.) influence the stopping of the particles, so as to decrease the rate of energy loss (stopping power). This phenomenon is called the "density

effect" and is taken into account by adding the correction term $-\delta$ in the Bethe fundamental stopping power formula (equation 1.2 for protons and 1.4 for electrons). With electrons the density effect becomes important at energies above 0.5 MeV but protons of even 1000 MeV are not significantly influenced by it. (BICHSEL, 1968).

The major uncertainty in equation (1.2) is the mean excitation energy I of the atoms of the target. The oscillator strengths f_i are not well known and I is determined from stopping power measurements.

The term $\sum \frac{C_i}{Z}$ in equation (1.2) represents the "shell corrections", which are necessary due to the fact that the atomic electrons contribute less to the stopping power of the medium if the velocity of the incident particle is comparable to their velocities in their orbits. These corrections are important for low-energy particles but little is known about them. For protons of 1 MeV in aluminium, shell corrections amount to about 4%. In medium and high Z elements, shell corrections are even more substantial (about 10% for 4 MeV protons in lead).

In the case of electrons of energy above 0.1 MeV, shell corrections amount to less than 1% and the term is often omitted from the stopping power formula.

As electrons show relativistic effects at energies above about 0.5 MeV, the collision mass stopping powers $\left(\frac{S}{\rho}\right)_{coll}$ for electrons which were needed for the comparison of tissue substitutes to the corresponding real tissues (see Chapter 4), were calculated using the relativistic formula 1.4. (BERGER and SELTZER, 1964; WHITE, 1974). In the case of compounds, the values of $\frac{Z}{A}$ and

MASS STOPPING POWER - HEAVY CHARGED PARTICLES

The mass stopping power $\frac{S}{\rho}$ of a material with atomic number Z and atomic weight A for a charged particle containing z protons is given by the Bethe equation:

$$\frac{S}{\rho} = - \frac{4\pi z^2 e^4 N_A Z}{m_e v^2 A} \left[\ln \frac{2 m_e v^2}{I(1-\beta^2)} - \beta^2 - \sum \frac{C_i}{Z} - \delta \right] \frac{MeV \cdot cm^2}{g} \qquad (1.2)$$

where : $N_A = 6.0225 \times 10^{23}$ atoms/mole (Avogadro number)

$\beta = v/c$, v = velocity of the particle

m_e = mass of electron

ρ = density of material in $g.cm^{-3}$

I = mean excitation energy of the atom defined by :

$$Z \ln I = \sum_i f_i \ln E_i \qquad (1.3)$$

where f_i = oscillator strength for the transition with excitation energy E_i

$\sum \frac{C_i}{Z}$ is the term for "shell corrections"

δ is the term for the "density effect"

Figure 1.3 Principal formulae for proton stopping powers

MASS STOPPING POWERS - ELECTRONS

$$\left(\frac{S}{\rho}\right)_{coll} = \frac{2\pi N_A r_e^2 m_e c^2}{\beta^2}\frac{Z}{A}\left[\ln\left\{\frac{\tau^2(\tau+2)}{2(I/m_e c^2)^2}\right\} + F^-(\tau) - \delta\right] \qquad (1.4)$$

where $F^-(\tau) = 1 - \beta^2 + \left[\frac{\tau^2}{8} - (2\tau+1)\ln 2\right](\tau+1)^{-2}$

$$\beta = \left[\tau(\tau+2)\right]^{1/2}(\tau+1)^{-1} = \frac{\text{velocity}}{c}$$

$m_e c^2$ = rest energy = 0.510976 MeV

τ = kinetic energy in units of $m_e c^2$

A = atomic weight

ρ = density

I = mean excitation energy = $Z(9.76 + 58.8\,Z^{-1.19})$ eV

δ = density effect correction

N_A = Avogadro's number

$r_e^2 = \left(e^2/m_e c^2\right)^2 = 7.9403 \times 10^{26}$ cm^2

$$\left\langle\frac{Z}{A}\right\rangle = \sum_i \omega_i \left(\frac{Z}{A}\right)_i \qquad (1.5)$$

$$\ln\langle I\rangle = \left(\left\langle\frac{Z}{A}\right\rangle\right)^{-1} \sum_i \omega_i \left(\frac{Z}{A}\right)_i \ln I_i \qquad (1.6)$$

$$\left(\frac{S}{\rho}\right)_{rad} = \sum_i \omega_i \left[\left(\frac{S}{\rho}\right)_i\right]_{rad} \qquad (1.7)$$

where ω_i is the proportion by weight of the i^{th} element .

Figure 1.4 Formulae used for electron mass stopping powers

lnI were replaced by $\langle \frac{Z}{A} \rangle$ and ln $\langle I \rangle$ calculated from elemental data using equations 1.5 and 1.6. The density effect corrections were derived using the procedures suggested by KIM (1973). Radiation stopping powers for electrons were calculated from the elemental data of BERGER and SELTZER (1964), and PAGES, et al., (1970) and applying the Bragg additivity rule (equation 1.7).

The multiple scattering of electrons travelling a path length ℓ in a material of density ρ is described by the mean square scattering angle, $\overline{\Theta}^2$. The elemental mass angular scattering powers $\left(\frac{\overline{\Theta}^2}{\rho \ell}\right)$, were derived from equations 1.8 and 1.9 as suggested by ICRU (1972). The choice of equation depends on the elemental atomic weight A and the momentum p_e of the electron. The mass angular scattering powers for compounds were calculated from elemental data and the additivity rule (equation 1.10).

1.2(ii) INTERACTIONS OF NEUTRONS WITH MATTER

Neutrons are uncharged particles and, like photons, are indirectly ionising particles. While photons are attenuated by photoelectric, Compton and pair production processes, neutrons are attenuated by interactions with atomic nuclei of the medium, giving rise to a complex spectrum of secondary charged particles through which energy is deposited in the medium.

In the case of biological tissues, the most important nuclear interactions for neutron energies up to 30 MeV have been summarised in ICRU report 26 (1977). Their characteristics had previously been reviewed by AUXIER, et al., (1968) who listed over 30 possible processes. These interactions include:

MASS ANGULAR SCATTERING POWERS - ELECTRONS

(a) ELEMENTS

If... $\left(\frac{280}{A^{1/3}} \cdot \frac{m_e c^2}{p_c c}\right) < 1$,

$$\frac{\overline{\Theta}^2}{\rho \ell} = 16\pi N_A \frac{Z^2}{A} \cdot r_e^2 \left(\frac{m_e c^2}{\beta p_e c}\right)^2 \ln\left[196 Z^{-\frac{1}{3}} \left(\frac{Z}{A}\right)^{1/6}\right] \quad (1.8)$$

If... $\left(\frac{280}{A^{1/3}} \frac{m_e c^2}{p_e c}\right) > 1$,

$$\frac{\overline{\Theta}^2}{\rho \ell} = 16\pi N_A \frac{Z^2}{A} \cdot r_e^2 \left(\frac{m_e c^2}{\beta p_e c}\right)^2 \ln\left[\frac{137 p_e c}{Z^{1/3} m_e c^2}\right]^{1/2} \quad (1.9)$$

(b) COMPOUNDS

$$\frac{\overline{\Theta}^2}{\rho \ell} = \sum_i \omega_i \left(\frac{\overline{\Theta}^2}{\rho \ell}\right)_i \quad (1.10)$$

Figure 1.5 Principal formulae used for electron mass angular scattering powers (symbols defined in Appendix 1)

a) Capture processes, b) Elastic scattering, c) Inelastic scattering (in which the neutron is re-emitted accompanied by a nuclear de-excitation gamma ray), d) Nonelastic scattering (interaction with a nucleus resulting in the emission of particles other than a single neutron) and e) Spallation (the nucleus is fragmented ejecting several particles and nuclear fragments).

The type of interaction which takes place depends on the neutron energy, the elastic scattering with hydrogen being by far the most important for all energies useful in radiotherapy. For energies up to 14 MeV, recoil protons deliver about 70%-90% of the absorbed dose, with the contribution decreasing with increasing neutron energy. (BEWLEY, 1963).

The capture processes $^{1}H(n,\gamma)^{2}H$ and $^{14}N(n,p)^{14}C$ are of particular importance at low and thermal neutron energies; the first gives a 2.2 MeV gamma ray and the second gives a 0.58 MeV proton which is absorbed at the capture site.

At higher energies the elastic $^{12}C(n,n)^{12}C$, $^{16}O(n,n)^{16}O$ and the nonelastic $^{16}O(n,a)^{13}C$ processes become very important in tissue.

One problem that complicates the derivation of the absorbed dose and its spatial distribution in tissue arises from the fact that neutrons transfer their energy to charged particles in the first step and these particles dissipate their kinetic energy at some point further away in the second step. Part of this energy, however, can escape from the irradiated medium.

The International Commission on Radiological Units and Measurements introduced the concept of kerma in order to treat the above problem in an approximation which does not take into account

the energy transport by the charged particles. The kerma, K, is defined as the quotient dE_{tr} by dm, where dE_{tr} is the sum of the initial kinetic energies of all charged particles liberated by indirectly ionising particles in a volume element of the specified material, and dm is the mass of the matter in that volume element.

$$K = \frac{dE_{tr}}{dm} \qquad (1.11)$$

Under conditions of charged particle equilibrium the kerma is equal in magnitude to the absorbed dose.

Tissue substitutes used in neutron dosimetry should be elementally correct so that they absorb and scatter both the neutron and the gamma ray component, which is present in all fast neutron beams, in the same way as the real tissue.

1.2(iii) BASIC ELEMENTAL DATA USED IN THIS WORK

In the case of photons (X - and gamma rays) interaction cross sections, attenuation and absorption coefficients and other requirements exist in tabulated form and are readily available.

The elemental cross sections of HUBBELL (1969) and STORM and ISRAEL (1970) compiled by WHITE (1974) on magnetic tape were used to calculate the total mass attenuation and energy absorption coefficients at 33 energy points in the range 10 keV-100 MeV, for both the substitutes and the real tissues.

Electron collision mass stopping powers, radiation stopping powers, and mass angular scattering powers for the same 33 energy points were calculated using elemental data and the formulae 1.4 to 1.10 as described in the previous section.

Stopping powers for protons were compiled and stored on magnetic tape. 38 energy points were considered in the energy range from 0.01 to 1000 MeV. For energies below 2 MeV, the values given by OLDENBURG and BOOZ (1972) were used. In the energy range from 2 to 1000 MeV the data were taken from BARKAS and BERGER (1964), and BERGER et al., (1966). 17 elements were considered in all, namely, ^{1}H, ^{6}C, ^{7}N, ^{8}O, ^{9}F, ^{11}Na, ^{12}Mg, ^{13}Al, ^{14}Si, ^{15}P, ^{16}S, ^{17}Cl, ^{19}K, ^{20}Ca, ^{26}Fe, ^{32}Cu and ^{58}I. For those elements for which no mass stopping powers existed readily available, the two-variable tables given by BARKAS and BERGER (1964) were used to obtain the proton mass stopping powers. The powers are given in these tables as a function of the proton kinetic energy and the mean excitation energy I. For this application it was necessary to know the correct I value for each element. Iadj - values, adjusted to take into account shell corrections were obtained from TURNER (1964), who gives Iadj/Z as a function of the atomic number Z, and averaged with the corresponding values given by BICHSEL (1968). Since only the logarithm of I enters the theory directly, (equation 1.2) a large uncertainty in the value of I, introduced only a small uncertainty in the value of the stopping powers. Based on the accuracy claimed for the data in the above references, the stopping powers obtained by using them will be accurate to within $\pm 2\%$.

Figures 1.6 and 1.7 show the electron and proton mass stopping powers respectively, for hydrogen, carbon and nitrogen, plotted as a function of energy. It is evident that while the data for carbon and oxygen are very similar, the data for hydrogen are

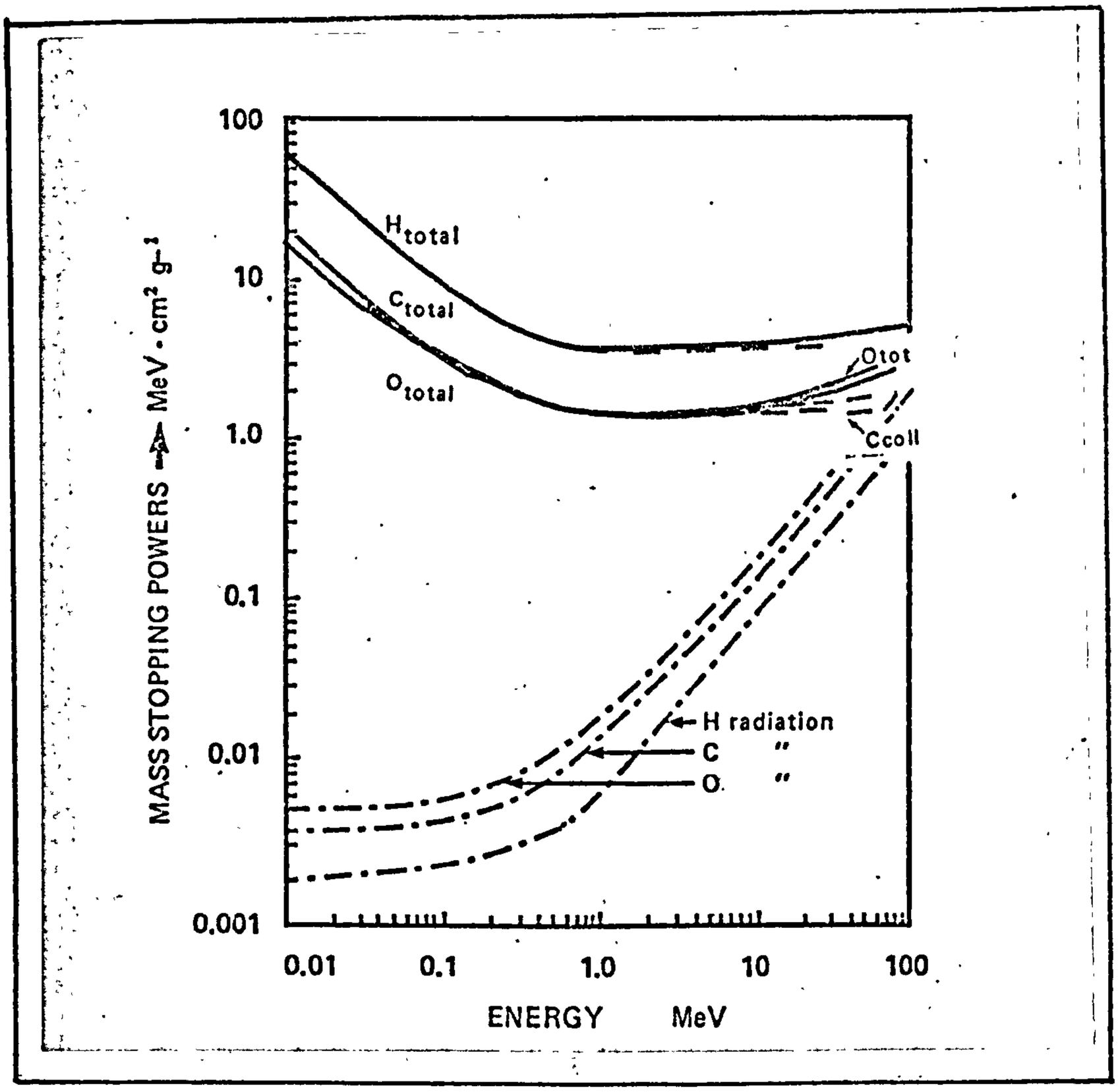

Figure 1.6 Mass stopping powers for electrons in hydrogen, carbon and oxygen

—— TOTAL · — · RADIATION — — COLLISION

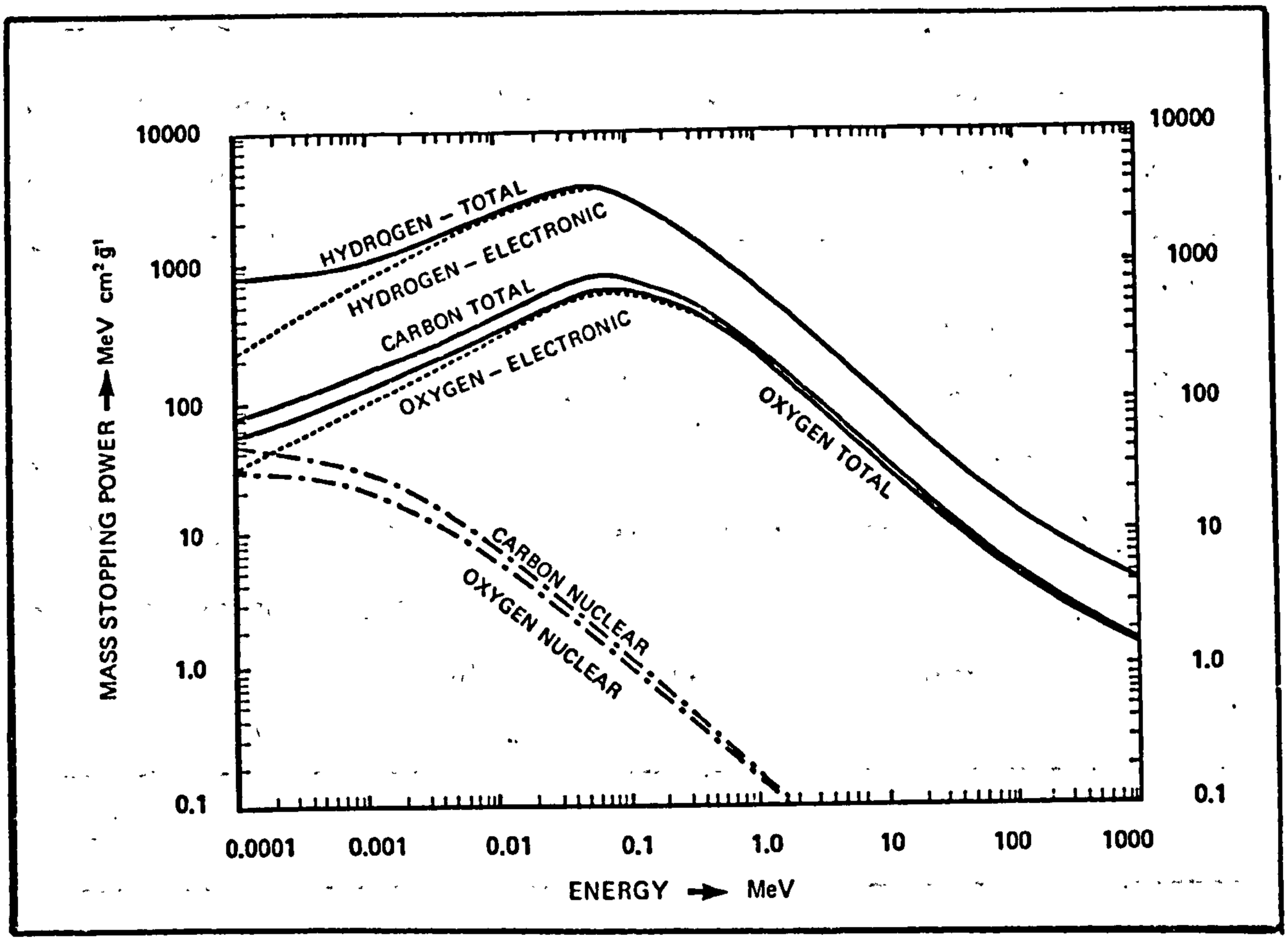

Figure 1.7 Mass stopping powers for protons in hydrogen, carbon and oxygen

much higher due to the fact that $\frac{Z}{A}$ for hydrogen is twice the $\frac{Z}{A}$ for other elements (equations 1.2 and 1.4). This supports the previous arguments on the significance of the hydrogen content of the substitutes.

The difference in the neutron interaction cross sections of carbon, nitrogen, oxygen and hydrogen was also investigated. Neutron cross sections were obtained from the Neutron Data Compilation Centre (CCDN, 91-GIF-SUR-YVETTE, B.P. No.9, FRANCE), on magnetic tape. Data from the Evaluated Neutron Data File (ENDF/B-IV) and from the Lawrence Livermore Evaluated

Neutron Data Library (ENDL, 1970) were used. The ENDF/B-IV can be used as a self-consistent source of cross sections, but unfortunately the cross sections in the resonance region are not explicitly given, but a set of parameters is listed from which the cross sections can be calculated by a rather time consuming computer program. In the resonance region the data from the ENDL were used and the curves for the neutron cross sections for H,C,N,O versus energy are given in Figure 1.8. For energies below 20 MeV, the data are based on a combination of experimental and theoretical results. Above 20 MeV, there are experimental data available to describe neutron-hydrogen collisions, but the available data on other nuclei are scant and the data are based on theoretical models.

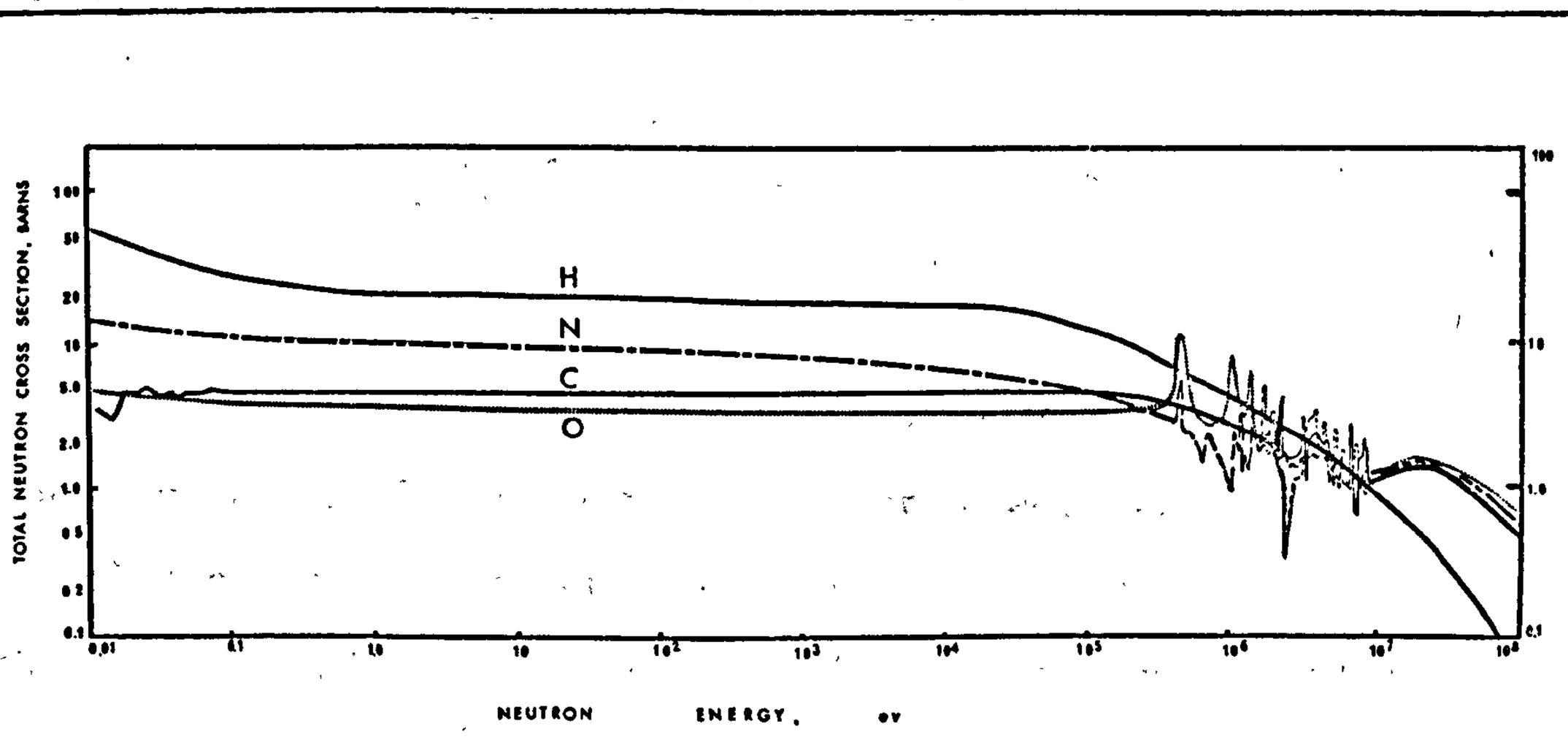

Figure 1.8 Neutron cross sections (σ_t) for H,C,N,O as a function of energy

Apart from the resonance region (0.3-9 MeV for oxygen, 2-9 MeV for carbon) where oxygen has some resonance peaks not present in the cross section (σ_t) of carbon, the total cross sections of C and O are very close to one another (4-5 barns at 0.01 eV and

about 1 barn at 10 MeV); so, when C replaces O in the plastic substitutes, the absence of some peaks will be compensated for by the slightly higher σ_t of C at lower energies and the neutron dose will not be affected significantly.

ICRU (report 26, 1977) used the ENDF/B-IV total neutron cross sections and calculated the kerma factors from 10 eV up to 30 MeV for 19 elements most of which appear in various tissues. (116 values of kerma factors for each element).

The kerma factor is defined as the quotient of the kerma (K) by the particle fluence $\Phi(E)$, and for a given energy it is equal to the product of the mass energy transfer coefficient $\left(\mu_{tr}/\rho\right)$ and the neutron energy En. (ICRU, report 26).

$$\frac{K}{\Phi(E)} = \frac{\mu_{tr}}{\rho} \cdot E_n \qquad (1.12)$$

The use of the kerma factors in neutron dosimetry requires some comment . The walls of the detectors used, do not have exactly the same composition as the real tissue; it is necessary, therefore, to multiply the response of the dosimeter by the ratio of kerma factor in tissue to kerma factor in the instrument, averaged over the neutron spectrum at the point of measurement, if accurate values of the kerma or the absorbed dose in tissue are to be obtained.

It is obvious that if the accuracy aimed is a few percent, it is important to take into account the exact composition of the tissue (or substitute) in which the dose is estimated.

Kerma factor ratios (substitute/real tissue) have been calculated for all the substitutes produced in this work and those for the recommended materials, are given in Chapter 4.

1.3 THE ADVANTAGES OF VARIOUS TYPES OF RADIATIONS IN RADIOTHERAPY

A cancerous tissue is formed of body cells growing out of control. While surgery aims to remove these cells, the aim in radiotherapy is to kill them by inflicting as much damage to the tumour as possible and at the same time minimising the dose delivered to the surrounding healthy tissues and thus sparing them. Sparing normal tissues is the feature that makes radiotherapy preferable to surgery in some cases.

What matters most in each case is the Therapeutic Ratio (T.R.), which is defined as the ratio of the normal tissue tolerance dose (N.T.T.D.) to the tumour lethal dose (T.L.D.). Above N.T.T.D. necrosis of the normal tissue starts to increase rapidly while above T.L.D. almost all the tumours are destroyed. (JOHNS and CUNNINGHAM (1969).

The ratio of tumour kill to normal tissue damage, can be improved either through better spatial dose distribution or through using a radiation with a larger Relative Biological Effectiveness at the tumour volume (RBE tumour) and a lower Oxygen Enhancement Ratio (OER), or through both. These concepts will be discussed in the following section.

The rationale for using particulate radiations in radiotherapy, is to increase this therapeutic ratio, and the criterion for the choice of the type of radiation to be used in each case, is the performance of each with regard to the above factors; by optimising the dose distribution, dose fractionation, RBE and OER, it is hoped to inflict the greatest possible amount of damage to the cancerous cells.

1.3(i) PHYSICAL FACTORS

Figure 1.9 shows the central axis depth dose curves derived from our measurements in the muscle equivalent liquid, MS/L1, with 5 different radiation modalities. (see also Figures 1.1 and 1.2). All the important physical characteristics of these radiations are clearly shown. Apart from adequate tissue penetration for a radiation modality, it is desirable to have controlled penetration and sharpness of dose distribution, so that sensitive healthy tissues near the tumour can be protected. Furthermore it is desirable to have the entrance dose smaller than the dose at any depth if possible.

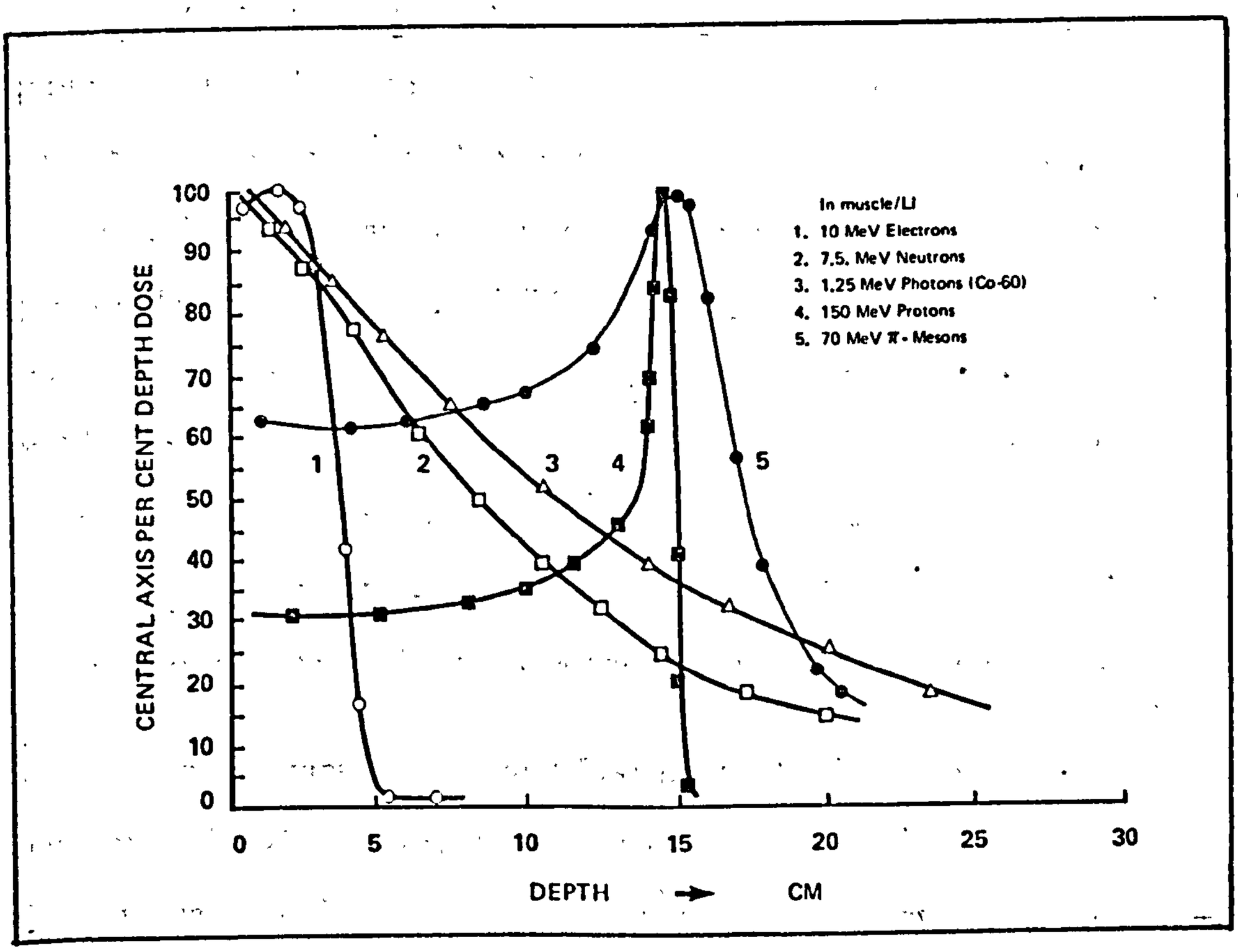

Figure 1.9. Central axis per cent depth doses in muscle, for various types of radiation

The above advantageous features are exactly what high energy beams of charged particles like protons, heavy ions and negative pions have. The depth of the peak can be controlled by energy absorbers, the beam allows a significant reduction of the dose to the tissue outside the target volume and beam collimation is relatively easy. It is obvious that protons have a more definite range, a narrower peak and a much sharper cut off; by superimposing many such beams (of varying range), one can treat extended tumour volumes to a uniform dose.

With pions the peak is wider and tails off resulting in some exit dose, due to the presence of electrons and muons in the beam, Pions have a unique property that makes them promising in radiotherapy; at the end of their range, negative pions are captured by the host nuclei which then disintegrate (star formation) emitting a number of particles, such as neutrons, protons, deuterons and other heavier fragments with high Linear Energy Transfer (LET). LET or LET_{∞} is defined as the energy transferred per unit length of track and is usually expressed in keV/μm); most of these secondary charged particles deposit their energy locally, resulting in a lower oxygen enhancement ratio (OER). Consequently, the killing of hypoxic cells is more effective in the peak region of the pion beam. (see following section).

With cobalt gamma rays and fast neutrons the dose falls off exponentially with depth, resulting in some exit dose; the depth of maximum dose depends on the energy and when megavoltage photons and neutrons are used the desirable skin sparing effect is observed. (Cobalt gamma rays : depth of maximum buildup = 0.5 cm; neutrons of energy = 7.5 MeV : depth of maximum buildup = 0.2 cm). In practice, neutrons have no physical advantages over

megavoltage X-and gamma rays.

Electrons in the useful energy range are easily scattered and absorbed in the irradiated medium. Electron beams of energy 3-10 MeV give such a dose distribution that allows the treatment of a superficial tumour to a nearly uniform dose while sparing the underlying deeper regions. The rapid fall off in the absorbed dose after the first few cm of tissue, however, is lost if higher energy electrons are used to treat deep seated lesions. Lower energy electrons are also very useful for treating skin tumours.

1.3(ii) BIOLOGICAL FACTORS

The presence of hypoxic but viable cells in many tumours has always been a serious problem in radiotherapy, because these cells are very resistant to X-rays. The sensitivity of cells to radiation was found to increase in the presence of oxygen and this is known as Oxygen Effect. The Oxygen Enhancement Ratio is defined as "the ratio of doses under hypoxic and oxygenated conditions needed to produce the same biological effect".

It is also known that equal doses of two different types of radiations do not always produce the same biological effect.

The Relative Biological Effectiveness of radiation A is defined by the relation:

$$(RBE)_A = \frac{\text{Dose of standard radiation for a biological effect}}{\text{Dose of radiation A needed for the same effect}}$$

In most comparisons, the standard radiation is cobalt-60 gamma rays or 250 kV_p X-rays.

RBE and OER depend on the LET of the radiation. In essence, LET describes the quality of the radiation. Table 1-I summarises

the range of LET values for the various types of radiations.

TABLE 1-I

LET VALUES OF VARIOUS RADIATIONS

Radiation	Range of LET, keV/μm
Electrons, X, γ	1 - 30
Protons	5 - 100
Pions, fast neutrons	3 - 900
Alpha particles	40 - 250
Heavy recoils	100 - 1000

As the LET of a radiation increases, the OER is reduced and approaches unity at about 200 keV/μm, while the RBE increases and reaches a maximum at about 100 keV/μm; with further increase in LET, the RBE decreases below its maximum because of dose saturation.

The RBE of charged particles in the Bragg peak ionisation region is known to be greater than that of charged particles in the plateau region, because of the higher LET of the particles towards the end of their range. Thus the ratio $RBE_{peak}/RBE_{plateau}$ is expected to be greater than unity. Consequently, if the Bragg peak region is made to coincide with the tumour containing volume, the ratio $RBE_{tumour}/RBE_{normal\ tissue}$ will be greater for beams of heavy charged particles than for X-ray, gamma ray, electron or neutron beams.

It is desirable to have OER values as close to unity as possible. For radiations that have a wide LET spread, even a small fraction

of high LET component is effective in reducing the OER significantly.

With the presence of more particles with higher LET in the peak region of heavy charged particle beams than in the plateau region, reduced OER and less recovery from sublethal damage are to be expected in the tumour region compared to the surrounding healthy tissues (ELLIS, et al., 1976).

X-rays and electrons are considered generally as low-LET radiations; their mean LET values are very similar and consequently the biological effectiveness of electrons is not expected to be different from that of megavoltage X-rays.

High-energy protons deposit an important part of their energy below 30 keV/μm and so behave to some extent like low-LET radiation (i.e. X-rays). (BEWLEY, 1971).

The RBE of fast neutrons is generally larger than unity and depends on the neutron energy spectrum. BIANCHI et al., (1978) used vicia faba roots (10-day growth) and found an RBE = 5.4 for 14 MeV neutrons; for higher energies the RBE value was found lower. RBE values derived from studies with mammalian cells, however, vary from 2.5-3.0. The OER of fast neutrons was investigated by a number of authors who report OER values ranging from 1.2 to 1.8 depending on the energy and on the biological system used; PARNELL, et al (1965) for example, used five mammalian systems and all their results lie in the region 1.6-1.8 for the OER of the neutron beam of the Medical Research Council cyclotron. These figures are less than the values of X-rays by a factor of 1.6 ± 0.1 (Gain factor). The

rationale for using fast neutrons in radiotherapy was centered originally almost exclusively on their reduced OER, hence their effectiveness in killing hypoxic cells.

In the case of negative pions, RBE values reported in the literature range from 2-3 and OER values range from 1.5 to 1.8. Table 1-II summarises the RBE and OER values derived from studies with mammalian cells, for all types of radiations used for therapeutic purposes. (PARNELL, et al., 1965; RAJU and RICHMAN, 1972; ARCHAMBEAU, et al., 1974; ELLIS, et al., 1976; RAJU and PHILLIPS, 1977).

TABLE 1-II

RBE & OER VALUES FOR VARIOUS TYPES OF RADIATION

Radiation	RBE	OER
X-and gamma rays and electrons	1	3.0
Protons (100-200 MeV)	Plateau 1 Peak 1	Plateau 3.0 Peak 2.5
Neutrons (1-20 MeV)	2.5-3.0	1.5-1.8
Negative pions (70 MeV)	Plateau 1.0-1.5 Peak 1.9-2.1	Plateau 3.0 Peak 1.8

ELLIS, et al., (1976), studied the distribution of high and low LET events in a perspex phantom irradiated with 70 MeV negative pions. Nuclear emulsions were placed at the surface of the phantom as well as in the plateau and peak position and the number, length and thickness of the observed tracks was considered. This work confirmed the existence of high LET events in the plateau region caused by interactions with pions in flight. Similar work with nuclear emulsions(KEMBER, et al., 1975), showed that low

and medium LET events (clusters and light tracks) are uniformly distributed through the whole range of the stopping negative pions. Heavy tracks in the peak region, however, were about three times the number in the plateau region. Determinations of event size distributions using a lithium drifted silicon detector and a ROSSI spherical "tissue equivalent" chamber showed a similar trend. The peak/plateau ratios for high LET events are between 4 and 6 and are dependent on the position in the plateau region; by comparing these high LET peak/plateau ratios with the overall values of 1.3-1.6, the effect of the low LET component is demonstrated. (ELLIS and PERRY, 1972, ELLIS, et al., 1976).

To conclude, the use of heavy charged particles is being proposed for treatment of cancer mainly for three reasons:

1) Superior depth dose distribution.

2) Higher RBE in the region of the Bragg-peak.

3) Lower OER and less recovery in the tumour.

Fast neutrons do not have the first advantage. Table 1-III shows a comparison of the various types of radiations. The high cost of the installations producing high energy heavy charged particles, some difficulty in localising the peak and, with pions the low dose rates available at present are the main reasons why some people might argue against the use of high energy particle beams in radiotherapy.

TABLE 1-III

COMPARISON OF VARIOUS RADIATION MODALITIES

Type of radiation	Spatial dose distribution	* $\frac{\text{RBE tumour}}{\text{RBE normal tissue}}$	$\frac{\text{OER tumour}}{\text{OER normal tissue}}$
X-and gamma rays	Exponential attenuation	1	1
Electrons (5-15 MeV)	Good for superficial tumours	1	1
Fast neutrons (1-20 MeV)	Exponential attenuation	~ 1	~ 1
Protons (100-200 MeV)	Very good for deep-seated tumours	~ 1	~ 1.2
Negative pions (70 MeV)	Good for deep-seated tumours	~ 1.4	~ 1.6

* If the Bragg-peak is made to coincide with the tumour area,

then: $\frac{\text{RBE peak}}{\text{RBE plateau}} = \frac{\text{RBE tumour}}{\text{RBE normal tissue}}$ and $\frac{\text{OER peak}}{\text{OER plateau}} = \frac{\text{OER tumour}}{\text{OER normal tissue}}$

CHAPTER 2

SIMULATION PROCEDURES AND THE FAMILY OF NEW TISSUE SUBSTITUTES

Various procedures can be applied to the simulation of body tissues, such as the "effective atomic number ($\bar{Z}$) method", the "basic data method" and the method of "elemental equivalence". The effective atomic number ($\bar{Z}$) method is applicable only to photon interactions and is the technique mostly employed before WHITE (1974) introduced the basic data method; the latter is applicable to photons and electrons.

A recent review of the literature (CONSTANTINOU and WHITE, 1977), has shown that some 80 tissue substitutes had been developed before 1974 and these simulate mainly muscle, lung and bone (46, 14 and 13 substitutes respectively). WHITE (1974) extended the range of simulated tissues by producing substitutes for fat, breast, skin, liver and thyroid as well as muscle, lung and bone. All these substitutes, however, were designed for photon and electron interactions. The number of substitute materials suitable for particulate radiation dosimetry and in particular neutrons, was very limited.

After a brief description of the first two simulation procedures, the application of the elemental equivalence method will be discussed and the whole range of liquid, gel and solid tissue substitutes produced in this work, most of which are TISSUE EQUIVALENT, will be presented.

2.1 THE EFFECTIVE ATOMIC NUMBER METHOD AND THE BASIC DATA METHOD

The atomic cross section for a photon interaction (photoelectric absorption, Compton scattering or pair production), generally depends on the photon energy and the elemental atomic number; the dependence on the atomic number Z can be expressed by the relationship :

$$\text{atomic cross section} \propto Z^x \tag{2.1}$$

where the value of the power x depends on the type of the process analysed and is reported to vary from 1 to 5 (HUBBELL, 1969). A compound may be regarded as a single element with an effective atomic number $\bar{Z}$, given by

$$\bar{Z} = \left(\sum_i a_i Z_i^x \right)^{\frac{1}{x}} \tag{2.2}$$

where a_i is the fractional electron content of the i^{th} constituent element with atomic number Z_i.

In the effective atomic number ($\bar{Z}$) method, the composition of the substitute is adjusted so that the value of its $\bar{Z}$ is as close as possible to that of the material being simulated. The mass attenuation coefficient $\frac{\mu}{\rho}$ for a compound, however, depends not only on the effective atomic number raised to a power x, but also on the electron density n_o, to which it is directly proportional (SPIERS, 1946).

$$\frac{\mu}{\rho} \propto n_o \left[\bar{Z} \right]^x \tag{2.3}$$

The reasons for the large errors in the properties of the substitutes produced by applying the $\bar{Z}$ method in the past are the following:

a) The method was usually applied only for photoelectric absorption.

b) The electron density (n_o) was not always considered in the simulation; this introduced errors especially in the energy range where Compton scattering predominates.

c) A single exponent is not enough to give adequate agreement between the substitute and the real tissue over a wide energy range. As the photon energy changes, different exponents are required. WHITE (1974) calculated values of the exponent x for the photoelectric process ranging from 3.5 at 10 keV to 3.9 at 100 keV instead of the popular 2.94. An exponent of 1.7 for coherent scattering has been found (WEBER and van den BERGE, 1969), while the pair production exponent has always been taken to be unity, although it has been shown that it decreases with energy (WHITE, 1977).

In the "basic data" method, fundamental photon and electron interaction data are used to establish the proportions of the compounds which make up the substitute. Once a base material has been chosen corrective additives are selected, which have coefficients (or powers) complementary to those of the base material; when base material and additives are mixed in the correct proportions, the radiation characteristics of the mixture will match those of the real tissue.

The selection of the corrective additives is based on the slopes of the "coefficient versus energy" curves. These coefficients (or cross sections for elements) on a log-log plot against energy form linear parts over certain energy ranges. The slope of these graphs for a compound depends upon the slopes of the graphs of the elements that make up the compound and the final slope for a substitute depends on the constituent compounds and their percentage weights. Figure 2.1

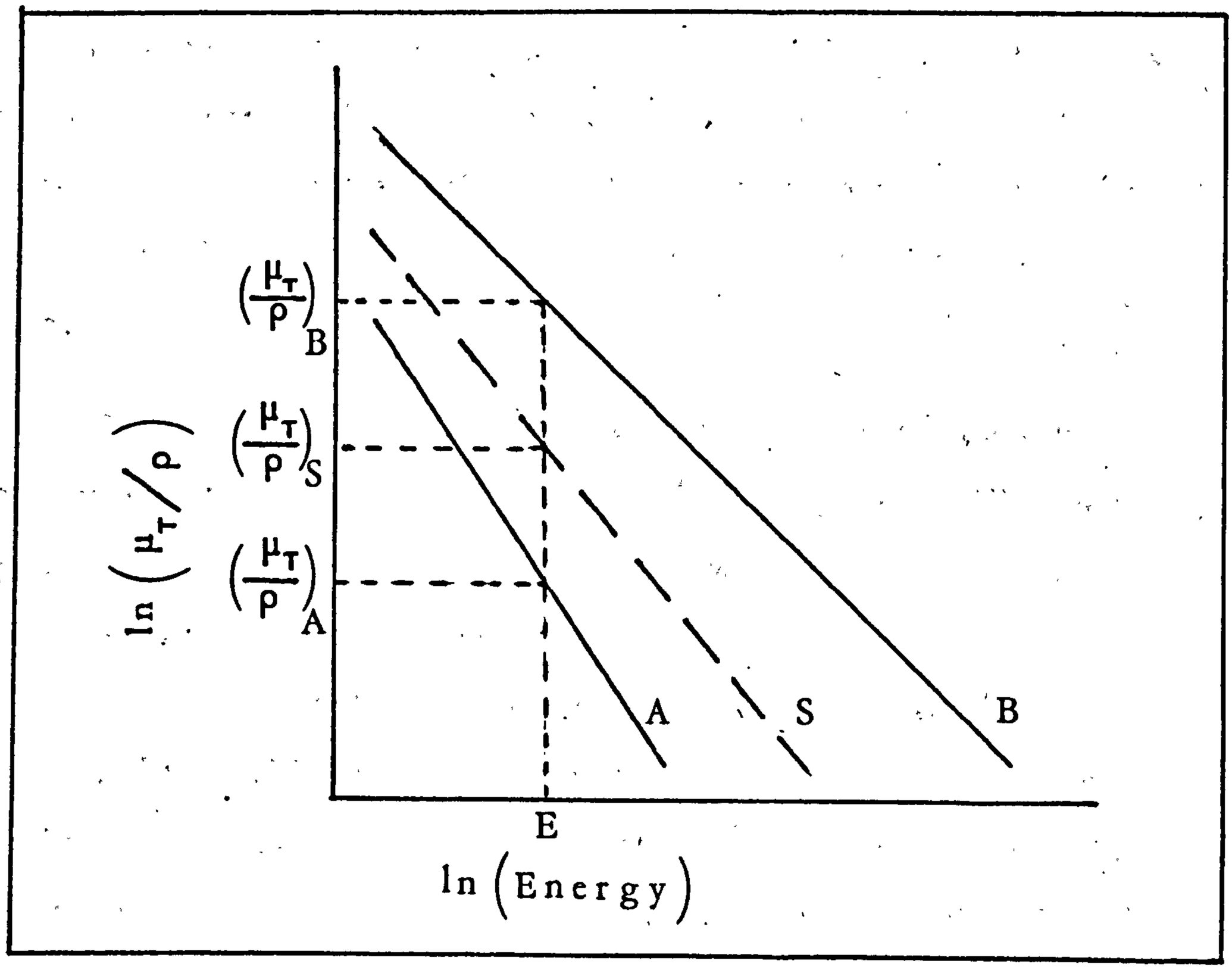

Figure 2.1 A schematic diagram to explain the principle of the "basic data" method of tissue simulation.

explains this principle schematically for photoelectric mass attenuation coefficients. If S is the substitute that simulates a tissue X and is composed of two components A and B and if the additivity rule is obeyed, then the corresponding coefficients $\left(\frac{\mu_T}{\rho}\right)_S, \left(\frac{\mu_T}{\rho}\right)_X, \left(\frac{\mu_T}{\rho}\right)_A$ and $\left(\frac{\mu_T}{\rho}\right)_B$ are related:

$$\left(\frac{\mu_T}{\rho}\right)_S = \left(\frac{\mu_T}{\rho}\right)_X = \omega_A\left(\frac{\mu_T}{\rho}\right)_A + \omega_B\left(\frac{\mu_T}{\rho}\right)_B \qquad (2.4)$$

where ω_A and ω_B are the proportions of A and B (by weight); but $\omega_A + \omega_B = 1$ and therefore,

$$\omega_A = \frac{\left(\frac{\mu_T}{\rho}\right)_S - \left(\frac{\mu_T}{\rho}\right)_B}{\left(\frac{\mu_T}{\rho}\right)_A - \left(\frac{\mu_T}{\rho}\right)_B} \qquad (2.5)$$

The agreement for other energies and other partial interactions will depend on the choice of materials. The limitations of the basic data method are: a) the additivity rule must be obeyed and b) the relationship between the coefficients (or stopping powers) and energy must be, or closely approximate to a linear function on a log-log scale.

In an attempt to calculate $\bar{Z}$ exponents for proton and pion interactions, the power law $\frac{S}{\rho} = a\ Z^x$ was applied. The least squares method for Z-values from 1 to 20 was used and a linear relationship of the form ln(mass stopping power) =lna+ x ln Z was fitted to the available data. This gave values of the exponent x from -0.26 to -0.75 for protons, and from -0.25 to -0.37 for pions. The fitting, however, was not good (coefficient of correlation about 0.75 for most energy levels). Consequently, the $\bar{Z}$ method was considered not useful for the formulation of tissue substitutes for particulate radiations.

As the proton mass stopping powers versus energy show some linearity on a log-log scale for certain energy ranges, it should be feasible to use the "basic data" method to produce substitutes for protons. This method, however, is not useful for neutrons because of the resonances in the neutron cross sections. It became clear, early in this work, that the best method to be applied to the formulation of tissue substitutes for particulate radiations, is that of "elemental equivalence". This method is discussed in the following section of this chapter.

2.2 THE ELEMENTAL EQUIVALENCE METHOD

The criteria for tissue equivalence have already been discussed and it has been made clear that the only way in which tissue substitutes suitable for all types of particulate radiations and photons can be formulated, is to make them have the same elemental composition and the same density as that of the real tissue. Consequently, the method of elemental equivalence was the simulation procedure of choice in the present work.

If a substitute is elementally correct and has the correct density, the only source of error in the determination of the dose absorbed in the real tissue will be due to "phase" differences, i.e. differences in chemical binding, the effect of which is expected to be minimal. Despite this, less than 10% of the published substitutes have been formulated using the elemental equivalence method.

2.2(i) APPLICATION OF THE ELEMENTAL EQUIVALENCE METHOD IN THE PAST

ROSSI and FAILLA (1956) were the first to apply the elemental equivalence method; in an attempt to reproduce an approximate formula for soft tissue ($C_5H_{40}O_{18}N$), they formulated a liquid system comprising a mixture of water/glycerol/Urea/sucrose, which had the formula $C_5H_{37.5}O_{18}N_{0.97}$. The method of arriving at this formula, however, was not explained in their publication. GOODMAN (1969), improved that liquid by removing sucrose.

The first solid tissue substitutes produced with the requirements of neutron dosimetry in mind, were those formulated and manufactured by SHONKA et al., (1958). The muscle substitute they produced consisted of polyethylene, nylon, carbon, calcium fluoride and silica, which were combined at temperatures of approximately 180°C in a

special mixer. A later variation of that product, in which the silica is excluded, is widely known as plastic A-150 (see Appendix 4). The plastic substitutes produced by Shonka presented electrical conductivities of a suitable magnitude (i.e. resistivity $< 5 \times 10^4$ $\Omega \cdot cm$) and this is the main reason why A-150 is, up to the present day, a popular material for the construction of ionisation chambers.

The composition of the original muscle substitute was decided from a set of simultaneous equations derived to satisfy a) the hydrogen content, b) the nitrogen content, c) the electrical conductivity d) Compton interactions and e) photoelectric interactions. The introduction of free carbon (13.5% by weight) for optimal conductivity resulted in an oxygen deficiency that was compensated for by the addition of smaller amounts of calcium, silicon and fluorine, to match the radiation attenuation characteristics of the simulated tissues.

FRIGERIO et al., (1972), used a simplified version of the GIBBS' method of canonical components (HUTCHINSON, 1964) and produced liquid systems which had the same elemental composition as the ICRU muscle. According to this method, the formula of each compound can be written as the sum of two or more components; for example, glycerol and urea can be written as $C_3H_8O_3 = C_3H_2(H_2O)_3$ and $NH_2CONH_2 = CH_2N_2(H_2O)$ respectively. In this way, the approximate soft tissue formula $C_5H_{40}O_{18}N$ can be written as: $C_5H_4N(H_2O)_{18}$. If urea is used to satisfy the needed one mole of nitrogen, then:

$$C_5H_{40}O_{18}N = 0.5\left[CH_2N_2(H_2O)\right] + C_{4.5}H_3(H_2O)_{17.5}$$

0.5 moles Urea + B

But the component B = 1.5 $\left[C_3H_2(H_2O)_3 \right]$ + 13(H_2O).

1.5 moles glycerol + 13 moles water.

Consequently,

1 mole $\left[C_5H_{40}O_{18}N \right]$ = 0.5 moles Urea + 1.5 moles glycerol + 13 moles water.

The formula weight is 402.378 so, to make one kilogram of mixture, 1000/402.378 times as many moles of each component as indicated above, have to be used.

The above two variations of the method of elemental equivalence, with slight modifications were used extensively during this work and as a result over 80 substitutes were formulated, which simulate various tissues, tissue components and body organs very closely. These formulations will be presented in the last section of this chapter.

2.2(ii) THE ELEMENTAL EQUIVALENCE METHOD AS APPLIED IN THIS WORK - SOME GENERAL COMMENTS

The formulation of the new substitutes was based on the following general principles:

a) The number of components should be kept to the minimum possible.

b) The components which are suitable for addition to a specified base material should be chosen from a "compound library", i.e. a group of chemical compounds selected to meet certain criteria (described in the next section).

c) The procedure should accurately establish the proportions (by weight) of the components of a tissue substitute.

d) The materials and techniques to be used should be such that the new substitutes can be manufactured in any ordinary workshop with a minimum requirement of simple equipment.

As it is not always possible to find a single rigorous solution in each case, the simulation procedure was not fully automated. A computer can be used interactively, saving time by doing calculations that are repetitive, in this case solving sets of simultaneous equations, but leaving it to the operator to choose the right compounds on the basis of compatibility, solubility, availability and likely cost factors.

The base materials used throughout this work were water for the liquid substitutes and epoxy resins for the solids, for reasons which are discussed in the following section. The viscosity and elemental composition of the resins, however, made the partial replacement of oxygen by carbon in the solid substitutes inevitable. Apart from that, resins proved to be very good insulators. A preliminary attempt to get conducting substitutes failed. Many samples of "resin + graphite" mixtures, with graphite up to 15% by weight, showed infinite resistance. The number of graphite grades is very large and for this reason the grade VULGAN XC - 72 used by Shonka in his conducting plastics, was also tested. The resistivity of the resulting sample was 800 times larger than that of a similar sample of A-150 plastic (8×10^4 Ω .cm as compared to 100 Ω .cm).

The application of the elemental equivalence method in the formulation of tissue substitutes during this work, followed a number of steps which are summarised here. Examples of the actual calculations are given in Appendix 2.

STEP 1: From the given elemental composition of the tissue to be simulated, derive its empirical formula and/or the number of moles needed per kilogram of substitute, for each constituent element (HOLDERNESS and LAMBERT, 1977).

STEP 2 : Scan the compound library (procedure not computerised) to find if there is a single compound with the same formula (or the same "percentage $\pm$0.5% by weight" for each constituent element, considering hydrogen as the critical element). If such a compound is found, use it as a "single component substitute with no trace elements in it", provided that its density does not differ from that of the real tissue by more than 2-3%.

STEP 3 : Decide on the compounds which will be used to satisfy the requirements for trace elements, i.e. elements whose proportion in the tissue is less than 0.5% by weight.

STEP 4 : Subtract the quantity of C, H, N, O already introduced with the compounds selected in Step 3 from the number of moles/kg derived in Step 1 for each element. Derive the empirical formula for the remaining C, H, N, O.

STEP 5 : Write the formula derived in Step 4 as the sum of two compound components (A and B). Consider water, gelatine or the selected epoxy resin system as an obligatory component (part A) for a liquid, a gel or a solid substitute respectively. Again, scan the library to find compounds with C, H, N, O contents equal to or bracketing those of part B. If no single compound having the same composition as part B is found, then the base material and the compounds with C, H, N, O contents bracketing those of part B are used in Step 6.

STEP 6 : Solve a set of simultaneous equations written to satisfy the requirements for C, H, N, O given in Step 4. Derive the exact proportions by weight of the various compound components.

STEP 7 : Calculate the density of the formulated substitute using equation 2.6, assuming that the volumes of pure substances are additive. This is an approximation which is partly responsible for the difference observed between calculated and measured density values.

$$\rho = 100 \left(\sum_i \frac{m_i}{\rho_i} \right)^{-1} \qquad (2.6)$$

where ρ = density of the mixture and

m_i = percentage by weight of the i^{th} constituent compound whose density is ρ_i .

The search of the compound library for a "single component" substitute usually produced a few interesting materials but rarely gave ideal systems.

All the trace elements put together, usually account for less than 1% of the total weight, but they should be included if absolute completeness is desirable. As it was difficult to find many alternative salt systems equally soluble and stable to satisfy the trace elements of a particular tissue, the same set was used whenever more than one liquid substitutes were formulated for the same tissue. The compounds for traces in gel systems are different from those for the corresponding liquids because gelatine, used as the main gelling agent, has sulphur as an impurity. Similarly, one single set of compounds was calculated for all the solid substitutes which simulate the same tissue.

The problem of matching the density of the real tissue, proved not to be a difficult one. In the case of liquids it was almost always possible to find alternative combinations of liquid components to formulate substitutes of lower, equal and higher density than that of the real tissue. In the case of epoxy resin based substitutes, the use of phenolic microspheres (PMS) with a relative density of approximately 0.2, solved the problem. Relatively small quantities of these hollow, gas-filled microspheres added to the resins reduced the bulk relative densities to below unity. The percentage of PMS (by weight) needed in each case, was derived from equation 2.6.

2.3 THE COMPOUND LIBRARY

A comprehensive library of selected chemical compounds was compiled at the beginning of this study, to facilitate the formulation of new tissue substitutes.

The following criteria were used in the selection of compounds for the library:

- A compound must not be carcinogenic (or suspected carcinogenic), corrosive, toxic, explosive, volatile, deliquescent, or unpleasant to use.

- A compound must not undergo internal reaction or absorb CO_2 from the air.

- A compound must be stable to radiation and with time, inert, commercially available and moderate in cost.

Compounds with melting point below 75°C were excluded from the list of solid compounds for use as additives in polymers and resins. Solids of lower M.P could be used either in wax-based substitutes or, if soluble in water, for the formulation of liquid substitutes. Liquid compounds with boiling point (B.P) below 65°C were excluded.

Advice was sought on the toxicity and carcinogenic properties of the selected compounds and those which had dubious properties were rejected (H.M.S.O, 1967; THE CHESTER BEATTY RESEARCH INSTITUTE, 1966; BROWNING, 1965). The compounds in the library were divided into five groups, namely, a) INORGANIC SOLIDS, b) ORGANIC SOLIDS, c) POLYMERS AND RESINS, d) LIQUIDS and e) SPECIAL AGENTS. High purity chemicals such as "Analar" grades were always used when these were available.

The list of inorganic compounds was compiled from the HANDBOOK OF CHEMISTRY AND PHYSICS (1971); the catalogue of HOPKINS AND WILLIAMS and BDH chemicals were consulted to ensure availability and acceptable cost (not more than £1 for 1g).

The above references together with the catalogues "ORGANIC CHEMICALS" (EASTMAN KODAK. Co), were the main sources for the organic compounds in the library. The compound library given by WHITE (1974) was also considered. The group of polymers and resins in that library, compiled from commercial literature and advice of experts in the field, was used in the new library with only few additions. The majority of the rest of WHITE's compound library, however, was rejected either on cost grounds or because they included elements not present in the real tissues.

A listing of the most useful compounds in the new library is given in Appendix 6. For convenience, this tabulation was generated via a computer-linked microfilm plotter.

The four epoxy resin systems CB1, CB2, CB3 and CB4 and the phenolic microspheres (PMS) used, have been described by WHITE et al., (1977). The nature of some of the special agents used in this work, however, require some comment.

The production of solid lung substitutes was made possible by the use of the liquid foaming agent DC1107 and the surfactant DC200/50.

DC1107 is a polymethyl hydrosilane cross-linking agent of the following syntactic formula:

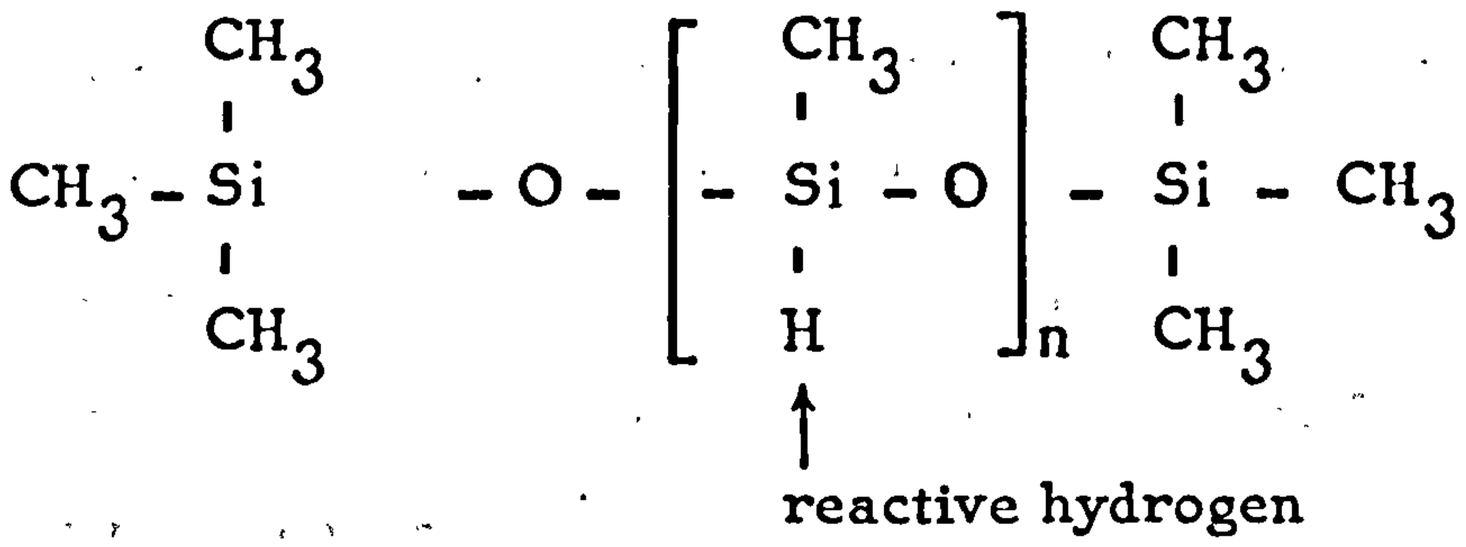

where n = 40-45 typically. The hydrosilane groups (= Si - H) react with acids, bases and amines liberating hydrogen. The formula of DC200/50 is similar, except that the reactive hydrogen is replaced by a methyl group ($-CH_3$).

Suppliers of the above products are listed in Table 2 of Appendix 5.

Water loaded polyester resins were not used because their composition is not stable, due to water loss.

The gelling agent of choice for the manufacture of gel substitutes was gelatine because its composition and density is very close to that of protein, a tissue component. Although gel substitutes usually find short-term applications, the addition of bacteriostatic agents (e.g. sodium azide) in tracer quantities, preserves them for longer periods. Other gelling agents like Agar (a sulfated polysaccaride), Guar (another polysaccaride gelled with borax) etc., were not used because of large uncertainties in their elemental composition.

2.4 ELEMENTAL COMPOSITION OF THE SIMULATED HUMAN BODY TISSUES

Recent publications on the elemental composition of biological tissues have indicated that there are large differences in the elemental contents of the tissues found in the human body. The composition of each tissue is subject to changes from the day to day metabolism and also variations with ageing. Liver, for example, undergoes rapid changes in size and protein metabolism (glycogen in particular). The composition of bone also varies both within and between various age groups. The relative density and the calcium content of young bone are less than that of mature bone but with further ageing these change again. Values for the calcium : phosphorus molar ratio and for the relative density of bone, varying from 1.37 to 1.80 and from 1.6 to 2.04 respectively, have been found in the literature. These differences are of significance for particulate radiation dosimetry, especia lly with neutrons.

Data for the most important human tissues and organs simulated in this work, were obtained from ICRU (NBS, 1964), KIM (1974), WOODARD (1964), and from the ICRP Reference Man document (ICRP, 1975). This document provides elemental data obtained from many sources on 81 organs, tissues and tissue components; it also gives their relative densities as well as their water : fat : protein contents. The ICRP task group had often, but not always, selected the average or the median of the available measurements. The percentages by weight of the constituents of some of the tissues given, however, total either more or less than 100%. In such cases either the oxygen or the carbon content was modified to bring the total to 100%.

The above correction is justified since oxygen and carbon are the most prevalent elements and a small subtraction or addition to them will cause the least overall change in density and absorbed dose.

The formula for "inner bone" was calculated from data supplied by SPIERS (WHITE, 1974); it is based on the ratio 22.4% hard bone to 77.6% red marrow, i.e. the average ratio of hard bone to red marrow in trabecular bone structures (percentages by weight).

In the case of breast tissue, a search for reliable formula showed that there are large variations in the composition of breast with age and subject. Apparently, breast tissue varies between the extremes of fat and muscle. In order to resolve the dilemma, WHITE (1974) considered a formula based on 50% FAT-50% WATER by weight and formulated solid substitutes useful for low energy photon mammography measurements. A formula for breast tissue, however, should contain, at the very least, nitrogen, phosphorus and sodium. Bearing this and the great variability of breast tissue in mind, it was decided to consider three different groups, namely:

AV.BR.I for young age : 25% FAT-75% MUSCLE

AV.BR.II for middle age : 50% FAT-50% MUSCLE

AV.BR.III for old age : 75% FAT-25% MUSCLE

The elemental composition of all the simulated human body tissues is given in Appendix 3.

2.5 THE RANGE OF TISSUE SUBSTITUTES DEVELOPED DURING THIS STUDY

Five groups of tissue substitutes were produced, namely, substitutes for Principal soft tissues (adipose, blood, muscle), Principal skeletal tissues (hard bone, inner bone, red marrow), Body organs (brain, kidney, liver, lung, thyroid), Average tissues (average breast, total soft tissue, total skeleton), and Tissue components (fat, protein, water). Tables 2-I to 2-V(pp 65-75) give the constituents of these substitutes, together with the percentage weights bracketed after each compound. The compounds for trace elements in each group of substitutes are given immediately after the first substitute of the group. Although the presence of trace elements was not found to affect the results of the depth dose measurements significantly, they are given for completeness. If a substitute was formulated to be used without trace elements in it, this will be indicated with the words "no traces".

About 60% of all substitutes given in this chapter are TISSUE EQUIVALENT and the remaining are QUASI-EQUIVALENT, except for the solid water substitute WT/SR1 described in section 2.5E. The elemental composition of these materials is given in Appendix 3, with that of the corresponding real tissues. Nearly all have been manufactured. Those formulae for which no relative density is given have not been manufactured but, from the experience gained in this study, they are considered to be practically feasible.

2.5A PRINCIPAL SOFT TISSUES

Sixteen new substitutes were produced to simulate three principal soft tissues, i.e. 4 for adipose, 3 for blood and 9 for muscle; they are grouped in Table 2-I (see pages 65-75 for Tables 2-I to 2-V).

The very low nitrogen and high hydrogen content of adipose tissue excluded the use of the epoxy systems CB1, CB2 and CB4 in the formulation of solid substitutes for adipose. The epoxy system CB3, however, proved to be particularly good and, in fact, it was selected as an adipose substitute from a "single material" search of the complete compound library (AP/SF2). Similarly, Ethoxyethanol and the epoxy system CB2 were selected as "single component" liquid adipose (AP/L1) and solid blood (BL/SR1) substitutes respectively.

The attempt to produce two-component gel substitutes for muscle (i.e. water + gelatine) gave products in which some of the carbon was replaced by oxygen. The introduction of an alcohol as a third component (ethanol or propanol) resulted in gel substitutes for muscle, both elementally correct and not subject to bacterial infection. (MS/G1 and MS/G2).

2.5B PRINCIPAL SKELETAL TISSUES

Matching the low hydrogen and high calcium and phosphorus contents of hard bone presented serious problems both in the liquid and solid phase. Formulae for liquid substitutes simulating hard bone (cortical) are not given because all of them suffered from the problem of insolubility of the best additives. The most soluble phosphate compound found in the compound library is di-potassium hydrogen phosphate; a solution of 160 grams of this compound per 100 ml of water is the best liquid substitute that could be manufactured to simulate hard bone. The K : P ratio is close to the Ca : P ratio

in bone (about 1.67), and the measured relative density of such a solution was found to be 1.68. This substitute was first proposed by WITT and CAMERON (1975), who used it as a general bone standard for the calibration and intercomparison of the systems they developed for measuring the bone mineral in vivo. This solution is stable at room temperature (20°C). Attempts to improve it by adding other soluble salts to satisfy the requirements for nitrogen, magnesium, sodium and sulphur, resulted in an oversaturated solution which, in less than a day, precipitated part of its solutes.

For solid bone substitutes, the low hydrogen content meant that the percentage of base material (epoxy resin system) that could be used was lower than needed to hold the calculated quantity of fillers, and many formulations representing elementally correct bone substitutes, gave a dough rather than a pourable mixture and had to be rejected. By relaxing the limit for the hydrogen requirement, the formulae of nine hard bone substitutes were produced with hydrogen up to 4.9% by weight and relative densities ranging from 1.58 to 1.82. The formulae of these substitutes are given in Table 2-II.

The use of $Ca(NO_3)_2$ in HB/SR1 seems to catalyse the reaction between resin and hardener and the curing process is completed in about one hour. This should be noted if this formula is used. HB/SF3 is very viscous but is pourable; HB/SR6 and HB/SR9 are so viscous that one should be careful when casting because the possibility of trapping air is high. The remaining hard bone substitutes are moderate in viscosity and present no problem in their manufacture; HB/SR4 seems to be the best from this point of view and samples of it were used in most of the experimental work described in Chapter 5.

The ICRU formula for hard bone (with 6.4% by weight hydrogen) was easier to simulate.

Table 2-II also gives the formulae for three inner bone and nine red marrow substitutes. Inner bone substitutes need only be covered with an outer layer of hard bone to simulate real bones on a macroscopic scale.

2.5C VARIOUS BODY ORGANS

The formulation and manufacture of tissue substitutes for various body organs was considered important for the construction of complete body phantoms for use in clinical dosimetry and other applications. Eleven substitutes were formulated for brain, two for kidney; two for liver, three for lung and three for thyroid (Table 2-III). All the liquid substitutes in this group are "TISSUE EQUIVALENT" while the solids are "QUASI EQUIVALENT".

The epoxy system CB2, on its own, was found to be acceptable for the simulation of kidney and liver in elemental composition but its relative density is higher than that of real kidney and liver (1.10 as compared to 1.05 and 1.07 respectively).

2.5D AVERAGE TISSUES

Table 2-IV shows the formulae of materials designed to simulate average tissues like "average breast", "total soft tissue" and "total skeleton".

The four liquid substitutes coded AV.BR* were produced to simulate an average breast formula based on 50% FAT-50% WATER by weight. The formulation of the solid substitutes of average breast, however, was based on the three combinations of FAT-MUSCLE as

described in section 2.4. Four out of five of these substitutes are solid flexible, with the epoxy resin system CB3 as base material. CB3, on its own, was selected as a substitute of average breast (50% FAT-50% MUSCLE) and is coded as AV.BRII/SF3. Its relative density is 1.02 instead of the required 0.99.

The human body can be considered as a combination of "total soft tissue" and "total skeleton"; consequently a number of substitutes were formulated for each. The last two substitutes for total skeleton (T.SK/L3 and T.SK/L4) are not clear liquid solutions but suspensions of calcium orthophosphate in a solution which contains the remaining components.

2.5E TISSUE COMPONENTS

The new ICRP document "Reference Man" shows that each tissue or organ is composed of WATER + FAT + PROTEIN + TRACE ELEMENTS. If it were possible to formulate protein and fat substitutes miscible with water, then by mixing the three under the right proportions one would be able to produce substitutes for any tissue or organ.

Gelatine was found to have elemental composition and relative density very close to protein; furthermore it is soluble in warm water (70-80°C). Unfortunately none of the formulated liquid substitutes for fat, is miscible with water. The use of gelatine as gelling agent, however, enables the formulation of gel systems which closely simulate real tissues (e.g. MS/G1, RM/G1, IB/G1).

The need for a solid material with the same photon attenuation characteristics as water, for various applications in diagnostic radiology, led to the formulation of an epoxy resin based

substitute for water (WT/SR1). This substitute was formulated using the "basic data method".

A critical theoretical evaluation was carried out for all the new substitutes and for most of those developed in the past. Some of them were selected and tested experimentally in order to verify the accuracy with which they simulate the corresponding real tissues. This will be discussed in Chapter 4 where a list of the recommended substitutes, new and old, will also be given.

TABLE 2-I SUBSTITUTES FOR PRINCIPAL SOFT TISSUES

No	Code	Constituents and percentage weights	Relative density	
			Measured	Calculated
		(i) ADIPOSE		
1	AP/SF1	Epoxy CB3(49.90); Polyethylene(38.47); Glucose(8.74); PMS(2.62); Traces(0.27). Compounds for traces: Na_2SO_4(0.156); S(0.037); K_2HPO_4(0.071); $CaHPO_4$(0.007)	0.92	0.92
2	AP/SF2	Epoxy CB3(100) - no traces	1.02	1.02
3	AP/L1	Ethoxyethanol (100) - no traces	0.93	0.93
4	AP/L2	H_2O(49.23); Traces(0.21); Propanol(48.28); Urea(1.71); H_3PO_4(2.73) Compounds for traces: NaCl(0.13); KCl(0.06); $CaCl_2$(0.006); $MgCl_2$(0.008).	0.92	0.93
		(ii) BLOOD		
1	BL/SR1	Epoxy CB2(100) - no traces	1.10	1.10
2	BL/L1	H_2O(70.96); Traces(1.44); Urea(5.99); Glycerol(9.02); Acetic acid(12.65). Compounds for traces: NaCl(0.45); $KHSO_4$(0.48); NH_4CNS(0.20); $Fe(NO_3)_3$(0.19); H_3PO_4(0.098).	1.08	1.07
3	BL/L2	H_2O(71.00); Traces(1.44); Urea(5.99); Ethanediol(6.08); Acetic acid(15.59).	1.06	1.05
		(iii) MUSCLE		
1	MS/SR1	Epoxy CB1(62.22); Polyethylene(28.58); Polyvinyl Acetate(7.74); Traces(1.635) Compounds for traces: K_2HPO_4(0.87); S(0.50); Na_2HPO_4(0.22); MgO(0.03); $CaCO_3$(0.02).	1.05	1.06
2	MS/SR2	Epoxy CB2(65.0); Acrylics(9.22); Urea(3.28); Polyethylene(21.06); Traces(1.635)	1.06	1.07

SR = solid rigid, SF = solid flexible, L = liquid, G = gel

PMS = phenolic microspheres

TABLE 2-I cont....

No	Code	Constituents and percentage weights	Relative density	
			Measured	Calculated
		(iii) MUSCLE cont....		
3	MS/SF3	Epoxy CB3(58.00); Acrylics(26.14); Polyethylene(8.88); Urea(5.51); Traces(1.635)	1.06	1.06
4	MS/SR4	Epoxy CB4(69.30); Polyethylene(25.51); PMS(0.70); Traces(1.635)	1.06	1.05
5	MS/SR5	Epoxy CB1(62.10); Polypropylene(32.36) Carbon(3.95); Traces(1.635)	1.07	1.07
6	MS/G1	H_2O(73.90); Traces(1.41); Gelatine(19.42); Ethanol(5.27) Compounds for traces: K_2HPO_4(0.87); Na.Cl(0.15); $NH_4H_2PO_4$(0.12); $Mg(NO_3)_2$(0.16); NaH_2PO_4(0.07) $Ca(NO_3)_2$(0.04)	1.06	1.04
7	MS/G2	H_2O(74.60); Traces(1.41); Urea(1.30); Gelatine(14.11); Propanol (6.68)	1.05	1.03
8	MS/L1	H_2O(62.53); Traces(2.43); Urea(7.43); Ethanediol(27.18); Acetic Acid(0.43) Compounds for traces: NaCl(0.13); $NaNO_3$(0.07); $KHSO_4$(1.36); H_3PO_4(0.63); $Ca(NO_3)_2$(0.03); $Mg(NO_3)_2 \cdot 6H_2O$(0.20)	1.07	1.07
9	MS/L1A	H_2O(62.53); no traces; Urea(7.50) Ethanediol(27.91)	1.06	1.06

TABLE 2-II SUBSTITUTES FOR PRINCIPAL SKELETAL TISSUES

No	Code	Constituents and Percentage weights	Relative density	
			Measured	Calculated
		(i) HARD BONE		
1	HB/SR1	Epoxy CB1(50.00); $Ca(NO_3)_2$(14.86); CaO(25.43); P(10.2); Traces(1.22)	1.75	1.70
		Compounds for trace elements: $MgSO_4$(1.04); Na_2SO_4(0.18)		
2	HB/SR2	Epoxy CB1(44.98); $CaHPO_4$(43.93); CaO(9.86); Traces(1.22)	1.66	1.60
3	HB/SF3	Epoxy CB3(35.78); Urea(7.34); $CaHPO_4$(43.91); CaO(7.44); $CaCO_3$(4.31); Traces(1.22)	1.69	1.60
4	HB/SR4	Epoxy CB2(39.21); Urea(5.77); CaO(9.86); $CaHPO_4$(43.93); Traces(1.22)	1.67	1.60
5	HB/SR5	Epoxy CB2(43.32); $CaHPO_4$(33.29); P(2.42); Urea(5.50); CaO(14.24); Traces(1.22)	1.60	1.55
6	HB/SR6	Epoxy CB4(47.91); $Ca_3(PO4)_2$(50.05); CaO(0.82); Traces(1.22)	1.76	1.71
7	HB/SR7	Epoxy CB4(52.54); CaO(21.48); P(7.61); $Ca_3(PO4)_2$(11.93); Urea(5.21); Traces(1.22)	1.58	1.55
8	HB/SR8	Epoxy CB4(48.97); $CaHPO_4$(11.83); CaO(26.19); P(6.37); Traces(1.22)	1.64	1.59
9	HB/SR9	Epoxy CB4(38.9); $CaHPO_4$(43.93); Urea(6.08); CaO(9.86); Traces(1.22)	1.82	1.74
10	HB/ POWDER 1	Calcium glycerophosphate(45.09); $Ca_3(PO4)_2$(22.67); $Ca(NO_3)_2$(23.25); Polyethylene(8.61); Traces(1.22)	–	1.77

SR = solid rigid, SF = solid flexible, L = liquid, G = gel

TABLE 2-II cont....

No	Code	Constituents and Percentage weights	Relative density	
			Measured	Calculated
		(i) HARD BONE cont....		
11	HB/ POWDER 2	$Ca_3(PO4)_2$(51,07); $CaCO_3$(5.02); Urea(8.51); Polyethylene(7.20); Traces(1.22)	-	1.96
12	HB/ PASTE	Glycerol(34.15); $CaCO_3$(4.05); Urea(7.92) $Ca_3(PO4)_2$(51.07); $CaSO_4$(1.35) Traces(1.22)	-	1.88
		ICRU BONE		
13	HB/SF1	Epoxy CB3(54.30); $Ca_3(PO4)_2$(34.73); C(4.32); CaO(1.725); Urea(3.93)	1.46	1.42
14	HB/G1	H_2O(34.33); Glycerol(15.70); K_2HPO_4(31.94); NaH_2PO_4(12.80); Gelatine(15.17)	-	1.40
		(ii) INNER BONE		
1	IB/SR1	Epoxy CB2(76.59); Polyethylene(8.44) $Ca_3(PO4)_2$(13.13); $NaNO_3$(0.243)	1.15	1.20
2	IB/G1	H_2O(68.98); Glucose(3.72); K_2HPO_4(10.80); $NaNO_3$(0.08); $Mg(NO_3)_2$(0.51); $KHSO_4$(0.47) Gelatine(14.05)	-	1.13
3	IB/L1	H_2O(36.64); Urea(5.45); Ethanediol(41.82) K_2HPO4(11.107); H_3PO4(1.62); $NaNO_3$(0.24)	1.14	1.18
		(iii) RED MARROW		
1	RM/SF1	Epoxy CB3(69.08); Polyvinyl Acetate(25.42); Polypropylene(1.92); Urea(2.27); PMS(0.8); Traces(0.05) Compounds for traces: K_2HPO_4(0.16); K_2SO_4(0.18) Na_2SO_4(0.02); $MgSO_4$(0.01); S(0.10)	1.04	1.03

TABLE 2-II cont....

No	Code	Constituents and percentage weights	Relative density	
			Measured	Calculated
		(iii) RED MARROW cont....		
2	RM/SR2	Epoxy CB2(65.13); Polyethylene(27.10); C(6.52); PMS(0.75); Traces (0.50)	1.03	1.05
3	RM/SF3	Epoxy CB3(59.4); Polyethylene(8.28); Urea(2.63); Polyvinyl Acetate(28.88) PMS(0.6); Traces(0.50)	1.03	1.03
4	RM/SR4	Epoxy CB4(63.7); Polyethylene(34.54) $NH_4 NO_3$(0.74); PMS(0.57); Traces(0.50)	1.03	1.03
5	RM/L1	H_2O(12.14); Glycerol(8.08); Urea(4.385) Pentanediol(75.33); Traces(1.34) Compounds for traces: Na Cl (0.20); K Cl(0.11); $K NO_3$(0.30); H_3PO_4(0.09) $(NH_4)_2 SO_4$(0.634)	-	1.01
6	RM/L2	H_2O(43.46); Ethanediol(51.21); Urea(4.38); Traces(1.34)	1.05	1.07
7	RM/L3	H_2O(64.14); Glycerol(34.42); Urea(4.38); Traces(1.34)	1.04	1.08
8	RM/G1	H_2O(79.10); Glucose(8.04); Traces(1.34) Gelatine (12.15)	1.07	1.06
9	RM/G2	H_2O(7.51); Glycerol(24.28); Pentanediol(55.19); Traces(1.34); Gelatine(12.25)	-	1.08

PMS = Phenolic microspheres

TABLE 2-III VARIOUS BODY ORGANS

No	Code	Constituents and percentage weights	Relative density	
			Measured	Calculated
1	BRN/SR1	(i) BRAIN Epoxy CB2(42.32); Polyethylene(33.23); Acrylics(22.05); PMS(0.60); Traces(1.82) Compounds for trace elements: NaH_2PO_4(0.93); K_2HPO_4(0.67); S(0.17); MgO(0.02); $CaCO_3$(0.02)	1.01	1.03
2	BRN/SR2	Epoxy CB2(42.32); Polyethylene(33.82) Acrylics(27.05); Traces(1.82)	1.04	1.06
3	BRN/SF3	Epoxy CB3(70.00); Polyethylene(8.38); Acrylics(19.85); Traces(1.82)	1.03	1.05
4	BRN/SF4	Epoxy CB3(70.00); Polyethylene(8.03); Acrylics(19.86); PMS(0.30); Traces(1.82)	1.00	1.03
5	BRN/L1	H_2O(67.60); Traces(2.27); Urea(2.77); Butanediol (27.36); Compounds for trace elements: $KHSO_4$(0.16); Na_2SO_4(0.56); KCl(0.48); H_3PO_4(1.07)	1.03	1.02
6	BRN/L2	H_2O(69.58); Traces(2.27); Urea(2.77); Pentanediol(25.38)	1.02	1.01
7	BRN/L3	H_2O(56.87); Traces(2.27); Urea(2.77); Ethanediol(24.44); Methanol(13.65)	1.03	1.00
8	BRN/L4	H_2O(60.70); Traces(2.27); Urea(2.77); Ethanol(9.81); Ethanediol(24.45)	1.04	1.01
9	BRN/L5	H_2O(55.11); Traces(2.27); Urea(2.77); Glycerol(18.15); Methanol(21.70)	1.03	1.00
10	BRN/L6	H_2O(62.45); Traces(2.27); Urea(2.77); Ethanol(14.35); Glycerol(18.15)	1.04	1.01
11	BRN/L7	H_2O(69.95); Traces(2.27); Urea(2.77); Glycerol(1.96); Propanol(23.05)	1.00	0.98

SR = solid rigid, SF = solid flexible, L = liquid, G = gel, PMS = phenolic microspheres

TABLE 2-III cont....

No	Code	Constituents and percentage weights	Relative density	
			Measured	Calculated
		(ii) KIDNEY		
1	KD/L1	H_2O(63.60); NaCl(0.47); K_2HPO_4(0.87); Urea(5.87); Ethanediol(29.29)	1.05	1.04
2	KD/SR1	Epoxy CB2(100) - no traces	1.10	1.10
		(iii) LIVER		
1	LV/SR1	Epoxy CB2(100) - no traces	1.10	1.10
2	LV/L1	H_2O(64.18); $KHSO_4$(1.02); NaCl(0.29) Urea(6.06); Ethanol(15.87); Glycerol(12.57)	1.06	1.03
		(iv) LUNG		
1	LN/SR1	Epoxy CB1(64.39); Polyethylene(26.50); Polyvinyl Acetate(6.72); Traces(1.09); Foaming DC1107(1.00); Surfactant DC200/50(0.30) Compounds for traces: K_2SO_4(0.42); S(0.14) Na_2HPO_4(0.50); MgO(0.02); $CaCO_3$(0.02)	0.30	0.30
2	LN/SF3	Epoxy CB3(58.00); Acrylics(33.65); Urea(4.00); Traces(1.09); DC1107(1.0); DC200/50(0.30)	0.29	0.30
3	LN/SR4	Epoxy CB4(63.51); Polyethylene(30.56); Traces(1.09); Urea(2.00); DC1107(1.0); DC200/50(0.3)	0.29	0.30

TABLE 2-III cont....

No	Code	Constituents and percentage weights	Relative density	
			Measured	Calculated
		(v) THYROID		
1	TH/L1	H_2O(62.90); NaI(0.90); NaCl(0.23); K_2HPO_4(0.44); Urea(4.71); Glycerol(31.00)	1.11	1.14
2	TH/L2	H_2O(62.10); NaI(0.90); NaCl(0.23); K_2HPO_4(0.44); Acetic Acid(11.46); Urea(4.71); Ethanediol(20.58)	1.08	1.08
3	TH/L3	H_2O(62.10); NaI(0.90); NaCl(0.23); Glucose(11.46); Urea(4.71); Ethanediol(20.58)	1.14	1.13

TABLE 2-IV AVERAGE TISSUES

No	Code	Constituents and percentage weights	Relative density	
			Measured	Calculated
1	AV.BR.I/ SF3	(i) AVERAGE BREAST Epoxy CB3(70.80); Acrylics(23.09); Urea(3.23); PMS(1.85); Traces(1.02) Compounds for traces: Na_2HPO_4(0.16); K_2HPO_4(0.65); S(0.18); $CaCO_3$(0.01); MgO(0.02)	1.00	1.01
2	AV.BR.II/ SR1	Epoxy CB4(61.50); Polyethylene(36.24); PMS(1.60); Traces(0.56) Compounds for traces: Na_2HPO_4(0.11); K_2HPO_4(0.43); MgO(0.01); $CaCO_3$(0.01)	0.99	0.98
3	AV.BR.II/ SF2	Epoxy CB3(68.61); Urea(1.34); Acrylics(14.11); Polypropylene(14.23); Phenolic microspheres(0.89); Traces(1.63)	0.99	0.99
4	AV.BR.II/ SF3	Epoxy CB3(100); - no traces	1.02	1.02
5	AV.BR.III/ SF1	Epoxy CB3(54.70); Glucose(10.85); Polyehylene(31.93); PMS(2.11); Traces(0.40) Compounds for traces: Na_2HPO_4(0.05); K_2HPO_4(0.22); MgO(0.01); S(0.12)	0.95	0.94
		* 50% FAT-50% WATER		
6	AV.BR*/ L1	H_2O(27.68); Ethoxyethanol(72.32)	0.97	0,96
7	AV.BR*/ L2	H_2O(32.43); Ethanol(20.72); Pentanediol(46.91)	0.96	0.94
8	AV.BR*/ L3	H_2O(32.43); Propanol(27.03); Butanediol(40.54)	0.96	0.95
9	AV.BR*/ L4	H_2O(29.72); Propanol(49.55); Glycerol(20.72)	0.93	0.93

TABLE 2-IV cont....

No	Code	Constituents and percentage weights	Relative density	
			Measured	Calculated
		(ii) TOTAL SOFT TISSUE		
1	T.S.T/L1	H_2O(42.06); Traces(1.54); Urea(5.20); Ethanediol(39.97); Propanol(11.27) Compounds for traces: NaCl(0.21); $NaHSO_4$(0.13); $NH_4H_2PO_4$(0.48); KCNS(0.49); $Mg(NO_3)_2\ 6H_2O$(0.13); $Ca(NO_3)_2$(0.08)	1.05	1.03
2	T.S.T/L2	H_2O(43.27); Traces(1.54); Urea(5.20) Ethanol(20.38); Glycérol(29.65)	1.02	1.01
3	T.S.T/L3	H_2O(40.04); Traces(1.54); Urea(5.20) Ethanediol(39.96); Ethanol(12.96)	1.04	1.02
		(iii) TOTAL SKELETON		
1	T.SK/SR1	Epoxy CB2(64.79); Urea(1.29); $CaHPO_4$(24.45); $Ca_3(PO_4)_2$(7.29) Traces(2.15) Compounds for trace elements: KNO_3(0.38); $MgSO_4$(0.60); $NaNO_3$(1.17)	1.39	1.35
2	T.SK/SF2	Epoxy CB3(60.46); Urea(3.90); $CaHPO_4$(31.08); $CaCO_3$(2.39); Traces(2.17)	1.40	1.36
3	T.SK/SF3	Epoxy CB3(52.56); Urea(4.27); $CaHPO_4$(24.44); $Ca_3(PO_4)_2$(7.29); Acrylics(9.42); Traces(2.17)	1.36	1.33
4	T.SK/L1	H_2O(51.32); $(NH_4)_2HPO_4$(12.96); K_2HPO_4(22.27); Glucose(11.60)	1.36	1.32
5	T.SK/L2	H_2O(27.31); $(NH_4)_2HPO_4$(12.96); K_2HPO_4(22.27); Glycerol(35.61)	1.40	1.36
6	T.SK/L3	H_2O(55.39); $(NH_4)_2HPO_4$(7.83); NH_4NO_3(3.27); Glucose(6.19) $Ca_3(PO_4)_2$(25.86)	1.34	1.33

TABLE 2-IV cont....

No	Code	Constituents and percentage weights	Relative density	
			Measured	Calculated
7	T.SK/L4	(iii) TOTAL SKELETON cont.... H_2O(42.16); $(NH_4)_2HPO_4$(7.83); Urea(2.45); Glycerol(20.24); $Ca_3(PO_4)_2$(25.84)	1.36	1.35

TABLE 2-V TISSUE COMPONENTS

No	Code	Constituents and percentage weights	Relative density	
			Measured	Calculated
		(i) FAT		
1	FT/SF1	ELVAX 220(100)	0.92	0.93
2	FT/SR2	Paraffin wax(68.57); Polyvinyl acetate(31.57)	0.93	0.96
3	FT/SR3	Palmitic acid(62.44); Borneol(37.56)	0.91	0.88
4	FT/L1	Ethyl oleate(76.61); Cyclohexanol(24.39)	0.89	0.89
5	FT/L2	Glycerol triolate(100)	0.92	0.92
		(ii) PROTEIN		
1	PR/SR1	Gelatine(100)	1.28	1.28
		(iii) WATER		
1	WT/SR1	Epoxy CB4(80.44); $CaCO_3$(5.77); Polyethylene(10.00); PMS(3.79)	1.00	1.00

CHAPTER 3

MANUFACTURE AND QUALITY TESTING OF THE NEW TISSUE SUBSTITUTES

In this chapter the various methods used for manufacturing the new substitutes will be described first and then the methods used for testing their quality will be discussed. An account of some of the problems encountered during the manufacture of these materials will also be given.

3.1 MANUFACTURING PROCEDURES

(i) EPOXY RESIN BASED SUBSTITUTES

The manufacture of epoxy resin based tissue substitutes has been described in detail by WHITE (1974,1977) and the necessary equipment is shown in Figure 3.1. One important improvement in the

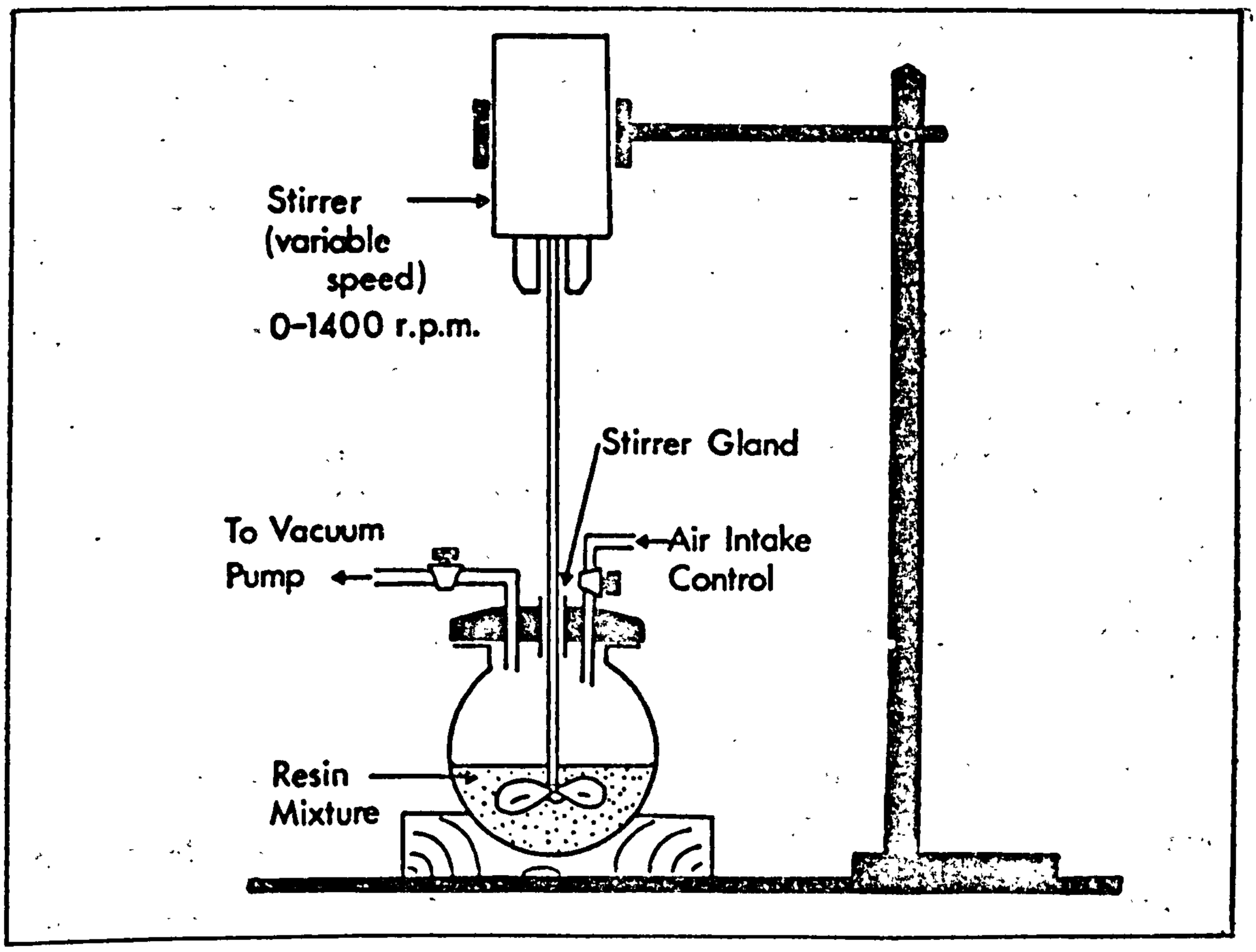

Figure 3.1 Equipment for manufacturing epoxy resin based substitutes

control of the homogeneity of the substitutes was achieved in the present work by the introduction and use of the vacuum degassing and pouring unit shown in Figure 3.2.

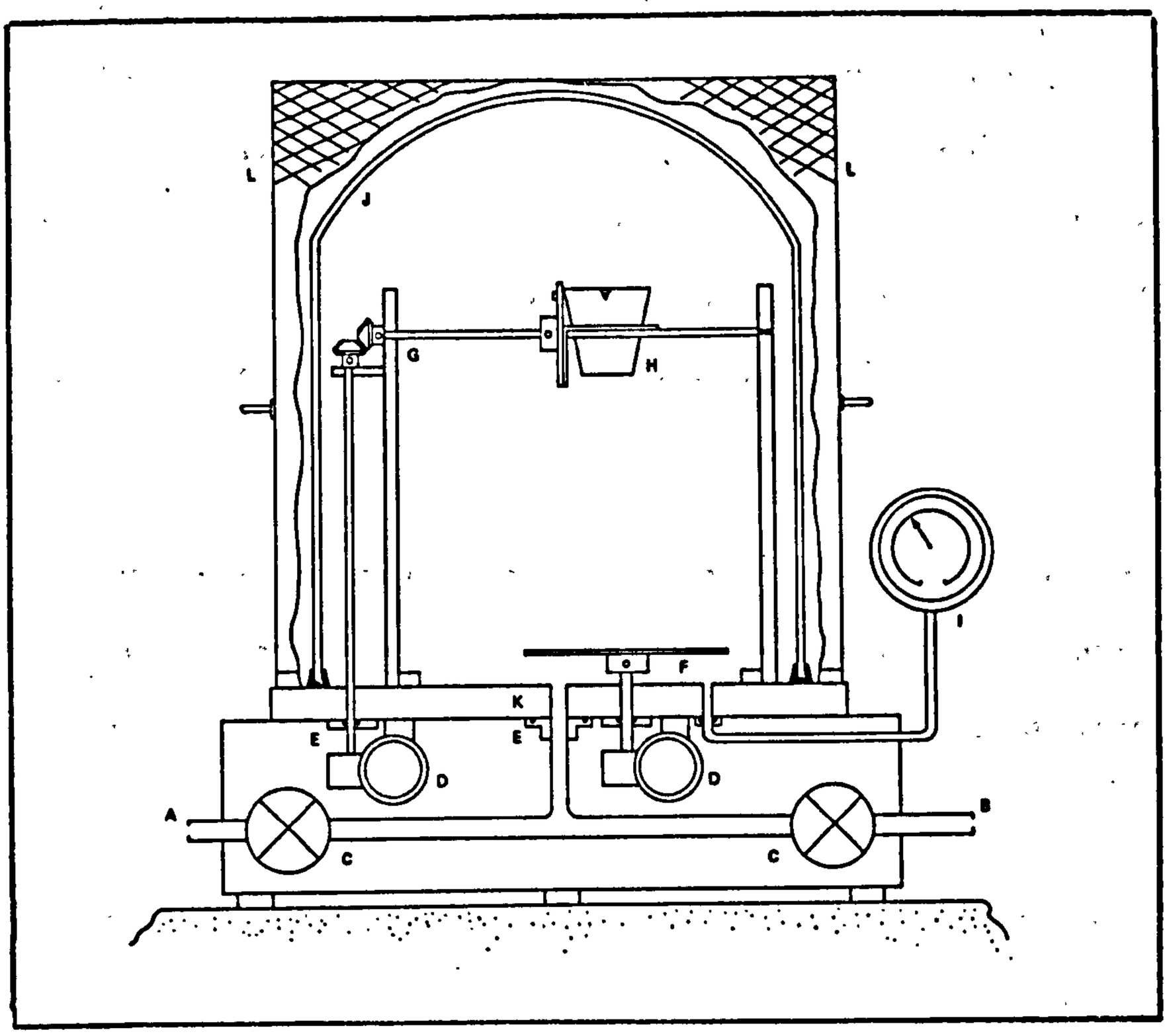

Figure 3.2 A vacuum degassing and pouring unit for use with synthetic resins

A : to vacuum pump
B : air intake
C : lever operated vacuum valves
D : handwheels for pouring gantry and rotating table
E : Vacuum seals
F : rotating table (23cm-diameter)
G : pouring gantry
H : dispenser
I : vacuum gauge
J : bell jar (acrylics 45cm-diam., with rubber seals)
K : steel base (2cm-thick)
L : Implosion shield

The necessary steps will be summarised here. Accurately measured quantities of resin, hardener and fillers are poured into a reaction vessel (500-5000 ml) and given a short manual mix. The system is then closed and the variable speed stirrer is used, with the blades of the rotor deep in the fluid to ensure a thorough mixing.

Once the desired mixing has been achieved, the blades are raised to just below the top surface of the fluid and the vacuum pump, to which the system is connected, is switched on while the stirring is continued. As the pressure is reduced the mixture rises in the vessel, due to trapped gases, but soon the rotating blades cause the foam to collapse (1-5 minutes depending on the quantity and the viscosity of the mixture). The blades are then lowered to their previous position and mixing under vacuum is continued for another 15-20 minutes; after that the stirrer is stopped and the vacuum released.

The mixture is now transferred into the dispenser of the vacuum degassing and pouring unit, the vacuum applied again (pressures below 5 mmHg achieved), and the mixture poured into the appropriate mould or tray.

If a vacuum pouring unit is not available, as the mixture is generally air-free, it could be cast into the mould under atmospheric pressure; in such case the mixture should be poured carefully at one point of the wall of the mould and left to flow slowly and fill the mould so that no air is trapped.

The time that these systems take to harden varies from 15 to 24 hours; if the sample, after it has hardened, is placed in an oven and heated to 80°C for 2-4 hours, the curing process is completed. When moulds of complex shape are used, it is better to leave the sample in the mould for at least 48 hours to avoid damaging it during demoulding.

As the curing of the resins is moderately exothermic the heat evolved could present problems when large objects have to be cast; these problems may be overcome by casting layers of suitably small thickness (2-3 cm) and allowing each layer to harden before pouring

the next. If a fan is used to blow air over the sample in the mould, the shrinkage, a function of the peak temperature attained, could be reduced to below 0.1% of the total volume. The use of moulds constructed of silicon rubber, PTFE, waxed aluminium, waxed perspex and melinex films, all with good "release" properties, ensures high quality end-products.

The viscosities of the base resin systems used $\left(\sim 25 \frac{Nt.sec}{m^2}\right)$ and their compatibility with some of the fillers were responsible for most of the problems encountered in the manufacture of solid substitutes. When the quantity of the filler was less than about 15% by weight, any difference between the densities of the filler and the resin resulted in separation, i.e. flotation or settlement accordingly. When the loading of fillers was high (e.g. hard bone), the removal of the air was rather difficult and this problem was overcome by using larger reaction vessels and so presenting a greater surface area for degassing; sometimes, however, adding the calculated quantity of fillers resulted in a dough rather than a pourable mixture. The quantity of a filler (additive) which can be dispersed into a known quantity of base material of a given viscosity, depends on the particle size of the filler; CB4, for example, can take up to 67% by weight of calcium carbonate OMYA BL (particle size about 50μm), but when "calcium carbonate BP" was used, with particle size of about 5μm, not more than 50% by weight could be used.

Compatibility of the resins and various fillers can also cause problems. It was noticed that nitrate compounds usually affected the curing process if used in quantities above 3-5% by weight. Ammonium nitrate, for example, inhibited the curing of the base material CB3; on the other hand, calcium nitrate seemed to catalyse the curing of CB1 and CB4; 10% of calcium nitrate in CB1 would cause the

mixture to harden in less than one hour thus making the handling of the system difficult.

Many formulae, otherwise ideal, were rejected on viscosity and compatibility grounds only.

3.1 (ii) LUNG SUBSTITUTES

The challenging problem of manufacturing solid, rigid or flexible, lung substitutes with correct elemental composition, porous nature and relative density if feasible, lead to the search for a suitable "blowing agent" which, when mixed with the epoxy resins would cause their volume to increase resulting in a foamed material of the required density.

Neither the concept of using shavings of muscle substitute turned on a lathe, nor that of using cellulose sponge soaked with sodium chloride solution (SHONKA and McGINLEY, 1976) was considered satisfactory. Cork was also rejected because of its unknown composition. The lung material suggested by ROGERS (1970) included components which, according to the author himself, are suspected carcinogenic (Moca) and others which may contain traces of volatile products known to be strong irritants to the mucous membranes and the skin (e.g. Adiprene).

The use of polyurethane foams was also avoided firstly because of the deleterious cyanate gases released during their manufacture, secondly because they must be contained and forced to overpack in strong metal moulds and thirdly because the maximum thickness that can be produced by this method is not more than 1 cm, if uniform density is to be achieved.

The aim was to stay away from too complex techniques which involve high temperatures and pressures. The solution to the problem was found when it was realised that one of the liquids sold by the firm "Dow Corning Ltd", namely DC1107, and used mainly in the paper industry, had such chemical composition that it could react with acids, bases, amines, etc., liberating hydrogen (see Section 2.3). The hydrosilane (≡Si -H) functional groups could, in theory, release up to 360 cm^3 of hydrogen gas per gram of liquid. This meant that approximately 1 cm^3 of this liquid would produce enough hydrogen to "blow" 100 grams of resin to more than 3 times its original volume, thus giving a bulk relative density below 0.3. By adjusting the amount of foaming agent it should be possible to produce lung substitutes of any required density.

In order to establish the relationship between the relative density of the lung phantom produced versus percentage of foaming agent, samples of muscle substitute MS/SR4 were made and different percentage by weight of DC1107 was added to each one of them (0.25%, 0.5%, 0.75%, etc). The experiment was repeated with the flexible muscle substitute MS/SF3. When the resulting lung substitutes cured, they were machined all to the same volume and weigh ed so that their relative density could be measured. Figure 3.3 summarises the results. With the rigid MS/SR4 the minimum relative density achieved was 0.25 corresponding to 0.95-1.0% by weight of foaming agent; with larger concentration of foaming agent, the sample originally rose and then collapsed.

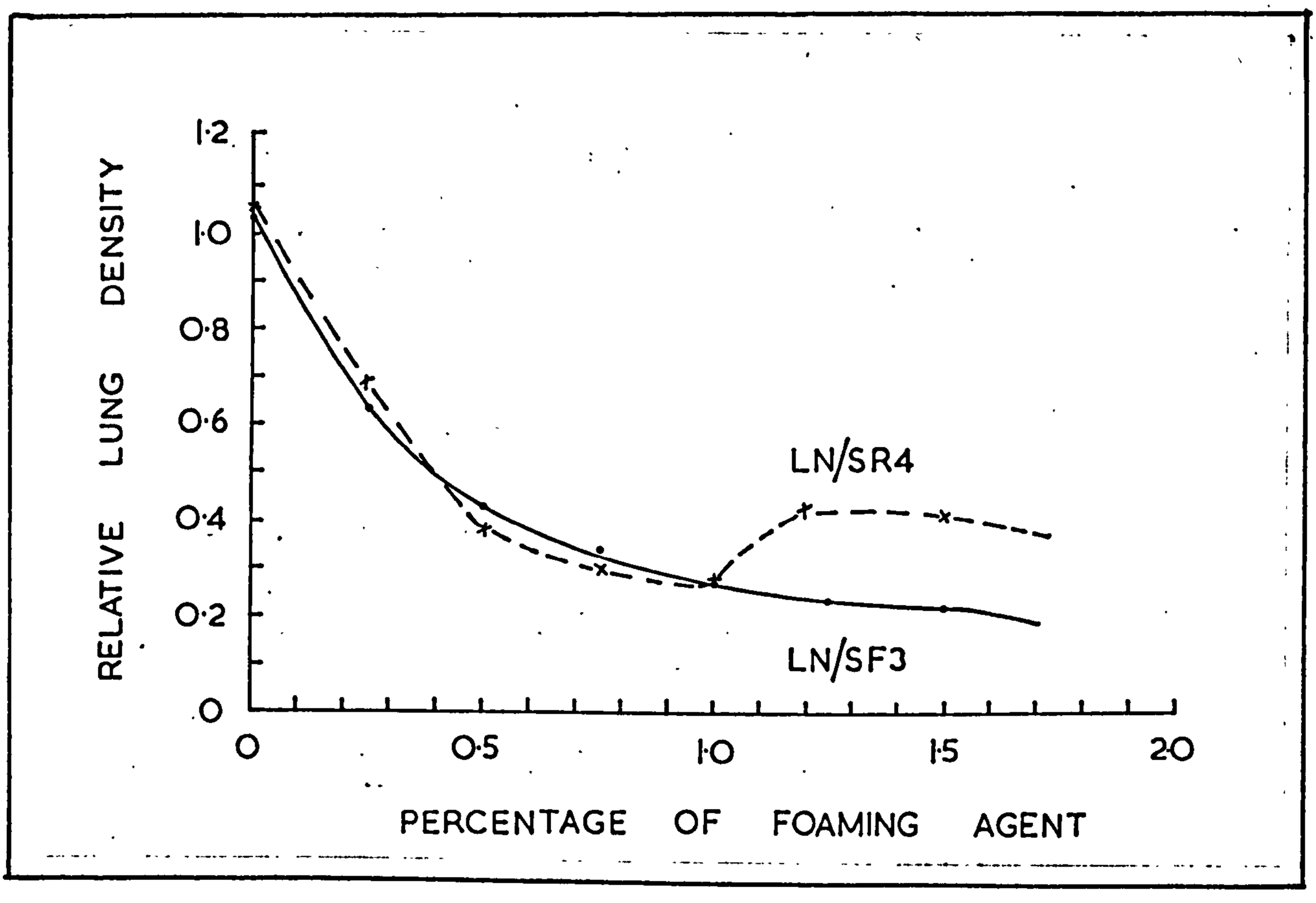

Figure 3.3 The lung substitute relative density as a function of the percentage (by weight) of foaming agent

The flexible product did not collapse even when the concentration of the foaming agent was increased up to 1.5% at which a relative density of 0.22 was obtained.

In order to control the size of the pores in the lung phantom, the liquid surfactant DC200/50 cs was found to be the best among several tested . The introduction of 0.25% by weight of surfactant was found to give acceptable results; if 1.0% by weight of foaming agent was used for example, the average diameter of the pores was about 2 mm.

The technique of manufacturing lung substitutes was standardised and is as follows:

First pre-calculated quantities of resin and fillers are thoroughly mixed in an open reaction vessel; then the surfactant is added and dispersed uniformly into the mixture by stirring at about 300-350 r.p.m; the stirrer is stopped when the mixing is considered thorough (5-10 minutes in all, depending on the quantity of the material) and the foaming agent is dispensed using a volumetric syringe or other precision dispenser (accuracy of $\pm 0.01 cm^3$ desirable). As the reaction starts as soon as the resin and the foaming agent come in contact, stirring is started immediately and continued for 30-40 sec. after which the mixture is poured into the open mould and left to rise under atmospheric pressure.

The time available after the foaming agent is added is limited and evacuation is precluded; consequently, a certain amount of air is always present, but its mass is so small that its effect on the chemical composition of the final product is negligible.

The lung substitutes that result from the above procedure can easily be moulded to any desired shape and they can be removed from the mould 48 hours later. The rigid samples can also be machined to any desired shape.

Using this procedure, reproducible results for densities over a wide range can be obtained. The question of uniformity of density when considering large volumes was also investigated; a 30 cm x 30 cm x 30 cm lung phantom (LN/SR4) with the desired relative density of 0.3 was made; when the density of several samples of it was measured, it was found to be 0.30 ± 0.02. This result was considered satisfactory.

Figures 7.1a and 7.1b show some lung phantom materials produced and used for measurements in this study.

3.1 (iii) LIQUIDS AND GELS

The mixing of several liquid and solid compounds to make various liquid and gel substitutes did not present any serious problems once the formulae of these substitutes were produced and a number of rules derived from experience were followed. The main difficulties encountered in this case resulted from the poor availability of solubility data for many compounds, especially organic liquids.

All too often, formulae which represented elementally correct substitutes had to be rejected because the addition of one component caused the precipitation of another compound. Consequently a certain amount of trial and error was inevitable.

In an attempt to keep the total vapour pressure (to which the volatility of a solution is proportional) below that of water, liquids with vapour pressure above 23.7 mmHg at 25°C, were avoided.

Water was preferred as base material for many reasons; it is one of the best solvents, readily available and cheap. Apart from this, various organs and tissues appear to be composed basically of fat, protein, water and trace elements. By mixing fat and protein substitutes with water in the desired proportions, substitutes for many organs or tissues can be made. A good step forward in this direction is due to the fact that gelatine, derived from bone by hydrolysis of collagen, has elemental composition close to that of protein. Unfortunately, attempts to formulate fat substitutes miscible with water failed; the use of gelatine, however, facilitated the formulation of many gel substitutes useful for short term applications.

When manufacturing liquid substitutes, the calculated quantity of water should always be measured into a beaker first. Then the inorganic compounds required to introduce the trace elements should be transferred and stirred into solution one by one in the order given in the formulae. It is important to wait until one is completely dissolved before the next is added; otherwise intermediate precipitates may be formed which, sometimes, are difficult to bring back into solution. Urea, used in most liquid tissue substitutes to satisfy the nitrogen requirement, is transferred next; finally any other organic liquids are transferred and stirred into solution.

In the case of gel substitutes, the water component with the trace elements already dissolved in it should be heated up to about 80°C and then the calculated quantity of gelatine added and dissolved; once a clear uniform solution is obtained it should be left to cool and approach room temperature, when the remaining organic components and a bacteriostatic agent should be added. The whole mixture can then be transferred into the reaction vessel of the mixing unit and the vacuum applied. Stirring under vacuum ensures the release of any air trapped in the mixture. The substitute can then be poured in polythene bags heat-sealed and left to gel before use. Figure 7.2 shows some of the liquid and gel tissue substitutes produced and used in this work.

3.2 SOME PHYSICAL INVESTIGATIONS FOR QUALITY TESTING

(i) RELATIVE DENSITY DETERMINATIONS

Relative density measurements were performed on the manufactured substitutes; these results are given with the calculated values in the Tables 2-I to 2-V. The calculations of relative density were made assuming that the volumes of pure substances are additive both in solid and in liquid phase. This is not always correct, especially in the liquid phase, because of ionic and molecular interactions; "partial solution density" data, however, are sparse.

Samples of each of the solid substitutes were accurately machined into cubes or parallelepipeds of known dimensions and the relative density was measured by a direct determination of mass and volume; the estimated error of measurement was 0.5%. The calculated values agreed with the measured ones to within 1% except in the case of the bone substitutes where disagreement up to 5% was observed. Samples of these bone substitutes were manufactured many times both in small quantities (100-200 g) and larger quantities (1-2 kg) and the results were reproducible indicating that the disagreement was not due to dispensing errors. It is likely that the density of the various grades of calcium compounds used was not the same as that quoted in the literature.

In the cases of liquid and gel substitutes, a 40 ml Hubbard Density Bottle was employed and occasionally the measurement was repeated with a 100 ml volumetric flask. The difference between calculated and measured density values here was about 2%. Most of this discrepancy is probably accounted for by the fact that the density of each component "in solution" is not the same as that of the pure substance which is found in the literature and was used in the calculations.

3.2(ii) HOMOGENEITY TESTS

The homogeneity of the manufactured solid substitutes was investigated mainly by using conventional radiography. Xeroradiography, end-of-range proton radiography and computerised axial tomography were used only in a few occasions. The end-of-range proton radiography proved to be superior to all the other methods for indicating air volumes within the sample. (KOEHLER, 1968, STEWART and KOEHLER, 1974).

Although most of the polymer fillers and the phenolic microspheres used were very fine powders with particle size of the order of 100 μm or less, some of the inorganic compounds used to introduce trace elements had to be ground and sieved; sieving to below 200 μm, however, proved to be very time consuming and as the samples produced were not to be used in making test objects for diagnostic purposes, except for two occasions described in Chapter 7, sieving the fillers to 200 μm was considered acceptable.

All the solid substitutes used in measurements during this work were tested radiographically, using 25-60 kVp X-rays. If bubbles of trapped air or pockets of undispersed high density filler were visible on a radiograph, the corresponding sample was rejected; air pockets of less than 50 μm, however, would not have been detected by this technique, unless end-of-range proton radiography was used. If flotation or precipitation of a filler was suspected in a sample, a radiograph was taken and scanned on a densitometer; if the variation in optical density was more than 5%, the sample was rejected.

A critical evaluation of the "tissue equivalence" of the manufactured tissue substitutes was considered to be very important and this is discussed in the next chapter.

CHAPTER 4

THEORETICAL AND EXPERIMENTAL EVALUATION OF THE VARIOUS TISSUE SUBSTITUTES

4.1 THEORETICAL EVALUATION

All the new tissue substitutes and most of those developed in the past have been evaluated theoretically by comparing the following radiation characteristics with similar data for the corresponding real tissues:

Mass stopping powers for protons.

Kerma factors.

Electron mass stopping powers and mass angular scattering powers.

Mass attenuation and energy absorption coefficients.

The recommended substitutes for each type of tissue and the calculated properties of some of them will be presented after a brief description of the computer programs developed for this theoretical evaluation.

4.1(i) COMPUTER PROGRAMS DEVELOPED DURING THIS STUDY

Three programs were developed during this study, namely ELISTB, PROTON and KERMAF. These programs were written in Fortran IV and run on the CDC computers of the University of London Computer Centre (U.L.C.C).

The program ELISTB is used to calculate the elemental composition (in terms of percentages by weight, w/o) and the relative density (SG) of any mixture of compounds, provided the formulae or elemental composition, the proportion by weight and the densities of these compounds are known. Table 4-I shows an example of the output of ELISTB, obtained in the form of microfilm.

TABLE 4-I TYPICAL OUTPUT OF THE COMPUTER PROGRAM ELISTB

MATERIAL BRN/L6 (SG 1.01)

WATER	62.45	C3H803	18.15	ETHANOL	14.36	NH2CONH2	2.77
KHSO4	.16	NA2SO4	.56	KCL	.48	H3PO4	1.07

	SUBSTITUTE (W/O)	REAL TISSUE (W/O)	RATIO (SUBST/REAL)
H	10.6822	10.7000	(.9983)
C	15.1398	15.3300	(.9876)
N	1.2902	1.2900	(1.0002)
O	71.6741	71.4000	(1.0038)
NA	.1813	.1790	(1.0127)
P	.3376	.3400	(.9928)
S	.1652	.1700	(.9717)
CL	.2292	.2290	(1.0009)
K	.3001	.3000	(1.0003)

The program PROTON uses elemental proton mass stopping power data at 38 energy points in the region from 0.01 MeV to 1000 MeV, the elemental or compound composition of the substitute and the Bragg additivity rule to compute the partial and total mass stopping powers of each substitute material. Stopping powers for the real tissue are then computed together with the ratio $\left(\frac{S}{\rho}\right)_{subst} / \left(\frac{S}{\rho}\right)_{tissue}$. The elemental stopping power data were stored on magnetic disc for convenience. Two subroutines are called by the main program, namely MM and GRAFFX. The first is used to determine the minimum and the maximum of an array of numbers (stopping powers or stopping power ratios). It then

prints the results with the appropriate headings. The second subroutine interacts with a plotting package for the line printer, written by the staff of the University College Hospital, London. This subroutine is called twice per substitute material. The first for the total mass stopping power of the substitute and the second for the stopping power ratios. Once these graphs are plotted on a linear-log scale, the mean, standard deviation and variance are computed and printed together with the minimum, maximum and range of values for each set.

The program KERMAF has a structure very similar to that of PROTON and uses the same subroutines. The 116 kerma factor values for each one of nineteen elements, including all of those which exist in real tissues, taken from ICRP report 26, were stored on magnetic disc and used to compute the total kerma factor values for each substitute in the energy range 10 eV to 30 MeV. The total kerma factor ratios (substitute/real tissue) are also computed and plotted against energy on a linear-log scale. The mean and standard deviation of these ratio values are also calculated and used to indicate how accurately each substitute simulates the corresponding real tissue for neutron interactions.

Figures 4.1a and 4.1b show examples of the graphical output of the programs PROTON AND KERMAF. The basic flow chart for these programs is shown in Figure 4.2. The program TABLE used for the computation of the photon and electron data for real tissues and tissue substitutes was developed by WHITE (1974). The data and formulae used in this program have been discussed in Chapter 1 (section 1.2 (iii)).

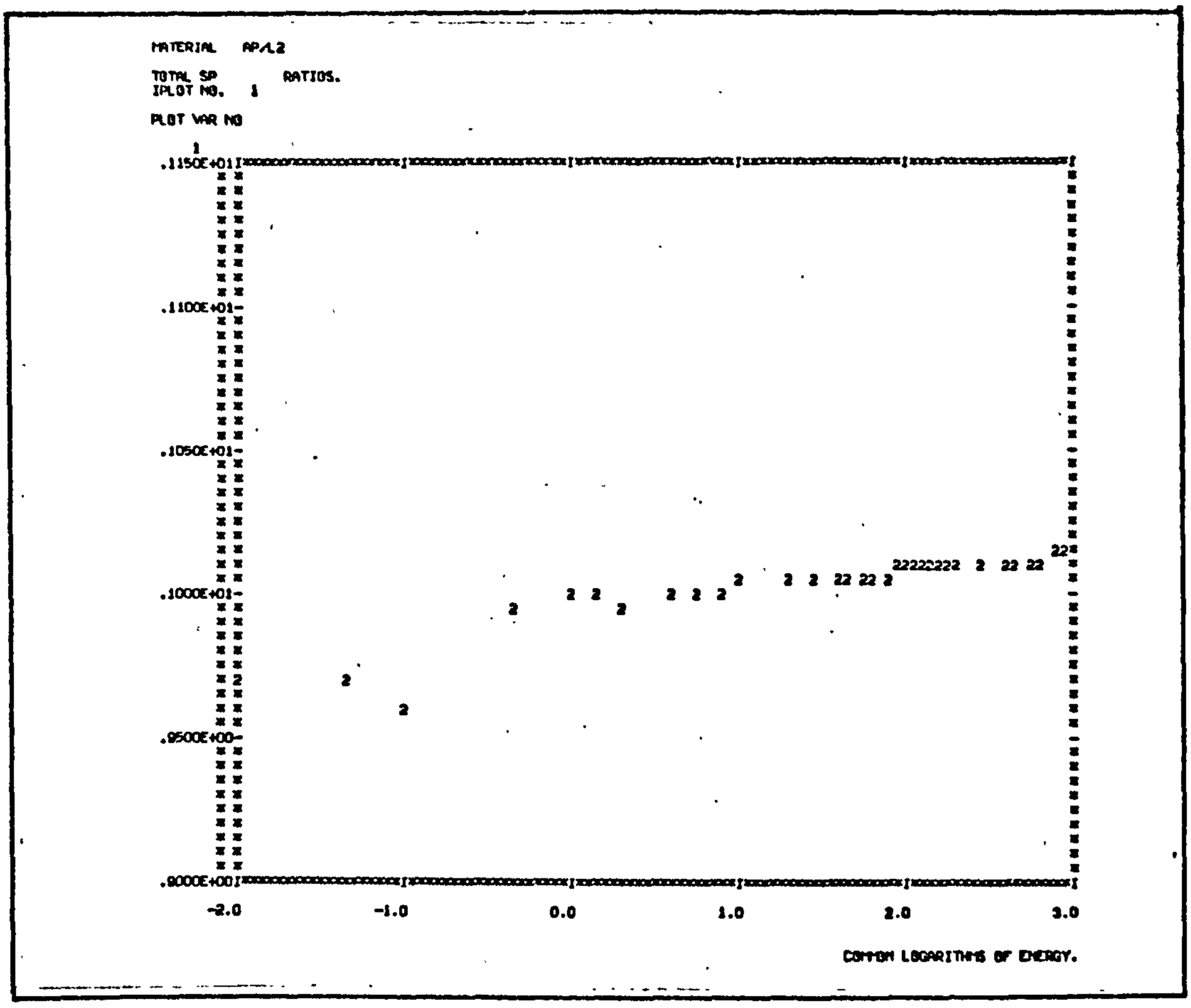

(a)

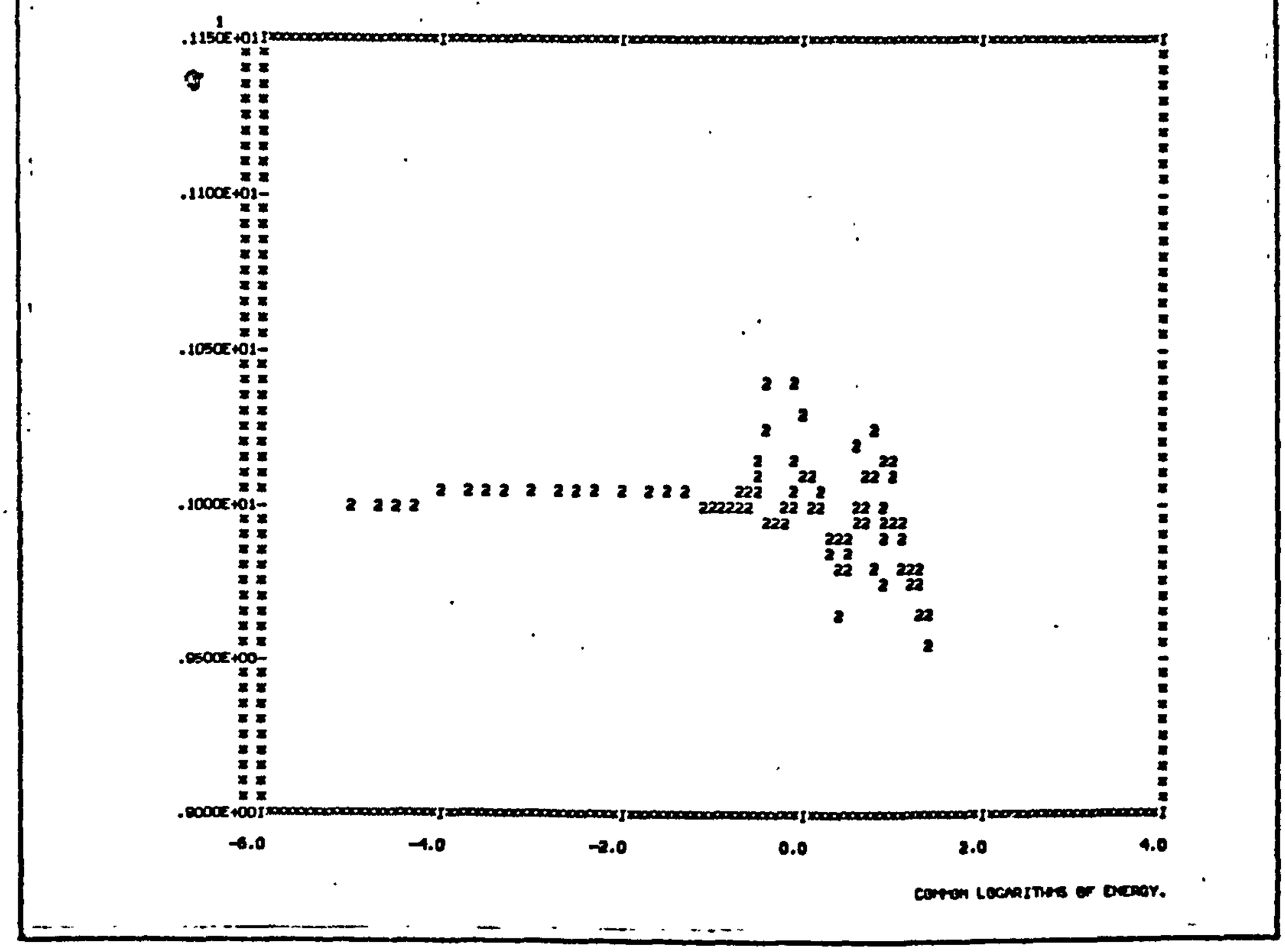

(b)

Figure 4.1. Graphical output of the programs PROTON and KERMAF.

(a) Proton mass stopping power ratios $\left(\frac{AP/L2}{Adipose}\right)$ against energy.

(b) Kerma factor ratios $\left(\frac{AP/L2}{Adipose}\right)$ against energy.

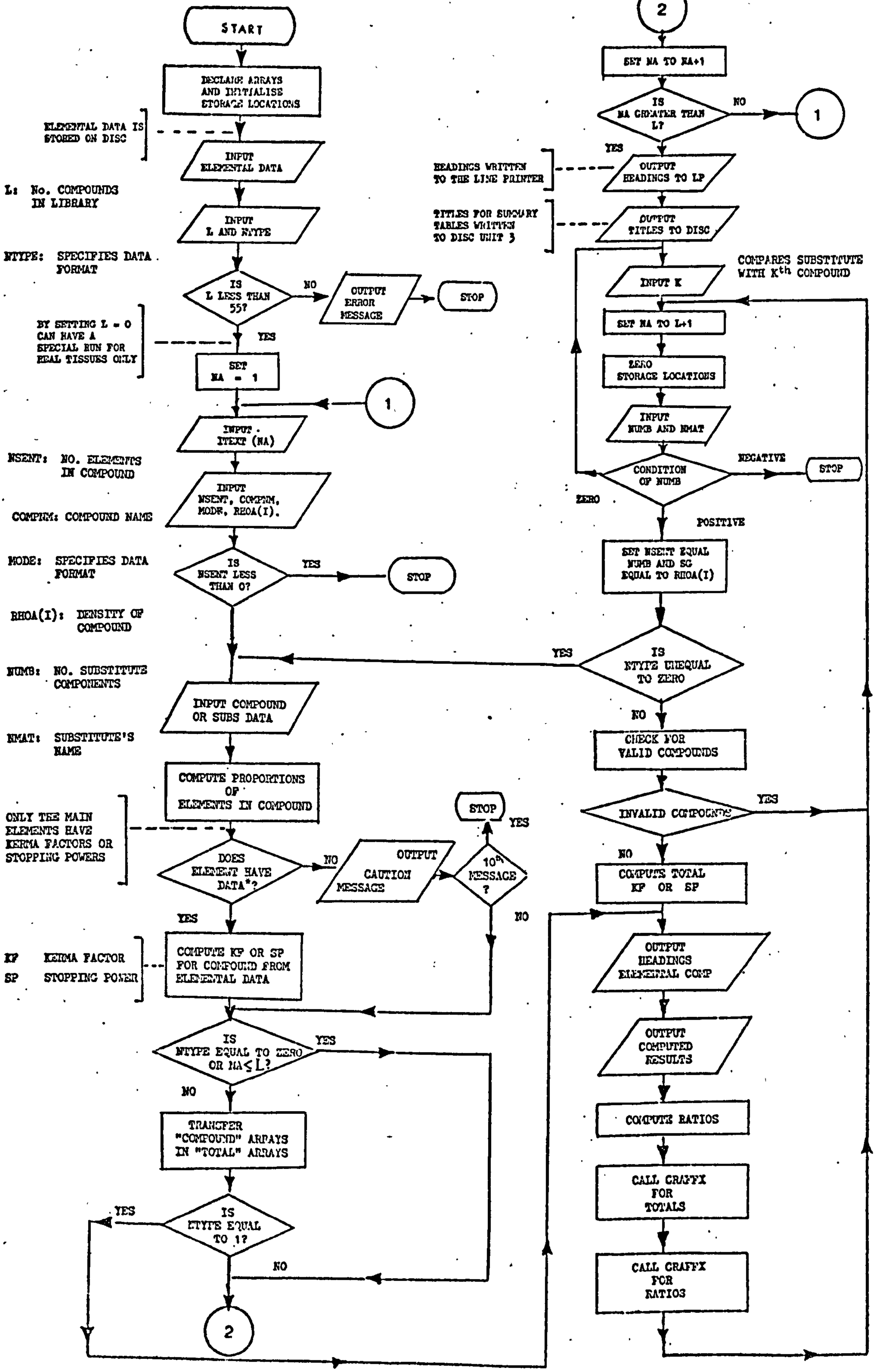

Figure 4.2. Basic flowchart for the programs PROTON and KERMAF.

4.1 (ii) RECOMMENDED TISSUE SUBSTITUTES AND THEIR CALCULATED RADIATION CHARACTERISTICS

The results of a comprehensive analysis of the radiation characteristics of all the new tissue substitutes, and of most of those published in the past (summarised in Appendix 4), for photons and electrons of 0.01 MeV-100 MeV, protons of 0.01 MeV-1000 MeV and neutrons of 11 eV-30 MeV, led to the classification of these materials according to the magnitude of the discrepancies in their radiation characteristics, when compared to those of the corresponding real tissues:

CLASS A materials : errors < 5%

CLASS B materials : errors from 5% to 20%

CLASS C materials : errors > 20%

All those substitutes which are "Class A for all types of radiations" are recommended for use in clinical dosimetry. Some of the "Class A" substitutes become Class B or even Class C when considered for photon energies below 0.1 MeV and such information is given in the classification. Similarly, some of the substitutes are Class A for one type of radiation but Class B or C for other radiation modalities. Tables 4-II (A to E) summarise the results of this classification and show the recommended substitutes. The calculated coefficient ratios, power ratios and kerma factor ratios of some of the recommended tissue substitutes are given in Tables 4-III and 4-IV.

TABLE 4-II CLASSIFICATION OF TISSUE SUBSTITUTE MATERIALS - RECOMMENDED SYSTEMS

A. PRINCIPAL SOFT TISSUES

TISSUE	SOLID	LIQUID	GEL OR POWDER	CLASSIFICATION				
							PHOTONS	
				Protons	Neutrons	Electrons	≥0.1 MeV	<0.1 MeV
i) ADIPOSE	AP/SF1			A	A	A	A	B
		AP/L2		A	A	A	A	B
	AP 6 (WHITE)			A	C	A	A	A
ii) BLOOD		BL/L1		A	A	A	A	A
		BL/L2		A	A	A	A	A
iii) MUSCLE	MS/SR1			A	A	A	A	C
	MS/SR4			A	A	A	A	C
		MS/L1		A	A	A	A	A
		FRIGERIO LIQU.		A	A	A	A	A
		GOODMAN LIQU.		A	A	A	A	B
		WATER		A	A-B	A	A	A
			MS/G1	A	A	A	A	A
			MS/G2	A	A	A	A	A
			FRIGERIO GEL	A	A	A	A	B
	A-150			A	A	A	A	C
	MS15 (WHITE)			A	A-B	A	A	A
	MS20 (WHITE)			A	C	A	A	A
	M3			A	B	A	A	A
	MIX D			B	C	A	A	B
	TEMEX			A	A-B	A	A	C

TABLE 4-II cont....

B. PRINCIPAL SKELETAL TISSUES

TISSUE	SOLID	LIQUID	GEL OR POWDER	CLASSIFICATION				
							PHOTONS	
				Protons	Neutrons	Electrons	≥ 0.1 MeV	< 0.1 MeV
i) HARD BONE	HB/SR1			A	B	A	A	A
	HB/SF3			A	B	A	A	B
	HB/SR4			A	B	A	A	B
	SB3 (WHITE)			A	C	A	A	A
			HB/POWDER 2	A	A	A	A	A
		WITT'S LIQUID		A	B-C	A	A	B
	SHONKA B100			B	C	B	A	C
ii) RED MARROW	RM/SF3			A	A	A	A	B
	RM/SR4			A	A	A	A	B
			RM/G1	A	A	A	A	B
iii) INNER BONE	IB/SR1			A	A	A	A	C
		IB/L1		A	A	A	A	B
	IB6 (WHITE)			A	B	A	A	A

Note: Aluminium, Magnesium, P.T.F.E, Sulphur and Spiers liquid, used to represent hard bone in the past, are Class C and are not recommended.

TABLE 4-II cont....

C. BODY ORGANS

TISSUE	SOLID	LIQUID	GEL OR POWDER	CLASSIFICATION				
				Protons	Neutrons	Electrons	PHOTONS ≥ 0.1 MeV	PHOTONS < 0.1 MeV
i) BRAIN		BRN/L4		A	A	A	A	A
		BRN/L6		A	A	A	A	A
	BRN/SR2			A	A	A	A	C
ii) KIDNEY		KD/L1		A	A	A	A	A
	KD/SR1			A	A	A	A	C
iii) LIVER		LV/L1		A	A	A	A	A
iv) LUNG	LN/SR4			A	A	A	A	C
	ALDERSON LUNG			A	C	A	A	C
	ROGER'S ADIPRENE			B	C	B	B	B
	STACEY LATEX			A	C	A	A	C
v) THYROID		TH/L2		A	A	A	A	A

TABLE 4-II cont....

D. AVERAGE TISSUES

TISSUE	SOLID	LIQUID	GEL OR POWDER	CLASSIFICATION				
							PHOTONS	
				Protons	Neutrons	Electrons	≥ 0.1 MeV	< 0.1 MeV
i) AVERAGE BREAST (50% FAT-50% MUSCLE)	AV.BR/SF3			A	A	A	A	B
(50% FAT-50% WATER)		AV.BR/L2		A	A	A	A	A
ii) TOTAL SOFT TISSUE		TST/L2		A	A	A	A	A
		TST/L3		A	A	A	A	A
iii) TOTAL SKELETON	TSK/SF3			A	A	A	A	A
		TSK/L1		A	A	A	A	B

E. TISSUE COMPONENTS

TISSUE	SOLID	LIQUID	GEL OR POWDER	CLASSIFICATION				
							PHOTONS	
				Protons	Neutrons	Electrons	≥ 0.1 MeV	< 0.1 MeV
i) FAT	FT/SF1	FT/L2		A	A	A	A	A
	ALDERSON FAT			A	A	A	A	A
				A	A	A	A	B
ii) PROTEIN	PR/SR1			A	B	A	A	B
iii) WATER	WT/SR1			A	B-C	A	A	A

TABLE 4-III CALCULATED COEFFICIENT AND POWER RATIOS FOR SOME RECOMMENDED TISSUE SUBSTITUTES (PHOTON AND ELECTRON DATA)

SUBSTITUTE	PHOTONS										ELECTRONS					
	$\left(\frac{\mu}{\rho}\right)_{subst.}/\left(\frac{\mu}{\rho}\right)_{tissue}$					$\left(\frac{\mu_{en}}{\rho}\right)_{subst}/\left(\frac{\mu_{en}}{\rho}\right)_{tissue}$					$\left(\frac{S}{\rho}\right)_{subst}/\left(\frac{S}{\rho}\right)_{tissue}$					$\left(\frac{\bar{\Theta}^2}{\rho\ell}\right)_{subst}/\left(\frac{\bar{\Theta}^2}{\rho\ell}\right)_{tissue}$
	ENERGY (Mev)															
	0.01	0.1	1.0	10	100	0.01	0.1	1.0	10	100	0.01	0.1	1.0	10	100	0.01-100
ADIPOSE																
AP/SF1	0.92	1.00	1.00	1.00	0.98	0.92	1.00	1.00	0.99	0.98	1.00	1.00	1.00	1.00	0.99	0.97
AP6 (WHITE)	1.00	0.97	0.97	0.98	1.00	1.00	0.97	0.97	0.98	1.00	0.95	0.96	0.96	0.97	0.99	1.02
BLOOD																
BL/L1	0.96	0.99	0.99	0.99	0.99	0.96	0.98	0.99	0.99	0.98	0.99	0.99	0.99	0.99	0.99	0.98
MUSCLE																
MS/SR1	0.70	0.99	1.00	0.96	0.90	0.68	0.95	1.00	0.96	0.92	1.01	1.01	1.00	0.99	0.93	0.85-0.86
MS/SR4	0.72	0.98	0.99	0.96	0.91	0.71	0.95	0.99	0.96	0.92	1.00	1.00	0.99	0.98	0.93	0.86
MS/L1	1.01	1.01	1.00	1.00	1.01	1.01	1.00	1.00	1.00	1.01	1.00	1.00	1.00	1.00	1.00	1.00
MS/G1	0.98	1.00	1.00	1.00	1.00	0.97	1.00	1.00	1.00	1.00	1.00	1.00	1.00	1.00	1.00	1.00
A-150 (SHONKA)	0.79	0.99	1.00	0.97	0.88	0.76	0.99	1.00	0.96	0.91	1.01	1.01	1.00	0.98	0.93	0.84-0.86
MS15 (WHITE)	1.03	0.99	0.99	0.98	0.94	1.05	1.00	0.99	0.98	0.95	0.99	0.99	0.99	0.99	0.96	0.92-0.93
HARD BONE																
HB/SR1	0.97	0.99	1.00	0.99	0.96	0.97	0.99	1.00	0.99	0.98	1.01	1.01	1.02	1.02	0.98	0.96
HB/SR4	0.91	0.99	1.01	0.99	0.96	0.91	0.96	1.01	0.99	0.97	1.03	1.02	1.03	1.03	0.98	0.95
HB/POWDER 2	0.98	0.99	1.00	1.00	0.99	0.98	0.99	1.00	1.00	0.99	1.00	1.00	1.00	1.00	0.99	0.99
SB3 (WHITE)	1.02	1.00	1.00	0.99	0.97	1.03	1.02	1.00	0.99	0.98	1.01	1.01	1.02	1.01	0.98	0.96-0.97
WITT LIQUID	1.05	1.01	1.01	1.02	1.04	1.07	1.02	1.01	1.02	1.03	1.01	1.01	1.01	1.02	1.03	1.05
BODY ORGANS																
BRN/L6	1.00	1.00	1.00	1.00	1.01	1.00	1.00	1.00	1.00	1.00	1.00	1.00	1.00	1.00	1.00	1.00
KD/L1	0.99	1.00	1.00	1.00	1.00	0.99	1.00	1.00	1.00	1.00	1.00	1.00	1.00	1.00	1.00	1.00
LN/SR4	0.78	1.01	1.02	0.99	0.91	0.76	0.98	1.02	0.98	0.94	1.03	1.03	1.02	1.01	0.96	0.92-0.93
AVERAGE TISSUES																
TST/L1	1.00	1.00	1.00	1.00	1.00	1.00	1.00	1.00	1.00	1.00	1.00	1.00	1.00	1.00	1.00	1.00
TSK/L1	0.93	0.99	1.00	1.00	1.01	0.92	0.99	1.00	1.00	1.01	1.00	1.00	1.00	1.00	1.01	1.02
TSK/SF3	0.97	1.00	1.00	0.99	0.96	0.97	1.00	1.00	0.99	0.98	1.01	1.01	1.01	1.00	0.98	0.96
TISSUE COMPONENTS																
FT/SF1	0.98	1.00	1.00	1.00	0.99	0.98	1.00	1.00	1.00	1.00	1.00	1.00	1.00	1.00	1.00	1.00
FT/L1	1.00	1.00	1.00	1.00	1.00	1.00	1.00	1.00	1.00	1.00	1.00	1.00	1.00	1.00	1.00	1.00
WT/SR1	1.05	0.97	0.97	0.96	0.95	1.06	1.00	0.97	0.96	0.95	0.97	0.97	0.97	0.97	0.95	0.88-0.89

RECOMMENDED TISSUE SUBSTITUTES (PROTON AND NEUTRON DATA)

SUBSTITUTE	PROTONS (0.01 MeV-1000 MeV)		NEUTRONS (10 eV-30 MeV)	
	TOTAL STOPPING POWER RATIOS $\left(\frac{\text{substitute}}{\text{tissue}}\right)$	STANDARD DEVIATION	TOTAL KERMA FACTOR RATIOS $\left(\frac{\text{substitute}}{\text{tissue}}\right)$	STANDARD DEVIATION
ADIPOSE				
AP/SF1	1.00	0.01	1.00	0.01
AP/6 (WHITE)	0.95	0.02	0.77	0.18
BLOOD				
BL/L1	0.99	0.01	1.00	0.01
MUSCLE				
MS/SR1	1.02	0.02	1.02	0.03
MS/SR4	1.01	0.02	0.96	0.02
MS/L1	1.00	0.00	1.00	0.01
MS/G1	1.00	0.02	1.00	0.01
A-150 (SHONKA)	1.02	0.02	1.03	0.03
MS15 (WHITE)	1.00	0.01	0.96	0.10
HARD BONE				
HB/SR1	1.01	0.01	1.10	0.03
HB/SR4	1.03	0.02	1.09	0.04
HB/POWDER 2	1.00	0.00	1.00	0.01
SB3 (WHITE)	1.01	0.01	0.94	0.10
WITT LIQUID	1.00	0.02	1.19	0.24
BODY ORGANS				
BRN/L6	1.00	0.00	1.00	0.01
KD/L1	0.99	0.01	1.00	0.01
LN/SR4	1.04	0.01	1.01	0.03
AVERAGE TISSUES				
TST/L1	1.00	0.00	1.00	0.01
TSK/L1	0.99	0.01	1.03	0.03
TSK/SF3	1.01	0.01	1.02	0.04
TISSUE COMPONENTS				
FT/SF1	1.00	0.00	1.00	0.01
FT/L1	1.00	0.00	1.00	0.01
WT/SR1	0.97	0.02	0.87	0.51

4.2 EXPERIMENTAL EVALUATION OF THE "TISSUE EQUIVALENCE" OF THE NEW SUBSTITUTES

The general objectives of the experimental work carried out during this study were two-fold, namely, to determine how accurately the new tissue substitutes simulate the corresponding real tissues and then to use these materials to measure the dose distributions from beams of various radiation modalities in tissues like muscle, brain, etc., and to investigate the effect of tissue heterogeneities on these dose distributions.

The experimental verification of the tissue equivalence of the new substitutes is described in this section while the dosimetric investigations using the new substitutes are discussed in Chapter 5. Comparative measurements were made for the following:

a) Muscle equivalent liquid (MS/L1) and solid muscle substitutes (MS/SR1 and MS/SR4) versus human muscle, beef steak and pork;

b) Brain equivalent liquid (BRN/L6) and brain solid substitute (BRN/SR2) versus human brain;

c) Fat equivalent solid (FT/SF1) versus beef fat;

d) Solid and liquid bone substitutes versus human bone.

The human tissues used in these comparisons were obtained from post-mortem investigations.

The cells shown in Figure 4.3, made of muscle or brain substitute accordingly, with cross sectional area 10 cm x 10 cm and variable thickness, were filled with the real tissues and immersed into the appropriate tissue equivalent liquid to displace an equal volume of that liquid; central axis depth doses and beam profiles were then measured in the liquid behind the cell and the results

compared with those obtained in the liquid alone and with those obtained when other solid substitutes were present in the liquid. The result will be discussed in the following sections of this chapter.

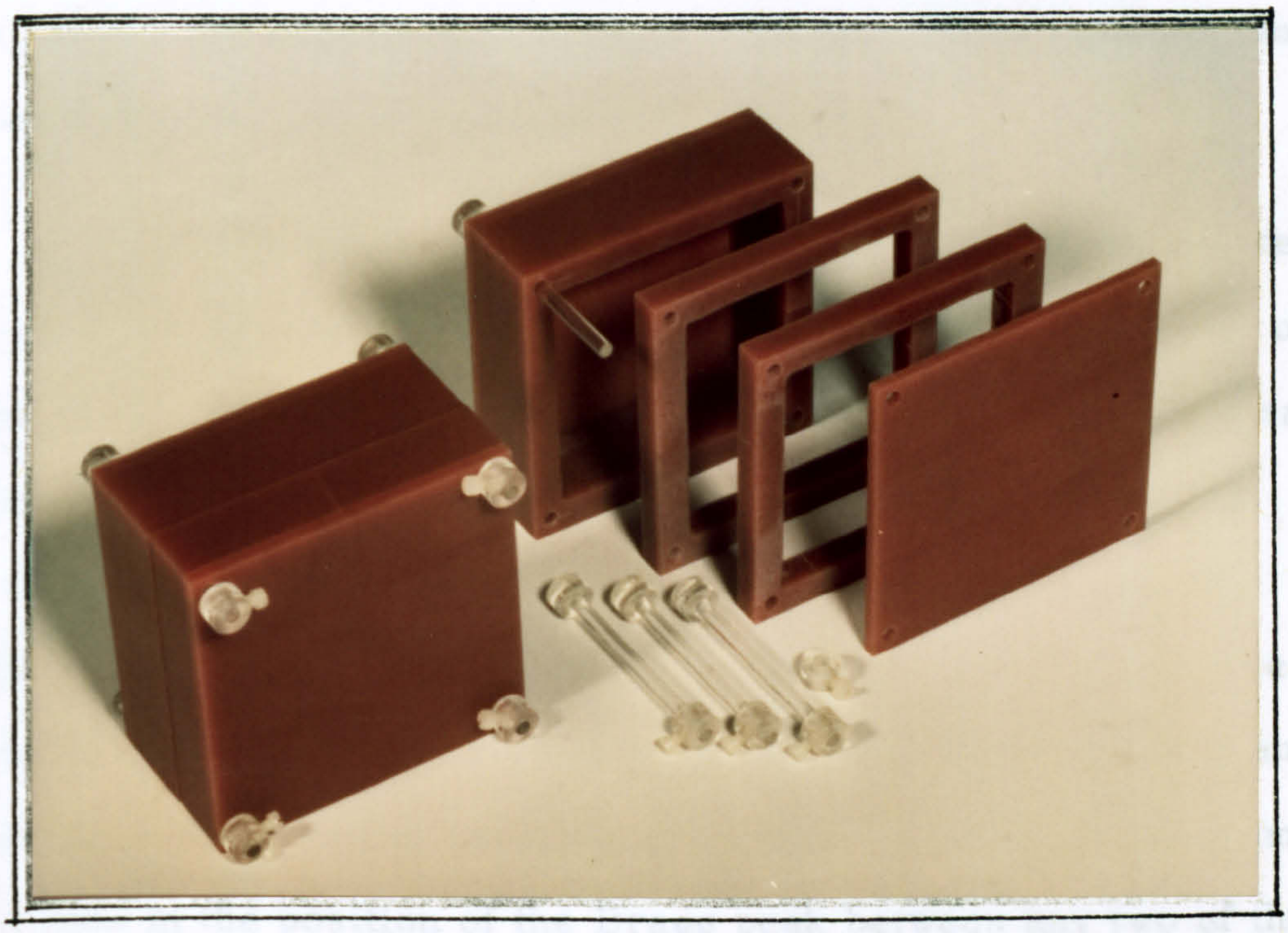

Figure 4.3 Cells used in the comparison of substitutes versus real tissues

4.2(i) HIGH ENERGY PROTONS

The 160 MeV proton beam from the synchrosyclotron of the Atomic Energy Research Establishment, U.K., was scattered with a 0.317 cm-thick copper plate. The resulting broad beam was about 5 cm diameter at the front face of the phantom, 1 m away from the end of the beam pipe line. When liquids were used, they were contained in a 15 cm x 15 cm x 25 cm perspex tank whose front wall was 0.3 cm thick.

A flat ionisation chamber (MC78), which is described later, was used to measure depth doses in MS/L1. A 5 cm-thick cell of human muscle was then immersed in the muscle liquid in the plateau region and the depth dose measurements in the liquid behind the muscle cell were repeated; the human muscle was sequentially replaced by beef steak, solid MS/SR1 and solid MS/SR4 muscle substitutes and each time the depth doses in the liquid behind them measured. The results are shown in Figure 4.4. The maximum difference in the position of the Bragg peak between any two of the above sets of measurements was less than 1 mm and if a correction for the slightly higher relative density of MS/L1 (1.07 instead of 1.06) was made, this difference was reduced to less than 0.2% of the peak depth. When MS/L1 with no trace elements in it was used (relative density 1.06), the results were identical with those obtained when the fixed human muscle sample was immersed in it.

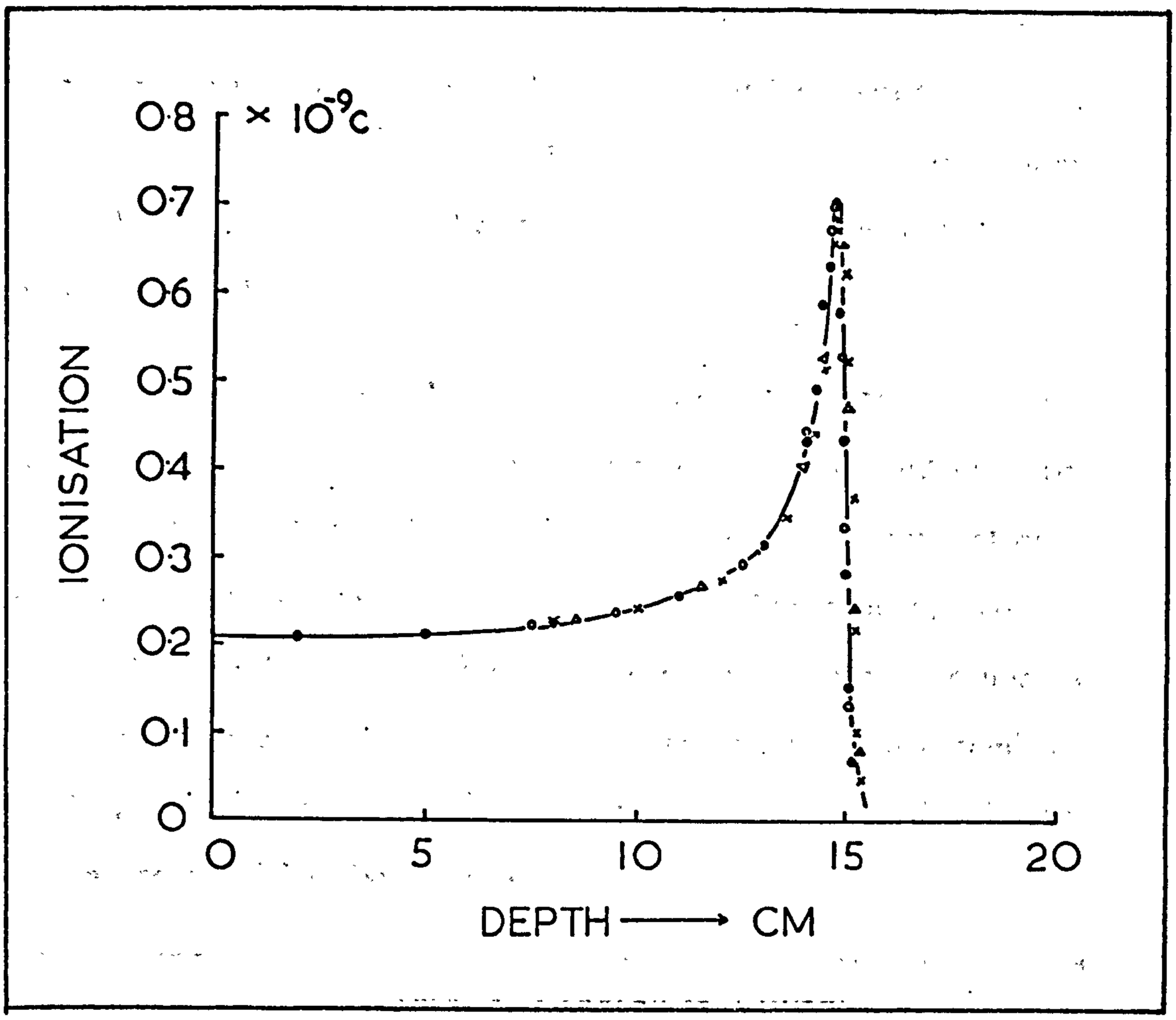

Figure 4.4 Muscle substitutes versus real human muscle with 150 MeV protons

- • MS/L1 (density = 1.07 g/cm^3)
- × with 5 cm human formalin fixed muscle
- ▽ with 5 cm beef steak
- σ with 5 cm MS/SR4 (density = 1.06 g/cm^3)

Figure 4.5 shows similar measurements for 5 cm-thick samples of beef fat and the solid fat substitute FT/SF1 placed, in turn, in the plateau region; the agreement between the two is good. The depth dose in MS/L1 is also plotted on this graph so that the displacement of the Bragg peak for fat relative to muscle can be estimated.

Another similar cell, made of brain substitute (BRN/SR2), was filled with human formalin-fixed brain and immersed in brain equivalent liquid (BRN/L6). The central axis depth ionisation curves in BRN/L6, with and without the real brain in it, are shown in Figure 4.6. The two sets of measurements are nearly identical; when a 5 cm-thick BRN/SR2 sample was immersed in BRN/L6, in the plateau region, however, the depth of the Bragg peak was reduced by about 1 mm.

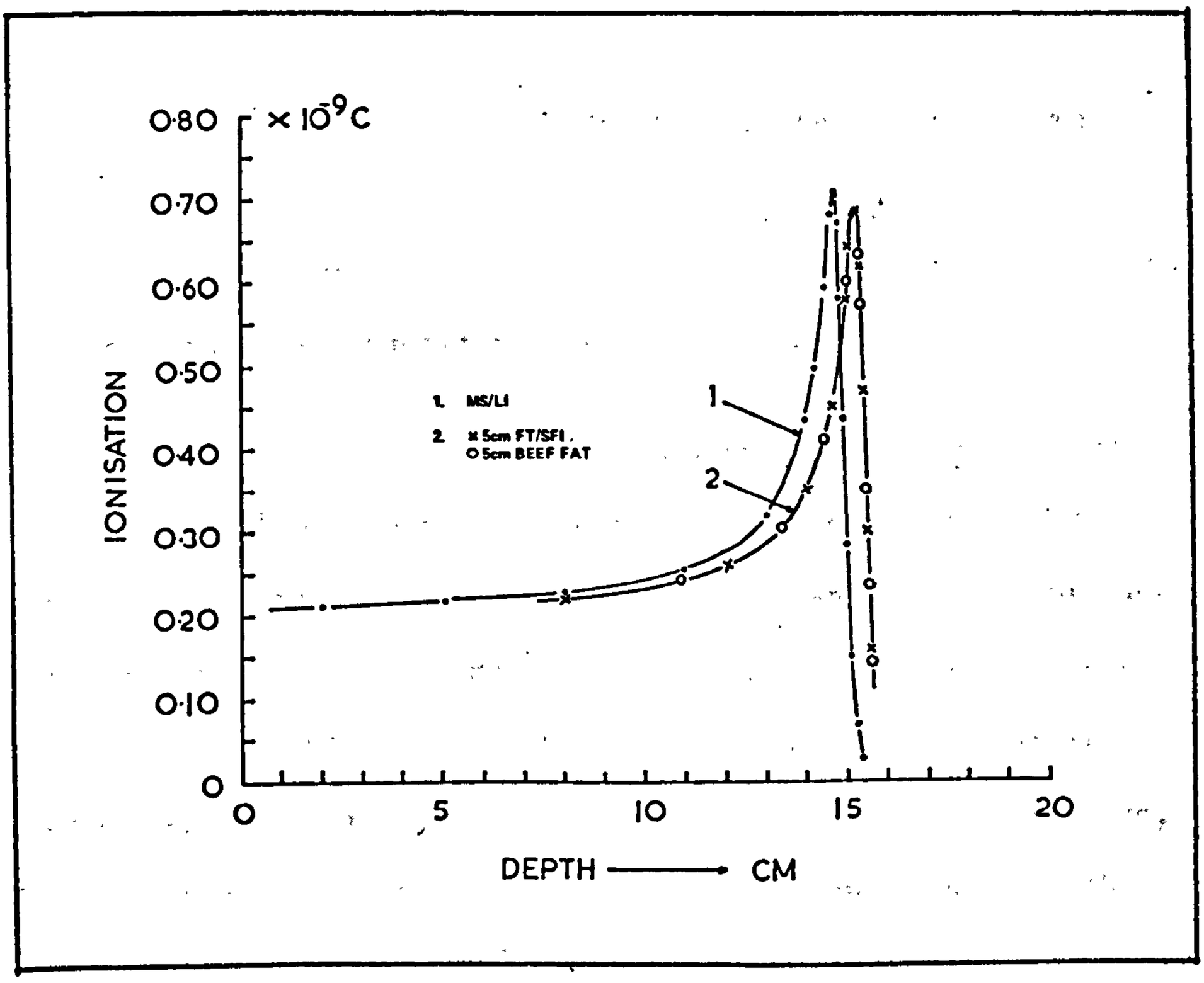

Figure 4.5 Fat substitute versus beef fat

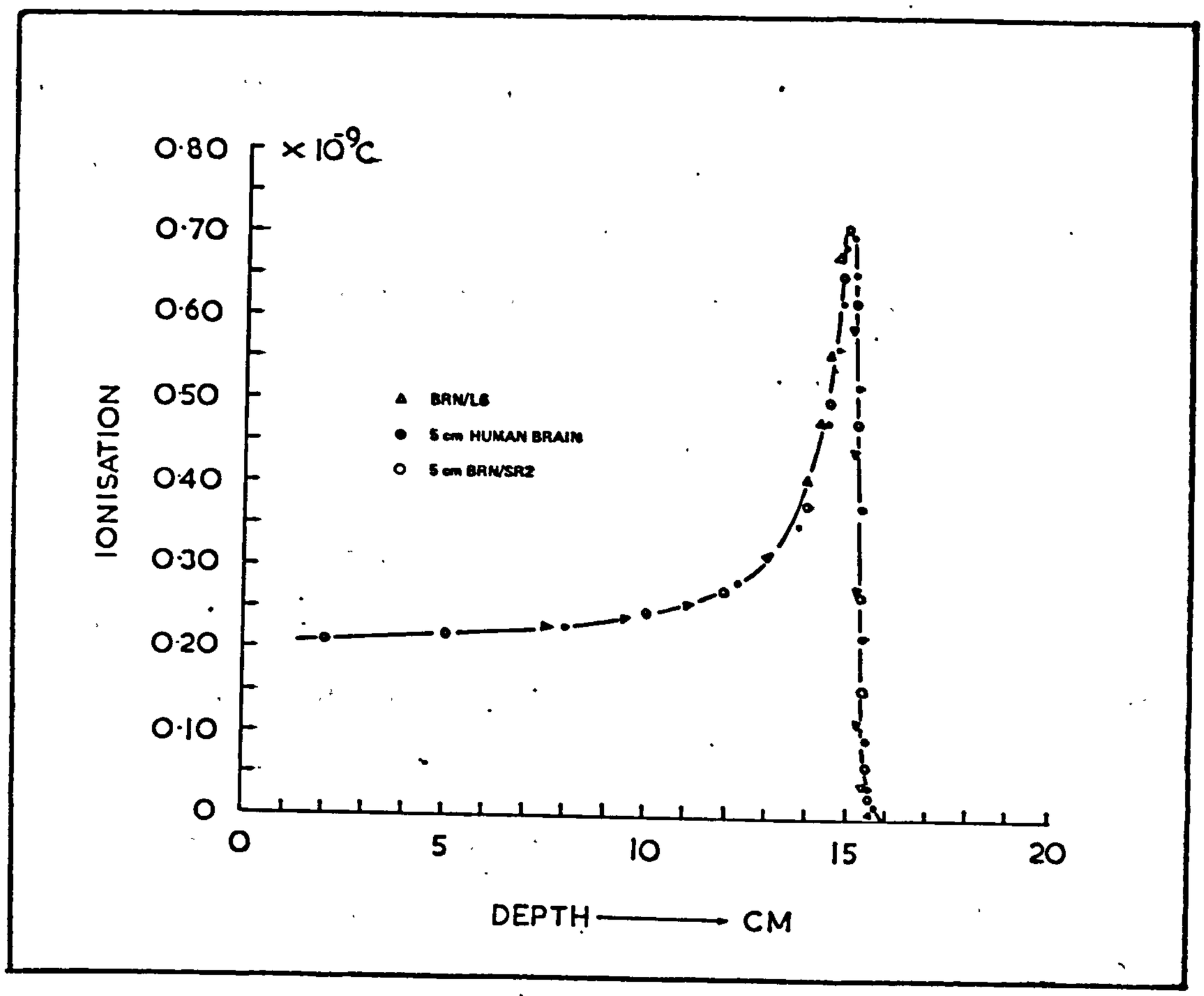

Figure 4.6 Brain substitutes versus real human brain

The slightly higher relative density (1.04 instead of 1.03) was found to be responsible for most of this displacement.

A preliminary series of measurements with various bone substitutes and sections of an ox tibia, showed that a density correction, when bone was present in the beam, would give the required position of the Bragg peak with an error not exceeding 4-5%. It was not possible to find areas of real bone to make absorbers of cross sections large enough to minimise experimental errors, so the above finding was accepted. The effect of bone as well as the correction necessary when bone is present in a proton beam are discussed later in the thesis.

4.2(ii) FAST NEUTRONS

A series of measurements similar to those described in the previous section was carried out using the fast neutron beam of the Medical Research Council cyclotron at the Hammersmith Hospital, London. Central axis depth doses were measured in muscle-equivalent liquid (MS/L1) and then 5 cm-thick samples of human muscle, beef steak, pork and MS/SR4 were immersed in turn, and the depth doses measured each time.

The total dose ($D_n + D_\gamma$) was measured with a 1 cm^3 spherical ionisation chamber (EG & G) whereas the gamma ray component of the dose was measured with a Geiger Muller counter covered with a ^6Li foil to absorb the slow neutrons. The total dose was normalised to the dose at 1.5 cm depth and the results, plotted versus depth, are given in Figure 4.7(a). Dose distributions perpendicular to the beam axis (beam profiles) were also measured in MS/L1 (at 9 cm depth) and then repeated with each of the above mentioned samples immersed in the liquid, in front of the dosemeter. The dose at points off the axis was normalised to the central axis dose which was taken as 100% (Figure 4.7(b)).

The difference between any two measurements at the same point, but with different samples, was generally of the order of $\pm 0.5\%$ and in no case greater than $\pm 0.8\%$. A statistical analysis of the differences observed in all the above measurements was made and these differences were found not to be significant; differences resulting from the variability of the machine itself (e.g. deuterons hitting the Be target off centre), amount to $\pm 1\%$; this also accounts for the fact that beam profiles measured under identical conditions are not always symmetrical.

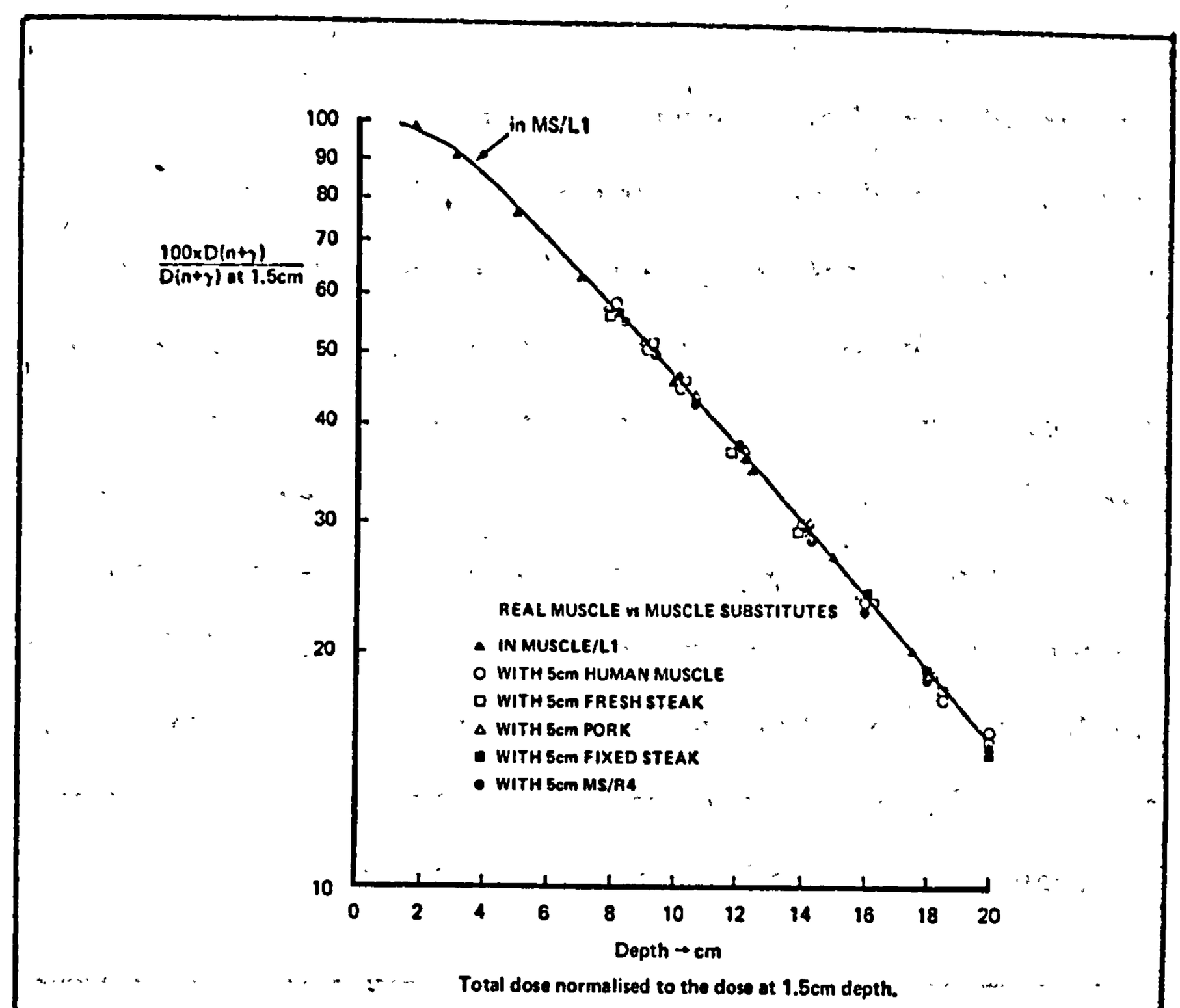

(a)

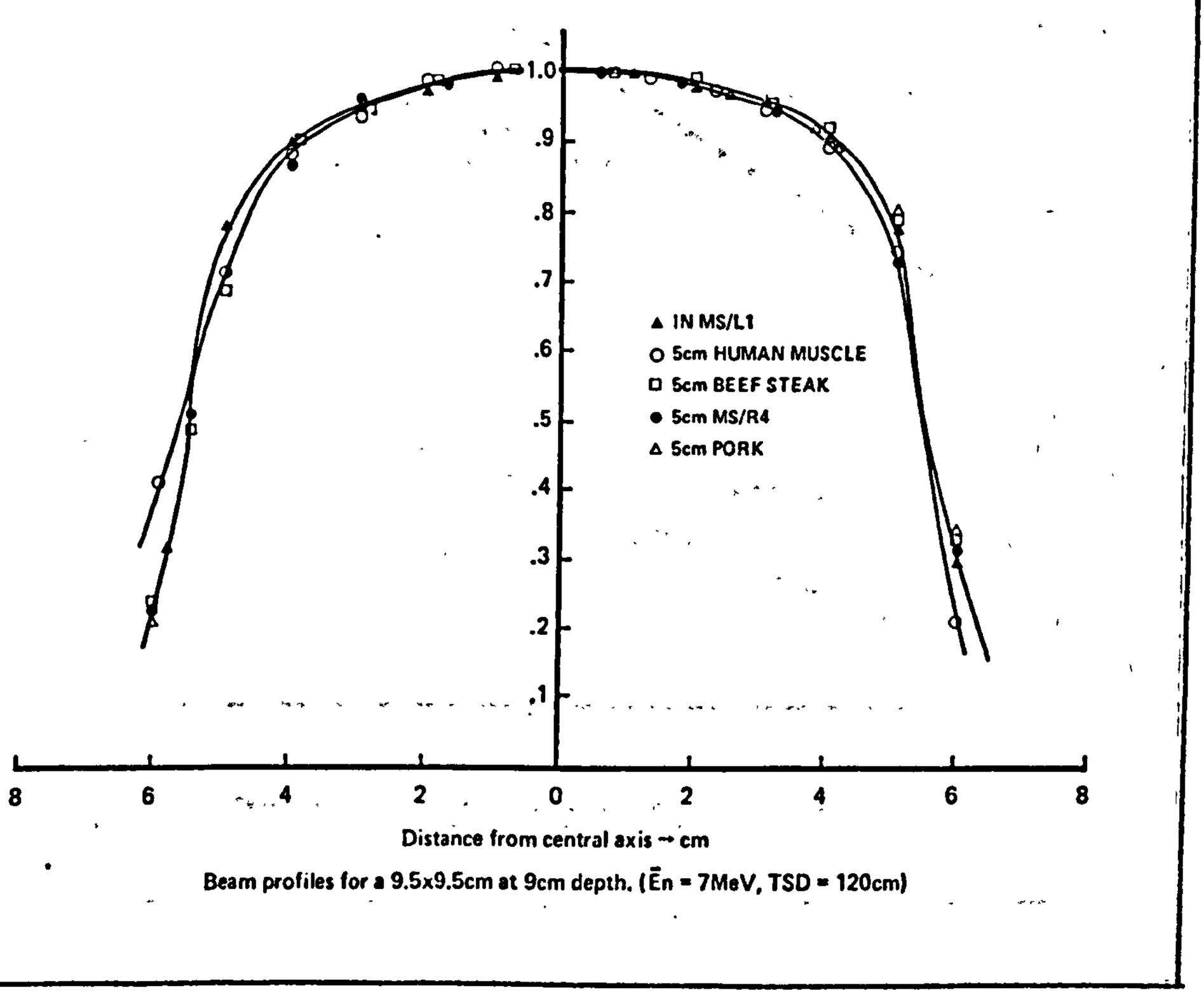

(b)

Figure 4.7 Comparison of muscle substitutes with real muscle using 7.5 MeV neutrons.

Brain substitutes were compared to human brain (both formalin fixed and unfixed), in the same way as above. The gamma ray component of the dose was also measured and subtracted from the total dose. The neutron depth doses, expressed as a percentage of the maximum neutron dose (at 2 mm depth for this neutron energy), are shown in Figure 4.8. Unfixed human brain and BRN/L6 gave nearly identical results whereas formalin fixed brain gave slightly higher and BRN/SR2 gave slightly lower depth doses than unfixed brain. In general, however, the neutron depth doses behind any brain sample, substitute or real, were found not to differ by more than 1%, i.e. they were within experimental error, the same.

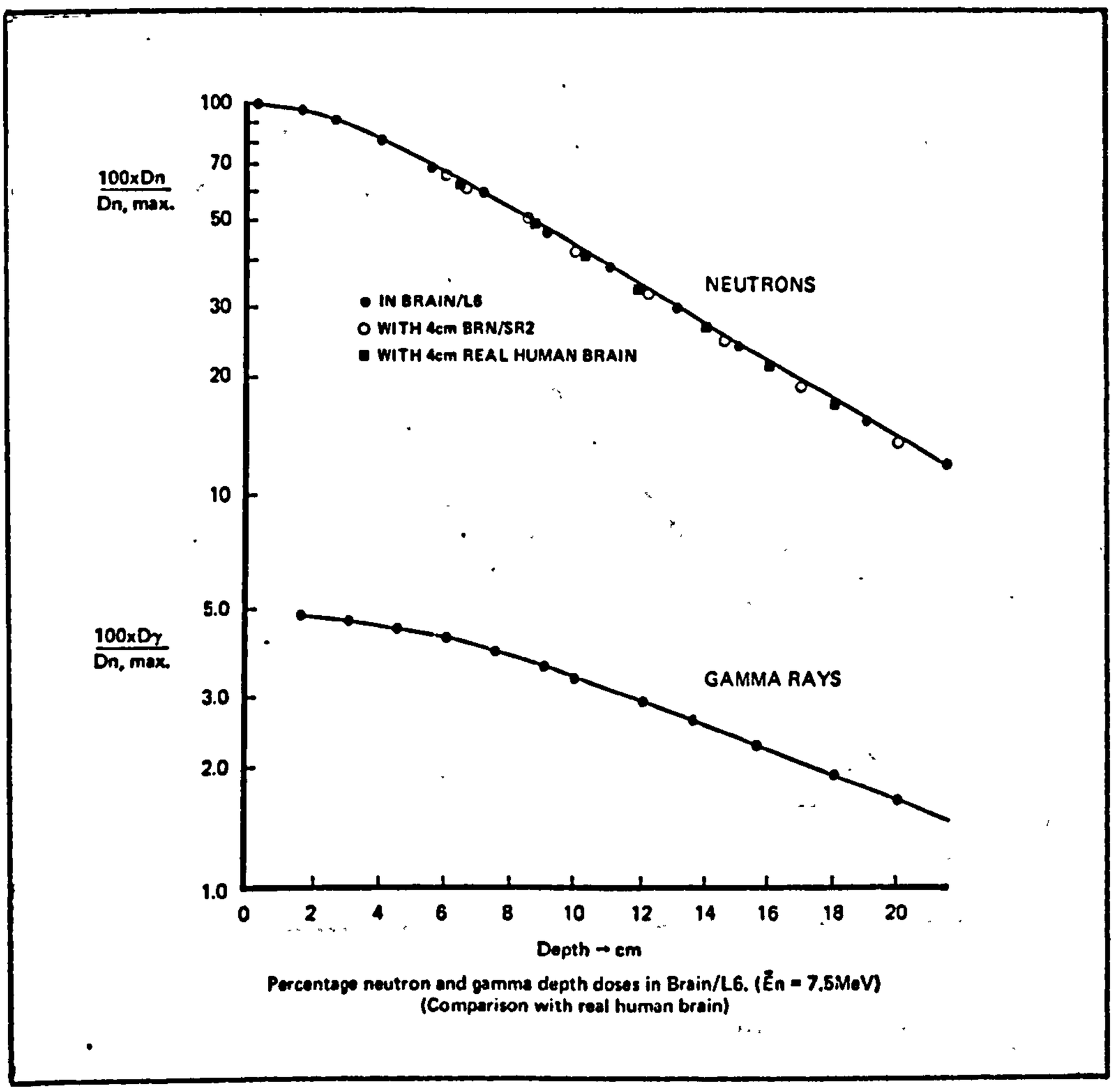

Percentage neutron and gamma depth doses in Brain/L6. ($\bar{E}n$ = 7.5MeV)
(Comparison with real human brain)

Figure 4.8 Brain substitutes versus real brain

Figure 4.9 shows the comparison of beef fat with FT/SF1 with the same beam of neutrons.

In this case the solid muscle substitute MS/SR4 was used as main phantom material and the fat samples placed in front of it, keeping the distance from the front surface of the composite phantom to the target unaltered (i.e. 120 cm). The neutron depth doses behind the beef fat sample are slightly higher (but not more than 1%) than those obtained with equal thickness of FT/SF1, mainly because of the difference in the width and height of the two samples (beef fat : 10 cm x 10 cm x 5 cm, FT/SF1 : 15 cm x 15 cm x 5 cm).

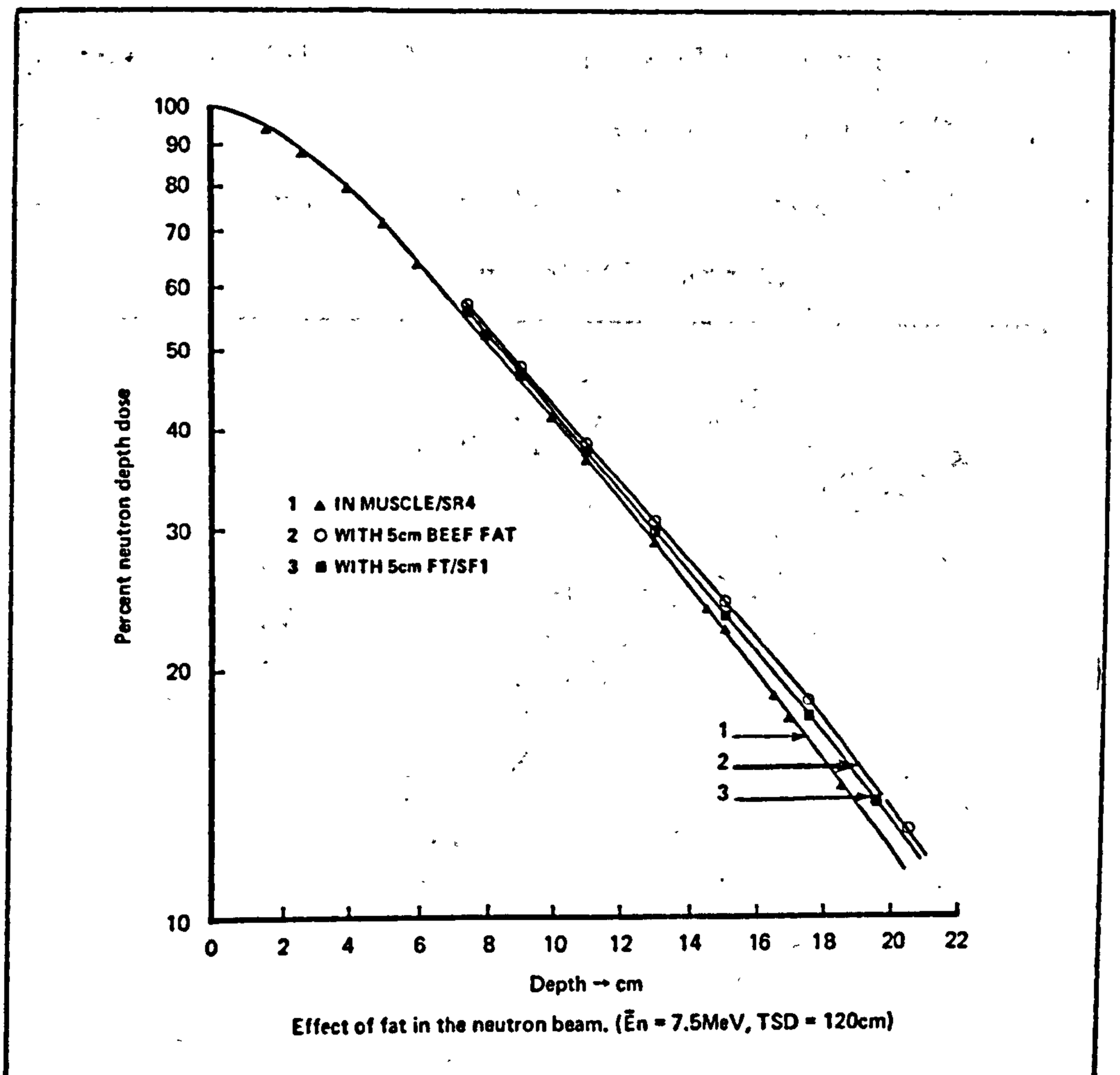

Effect of fat in the neutron beam. ($\bar{E}n$ = 7.5MeV, TSD = 120cm)

Figure 4.9 - Fat substitute versus beef fat

This difference in geometry was cancelled out when the tissue cells were immersed in the liquids in all the previous examples.

It is evident that the higher hydrogen content of fat, although it may result in higher neutron absorbed dose in the fat itself, is more than compensated by its lower density; the net effect is that the neutron doses behind it are higher than in muscle alone, without any fat present.

Finally, a comparison between bone substitutes and real bones was attempted. For this, a cylindrical container with 5 cm internal diameter and 0.5 cm-thick wall, made of MS/SR4 was placed in the perspex tank touching its front wall and displacing muscle equivalent liquid (MS/L1). This allowed the introduction of liquid bone substitutes into the muscle equivalent liquid (MS/L1). The ionisation chamber could move behind the cylinder, in the liquid, the movement being controlled remotely (Figure 4.10).

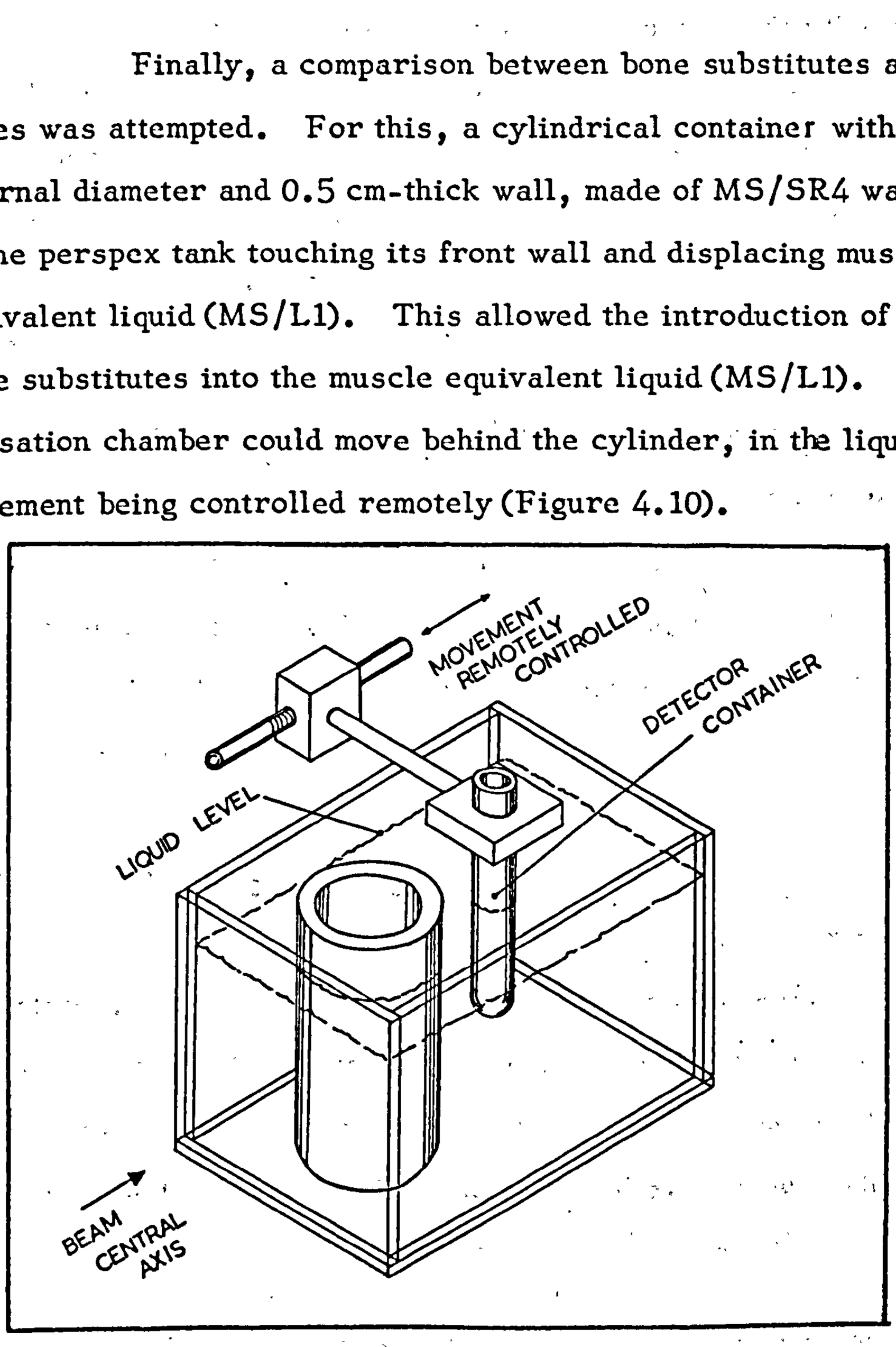

Figure 4.10 Setup used for the comparison of real bones with bone substitutes

Three real bone samples and three cylinders of solid bone substitutes, (T.SK/SF3, HB/SF3 and HB/SR9), machined to dimensions similar to those of the real bones (femur, about 3 cm diameter) were immersed, in turn, into the cylinder, displacing the liquid bone substitute. The depth doses were measured at two depths, namely 9 cm and 15 cm, with the cylinder containing TSK/L1 and then a hard bone liquid substitute (WITT and CAMERON 1975).

The total doses measured at 9 cm depth for the various liquid bone substitutes and the real bone samples were all lower than those measured in muscle equivalent liquid alone; the difference between the total doses behind any combination of two bone samples, real or substitutes, however, did not exceed 0.5% of the maximum dose.

An attempt to verify whether the lower total dose was due to lower neutron or lower gamma ray components of the dose, did not give conclusive results. Measurements with slabs of solid bone substitutes, however, indicated, consistently, that the difference was due to a reduced gamma ray component of the dose; this will be discussed in Chapter 5.

4.2 (iii) COBALT-60 GAMMA RAYS

Although the new substitutes were designed for particulate radiations, they were also tested with cobalt-60 gamma rays. There was no doubt about the accuracy of simulation for the liquid substitutes which have both correct elemental composition and relative density. It is the effect of the partial replacement of oxygen by carbon in the solid substitutes that had to be verified experimentally.

Since Compton scattering is the predominant process at the energy of cobalt-60 gamma rays, it is the electron density

(electrons/cm^3) that is important in this case. Consequently, no great difference was to be expected, for example, between MS/L1 which is elementally correct and MS/SR4 in which three quarters of the oxygen content of muscle have been replaced by an equal amount of carbon (oxygen = 15.55% instead of 72.89%, by weight).

The tissue equivalence of some of the new substitutes was tested with cobalt-60 gamma rays in the same way as with protons and neutrons. The field size and SSD employed were 10 cm x 10 cm and 75 cm respectively.

Figure 4.11 shows the results of the comparison of MS/L1, MS/SR4, beef steak and human muscle. On the same graph the results

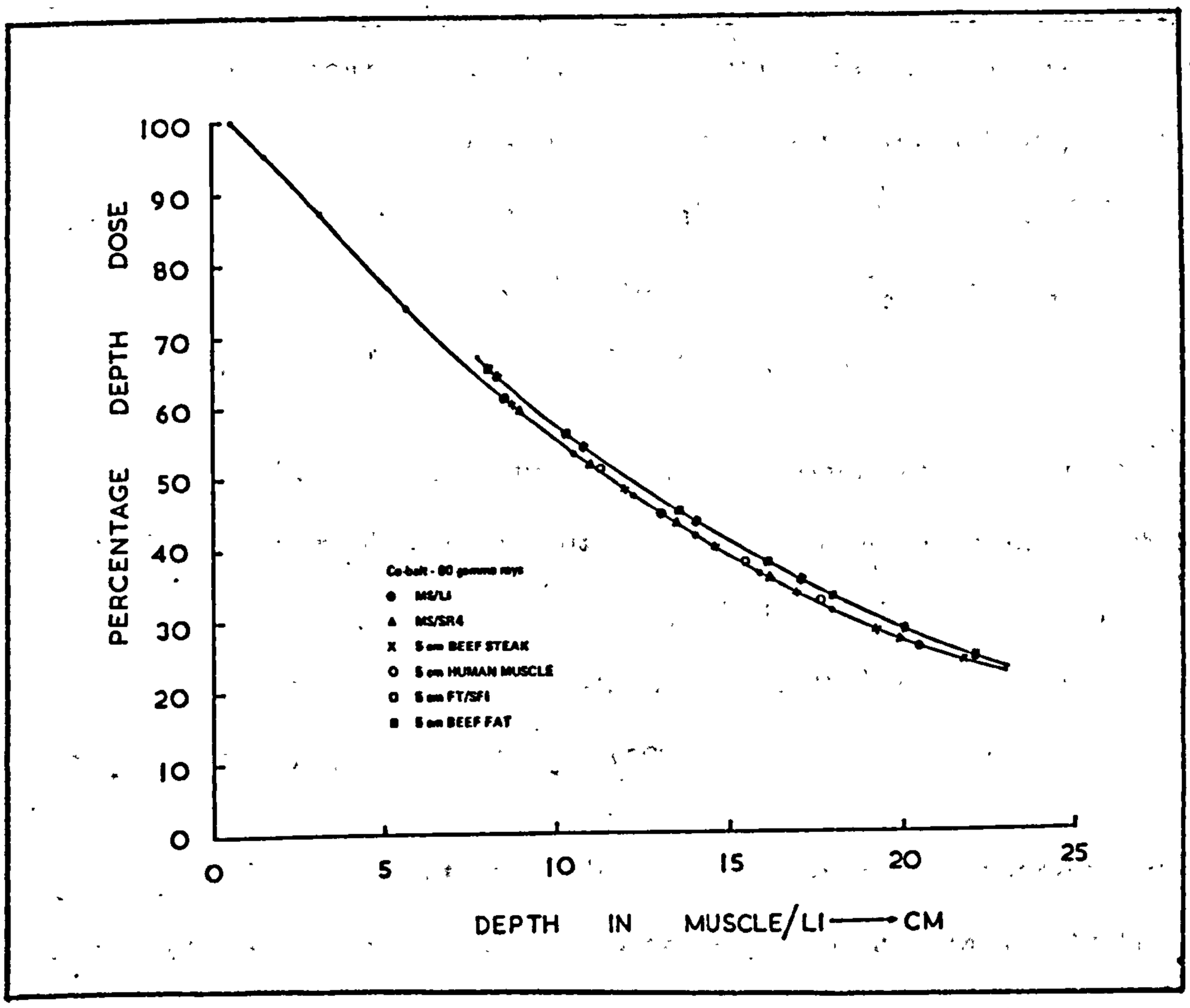

Figure 4.11 Comparison between substitutes and real tissues with cobalt-60 gamma rays

of the comparison of FT/SF1 with beef fat are also given for the same 10 cm x 10 cm field size. It was found that in no case did the readings at the same depth differ by more than 1% which indicates that the simulation of the real tissues at this photon energy is very accurate. However, when cylinders of hard bone substitutes (HB/SF3, HB/SR4) were compared to real human bones of approximately the same shape, the depth dose measured behind the substitutes was up to 2% lower than the dose measured at the same point behind the real bones. The setup and method used in this comparison was the same as that already described in the comparison of bones using fast neutrons (Figure 4.10). The two bone substitutes themselves were found to be within 0.5% of each other.

4.2(iv) 120kVp X-RAYS

The accuracy with which the various substitutes simulate the corresponding real tissues at photon energies below 100 keV (Diagnostic range) was tested using the general purpose EMI CT5005/2085 scanner of the Middlesex Hospital, London, operating at 120 kVp, 33 mA (4.5 mm Al filtration).

The CT-numbers obtained in computerised tomography (CT), for a given photon energy, appear to have a linear relationship with the linear attenuation coefficient (μ) of the material which is reconstructed in each picture element (pixel) (McCULLOUGH et al., 1976, WHITE and SPELLER, 1978).

The derivation of the μ-value from the measured CT-number of the various tissues is needed if these data are to be used in dose calculations for radiotherapy treatment planning. In order to find the exact analytical expression for this relationship and subsequently derive the μ-values from the CT-numbers measured

during a scan, it is necessary to know the effective energy (E_{eff}) of the X-ray beam in use.

The E_{eff} of the X-ray beam of the CT-5005 scanner used, was measured using the "KEVLIQUID" method proposed by WHITE and SPELLER (1978) and was found to be 67 $\pm$0.5 keV. Each of the liquids used is a two-component solution (ethanol + carbon tetrachloride) denoted by keV1. The relative volume of each component is calculated so that the μ-value of each KEVLIQUID equals that of water only at one specific energy (water is used as standard material). In this way, several KEVLIQUIDS can be formulated and used as "keV indicators".

The actual E_{eff} of the X-ray beam can be found by scanning the keV indicators (KEV1/60, KEV1/62, KEV1/64 etc) sequentially and selecting the one that has the same CT-number as water.

In practice, a 20 cm diameter solid phantom was used; the phantom was made of the water substitute WT/SR1. 2.5 cm diameter polypropylene tubes, each filled with one KEVLIQUID, were inserted in a hole of the same diameter drilled at the centre of the phantom and scanned, one at a time. Water was also scanned on its own. After each scan, the mean CT-number and the standard deviation were determined within a circle of radius equal to 5 pixels. The measured CT-numbers were plotted against "indicated keV" and the value E_{eff} = (67 $\pm$0.5)keV was derived from the graph using the CT-number for water; consequently the μ-value, at 67 keV, for each of the KEVLIQUIDS was computed. Table 4-V shows the exact values.

TABLE 4-V MEASURED AND COMPUTED DATA FOR THE KEVLIQUIDS

"Indicated keV" liquids	Measured CT-number	Standard deviation	Computed μ (cm^{-1})
KEV1/60	-26.13	2.40	0.189
KEV1/62	-21.50	2.36	0.191
KEV1/64	-16.80	2.53	0.193
KEV1/66	-11.39	2.35	0.195
KEV1/68	- 6.94	2.53	0.197
KEV1/70	- 2.48	2.30	0.199
KEV1/72	+ 2.43	2.42	0.201
WATER	-10.77	2.30	0.196

A linear relationship of the form $\mu = a_0 + a_1 \times (\text{CT-number})$ was fitted to the data of columns 2 and 4 of Table 4-V using the method of least squares; the equation for the "best fit" straight line was found to be:

$$\mu = 0.1999 + 0.00042 \times (\text{CT-number}) \qquad (4.1)$$

It is evident that these KEVLIQUIDS can also be used to test the linearity of the scanner.

Having established the E_{eff} of the machine and the exact relationship between CT-numbers and μ-values, a series of tissue substitutes were scanned, in turn, using the same phantom and the same machine working conditions; the μ-values for these substitutes, derived from their measured CT-number using equation 4.1, were compared to those of the corresponding real tissues which were calculated from basic elemental data as suggested by WHITE and FITZGERALD (1977). Table 4-VI gives the actual values and in the last column the values of

the coefficient ratios, which indicate the accuracy of simulation at this low energy, are given.

TABLE 4.VI MEASURED AND CALCULATED μ-VALUES FOR SUBSTITUTES AND REAL TISSUES

Real tissue or substitute	Measured CT-number	Standard deviation	$\mu_{exper.}$ (cm^{-1}) (67 keV)	$\mu_{calc.}$ (cm^{-1}) (67 keV)	$\frac{\mu_{subst.exper}}{\mu_{tissue\ calc.}}$
ICRU MUSCLE				0.198	
H_2O	-10.77	2.30	0.195	0.196	0.99
MS/L1	11.68	2.50	0.205	0.205	1.03
MS/SR1	3.05	2.28	0.201	0.200	1.01
MS/SR4	-2.33	2.30	0.199	0.197	1.00
BLOOD (WHOLE)				0.206	
BL/L1	31.99	2.41	0.213	0.201	1.03
BRAIN				0.201	
BRN/L3	5.23	2.23	0.202	0.198	1.00
BRN/L6	9.51	2.23	0.204	0.199	1.01
BRN/SR2	0.13	2.59	0.200	0.200	0.99
HARD BONE				0.497	
HB/SR4	557.68	4.76	0.434	0.413	0.87
SB4	625.95	5.83	0.463	0.478	0.93
WITT'S LIQUID	578.75	4.52	0.443	0.474	0.89
TOTAL SKELETON				0.321	
S.SK/L1	257.60	2.60	0.308	0.292	0.96
T.SK/SF3	248.10	2.70	0.304	0.297	0.95
FAT				0.174	
FT/L1	-79.43	2.50	0.166	0.168	0.96
TOTAL SOFT TISSUE				0.200	
TST/L1	7.61	2.40	0.203	0.200	1.01

The difference between experimental and computed μ-value for the same material is generally of the order of 1-2%, except in the case of hard bone substitutes where the maximum difference was 7%.

CHAPTER 5

THE USE OF THE NEW TISSUE SUBSTITUTES IN DOSIMETRIC INVESTIGATIONS RELEVANT TO RADIOTHERAPY

Beams of X-rays, gamma rays, electrons and neutrons are used in radiotherapy on a routine basis, while clinical trials with high energy protons and negative pions are in progress in various countries. The formulation and manufacture of the new tissue substitutes for particulate radiations, offered the opportunity for dosimetric measurements with these radiation modalities. It also made possible the investigation of the effect of air spaces, lung, fat and bone on the dose distributions in composite phantoms.

Dose distributions were measured in a muscle equivalent liquid (MS/L1), a solid muscle substitute (MS/SR4) and a brain-equivalent liquid (BRN/L6). Since water has been widely used as muscle substitute in the past, measurements were also made in water, so that the difference between muscle and water when the two are used under identical conditions could be investigated. In this chapter, the measurements carried out with beams of 150 MeV protons, 7.5 MeV neutrons, 10 MeV electrons, 70 MeV negative pions and alpha particles of energy up to 5 MeV will be discussed in turn.

5.1 PRE-THERAPEUTIC MEASUREMENTS WITH HIGH ENERGY PROTONS

The physical characteristics of high energy protons have been reviewed by KOEHLER and PRESTON (1972); more recently, ARCHAMBEAU et al., (1974) reviewed the clinical status of proton radiation therapy. The measurement of a number of parameters determining the depth dose distribution of a high energy proton beam

is a necessary pre-requisite of patient treatment. Such measurements would enable a credible and reproducible method of dose administration to be established.

As plans to use the 160 MeV proton beam from the synchrocyclotron of the Atomic Energy Research establishment, U.K., (A.E.R.E) for radiotherapy exist, all the relevant physical parameters of that proton beam were measured during this study. The central axis depth doses, the depth of the Bragg peak, the peak. width, peak/plateau ratio and beam profiles in MS/L1, BRN/L6 and water have been established. The effect of air spaces, lung, fat and bone on the depth doses was also investigated and a simulated patient treatment was attempted, with promising results.

5.1(i) MATERIALS AND METHODS

Protons of (160 $\pm$ 2)MeV were focussed onto a 0.317 cm-thick copper scatterer, from which they emerged having a roughly Gaussian intensity distribution with distance from the beam axis, with a mean energy of about 150 MeV. A transmission ionisation chamber placed in the beam, 10 cm away from the scatterer, was used as beam monitor. The scatterer-phantom distance was 1 metre and the 50% level width of the beam profiles, measured with a silicon diode detector at 0.5 cm and 15.5 cm-depth in water, was 4.8 cm and 6.0 cm respectively.

The detectors used within the phantom could be moved by remote control along the horizontal axis of the beam, as well as laterally and vertically in a plane normal to the beam direction. Figure 5.1 shows a photograph of the setup. The focussing magnets, scatterer, transmission monitor chamber and the detector in the liquid phantom are clearly visible. The detector signals were fed

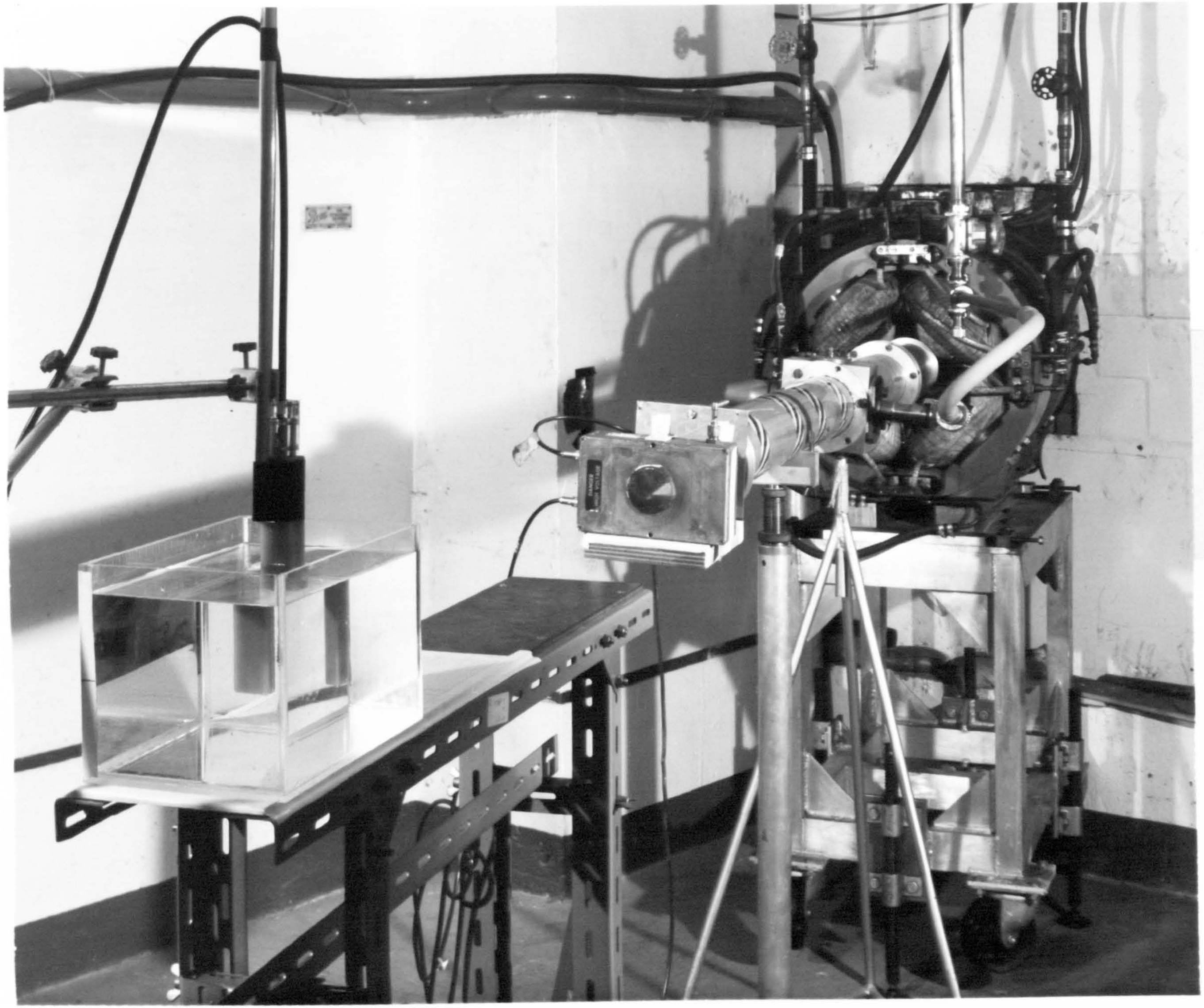

Figure 5.1

The proton beam line and setup used. (160 MeV synchro-cyclotron. A.E.R.E, U.K)

into a KEITHLEY 602 electrometer connected to a digital voltmeter. Whenever the detectors were used in a liquid phantom, they were inserted in special sleeves made of the appropriate solid substitute (bone: HB/SR4, muscle: MS/SR4 or MS/SR1 and brain: BRN/SR2), and machined to the exact shape of the detector. These are illustrated in Figure 5.2. The 0.2 cm^3 cylindrical ionisation chamber was obtained from the Rutherford Laboratory.

The plane parallel plate (flat) ionisation chamber (MC78) also illustrated in Figure 5.2, was made by painting the h.t., guard and collector plates onto strips of a muscle substitute (MS/SR1), using colloidal graphite (dag). It was assembled using a 1 mm-thick strip of Perspex as a spacer. The air-filled collecting volume was formed by removing a 1 cm-diameter section of the spacer. The chamber followed the design used at the Medical College of St Bartholomew's Hospital and described by ELLIS and READ (1969). The outer surface of the stem of this chamber had to be coated with dag which was grounded to eliminate fluctuations of the signal, arising from mains pick-up. A similar chamber made of Perspex (MC38), gave results which agreed within $\pm$ 1% with those of the chamber MC78 described above, provided a density correction was made for the presence of Perspex.

A silicon diode (AERE) was also used at a later stage in this series of measurements; this diode has a surface of about 1 mm^2 and a depletion zone of the order of 0.2 mm-thick and is encapsulated in a disc of epoxy resin (diameter = 1 cm) at a depth of 0.5 mm.

The polarizing voltage used was 250 Volts for the 0.2 cm^3 cylindrical chamber and 300 Volts for the flat chambers and the diode. The alignment of each detector in the beam was generally made by means of vertical and horizontal scans normal to the direction of the

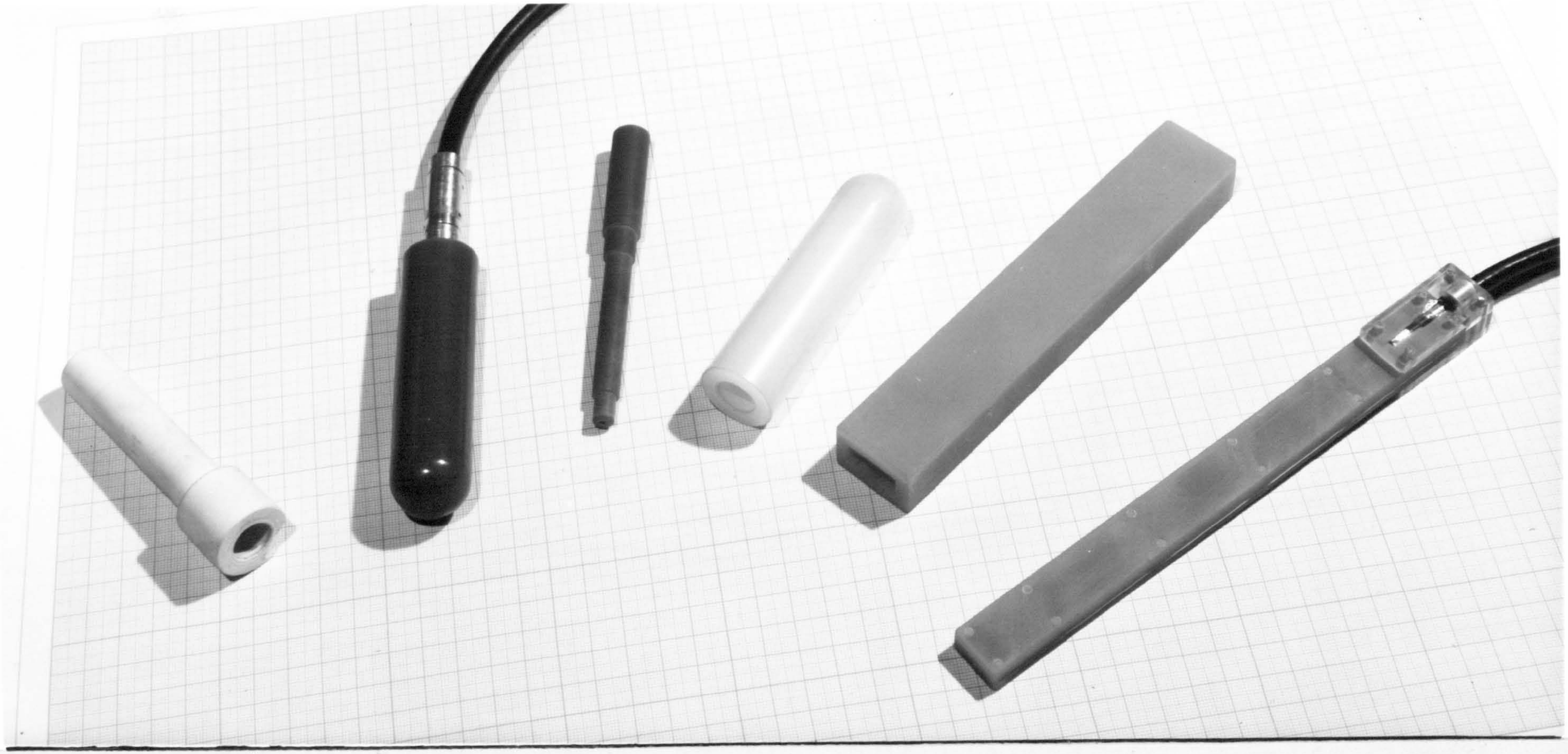

Figure 5.2 From the left: A "bone" sleeve; the 0.2 cm^3 cylindrical ionisation chamber (made of A-150 conducting plastic) in its "muscle" sleeve; a dummy of the cylindrical chamber; a "brain" sleeve and the plane parallel plate ionisation chamber (MC78) with its "muscle" sleeve

beam, except in the case of measurements with the collimated beam, when a paraxial LASER beam was used in addition.

5.1(ii) MEASUREMENTS WITH A SCATTERED BUT UNCOLLIMATED PROTON BEAM

Working with the 150 MeV proton beam described above, the ionisation produced along the central axis of the beam in water, brain equivalent liquid (BRN/L6) and muscle equivalent liquid (MS/L1) was measured with the flat ionisation chamber (Perspex MC38).

In practice, the signal from the chamber was integrated over the time needed for the "monitor" ionisation chamber to collect a preset electric charge of 1×10^{-7}C (scale 1000×10^{-10}C on the integrator).

The results are summarised in Figure 5.3 and Table 5-I.

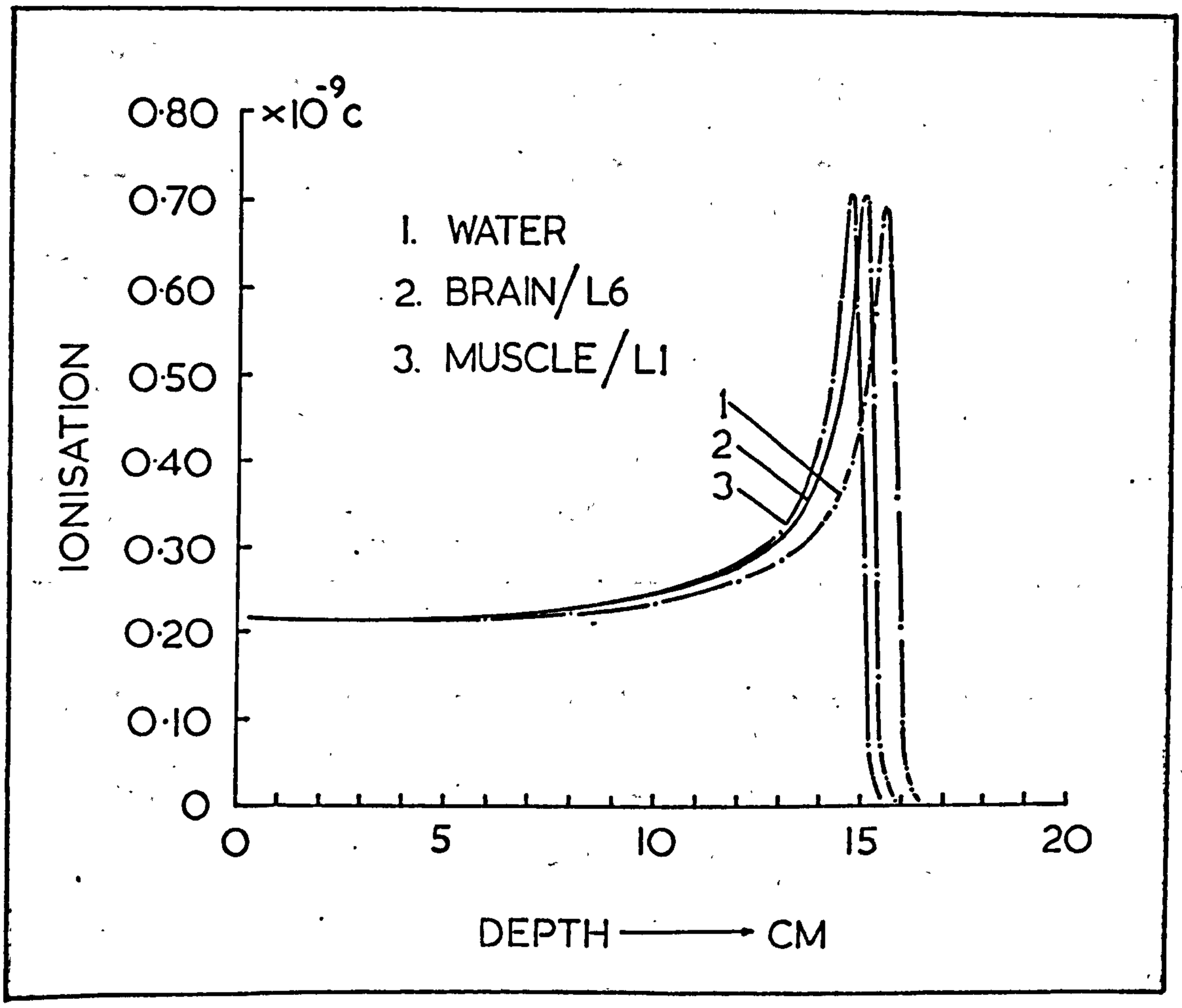

Figure 5.3 Central axis depth dose curves for 150 MeV protons. (Scattered but uncollimated beam)

TABLE 5-I VARIOUS PHYSICAL PARAMETERS OF 150 MeV PROTONS IN MUSCLE, BRAIN AND WATER (SCATTERED BUT UNCOLLIMATED BEAM)

PARAMETER *	MATERIAL		
	MS/L1	BRN/L6	WATER
Depth of peak (cm)	14.73	15.04	15.57
Peak height ($\times 10^{-9}$C)	0.71	0.70	0.68
Range to half maximum (cm)	15.06	15.37	15.92
Extrapolated range (cm)	15.38	15.59	16.20
Full width at 80% level (cm)	0.45	0.45	0.45
Full width at half maximum (cm)	1.50	1.53	1.56
$\frac{\text{Peak}}{\text{entrance}}$ ratio	3.38	3.35	3.26
$\frac{\text{Peak}}{\text{Plateau (5 cm)}}$ ratio	3.29	3.24	3.23
$\frac{\text{Peak}}{\text{Plateau (10 cm)}}$ ratio	2.90	2.91	2.93
Drop 100 → 20% (distance in cm)	0.45	0.46	0.47

* 1. Correction for the presence of the Perspex wall of the tank applied.

2. Entrance value obtained by extrapolation of the curve to "zero depth".

The effect of hard bone and fat on the depth of the Bragg peak, the peak height, the range and the other physical parameters was investigated by introducing various thicknesses of the tissue heterogeneity in muscle equivalent liquid. In order to investigate the effect of lung, a composite phantom consisting of 3 cm-thick solid muscle substitute (MS/SR4) and then various thicknesses of lung followed by muscle equivalent liquid (MS/L1 in the Perspex tank), was used, as Figure 5.4 indicates (the effect of fat is shown in Figure 4.5). Table 5-II gives a summary of the results.

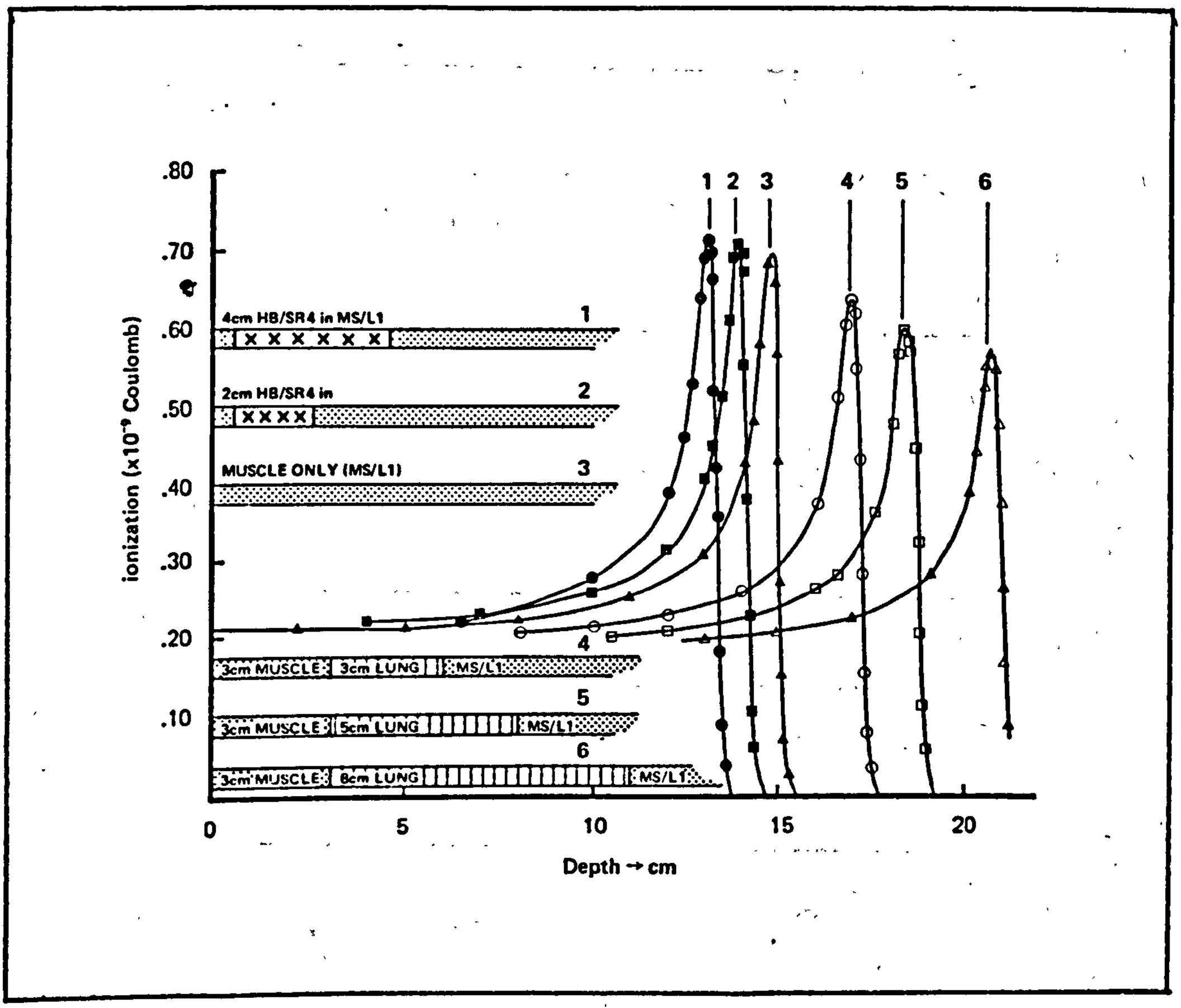

Figure 5.4 Effect of hard bone and lung on the central axis depth dose curve of 150 MeV protons.

TABLE 5-II EFFECT OF THE PRESENCE OF LUNG, FAT AND BONE IN MUSCLE, ON THE PHYSICAL PARAMETERS OF A 150 MeV PROTON BEAM

PARAMETER *	MATERIALS - SETUP					
	2 cm HB/SR4 - MS/L1	4 cm HB/SR4 - MS/L1	5 cm FT/SF1 - MS/L1	3 cm MS/SR4 - 3 cm LN/SR4 - MS/L1	3 cm MS/SR4 - 5 cm LN/SR4 - MS/L1	3 cm MS/SR4 - 8 cm LN/SR4 - MS/L1
Depth of peak(cm)	13.88	13.08	15.28	16.93	18.43	20.68
Peak height(x 10^{-9} C)	0.72	0.73	0.68	0.65	0.61	0.58
Range to half maximum (cm)	14.20	13.38	15.58	17.26	18.78	21.08
Extrapolated range (cm)	14.43	13.63	15.83	17.48	19.04	21.38
Full width at 80% level (cm)	0.50	0.50	0.45	0.52	0.53	0.54
**FWHM (cm)	1.50	1.50	1.50	1.70	1.80	1.90
Peak/plateau(5 cm)	3.18	3.22	-	-	-	-
Peak/plateau(10 cm)	2.75	2.58	2.85	2.97	3.02	2.94
Drop 100 → 20% distance in cm	0.48	0.40	0.40	0.45	0.50	0.55

* Correction for the presence of Perspex applied

** FWHM = Full width at half maximum

Because of the importance of the effect of skull bone on the depth of the Bragg peak when such a proton beam is used for the treatment of the pituitary gland or any brain tumours, various thicknesses of hard bone and total skeleton substitutes were immersed in brain equivalent liquid (BRN/L6), touching the front wall of the Perspex tank (15 cm x 15 cm x25 cm) and the scans along the central axis of the beam in the brain liquid were repeated. Figure 5.5 and Table 5-III give the relevant data.

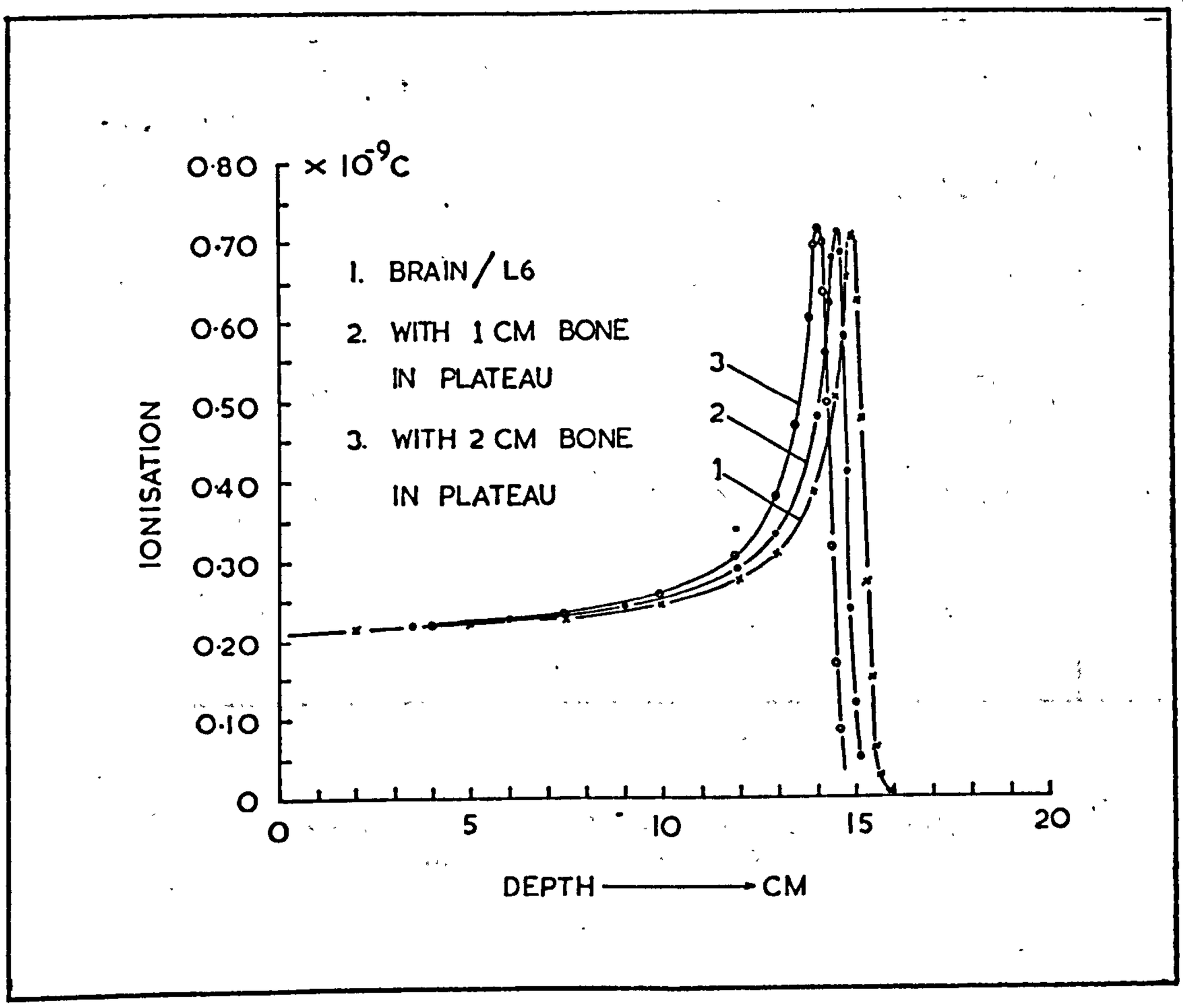

Table 5.5 The effect of bone on the central axis depth dose curve of 150 MeV protons in a brain equivalent liquid

TABLE 5-III EFFECT OF BONE ON THE DOSE DISTRIBUTION FROM 150 MeV PROTONS IN BRAIN

PARAMETER *	MATERIALS - SETUP			
	BRN/L6	1 cm HB/SR4 - BRN/L6	2 cm HB/SR4 - BRN/L6	2 cm TSK/SF3 - BRN/L6
Depth of peak (cm)	15.04	14.59	14.14	14.59
Peak height ($\times 10^{-9}$C)	0.70	0.71	0.72	0.71
Range to half maximum (cm)	15.37	14.90	14.45	14.91
Extrapolated range (cm)	15.59	15.11	14.69	15.19
Full width at 80% level (cm)	0.45	0.50	0.45	0.46
FWHM (cm)	1.53	1.54	1.60	1.65
$\frac{\text{Peak}}{\text{entrance}}$ ratio	3.35	3.38	3.40	3.38
$\frac{\text{Peak}}{\text{Plateau (5cm)}}$ ratio	3.24	3.18	3.19	3.20
$\frac{\text{Peak}}{\text{Plateau (10 cm)}}$ ratio	2.91	2.84	2.79	2.85
Drop 100 → 20% (distance in cm)	0.46	0.46	0.48	0.50

* Correction for the presence of Perspex (front wall of tank and front plate of chamber MC38) applied

As the pituitary gland is situated in the bony structure of the pituitary fossa (sella turkika), the effect of bone being very close to the detector was investigated; a "bony sleeve" was made for the 0.2 cm^3 cylindrical ion chamber which had a uniform thickness of 0.5 cm all round the sensitive volume of the detector (see Figure 5.2). The depth of the peak in MS/L1 was found to be 1 mm less than it was with the "muscle sleeve for the detector and 0.5 cm-thick slab of the same bone substitute (HB/SR4) placed in the plateau region". It was assumed that the extra 1 mm reduction of the peak depth observed was due to backscatter from the back half of the "bone" sleeve. The measurement was repeated with another sleeve whose back half was HB/SR4 (hard bone) and the front half MS/SR4 (muscle). Again the depth of the peak and the extrapolated range were found to be approximately 1 mm smaller than those in the "muscle only" situation, which indicated the presence of some backscatter from the 0.5 cm-thick bone behind the sensitive volume of the ionisation chamber. The observed reduction in peak depth is possibly due to a change of the effective measuring position in the cylindrical volume of the chamber. This is discussed later in this chapter.

The presence of air pockets in the path of the proton beam causes a distal shift of the Bragg peak in a phantom. Two polypropylene tubes, closed at both ends, with internal diameters 1.6 cm and 2.5 cm respectively were introduced, in turn, in the plateau region so that their long axis was perpendicular to the axis of the proton beam. On both occasions, the scans along the central axis of the beam showed a distal movement of the peak by 0.9t (t = diameter of air tube). The observed reduction in the peak height, was more than the inverse square law would predict by about

10% of the peak height in muscle. This is probably because the muscle liquid in front of the air space acts as a second scatterer; this combined with the presence of the air space (i.e. extra distance to be travelled) result in a further spreading of the proton beam and so the number of protons per unit area in the peak region, on which the peak height depends, becomes smaller than it would have been without the presence of air in the beam.

In order to study the effect of differences in chemical composition of the various tissue substitute materials, the depth of the Bragg peak and the extrapolated range in water, BRN/L6 and MS/L1 were multiplied by the density of each material, to obtain the "equivalent thickness" of both the peak depth and the extrapolated range in g/cm^2. In this way, the effect of differences in density between the various materials is eliminated (density correction). In the case of composite phantoms, the path length in each type of substitute material was multiplied by the corresponding density to derive the "total equivalent thickness" in g/cm^2. The relevant data are given in Table 5-IV.

TABLE 5-IV BRAGG PEAK DEPTH AND EXTRAPOLATED RANGE - EQUIVALENT THICKNESS IN VARIOUS MATERIALS

Materials	Equivalent thickness of peak depth (g/cm^2)	Equivalent thickness for extrapolated range (g/cm^2)
Water	15.57	16.20
BRN/L6	15.64	16.22
MS/L1	15.76	16.45
3 cm MS/SR4) + 8 cm LN/SR4) + MS/L1)	15.88	16.55
5 cm FAT + MS/L1	15.60	16.19
4 cm HB/SR4 + MS/L1	16.38	16.97

The conclusion from this analysis is that, after correcting for density, only a very small variation in peak depth equivalent thickness remains to be accounted for. This variation could be attributed to the differences in chemical composition among the tissue substitutes considered. Fat is probably the most effective in stopping protons, on a gram for gram basis, because of its higher hydrogen content. The depth of the Bragg peak (in g/cm^2) in a "5 cm fat + muscle" phantom is about 1% smaller than that in muscle alone.

When "4 cm-thick hard bone + muscle" is considered, the peak depth equivalent thickness is found to be 4% larger than that in "muscle alone"; in other words, despite its higher density, hard bone is less effective in stopping protons than muscle, on a gram for gram basis (low hydrogen content in hard bone).

To summarise, a density correction is adequate for calculating the peak depth in a given phantom from measurements in water except when lung or thick bones are present.

The peak height is increased by about 0.5% per cm of bone present in the path of the protons, while it is reduced by about 2.5%-3.0% per cm of lung and by about 0.6% per cm of fat traversed.

For clinical purposes one needs to have certain measured data and a set of "isodose shift" factors to correct the dose distribution for the presence of heterogeneities. Such correction factors have been derived during this work and are given in Table 6-I of next chapter.

5.1(iii) MEASUREMENTS WITH A SCATTERED AND COLLIMATED PROTON BEAM

The advantage of proton beam therapy lies in the narrow well-defined beams which can be obtained by collimating the scattered beams. However, the plateau shape, the width and height of the Bragg peak and the peak/plateau ratio are modified when the proton beam is collimated. These effects were measured using the 150 MeV scattered proton beam described above but collimated with a 10 cm x 10 cm x 3.7 cm block of brass which had a 0.7 cm diameter hole at its centre. This collimator was positioned between the beam monitor ion chamber and the phantom, and 3 cm in front of the latter. The intensity distribution of the collimated beam when it entered the phantom was essentially uniform.

Central axis depth doses and beam profiles in a plane normal to the beam direction were measured at various depths in water, brain equivalent liquid (BRN/L6) and muscle equivalent liquid (MS/L1). Figure 5.6 shows the central axis "depth-ionisation" curves obtained from measurements in the above liquids, using the 0.2 cm^3 cylindrical ionisation chamber. By using the appropriate calibration factor, the percentage depth doses can be derived from these curves. Table 5-V gives the results of the above measurements. The results from scans along the central axis of the beam in water and BRN/L6 using the silicon diode of the AERE are also shown in this Table for comparison.

Central axis depth dose scans with mixed materials were also carried out in the collimated proton beam, to determine the effect of various thicknesses of bone on the depth dose distributions in muscle and brain. The results agreed with those obtained with the uncollimated proton beam of the same energy, i.e. a proximal displacement of the Bragg peak by 4 mm per cm of hard

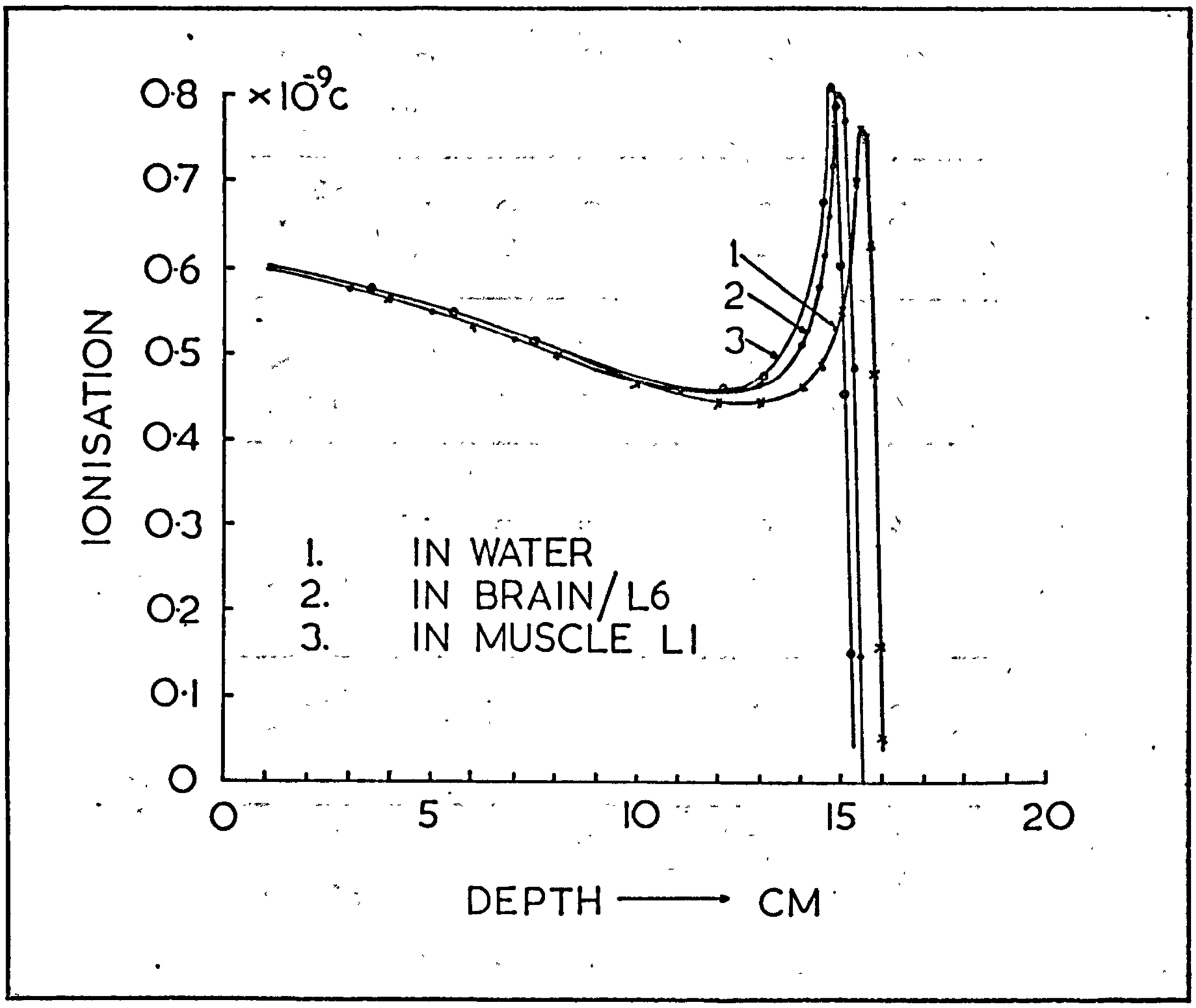

Figure 5.6 Central axis depth dose curves with a 150 MeV scattered and collimated proton beam (0.2 cm^3 cylindrical ion chamber

bone traversed in the case of muscle equivalent liquid behind the bone, and 4.5 mm per cm of hard bone in the case of brain equivalent liquid behind the bone.

Figure 5.7 shows part of an isodose map of the 7 mm diameter collimated beam used, derived from measurements with the 0.2 cm^3 cylindrical ionisation chamber in the brain equivalent liquid BRN/L6. Although the silicon diode was found to give better spatial resolution, as it is expected from its size, it was also found to have a response which changes with depth in the phantom (i.e. with energy of the beam); for this reason the beam profiles obtained with the

TABLE 5-V RESULTS OF MEASUREMENTS IN A 150 MeV SCATTERED AND COLLIMATED PROTON BEAM

Detector	Material	Peak depth cm	Peak depth g/cm^2	Range to half maximum cm	Range to half maximum g/cm^2	Extrapolated range cm	Extrapolated range g/cm^2	Peak height $\times 10^{-9}$C	Full width at the 70% level (mm)	Peak / Plateau (5 cm)	Peak / Plateau (10 cm)	100 → 20% (cm)
0.2 cm^3 cylindrical ion chamber	Water	15.55	15.55	15.96	15.96	16.18	16.18	0.76	0.75	1.39	1.64	0.50
	BRN/L6	15.04	15.60	15.39	15.97	15.64	16.20	0.80	0.80	1.46	1.70	0.50
	MS/L1	14.76	15.79	15.13	16.19	15.41	16.49	0.81	0.75	1.46	1.70	0.50
silicon diode	Water	15.31	15.31	15.66	15.66	15.90	15.90	0.28	0.75	1.56	1.74	0.50
	BRN/L6	14.75	15.28	15.10	15.70	15.30	15.95	0.30	0.75	1.67	1.84	0.45

$0.2\ cm^3$ chamber were used. When the $\frac{\text{ion chamber signal}}{\text{silicon diode signal}}$ ratio was measured at a later stage, the readings from the silicon diode's transverse scan at a depth of 5 cm in BRN/L6 were corrected and expressed as a percentage of the maximum peak height. The full width of this corrected beam profile at the 20% level (= width of the 20% isodose at that depth), was about 1 mm smaller than the width obtained with the $0.2\ cm^3$ ion chamber.

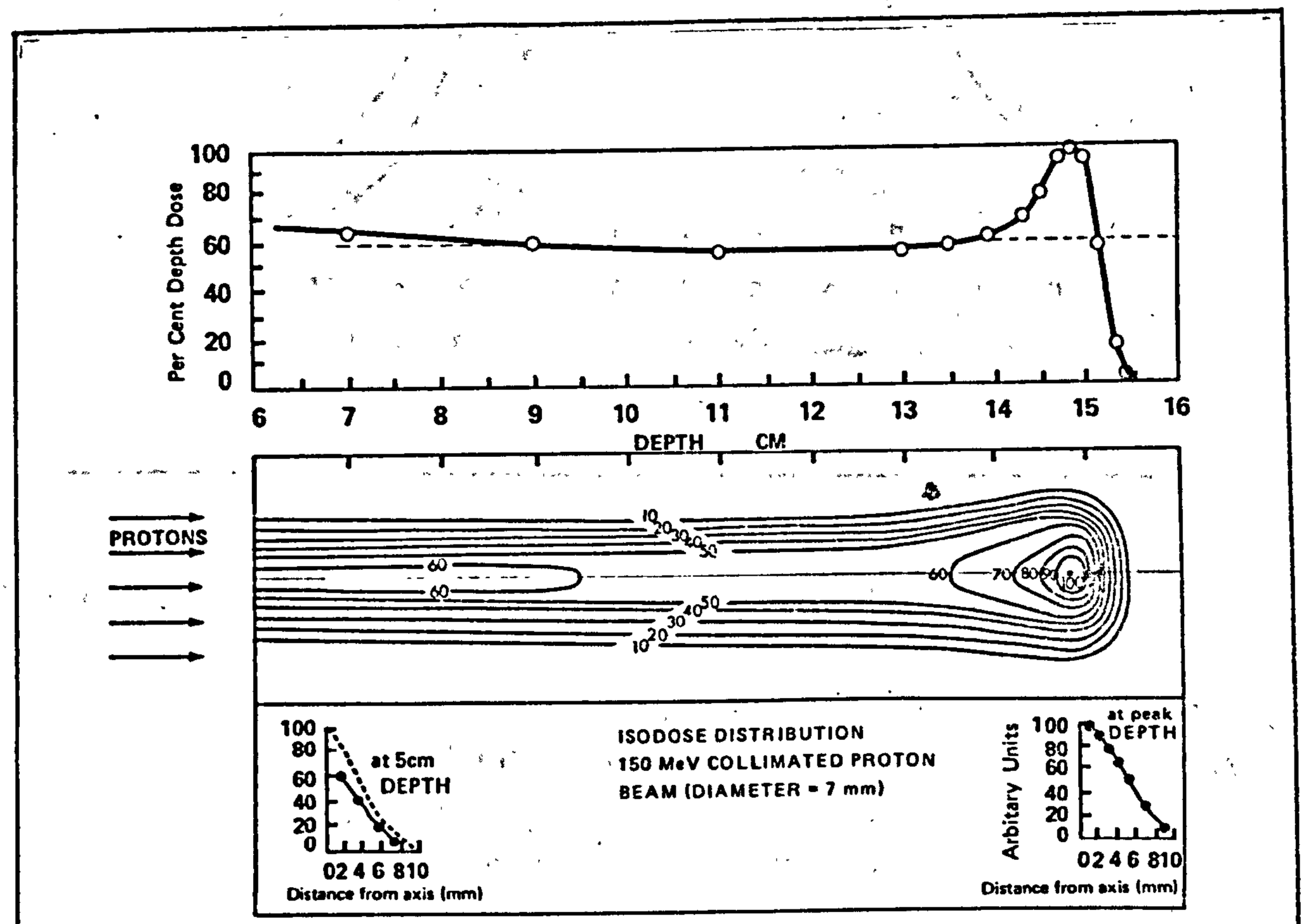

Figure 5.7 Part of the isodose map of the 150 MeV collimated (0.7 cm diameter) proton beam of the AERE, U.K.

The effect of the different chemical composition and density of various materials on the scattering of the collimated proton beam was also investigated. Figure 5.8 shows the beam profiles at the depth of the Bragg peak in BRN/L6, measured with

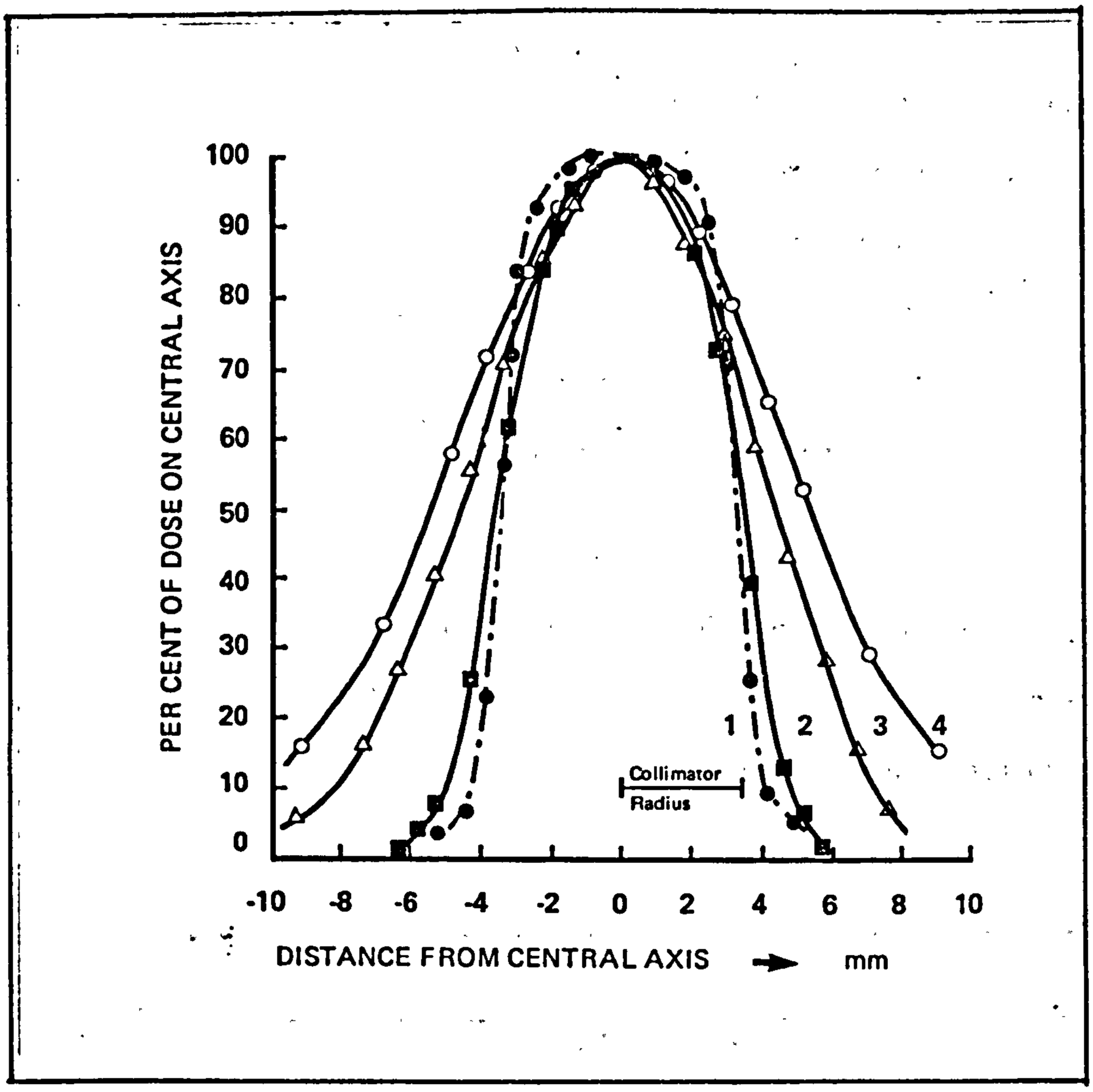

Figure 5.8 Profiles of the collimated proton beam.

1) In air, 7 cm from the collimator (silicon diode)
2) In air, 18 cm from, the collimator(silicon diode)
3) In BRN/L6, at the depth of the peak(silicon diode)
4) In BRN/L6, at the depth of the peak (0.2 cm^3 cylindrical ionisation chamber)

the AERE silicon diode (3) and with the 0.2 cm^3 cylindrical ionisation chamber (4). The profiles of the beam in air, at distances of 7 cm and 18 cm from the collimator (1 and 2 respectively), obtained with the diode, are given for comparison.

The silicon diode was used to measure the beam profiles behind various thicknesses of fat, muscle and bonesubstitutes. The diode was moved vertically (i.e. normal to the beam axis), in air, 2 cm behind the absorber. The results are summarised in Figures

5.9 and 5.10. Figure 5.9 shows the beam profiles behind 5 cm, 10 cm and 13 cm of MS/SR4 (muscle's relative density = 1.06) and 10 cm HB/SR4 (relative density = 1.67); the width of the beam profile (and particularly at the 60% level where the derivative is a maximum), is considered as a measure of the beam scattering and depends on the type and the thickness of the material traversed by the proton beam.

Figure 5.10 shows that as the absorber thickness is increased, the beam is broadened but the effect of the differences in chemical composition between the various materials is not evident.

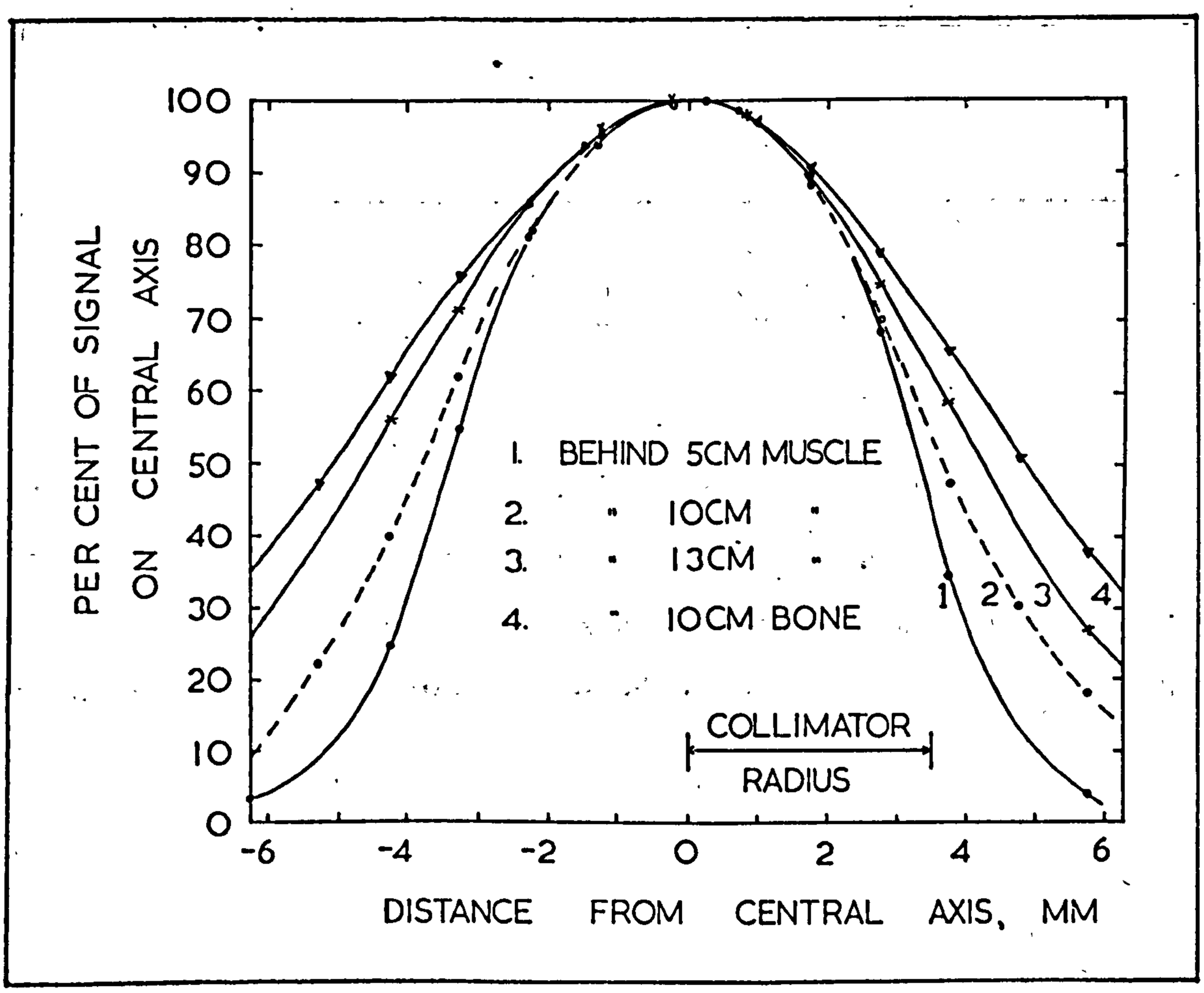

Figure 5.9 Beam profiles behind samples of muscle and bone substitutes

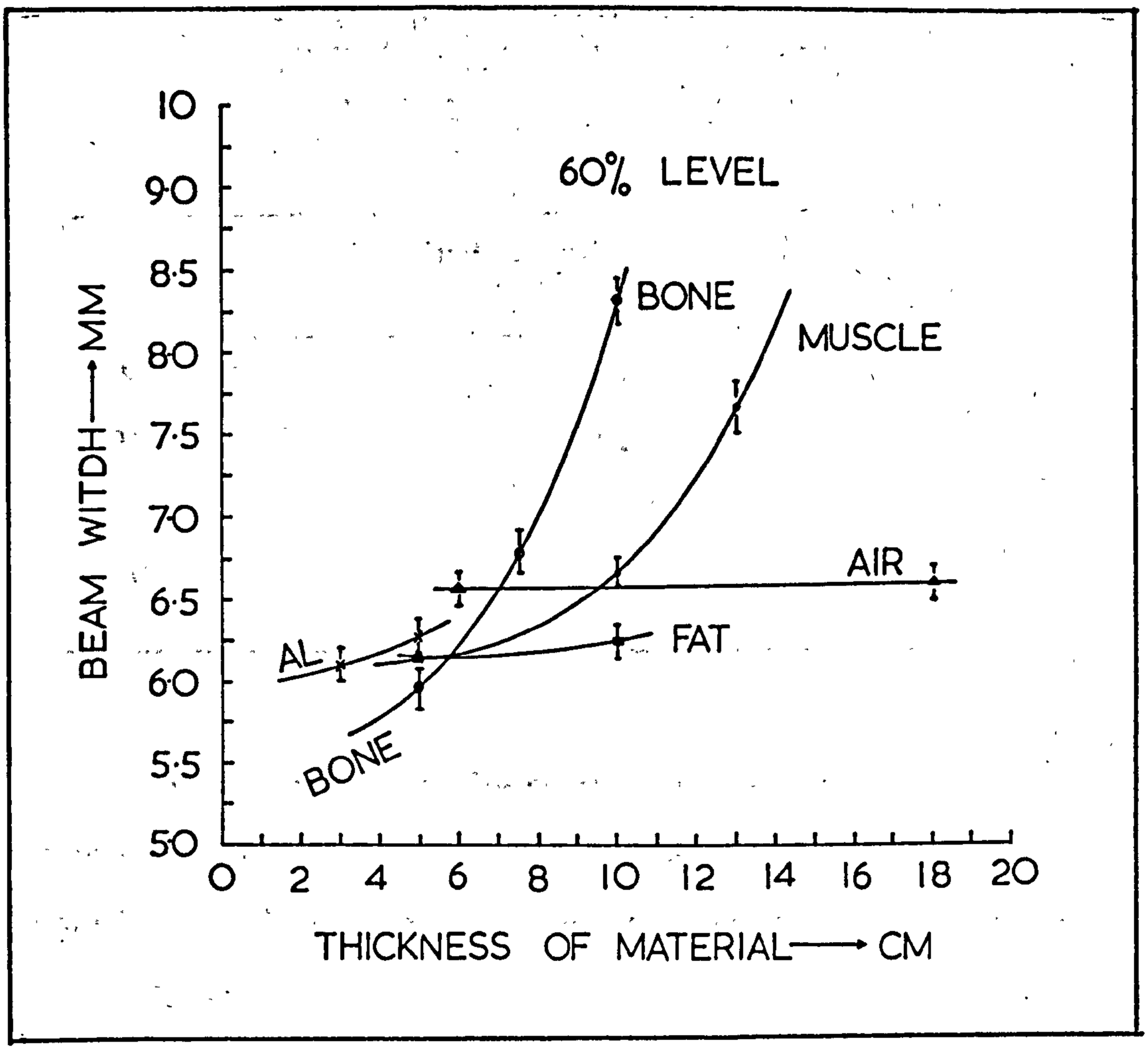

Figure 5.10 Variation of beam profile width with thickness of absorber, for various materials

By multiplying the thickness of each material by its density and looking at the beam width that corresponds to the same "equivalent thickness" of each material, for example 10 g/cm^2, one finds that muscle causes more scattering than any other material (see Table 5-VI).

TABLE 5-VI BEAM PROFILE WIDTH AT THE 60% LEVEL FOR THE SAME EQUIVALENT THICKNESS OF VARIOUS MATERIALS

Material	Profile width for 10 g/cm^2 of absorber (mm)
MS/SR4	6.55
HB/SR4	6.35
FT/SF1	6.30
Al	6.10

From the results of the measurements presented in this section a comparison between the collimated and uncollimated 150 MeV proton beam used was made and revealed the following (in summary).

a) By comparison with the uncollimated proton beam, the peak height is reduced when the beam is collimated. Using the 0.2 cm^3 cylindrical ion chamber, for example, the peak height in water was found 2.22×10^{-9}C for the uncollimated beam and 0.76×10^{-9}C for the collimated beam.

b) The $\frac{\text{Peak}}{\text{Plateau (10 cm)}}$ ratio in water is reduced from 1.85 for the uncollimated to 1.64 for the collimated proton beam (0.2 cm^3 ion chamber).

c) The width of the Bragg peak and the slope of the post-peak part of the depth dose curve do not change significantly.

5.1 (iv) COMPARISON BETWEEN SILICON DIODES AND IONISATION CHAMBERS USED IN PROTON DOSIMETRY-EFFECTIVE MEASURING POSITION FOR A CYLINDRICAL IONISATION CHAMBER

Small silicon diodes can be used as detectors for particulate radiations but radiation damage limits their application to low intensity beams (a few nanoamperes). The plan to plot isodose curves of the proton beam used in this work in various tissue equivalent materials, prompted a comparison between the silicon diode available at the AERE and the three air-filled ionisation chambers described in section 5.1(i), namely two plane parallel plate ionisation chambers (MC38 and MC78) and a 0.2 cm^3 cylindrical ionisation chamber.

All four detectors were used, in turn, to measure the depth dose distribution in a water phantom. Beam profiles were measured in the plateau and the peak region and used for the alignment of the detector in each case. The agreement between the two flat ionisation chambers was very good; after the necessary corrections for the presence of Perspex (of which the MC38 is made), the differences in the various parameters measured by the two chambers were smaller than 0.5% of the corresponding average value. Figure 5.11 shows the "relative ionisation versus depth" curves for the MC78 plane parallel plate (flat) ionisation chamber (1), the 0.2 cm^3 cylindrical chamber (3) and the silicon diode (2), obtained by scanning along the central axis of the uncollimated proton beam, in water. The signal of the 0.2 cm^3 chamber was divided by 4 in order to read on the same scale.

A similar comparison was made between the 0.2 cm^3 cylindrical chamber and the silicon diode in water, using the 0.7 cm-diameter collimated beam. The relevant data are summarised

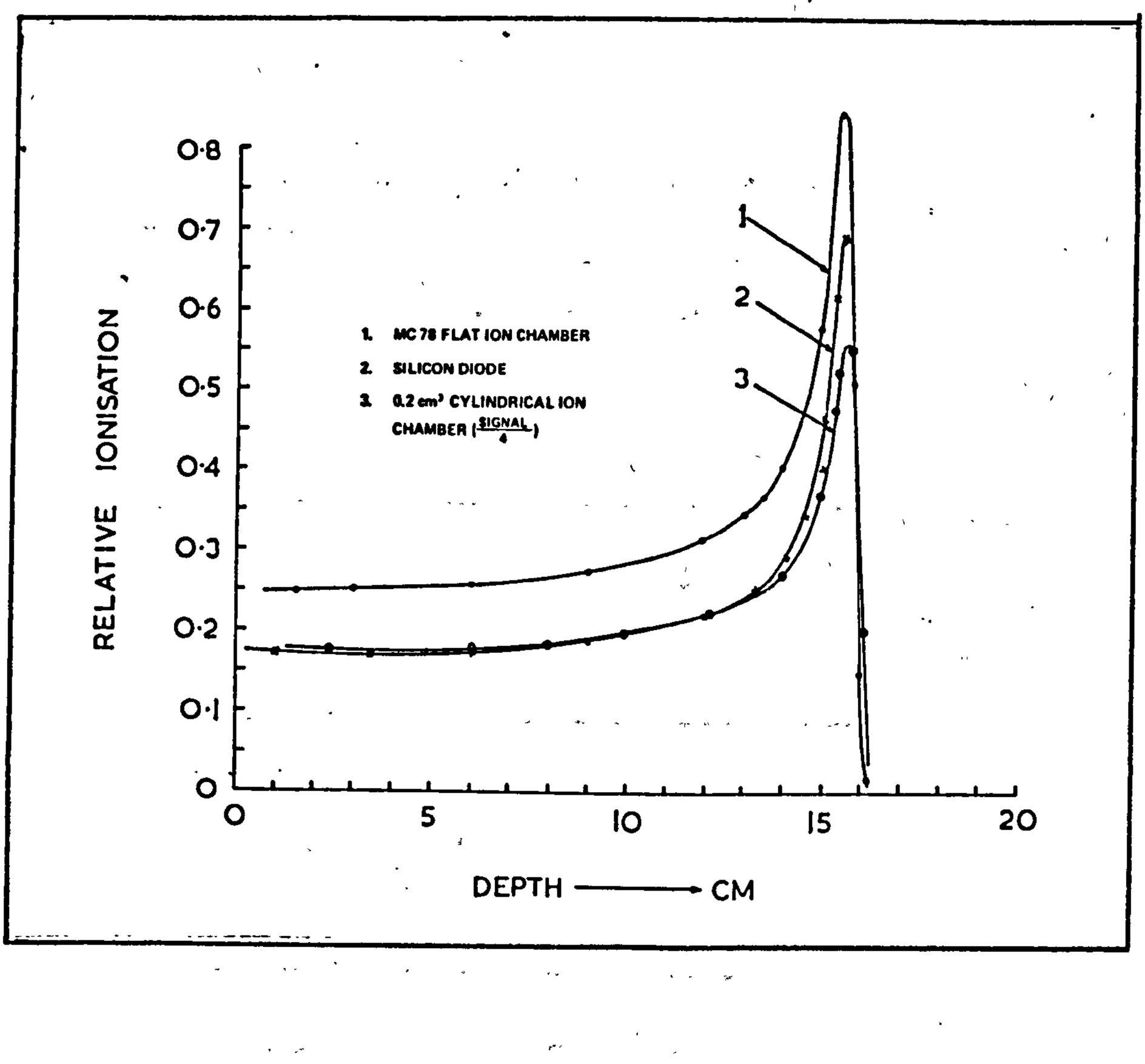

Figure 5.11 Central axis "relative ionisation versus depth" curves for 150 MeV protons in water, measured with three different detectors.

in Table 5-VII. These measurements indicated that the silicon diode has better spatial resolution than the ionisation chambers used in this work, but that its response varied with depth (hence proton energy). Secondly, the effective point of measurement in the cylindrical ionisation chamber is neither at the front face nor at the centre of the sensitive volume of the chamber but in between the two. Table 5-VII (and Figure 5.17) also indicate that the depth of the peak and the extrapolated range of the collimated beam used, were about 2 mm smaller than those of the uncollimated beam. The above observations are discussed in turn.

TABLE 5-VII COMPARISON OF THREE DETECTORS, IN WATER. COLLIMATED VERSUS UNCOLLIMATED PROTON BEAM

Scattered 150 MeV proton beam	Detector	Peak depth (cm)	Extrapolated range (cm)	Peak height x 10^{-9}C	Peak / Plateau(10 cm)	Full width at the 70% level (cm)
Uncollimated	Silicon diode	15.56	16.15	0.69	3.54	0.70
	Flat ion chamber (MC78)	15.57	16.17	0.84	2.99	0.80
	0.2 cm^3 cylindrical ion chamber	15.70	16.31	2.22	2.85	0.80
Collimated	Silicon diode	15.31	15.90	0.28	1.74	0.70
	0.2 cm^3 cylindrical ion chamber	15.55	16.18	0.76	1.64	0.80

* Drop 100 ⟶ 20% within 0.45-0.50 cm in all occasions

** All values corrected for the presence of the Perspex tank front wall

The most probable reason for the difference in the peak depth and extrapolated range values between the collimated and uncollimated beam, would be a small variation in the energy of the proton beam. The measurements with the collimated beam were made on a different day, with slightly modified "beam focus conditions". Consequently, a change of about 1 MeV in the energy of the proton beam, enough to account for the above discrepancy, would be possible.

The improved spatial resolution of the silicon diode is due to its smaller area (about 1 mm^2); the ionisation chambers integrate their signal over a wider area (about 36 mm^2 for the 0.2 cm^3 cylindrical chamber and about 80 mm^2 for the two plane parallel plate ionisation chambers). No convincing explanation has been found, however, for the variation of the diode's response with proton energy. Figure 5.12 shows the variation of the ratio $\frac{\text{ion chamber signal}}{\text{silicon diode signal}}$ for the three detectors under discussion. (Note that the ratio $\frac{\text{MC78 chamber signal}}{\text{silicon diode signal}}$ was multiplied by 2.5 in order to read on the same scale).

KOEHLER (1967) also worked with ionisation chambers and silicon detectors and investigated the possibility of columnar recombination in the ion chamber by varying the bias voltage. He concluded that recombination in the ion chamber is not the cause of the variation in the signal ratio. He also found that pre-exposing the diodes to massive doses ($\sim 10^6$ rads) of radiation, reduces the change in their sensitivity during subsequent use at low beam intensities.

Other reasons which could be partly responsible for the above effect are a change in the energy needed per ion pair in the diode (W-value for silicon $\simeq$3,6eV), or excitation of the crystal lattice or nuclear interactions, the possibility of which increases

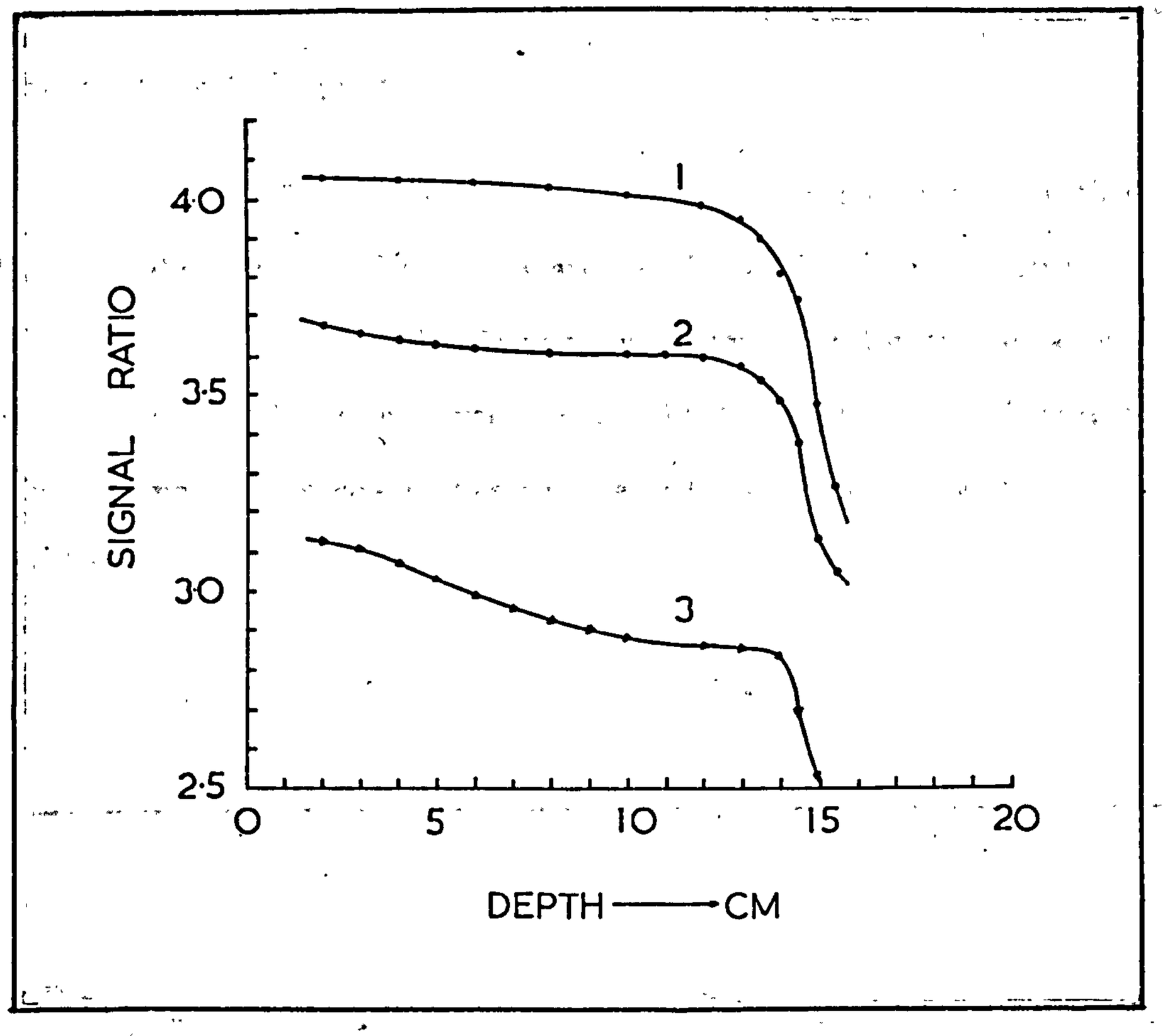

Figure 5.12 Variation of the ratio

$$\frac{\text{ion chamber signal}}{\text{silicon diode signal}}$$

with depth in water

A) Uncollimated beam:

1) $\frac{0.2\ cm^3 \text{ cylindrical chamber signal}}{\text{silicon diode signal}}$

2) $\frac{\text{MC78 flat ion chamber signal}}{\text{silicon diode signal}} \times 2.5$

B) Collimated beam (0.7 cm diameter)

3) $\frac{0.2 cm^3 \text{ cylindrical chamber signal}}{\text{silicon diode signal}}$

as the protons slow down. Whatever the reason, the sensitivity of the silicon diode is reduced in the plateau region where the energy of the protons is higher.

Figures 5.13 and 5.14 illustrate our measurements with the silicon diode of the AERE in water and BRN/L6 respectively. The beam profiles show the progressive broadening of the beam as the depth in the phantom increases. At the depth of the Bragg peak the beam profile approximates in shape to a Gaussian (normal) distribution.

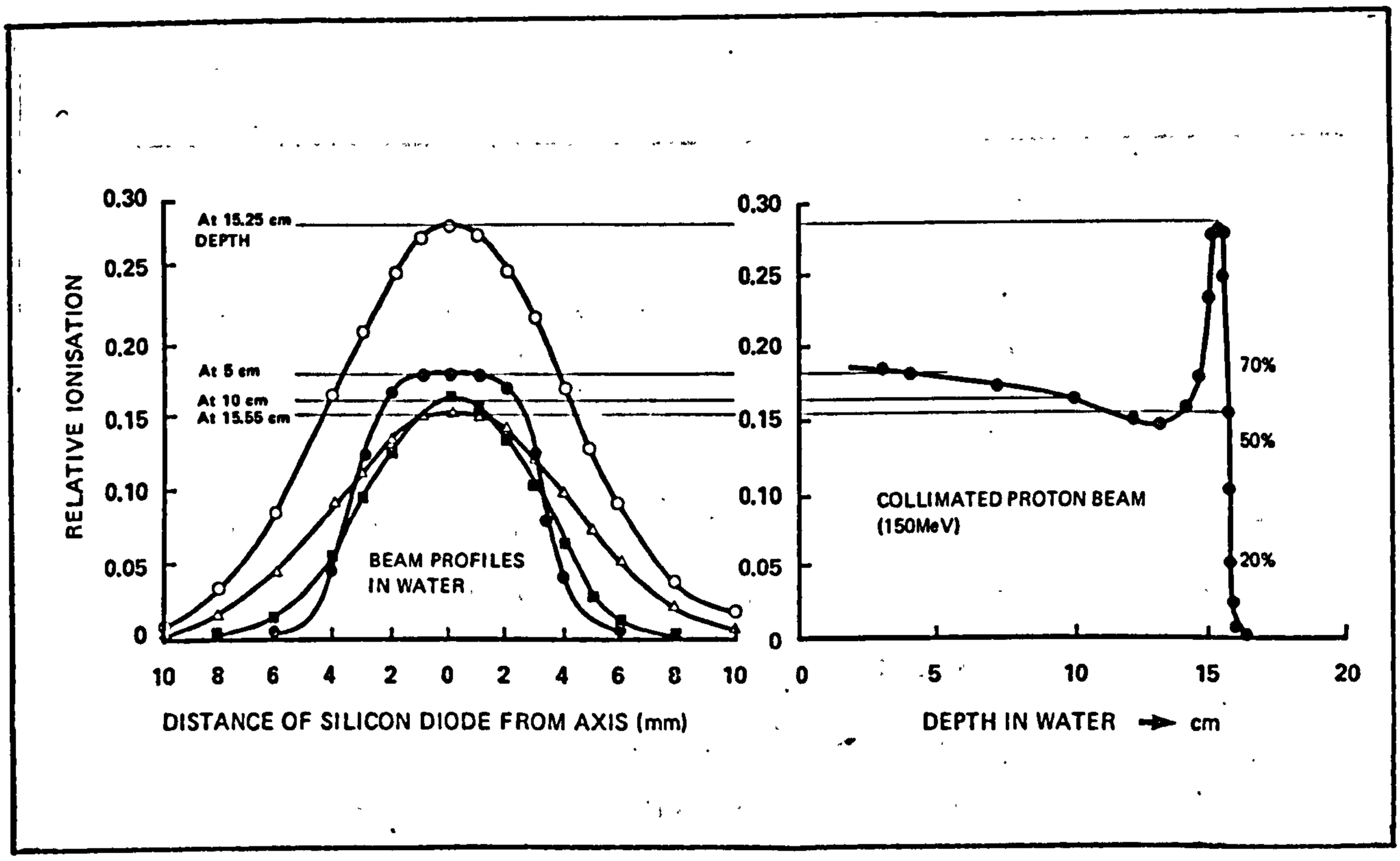

Figure 5.13 Variation of beam width and diode signal with depth in water

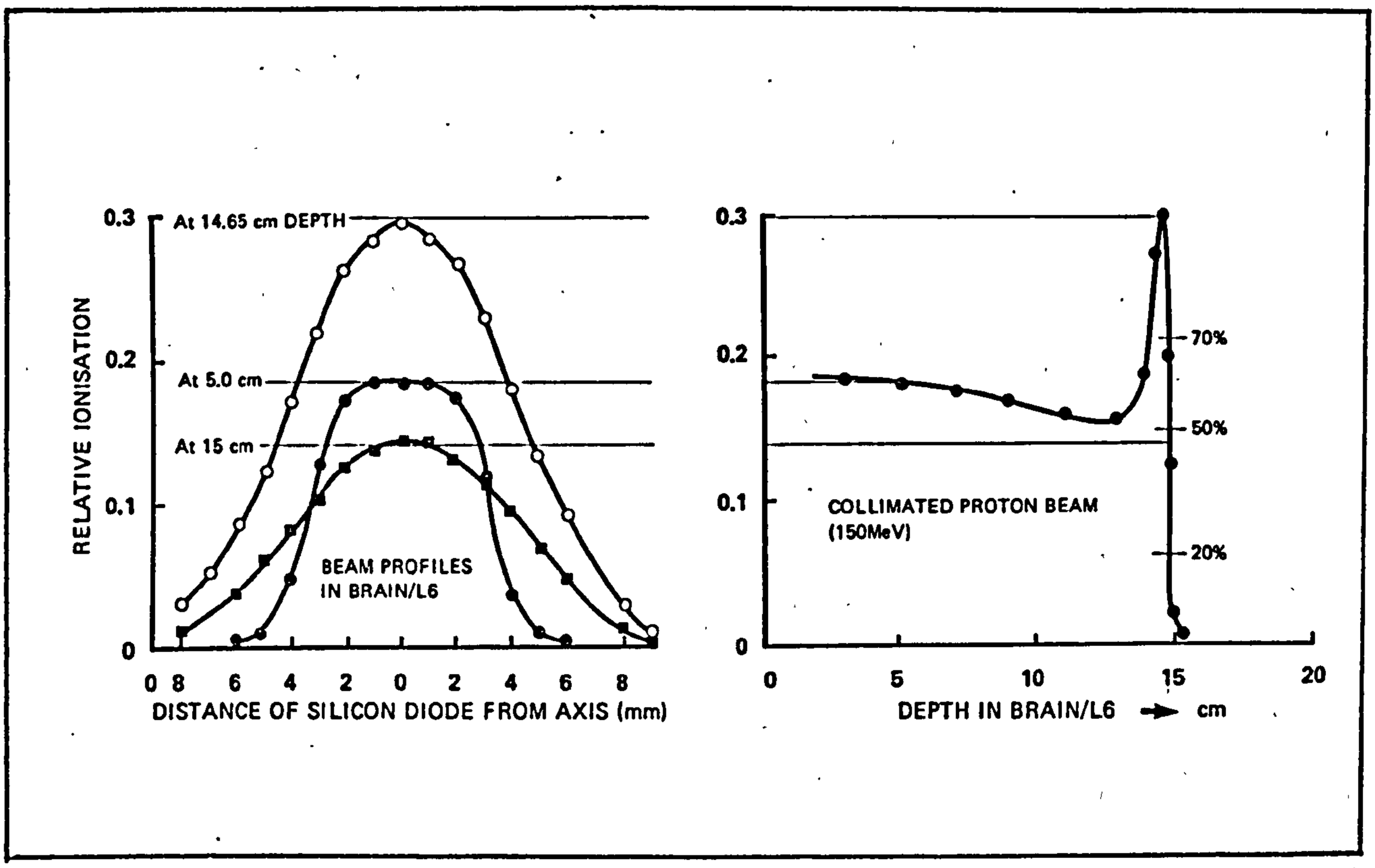

Figure 5.14 Variation of beam width and diode signal with depth in a brain equivalent liquid

The effective measuring position for the 0.2 cm^3 ion chamber was found to be different in the collimated and uncollimated proton beam. The diameter of the cylindrical cavity of the chamber is 6 mm and Figure 5.15 shows that the depth of the peak and the extrapolated range for the collimated beam, measured with the cylindrical ion chamber are greater than those measured with the silicon diode by 2.0-2.5 mm, i.e. about 0.7 to 0.8 times the radius of the chamber's sensitive volume. The relationship is illustrated in the schematic diagram of Figure 5.16.

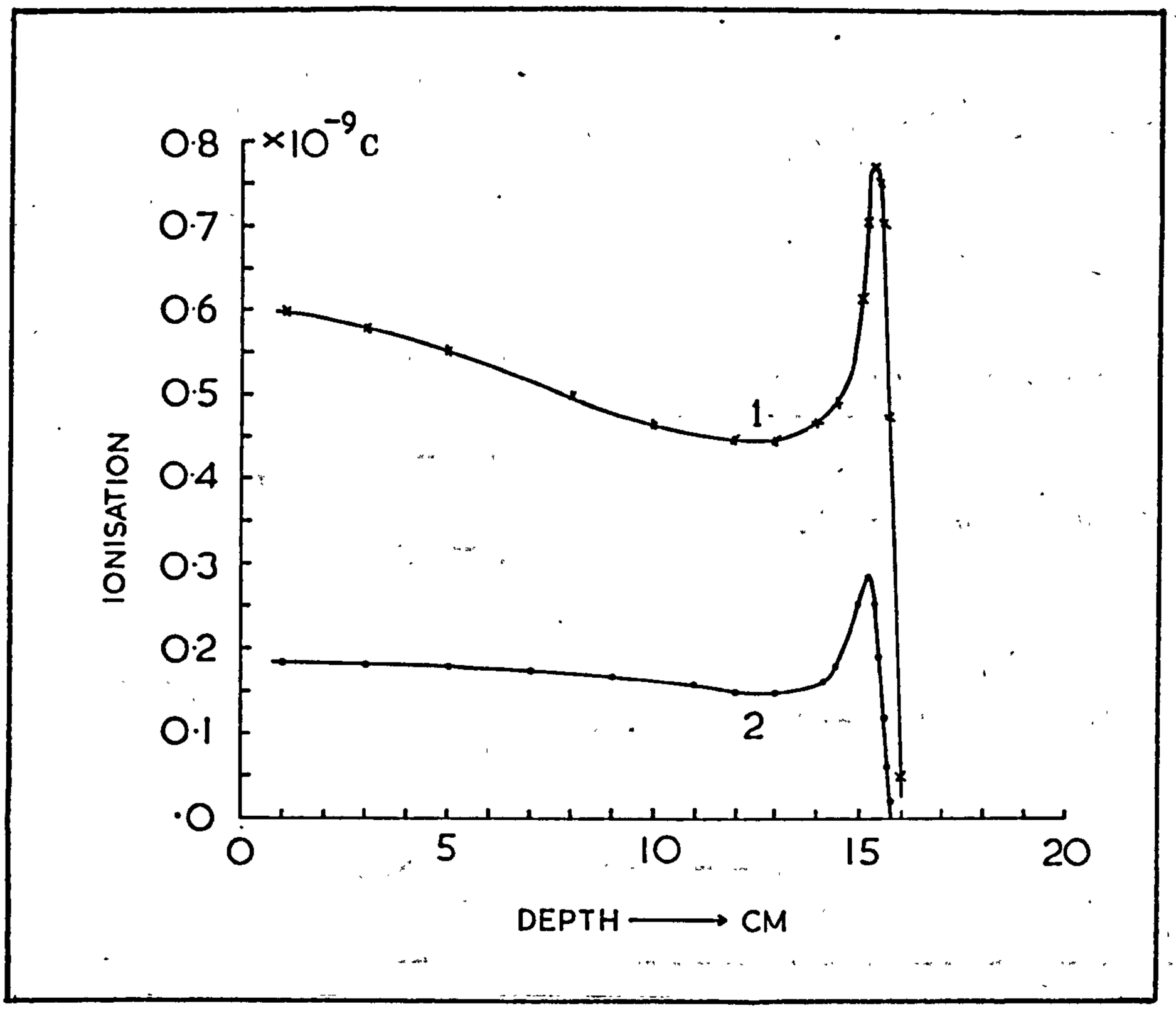

Figure 5.15 Ionisation along the central axis of the collimated proton beam (150 MeV)

1. 0.2 cm^3 cylindrical ion chamber in water

2. Silicon diode in water

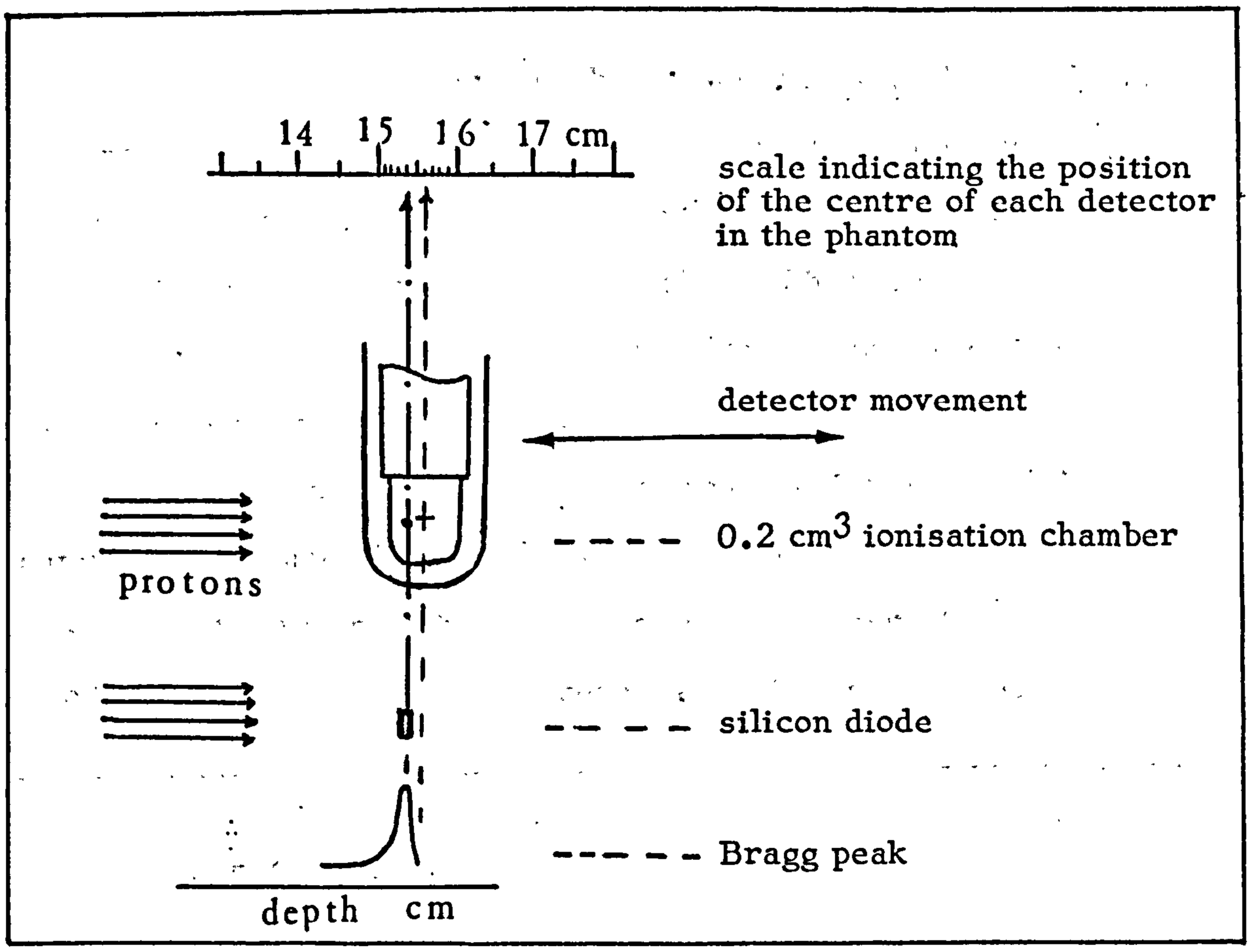

Figure 5.16 The silicon diode gives the true position of the Bragg peak. When "maximum signal" is recorded with the 0.2 cm^3 cylindrical chamber, its centre is at a depth greater than the depth of the peak

With the uncollimated beam, the difference in the peak depth and the extrapolated range, derived from measurements with the cylindrical and the flat ion chambers (as well as the diode) is about 1.5 mm; i.e. the effective measuring point for the cylindrical ion chamber lies approximately 0.5 x Radius in front of its centre; the difference from the collimated beam situation is probably due to the presence of extra scatter when the beam is not collimated. In the case of the plane parallel plate ionisation chamber, the effective plane of measurement is at the front face of the sensitive volume as the proton fluence is the same through the volume.

The values of "range to half maximum" and "extrapolated range" derived with the flat ion chamber in water, using the uncollimated beam, are about 2.5% and 4% respectively larger than the calculated range values given by BICHSEL (1968) and BARKAS and BERGER (1964) for the same proton energy (150 MeV). When the values measured with the collimated beam are considered, however, the above differences are reduced to 1.0% and 2.5% respectively.

Figure 5.17 shows the results of measurements with the silicon diode in water, with the uncollimated (1) and with the collimated beam (2). The experimental error in the measurement of the correct position of the diode was less than 0.5 mm as repeat experiments showed.

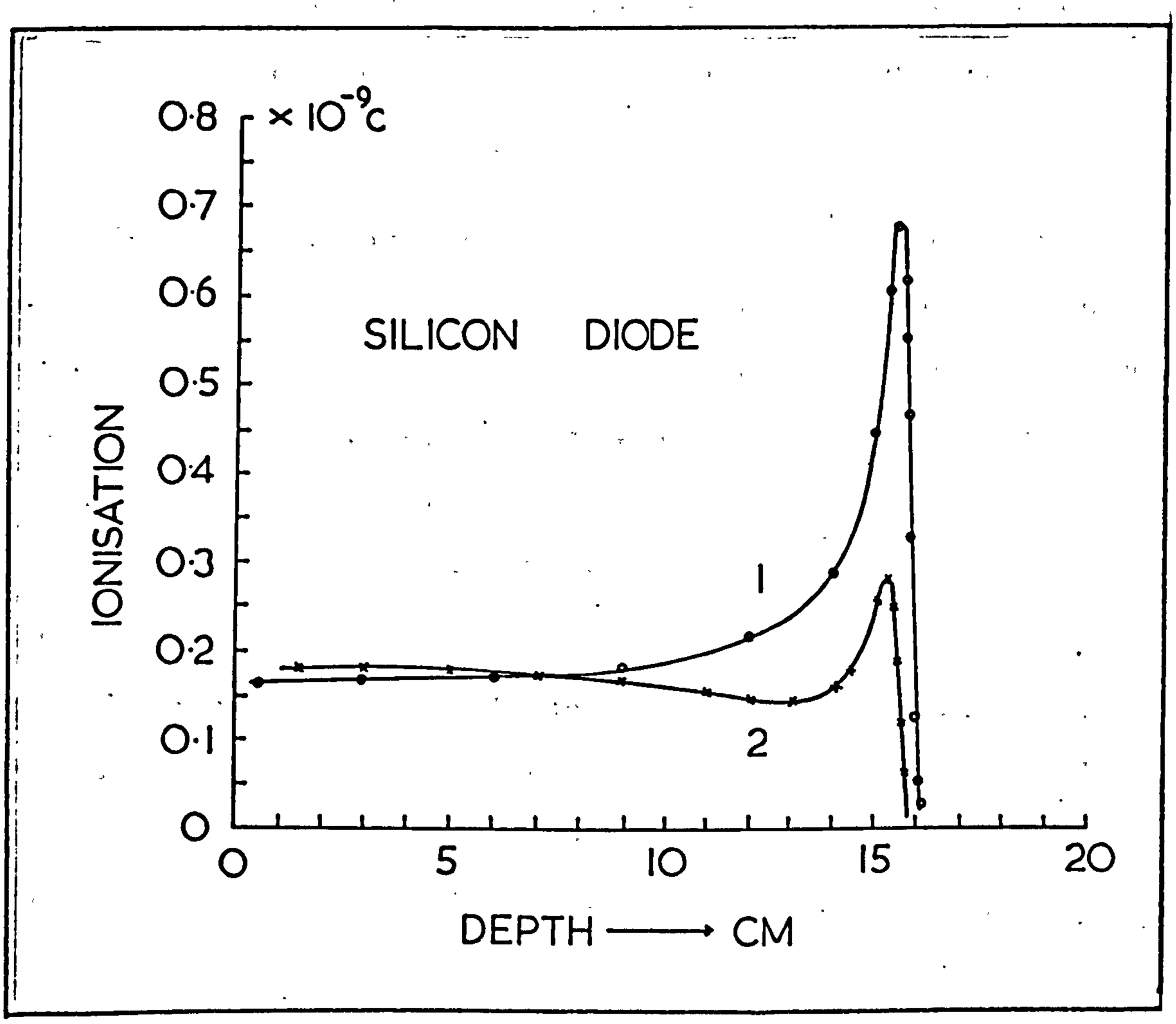

Figure 5.17 Central axis "ionisation versus depth" curves for 150 MeV protons, in water

1. Broad beam
2. Collimated beam

5.1(v) A SIMULATED PATIENT TREATMENT

The Bragg peak of a high energy proton beam is narrow and has a sharp cutoff; by superimposing many such beams, extended tumour volumes can be treated to a uniform dose. The dose distribution obtainable with parallel opposed field irradiation is shown schematically in Figure 5.18. Plans designed to irradiate a 2 cm-thick tumour centered in a 20 cm slab of tissue a) with cobalt-60 gamma rays and b) with 150 MeV protons are compared. By the use of bolus material the proton Bragg peak can be made to coincide with the tumour area. The advantage of protons over photons in this respect is obvious; in the photon isodose distribution, the normal tissues outside the tumour volume receive about the same or even more dose than the tumour while with protons the normal tissue dose is greatly reduced.

In view of the proposed use of the AERE synchrocyclotron for pituitary proton radiotherapy, an experiment was carried out to discover how accurately the Bragg peak can be positioned "on target" in practice. A Perspex tank with 1 cm-thick front wall was filled with brain equivalent liquid (BRN/L6) and the 0.2 cm^3 cylindrical ion chamber was used to scan along the central axis of the collimated proton beam (0.7 cm diameter). At the position of the maximum signal (Bragg peak) the dial indicated a depth of 14.90 cm. A real skull, with average thickness of the temporal bone at the level of the pituitary equal to 3 mm, was mounted on a Perspex circular base so that it could be rotated round a vertical axis through the centre of the pituitary fossa.

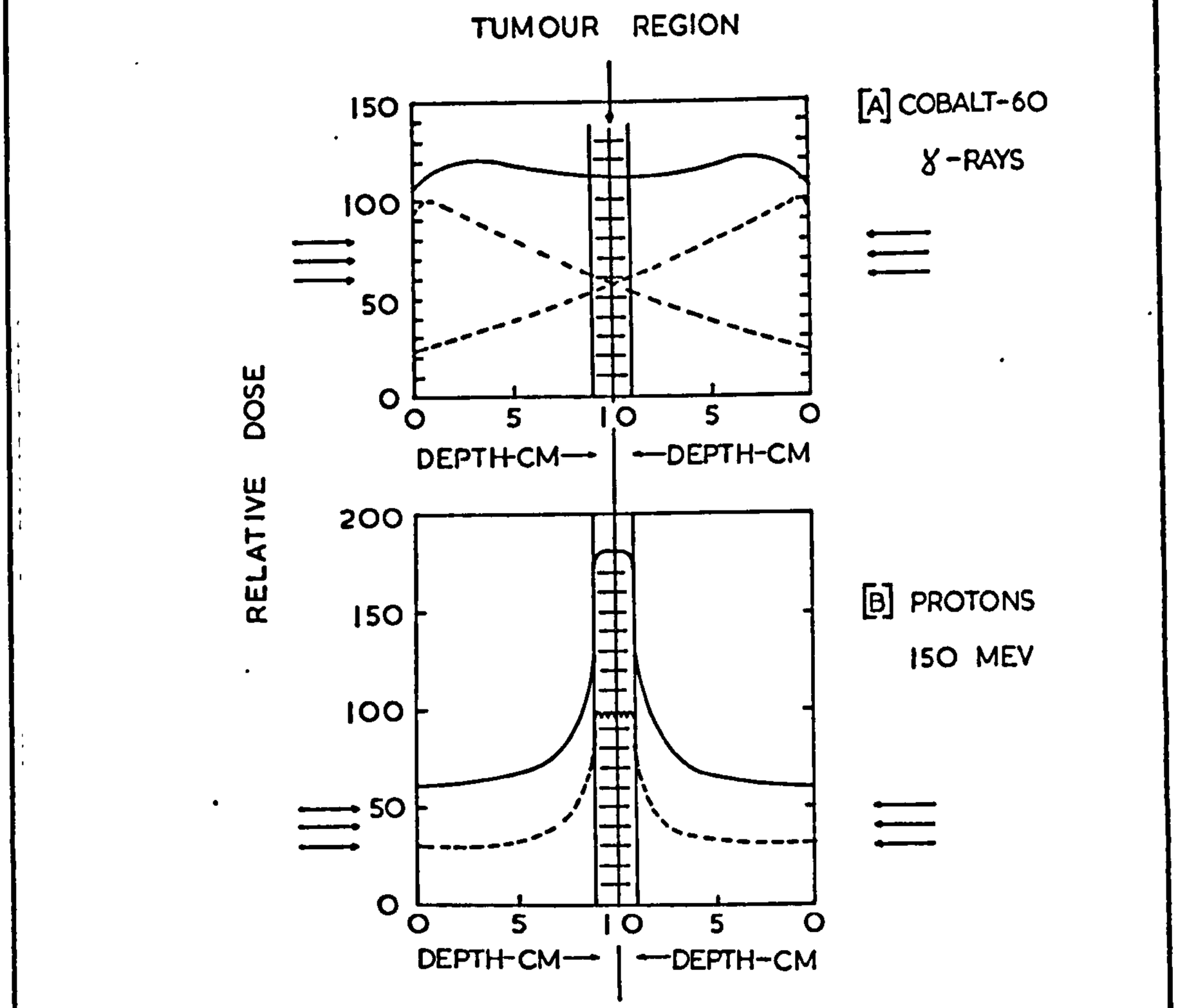

Figure 5.18 Dose distributions with parallel opposed fields. Comparison of 150 MeV protons to cobalt-60 gamma rays

Our previous measurements indicated that a 3 mm-thick bone in front of brain tissue would reduce the depth of the Bragg peak by 1.5 mm (4.5 mm per cm of bone in front of BRN/L6). Consequently, the skull was immersed in the brain equivalent liquid, with the centre of the pituitary fossa at 14.90 cm -0.15 cm = 14.75 cm from the entry face of the tank (Figure 5.19). The 0.2 cm^3 chamber was then clamped so that its sensitive volume was "sitting" in the pituitary depression. The presence of the anterior and posterior clinoid bony processes allowed 3-4 mm movement of the ion chamber on either side of the centre, but this was enough to find the pre-peak, peak and

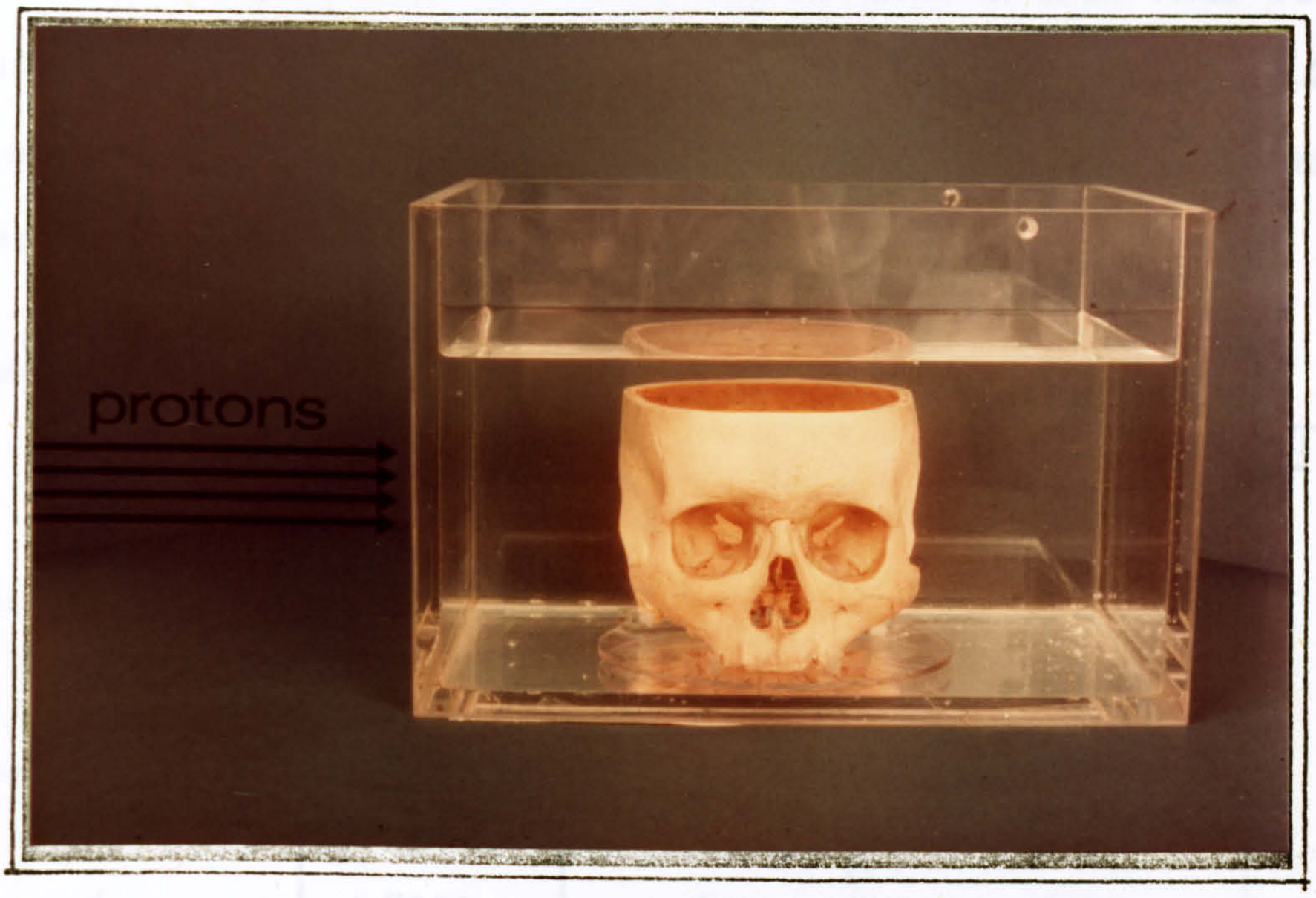

Figure 5.19 Setup for test of "positioning the Bragg peak on target"

post-peak positions. When the proton beam was turned on, the remotely controlled movement of the ion chamber along the axis of the beam indicated that the ionisation was maximum when the detector was at a depth of 14.75 cm, i.e. exactly as planned. The dose to the pituitary, for a preset 1×10^{-7}C on the transmission chamber used as beam monitor, was calculated from the measured peak height and the calibration factor of the 0.2 cm^3 ion chamber. It was found equal to 10.87 rad. With the available beam intensities, however, doses of 10,000 rad could be administered in a few minutes. For a 15 cm wide skull, the skin dose would be about 64.0% of the peak dose as Figure 5.15 indicates (i.e. 6.96 rad in this case).

The above exercise was repeated 4 times, but each time the skull was rotated by 10° clockwise. The maximum displacement of the Bragg peak observed was 0.5 mm and this was mainly due to a small variation in the thickness of the skullbone. Based on the

above results, the skin dose for a tumour dose of 5000 rads was calculated. Table 5-VIII gives the results for the case of 1, 4, 8 and 12-portal treatments; the inherent advantage of the multi-portal treatment with high energy proton beams is obvious.

TABLE 5-VIII TUMOUR AND SKIN DOSES FOR A MULTIPORTAL PITUITARY TREATMENT WITH 150 MeV PROTONS

Number of portals	Tumour dose (rads)	Skin dose (rads)	Skin dose as a percentage of tumour dose
1	5000	3200	64.0
4	5000	800	16.00
8	5000	400	8.00
12	5000	266	5.33

In practice, a plastic bag stuck on to a thin Perspex plate and filled with brain equivalent liquid could be used as a variable-length energy degrader for the adjustment of the position of the Bragg peak. The mechanics of the proposed patient treatment on the AERE synchrocyclotron have been described by WHITEHEAD (1974).

5.2 FAST NEUTRON DEPTH DOSES IN VARIOUS TISSUE SUBSTITUTES AND IN COMPOSITE PHANTOMS

In view of the current use of fast neutrons in cancer therapy, it is desirable to know the depth dose characteristics of fast neutron beams in various tissues. The new tissue substitutes were used to study the physical characteristics of the fast neutron beam produced by the cyclotron of the Medical Research Council (MRC) at the Hammersmith Hospital, London.

5.2(i) DOSIMETRY AND EQUIPMENT

The contamination of fast neutron beams with gamma radiation and the complex manner in which neutrons interact with tissue makes neutron dosimetry more difficult than the dosimetry of photons and electrons. Gamma rays result from neutron production processes in the target, from interactions of neutrons with the collimators and from interactions in the tissue being irradiated (probably mainly 2.2 MeV gamma rays from thermal neutron capture in hydrogen).

The measurement of the total dose (neutrons + gamma rays) is usually made with a "tissue equivalent" chamber. Uncertainties in the knowledge of the W_n value, the energy required to produce an ion pair in the gas of the chamber, and the replacement of most of the oxygen content of the plastic from which the ion chamber is made by carbon, may result in errors of up to 10% in the neutron component of the total dose.

The gamma ray component of the total dose varies with field size and with depth in the phantom and is usually measured with detectors of low sensitivity to neutrons. For example, ionisation chambers constructed from non-hydrogenous materials, specially

designed Geiger counters and photographic films may be used.

Whenever relative dose measurements are required, activation methods can be used for neutron dosimetry, for example, $^{32}S(n,p)^{32}P$, in which the product is a beta-emitter with a half life of 14.3 days. The dose in the patient during treatment can be measured by using activation of aluminium pellets or by exposing thermoluminescent dosimeters in lead and polythene to record the neutron dose and the gamma-ray dose separately.
(The product in the $^{27}Al(n,p)^{27}Mg$ reaction has a half life of 9.5 minutes and emits a gamma ray of 0.83 MeV).

The M.R.C. cyclotron accelerates deuterons up to 16.7 MeV and these hit a 0.8 mm-thick beryllium target backed by copper. The fast neutron beam produced, has a spectrum extending from zero to about 17 MeV with a mean energy of 7.5 MeV. The dose rate at 120 cm from the target is 40-50 rad per minute (BEWLEY and PARNELL, 1969, PARNELL, 1971). The total dose was measured with a 1 cm^3 spherical ionisation chamber (EG&G, Wellesley, Mass). A tissue equivalent gas was flowing through the chamber during the measurements (64.4% methane; 32.4% carbon dioxide; 3.2% nitrogen; percentages by volume). The signal from the ionisation chamber was integrated using a Keithley 610R electrometer for a preset number of divisions on the beam monitor. The ionisation chamber was operated at a bias voltage of -300 volts.

When used in a solid phantom, this ion chamber was first covered with a sleeve specifically made from the same material as the phantom and then inserted in the appropriate hole of a 20 cm x 20 cm x 3 cm slab of that material (see Figure 5.20). The chamber was moved back through the phantom by changing the position of the slab (in which it was inserted) in the stack. When used in a liquid

phantom, the chamber (without build-up cap) was enclosed in a water tight Perspex cylinder and moved along the central axis of the beam by a remote control mechanism, readings being taken at discrete depths. The total dose ($Dn + D_\gamma$) at each point was obtained by multiplying the integrated signal (nC) with the factor 3.049 rad/nC, obtained from a calibration of the chamber with caesium gamma rays (BEWLEY and PARNELL, 1978).

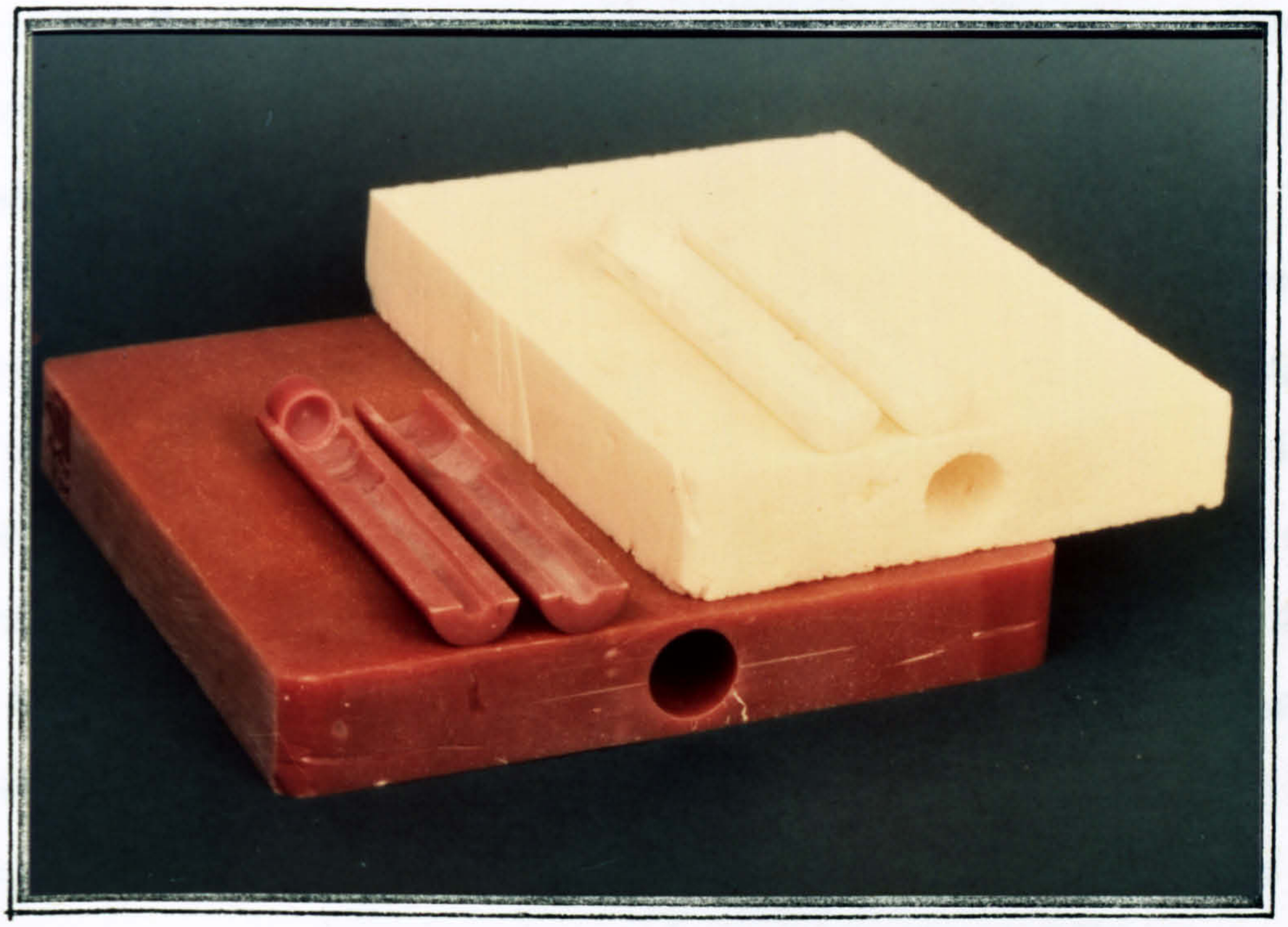

Figure 5.20 Sleeves and plates for the 1 cm^3 EG&G spherical ion chamber

The gamma-ray component of the dose was measured with a Geiger counter (Mullard GM D6) which was covered with a 2 mm-thick ^6Li foil to absorb the slow and thermal neutrons. The setup was the same as above except that when the counter was used in liquids it was protected with a plastic tube cover. The number of counts for a preset 1 division on the beam monitor was measured with an Ortec dual counter-timer, corrected for the resolving time of the counter (dead time = 15 μsec) and, after subtraction of the background counts, converted into rads/division using the calibration

1.26×10^6 counts/rad. (BEWLEY and PARNELL, 1978). The bias used for the Geiger counter was +500V.

5.2(ii) NEUTRON DEPTH DOSES IN MUSCLE, BRAIN AND WATER

The penetration of the neutron beam in tissue is the most important physical parameter for radiation beam therapy. In Figure 1.9, among others, the central axis percent neutron depth dose from the MRC cyclotron is compared to that of cobalt-60 radiation (our measurements). The neutron depth dose curve (9.5 cm x 9.5 cm field, at a target-skin distance of 120 cm) shows that the 50% dose is at 8.5 cm depth and on this account the range of tumours which can be treated with this machine is limited to head and neck or superficial and breast tumours. In order to match the penetration of cobalt-60 gamma rays, it is necessary to use either 14 MeV neutrons from the $T(d, n)^4$ He reaction (but unfortunately dose rates of only few rads per minute have been achieved with this reaction so far), or neutrons generated by deuterons of at least 30 MeV energy on beryllium. To match the skin sparing given by cobalt-60 radiation it is necessary to use deuterons of at least 50 MeV energy on beryllium (BEWLEY, 1971).

The effect of field size on the percentage neutron depth doses was studied using a 20 cm x 20 cm x 20 cm phantom made of solid muscle substitute (MS/SR4). The smallest depth at which measurements were made in this phantom was 1.5 cm and the neutron dose at this depth, for a 9.5 cm x 9.5 cm field, was estimated to be 93.5% of the maximum neutron dose (Dn .max at 0.2 cm, BEWLEY and PARNELL, 1969). Consequently, all readings obtained with a 9.5 cm x 9.5 cm fields were normalised to 93.5% at 1.5 cm deep. The neutron dose

was derived by subtracting the gamma ray dose (D_γ) from the total dose ($Dn + D_\gamma$). Figure 5.21 shows the results of these measurements for three field sizes; the gamma ray dose, expressed as a percentage of Dn maximum is also given, while Figure 5.22 shows the gamma-dose as a percentage of the local neutron dose. The percentage rises steadily with depth. As the RBE of photons relative to neutrons is about one-third, a 12-15% gamma-dose at 15 cm depth represents 4-5% of the biologically effective dose.

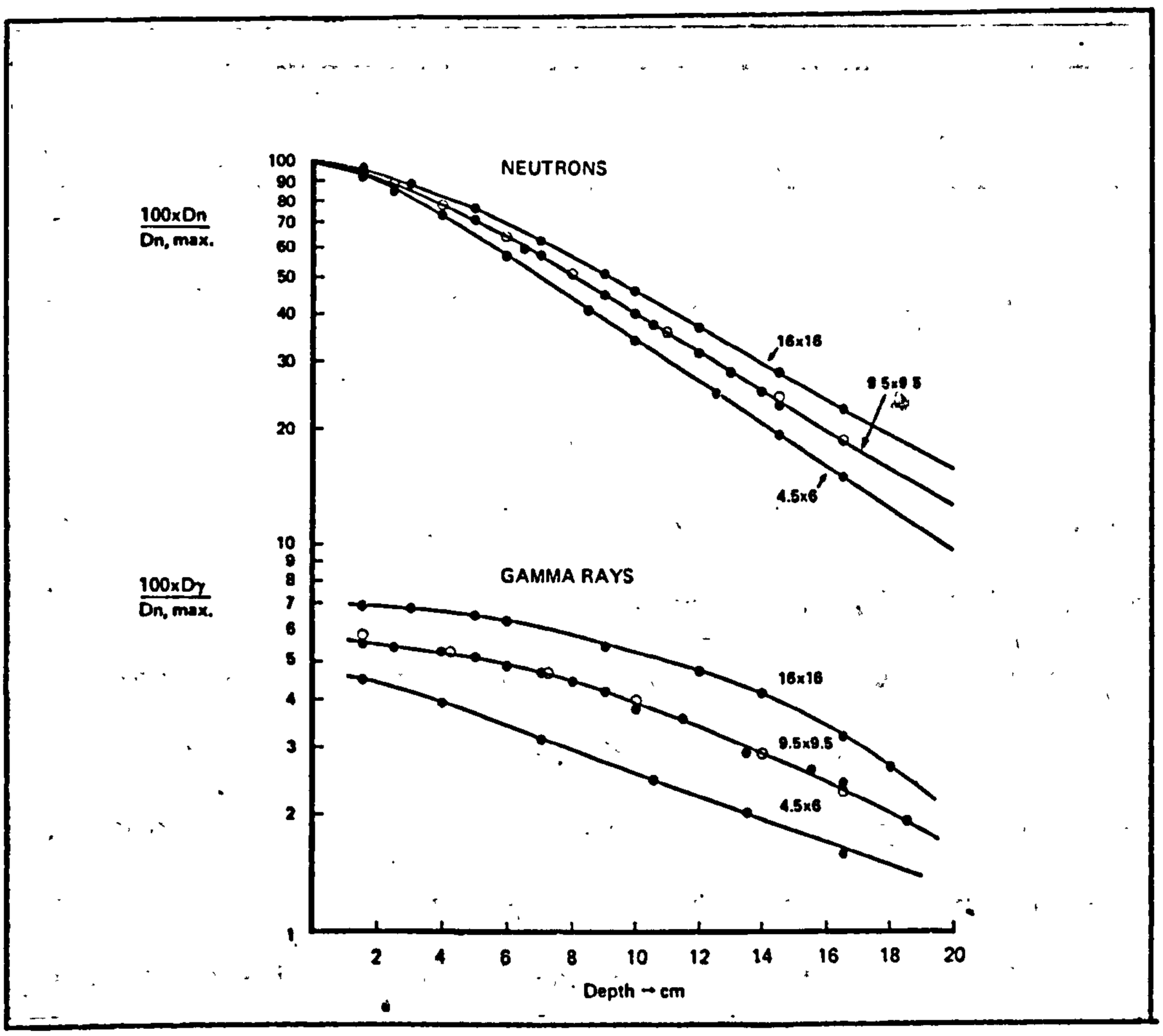

Figure 5.21 Central axis neutron and gamma ray depth doses as a percent of the maximum neutron dose ($\bar{E}n$ = 7.5 MeV, TSD = 120 cm).
Closed circles : in MS/SR4
Open circles : in MS/L1

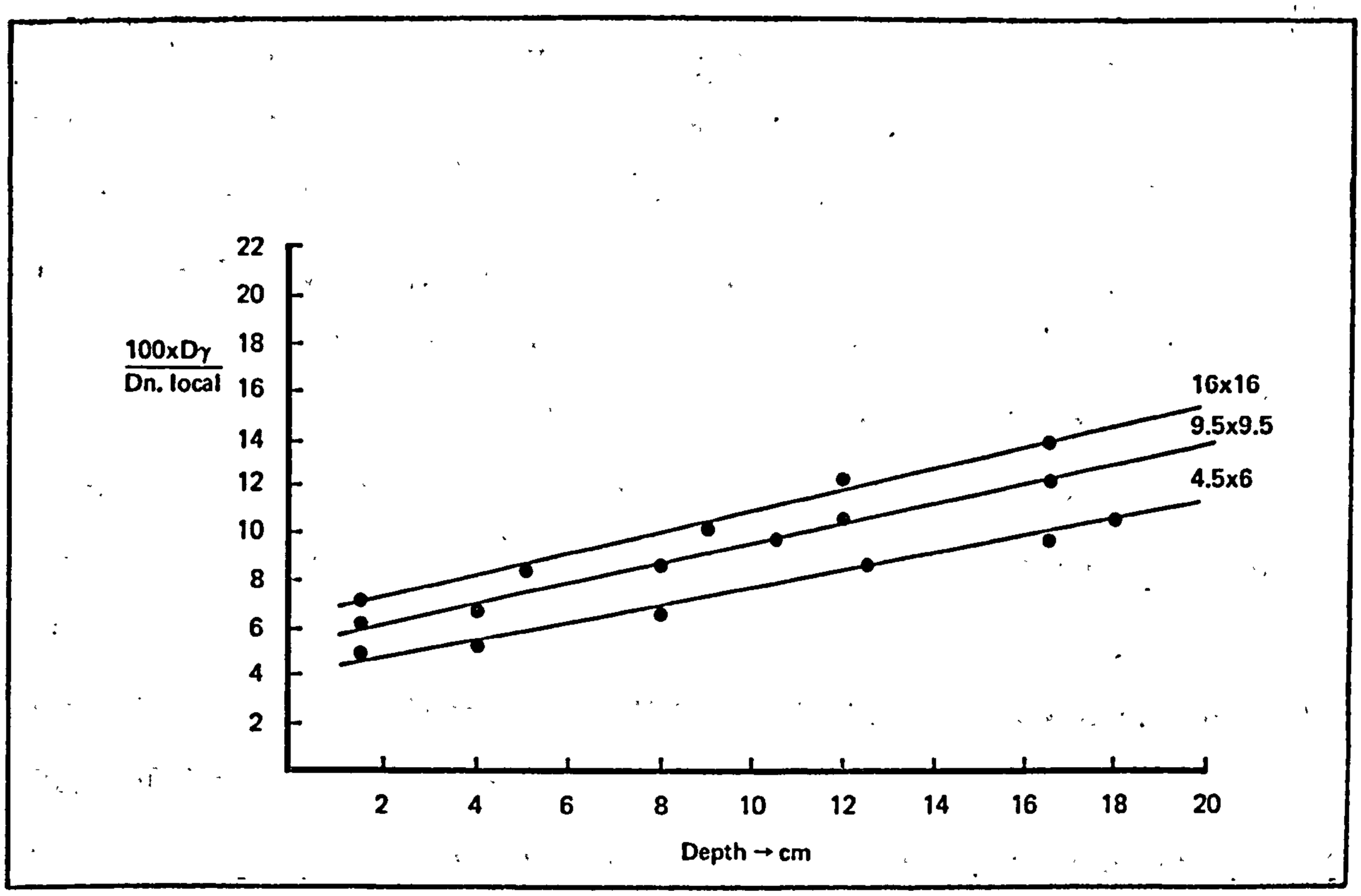

Figure 5.22 Dose due to gamma rays as a percentage of the local neutron dose in muscle (En = 7.5 MeV, TSD = 120 cm)

Measurements of the neutron dose repeated in the same phantom on different days gave an average difference of 0.5% of the maximum neutron dose and in no case did the difference between any two sets of measurements at the same depth differ by more than 1%. The calibration of the cyclotron output on 7 different days gave a mean value of 0.98 neutron-rad per division, with a standard deviation of 0.01, i.e. the variability of the machine output is about 1% (calibration at 120 cm TSD, in air, at 22°C and 760 mmHg, for a 9.5 cm x 9.5 cm field).

Beam profiles in muscle for a 9.5 cm x 9.5 cm field obtained by scanning transversely at 9 cm depth, have already been given in Chapter 4 (Figure 4.7).

A comparison between muscle and brain equivalent liquids (MS/L1, BRN/L6) and water was made and the corresponding neutron depth dose curves, measured with a 9.5 cm x 9.5 cm field at 120 cm TSD, are given in Figure 5.23. The curves show that muscle, despite its lower hydrogen content attenuates neutrons more effectively than water because its higher relative density more than compensates for the difference in hydrogen. The curve for brain equivalent liquid lies between the two. The difference between MS/L1 and water at 15 cm depth is 1.5% of the maximum neutron dose while the difference between MS/L1 and BRN/L6 at the same depth is 0.7% of the maximum neutron dose. Table 5-IX gives the measured neutron depth doses in water and in muscle and brain equivalent liquids.

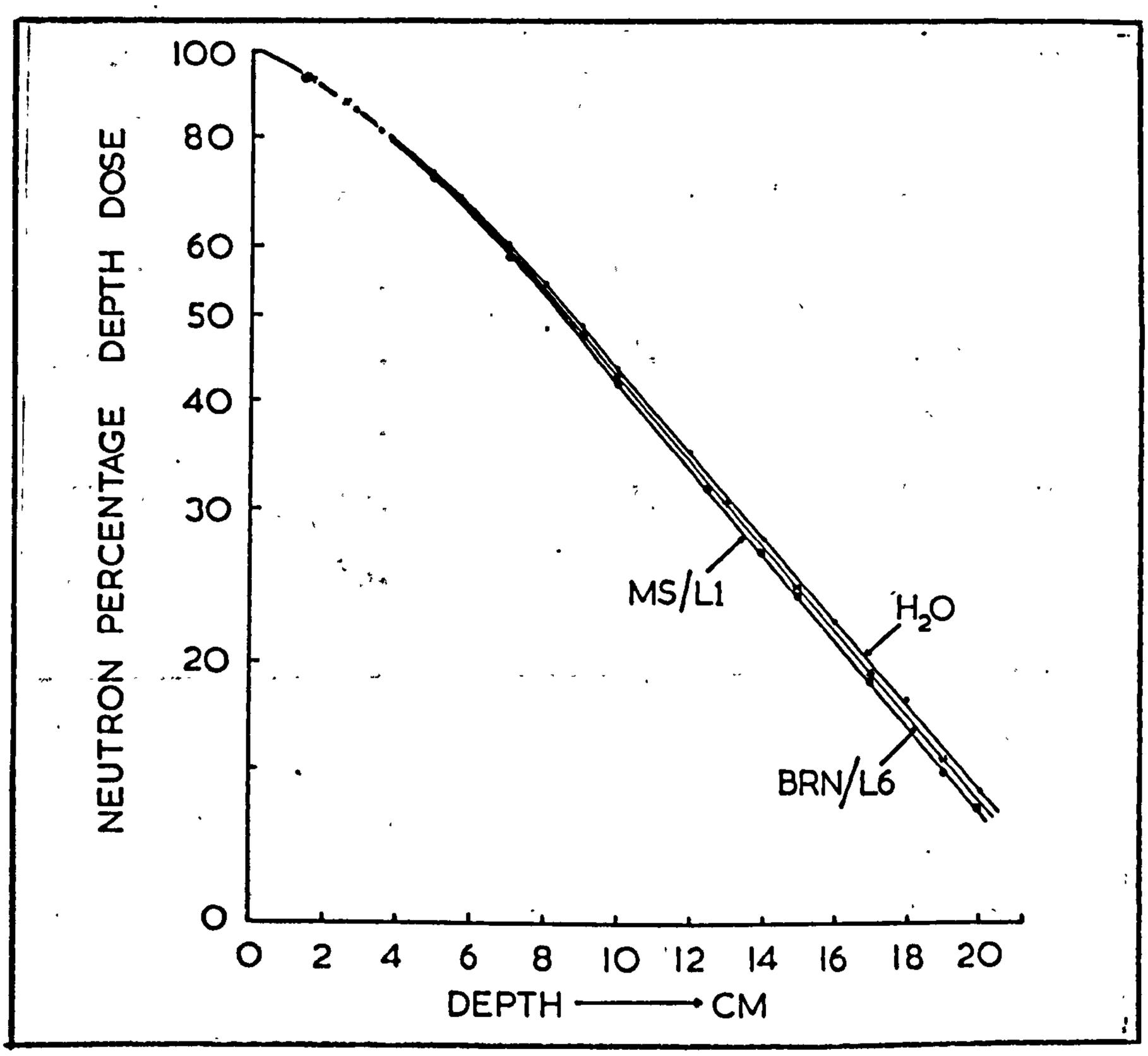

Figure 5.23 Comparison of muscle, brain and water

TABLE 5-IX CENTRAL AXIS PERCENTAGE NEUTRON DEPTH DOSES IN MUSCLE, BRAIN AND WATER

($\bar{E}n$ = 7.5 MeV, 10 cm x 10 cm, TSD = 120 cm)

DEPTH (cm)	MUSCLE (MS/L1)	BRAIN (BRN/L6)	WATER
0.2	100.0	100.0	100.0
1.0	96.0	96.0	96.0
2.0	90.8	90.9	91.0
3.0	84.5	84.8	85.0
4.0	77.5	77.8	78.0
5.0	71.9	72.3	72.8
6.0	65.0	65.5	66.2
7.0	58.5	59.1	60.0
8.0	52.5	53.1	54.0
9.0	47.0	47.6	48.5
10.0	42.0	42.7	43.5
12.0	33.5	34.2	35.0
14.0	26.5	27.2	28.0
16.0	21.0	21.7	22.4
18.0	16.8	17.3	18.0
20.0	13.3	13.8	14.5

In an attempt to compare water with "unit density" muscle, the measurements in MS/L1 were used. In order to derive the neutron percentage depth dose in "unit density" muscle, the actual depth of the chamber was multiplied by the density of the muscle substitute and the corresponding neutron dose was reduced by a factor $(f + d)^2/(f + 1.06\,d)^2$, to allow for the inverse square law effect between the true and the "corrected" depths (f = TSD, d = true depth in MS/L1). The results are shown in Figure 5.24. The neutron depth doses in "unit density" muscle quoted in supplement 11 of the British Journal of Radiology and used at the Hammersmith Hospital, are also shown. The neutron depth doses in water are closer to those in muscle equivalent liquid than the corresponding doses in unit density muscle.

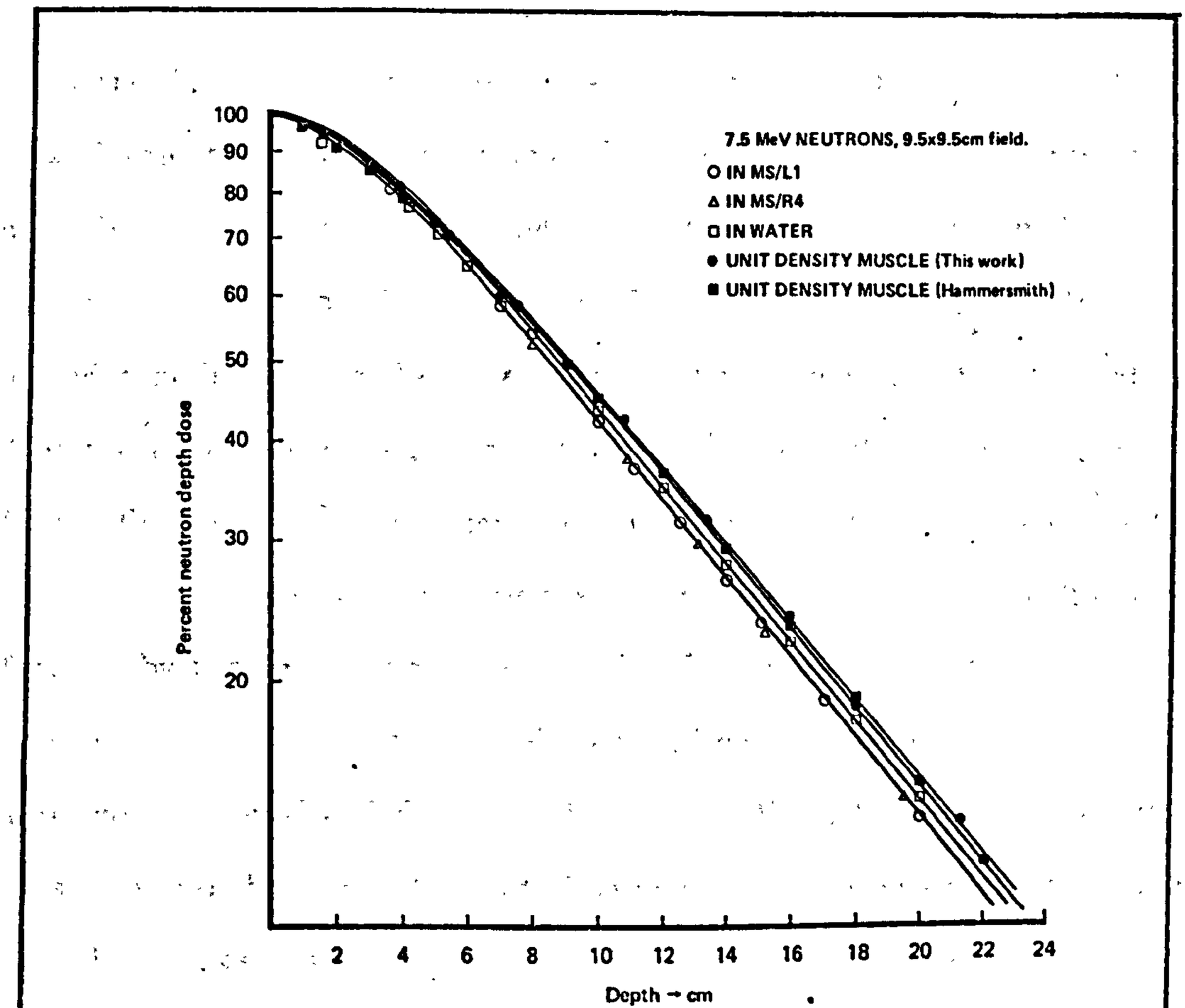

Figure 5.24 Muscle, unit density muscle and water

5.2(iii) NEUTRON DEPTH DOSE CURVES IN COMPOSITE PHANTOMS

The effect of various thicknesses of lung, fat and bone on the neutron depth doses in phantoms consisting of muscle + heterogeneity + muscle, was investigated using the MRC cyclotron neutron beam. Isodose shift factors derived from these measurements for use in manual and computerised treatment planning, are presented and discussed in Chapter 6. The presence of lung may result in neutron doses in the tissues behind it higher by a factor of up to 2 or even more than the dose at the same depth in "muscle alone", depending on the thickness of lung traversed by the beam and the distance of the point behind the lung (see Figure 6.1 and Table 6-II).

The effect of fat is much less pronounced. The neutron depth doses in muscle behind a 5 cm-thick fat sample have been given in Figure 4.9. As far as bone is concerned, our measurements showed that the total dose in muscle behind various thicknesses of "hard bone" and "total skeleton" substitutes is slightly reduced. 4 cm of TSK/SF3 or 3 cm-thick slabs of HB/SR4 (10 cm x 10 cm) caused a reduction in the total dose behind them, in MS/SR4 of about 1% of the maximum dose. (see Figure 5.25). Repeated measurements of both the total and the gamma-dose indicated that the above reduction was due to a lower gamma-dose while the neutron depth doses were not affected by the presence of bone (see Figure 5.26). Similar results were obtained when the depth doses in brain and "bone + brain" were measured. McGINLEY and McLAREN (1975), however, used the Naval Research Laboratory cyclotron (35 MeV deuterons on a thick beryllium target) and from their measurements they concluded that bone (B100 plastic) attenuates neutrons of that energy (about 16 MeV) more effectively than muscle and therefore produce a shadowing effect (up to 15% reduction in the total dose at 8.6cm behind the 4.8 cm-

thick bone samples used).

The absorption of energy per gram of bone is only about half that in soft tissue but as the density of bone is higher the energy absorbed per unit volume in bone relative to soft tissue is about 0.85, while in fatty tissue it is about 1.15 (BEWLEY, 1963, 1975).

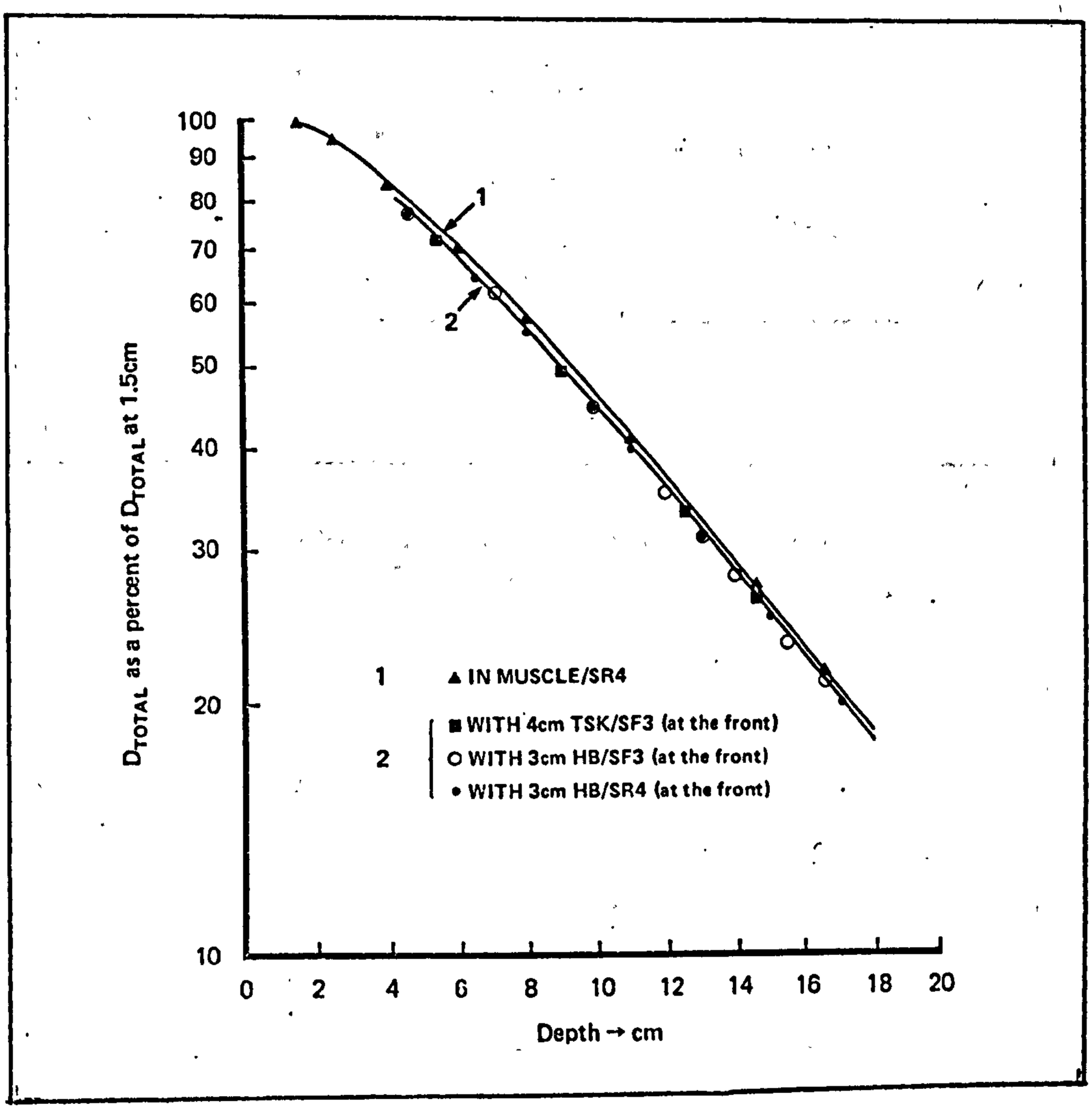

Figure 5.25 Total dose normalised to the dose at 1.5 cm depth.
($\bar{E}n$ = 7.5 MeV, TSD = 120 cm)

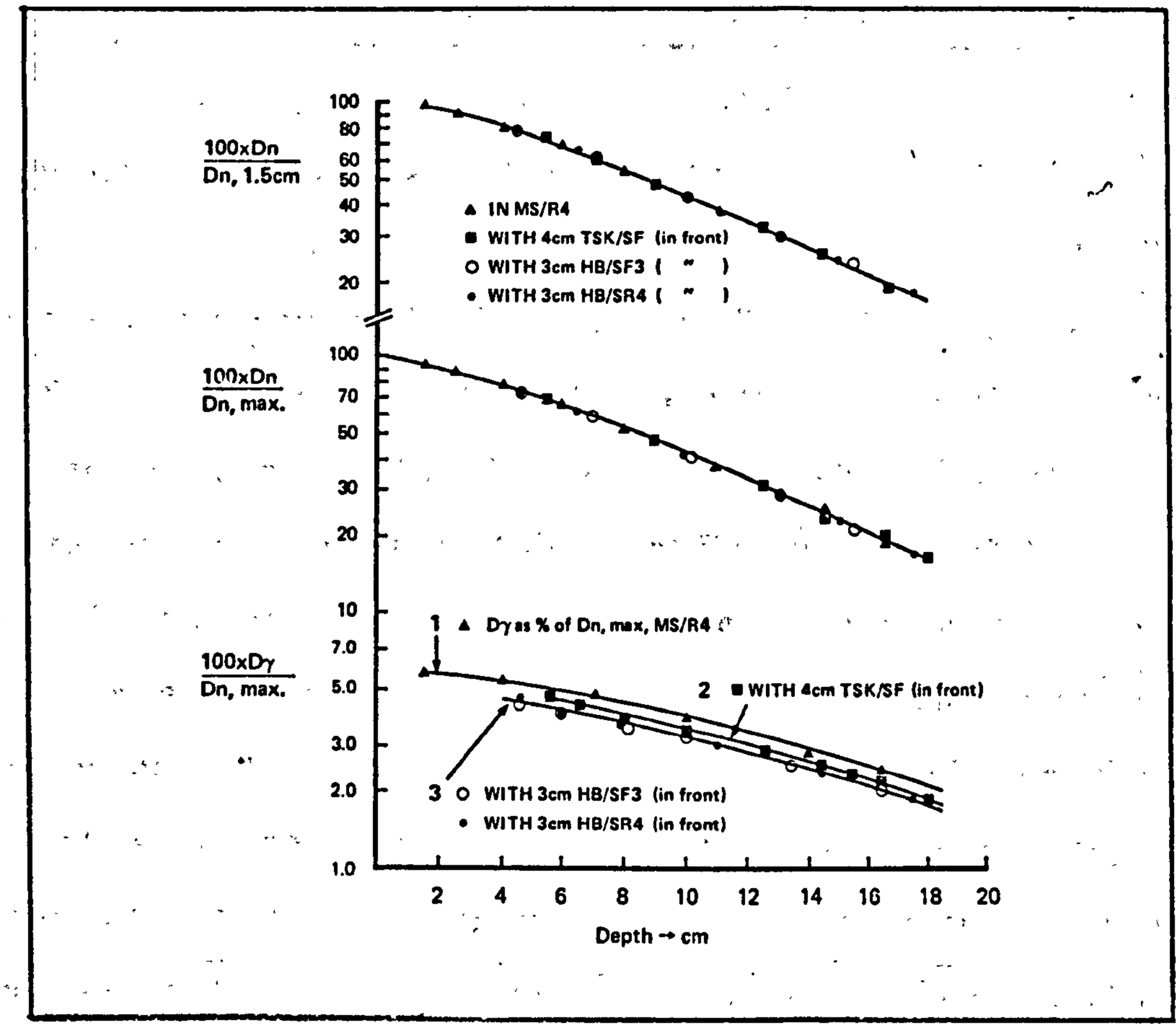

Figure 5.26 Effect of bones in the neutron beam ($\bar{E}n$ = 7.5 MeV, TSD = 120 cm)

5.3 DOSE DISTRIBUTIONS FROM A 10 MeV ELECTRON BEAM IN VARIOUS TISSUE SUBSTITUTES

(i) EQUIPMENT AND METHOD OF MEASUREMENT

The electron beam of the MEL SL75 linear accelerator of the London Hospital was mainly used for this series of measurements. The only detector used here was a flat ionisation chamber made of Perspex, as described by NAYLOR and WILLIAMS (1972). The air-filled disc shaped cavity of this "electron chamber" has 1 cm diameter and 3 mm depth. The holder on which the electron chamber was mounted was bent so that the front flat surface of the chamber's cavity is at right angles to the axis of the electron beam. This holder was clamped on a system which allowed remote control of the horizontal movement of the electron chamber, both along the central axis of the beam and normal to it. The 45 cm x 45 cm x 45 cm Perspex tank used was filled with water and the electron chamber was immersed in it. At the beginning of each measurement, the chamber was touching the inner surface of the tank's front wall, which was machined to a thickness at the centre of 2.5 mm. As the thickness of the front wall of the chamber itself is 1 mm, the first measurement in each set corresponded to a depth of 3.5 mm. The front face of the phantom was in contact with the end of the collimator in use.

A built-in transmission chamber was used to monitor the electron beam. The signals from the monitor and the electron chamber were fed into an ionisation current comparator (ratiometer circuit). The ratio of the signal of the electron chamber to that of the monitor, was taken from the output of the comparator and used to control the Y-axis movement of an X-Y plotter. In the X direction, the plotter moved as a slave of the corresponding movement of the electron chamber in the water tank, i.e. along the central axis

of the beam for depth dose measurements and transversely to it when beam profiles were taken. The plotter was adjusted to 100% where the signal ratio was maximum in each case.

The electron beam from the linear accelerator of the Medical College of St Bartholomew's Hospital was also used and the depth doses from this beam in muscle were measured with thermoluminescent dosimeters (TLD chips). The results will be presented and discussed in the next section.

5.3(ii) DOSE DISTRIBUTIONS IN WATER, MUSCLE AND BONE

The central axis depth dose curve from the 10 MeV electron beam was measured first in water for a 10 cm x 10 cm field. Then the central axis depth dose curve for the same field in water was measured using the 8 MeV electron beam of the same accelerator (MEL SL75). The results are shown in Figure 5.27 in which the data given by Jones in supplement No.11 of the British Journal of Radiology (1972) for 15 MeV and 20 MeV are given in addition. The discrepancy between the data given in the above reference for 10 MeV electrons and our measurements for the same energy, expressed as "depths of percentiles", was less than 1 mm.

Figure 5.28 shows the isodose distributions for 10 MeV electrons and cobalt-60 gamma rays (SSD = 75 cm) derived from our measurements in water. Figures 5.27 and 5.28 make the advantage of electron beams up to 10 MeV in the treatment of superficial tumours obvious.

The effect of field size was investigated by using various applicators from 3 cm x 3 cm up to 12.5 cm x 12.5 cm. The central axis percentage depth dose curves changed slightly by increasing the

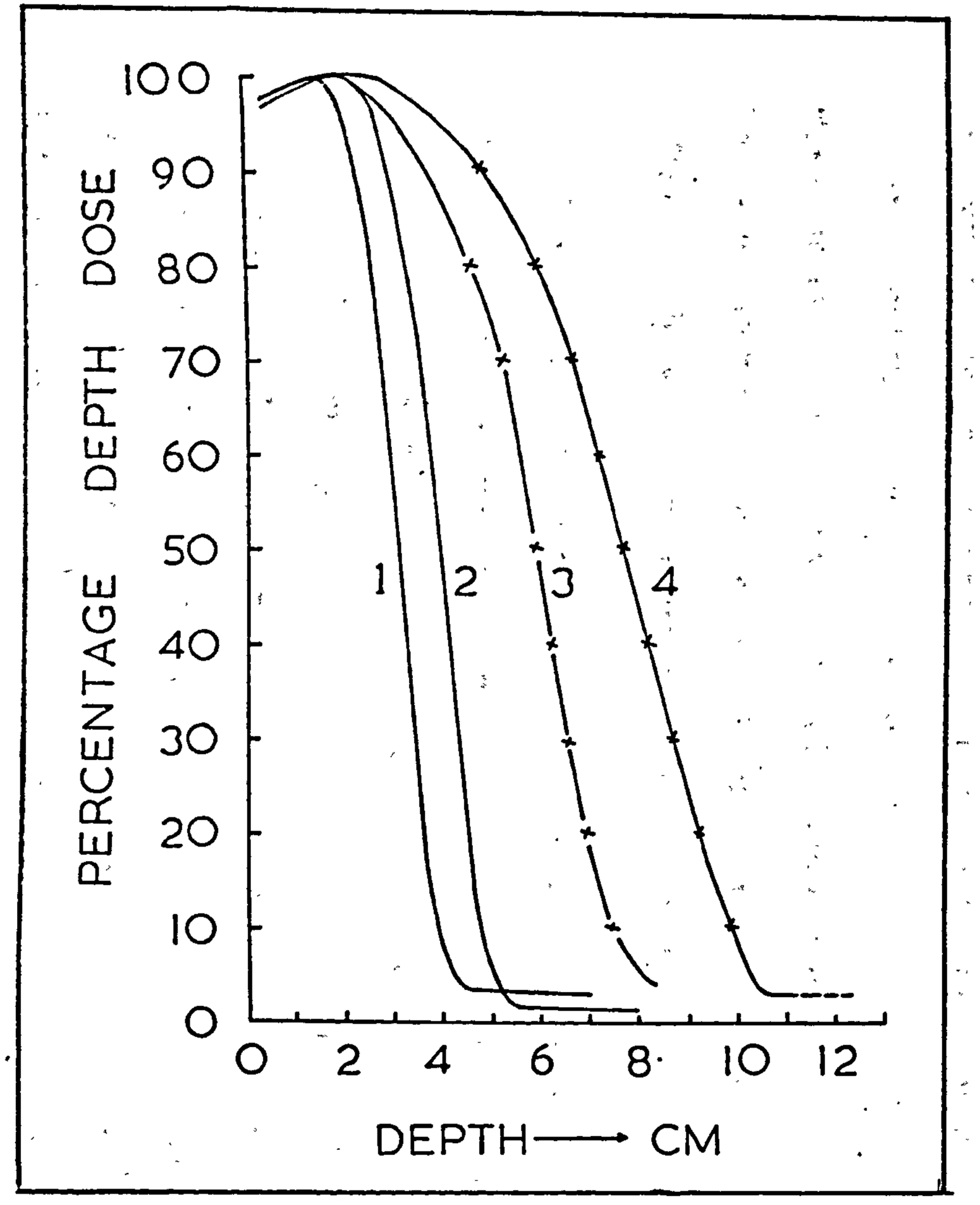

Figure 5.27 Central axis depth dose curves for electrons of various energies, in water (10 cm x 10 cm)
(1) 8 MeV, (2) 10 MeV, (3) 15 MeV, (4) 20 MeV

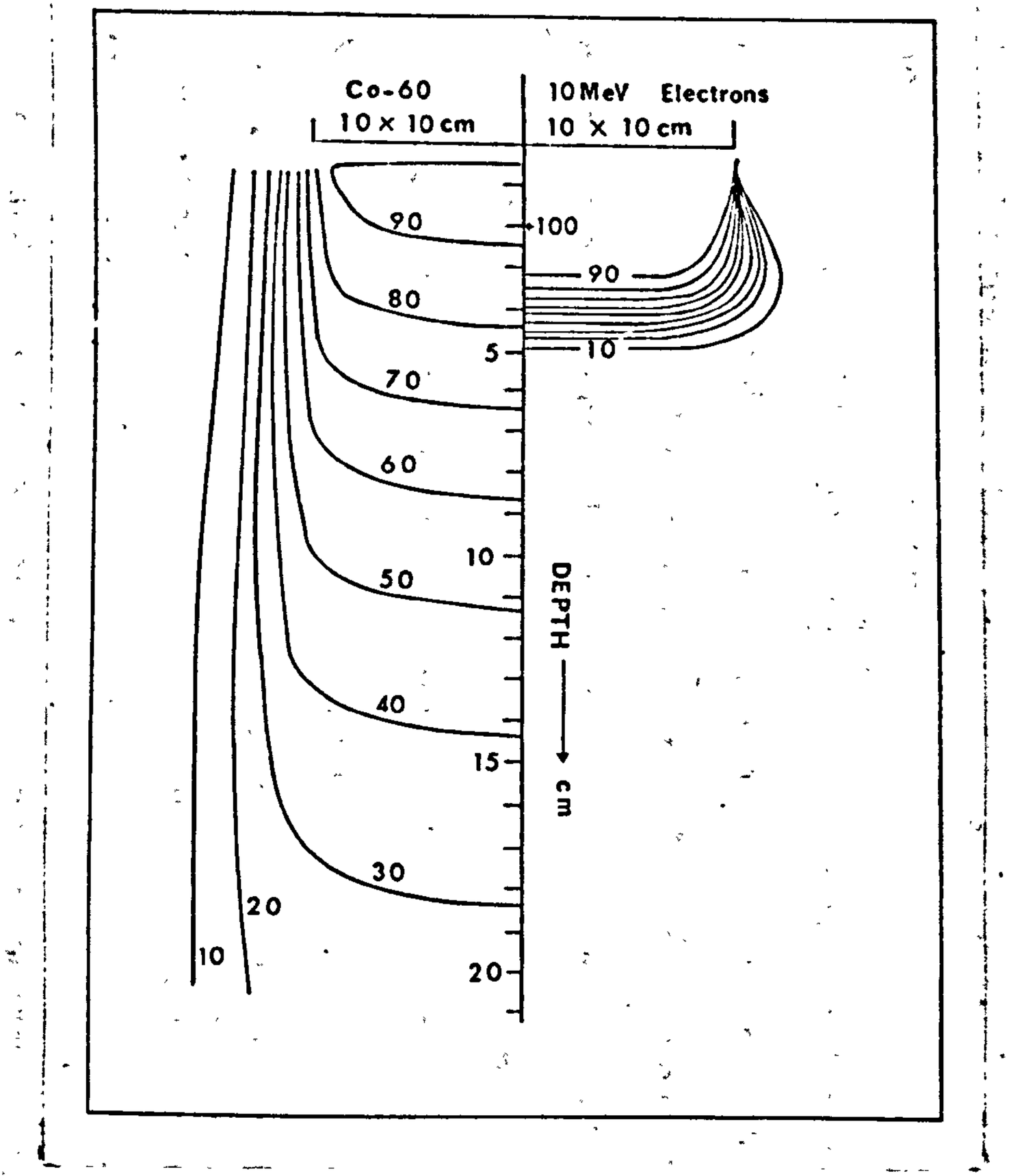

Figure 5.28 Isodose distributions in water. Comparison of cobalt-60 gamma rays with 10 MeV electrons

field size from 3 cm x 3 cm to 7 cm x 7 cm but were nearly identical for field sizes larger than 7 cm x 7 cm. Figure 5.29 shows the central axis depth dose curves for two applicator sizes, namely 3 cm x 3 cm and 10 cm x 10 cm. This "saturation" in the effect of field size on the depth doses would be expected from the finite range of 10 MeV electrons in water. The measurement of central axis percentage depth doses in muscle was made by adding, sequentially, 0.5 cm-thick slabs of muscle substitute MS/SR1 in front of the tank and taking readings with the electron chamber immersed in water and kept in contact with the inner surface of the front wall of the Perspex tank. The measurement of the percentage depth doses in bone was carried out in a similar way. Figure 5.30 shows the results. In Table 5-X the percentage depth doses from 10 MeV electrons in water, muscle and bone are expressed as depths of percentiles. In order to find out what the effect of the different chemical composition of the above materials on the depth doses is, the 50% percentile depth and the extrapolated range were multiplied by the density of the corresponding material and the results are given in Table 5-XI. The depth at which the dose is 50% of the maximum, when expressed in g/cm^2, differs between water and bone by only 4% of the value in water, while the difference between water and muscle is less than 1%.

Figure 5.31 shows the central axis depth dose curve in muscle (MS/SR4) derived from measurements in the pulsed electron beam of the linear accelerator at the Medical College of St Bartholomew's Hospital, London, using thermoluminescent dosimeters (TLD chips). The dose rate obtainable from this machine is in the Krad/sec range. The data for 15 MeV electrons, 10 cm x 10 cm field, given by JONES (1972) are plotted on the same graph for comparison. The differences between the two curves could be due to the following reasons:

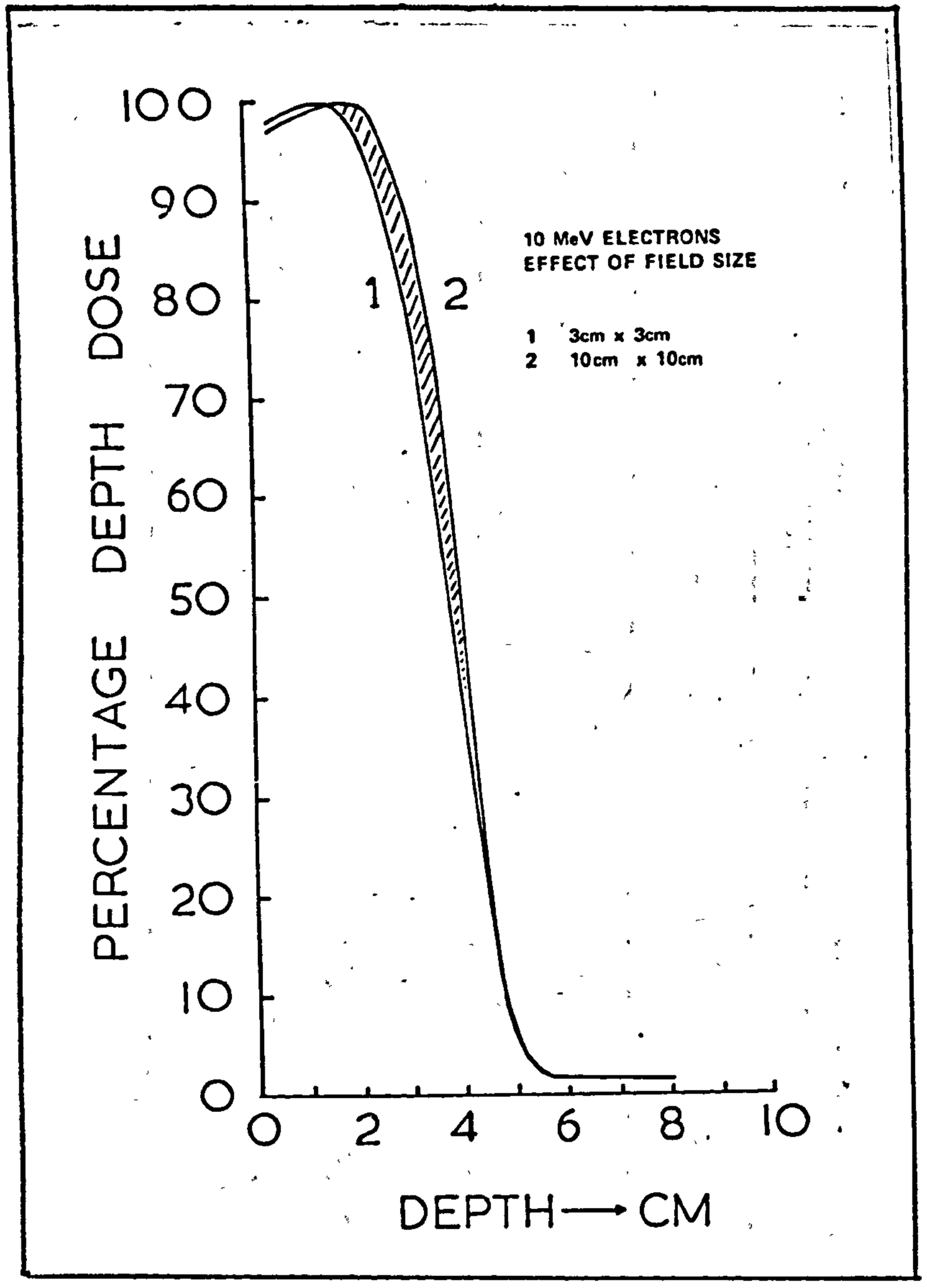

Figure 5.29 The effect of field size on the central axis depth dose curves from 10 MeV electrons in water

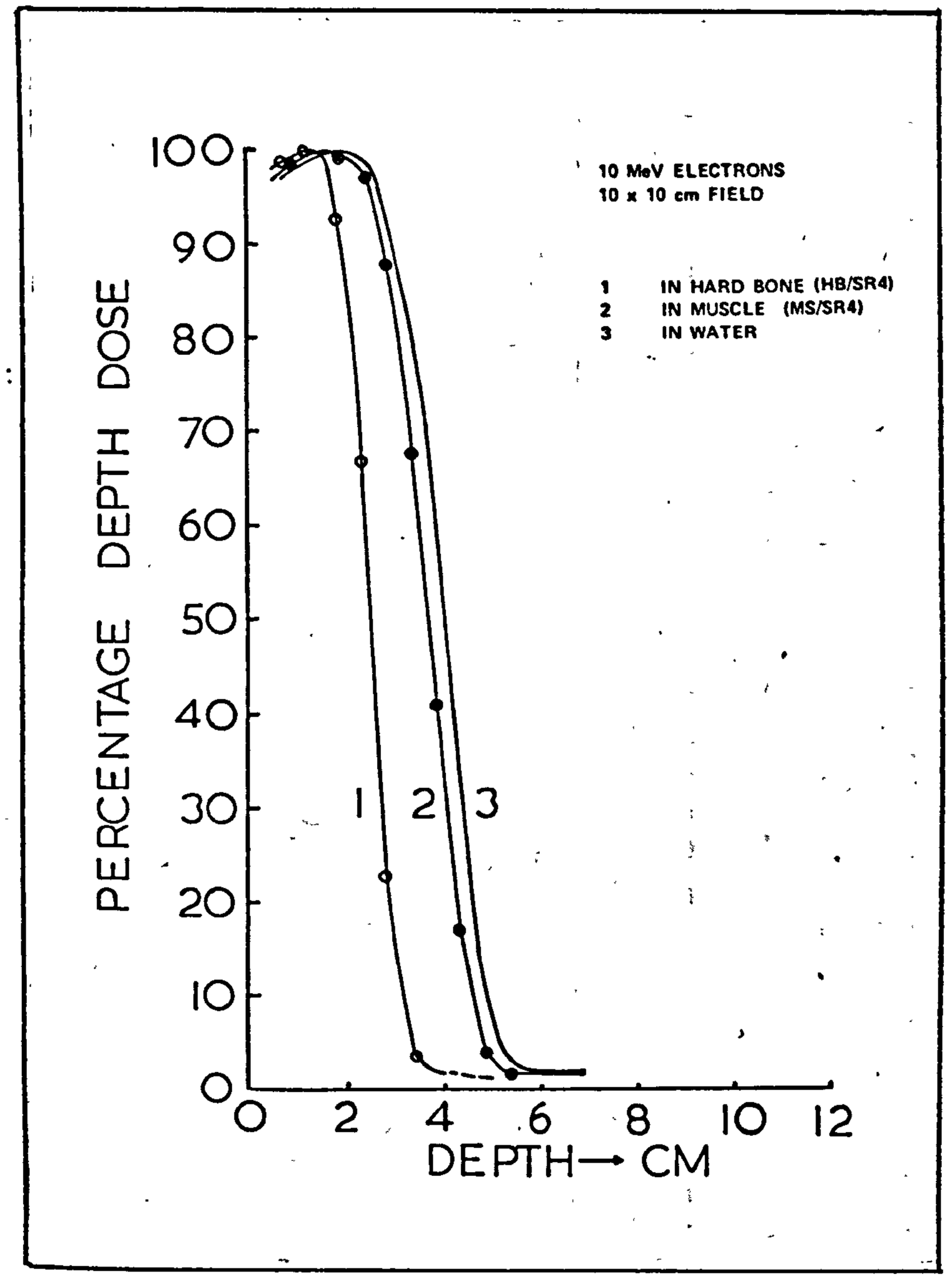

Figure 5.30 Central axis depth dose curves from 10MeV electrons in water, muscle (MS/SR4) and bone (HB/SR4)

TABLE 5-X CENTRAL AXIS PERCENTAGE DEPTH DOSES EXPRESSED AS DEPTHS OF PERCENTILES. 10 MeV ELECTRONS (10 cm x 10 cm)

PERCENTILE	DEPTHS OF PERCENTILES (cm)		
	IN WATER	IN MUSCLE	IN HARD BONE
100	2.0	1.7	1.4
90	3.0	2.8	1.9
80	3.4	3.1	2.1
70	3.6	3.4	2.3
60	3.8	3.6	2.4
50	4.0	3.8	2.5
40	4.2	3.9	2.6
30	4.4	4.1	2.7
20	4.6	4.3	2.9
10	4.9	4.6	3.2

TABLE 5-XI DEPTHS OF THE 50% DOSE AND EXTRAPOLATED RANGES IN WATER, MUSCLE, BONE. 10 MeV ELECTRONS (10 cm x 10 cm)

MATERIAL	DEPTH OF 50% DOSE		EXTRAPOLATED RANGE	
	cm	g/cm^2	cm	g/cm^2
Water	4.00	4.00	5.00	5.00
Muscle	3.80	4.03	4.70	5.03
Hard Bone	2.50	4.17	3.10	5.15

i) The distance from the scatterer to the front surface of the phantom was about 5 m and no beam defining applicator was used. The scatterer-phantom distance for the data given by JONES (1972) was much smaller, hence the divergence of the beam was more pronounced, resulting in the maximum being at a smaller depth.

ii) The average energy of the pulsed electron beam used at the position of the phantom was (15.3 $\pm$ 0.4) MeV instead of 15 MeV (LOVELL and SHEN, 1976)

iii) The dimensions of the phantom used were only 10 cm x 10 cm x 10 cm.

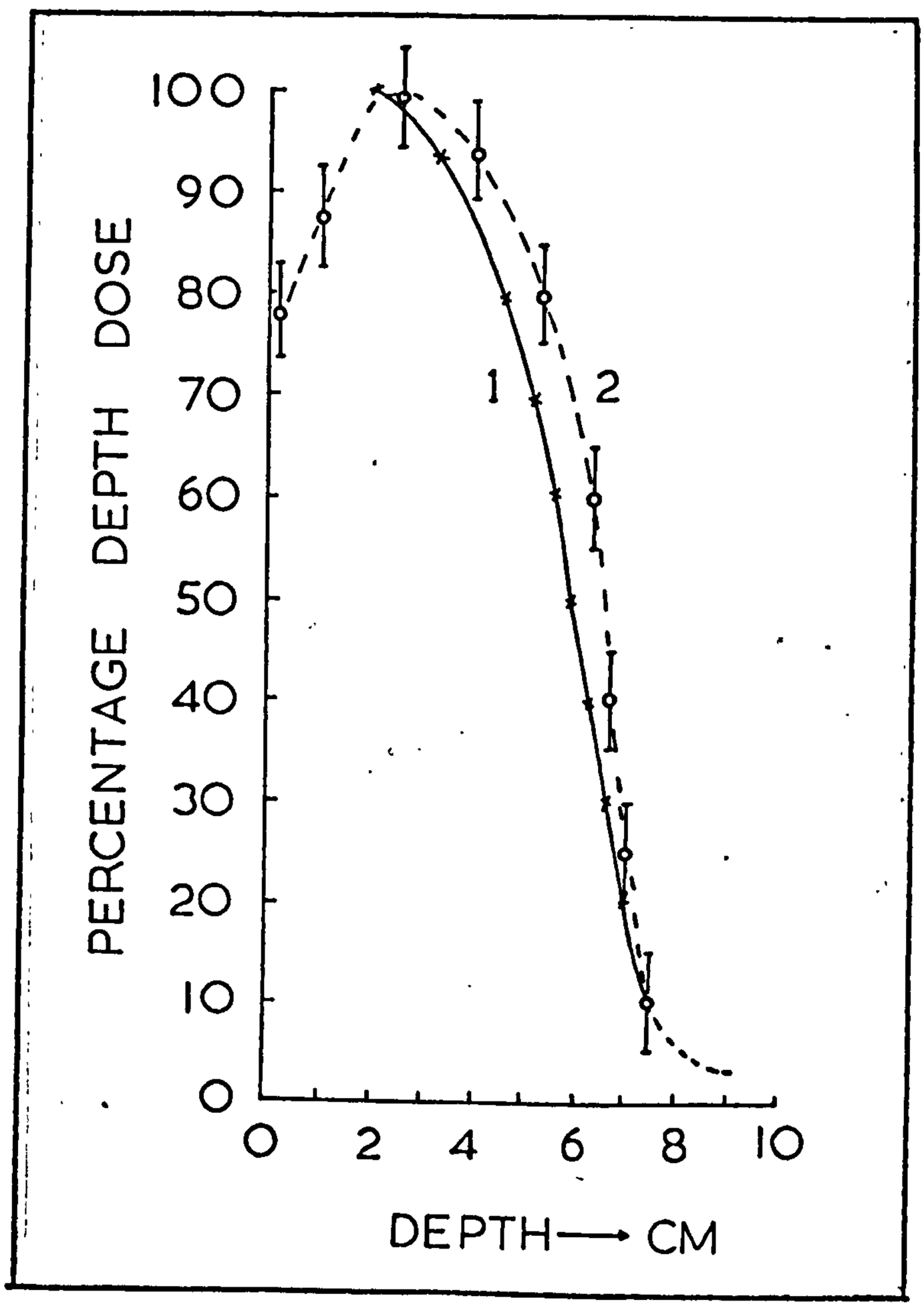

Figure 5.31 Central axis percentage depth doses from 15 MeV electrons

1. Data from supplement 11 of British Journal of Radiology (1972)
2. Measured in muscle (MS/SR4) at 5 m distance from the scatterer

5.3(iii) DOSE DISTRIBUTIONS IN COMPOSITE PHANTOMS

Central axis percentage depth dose measurements with 10 MeV electrons were made in composite phantoms consisting of various thicknesses of bone + water, fat + water, muscle + lung + water, muscle + air + water and finally muscle + bone + lung. The resulting depth dose curves were used to derive the "isodose shift factors" discussed in the next Chapter (Table 6-I). Figures 5.32 to 5.36 illustrate the results of these measurements. The solid curves were plotted by the X-Y plotter, and give the percentage depth doses at various depths in water with different thicknesses of "overlying tissue heterogeneity". From Figure 5.32 it is evident that the dose in water immediately behind 0.5 cm or 1 cm-thick bone is slightly higher than the dose in "water only" but this increase in dose is sufficiently small to be neglected under most clinical conditions. The isodose shift factor for lung was found to depend on the thickness of the lung traversed but it was found to be the same irrespective of the position of the lung in the composite phantom. Figure 5.34 shows the case of 2 cm muscle followed by various thicknesses of lung and this followed by water. Similarly Figure 5.35 shows the effect of 1 cm, 2 cm and 4 cm air gap in the composite phantom. Again, the position of the air gap in the phantom was not found to have any influence on the "shift" of the depth dose curve. Finally, Figure 5.36 shows a comparison of the depth dose curve in water with that obtained when 1.3 cm of muscle is followed by 1 cm of hard bone and this followed by lung. It is obvious that unless corrections are made for the presence of tissue heterogeneities, the dose distributions obtained from measurements in a water phantom alone are not satisfactory for accurate patient dosimetry.

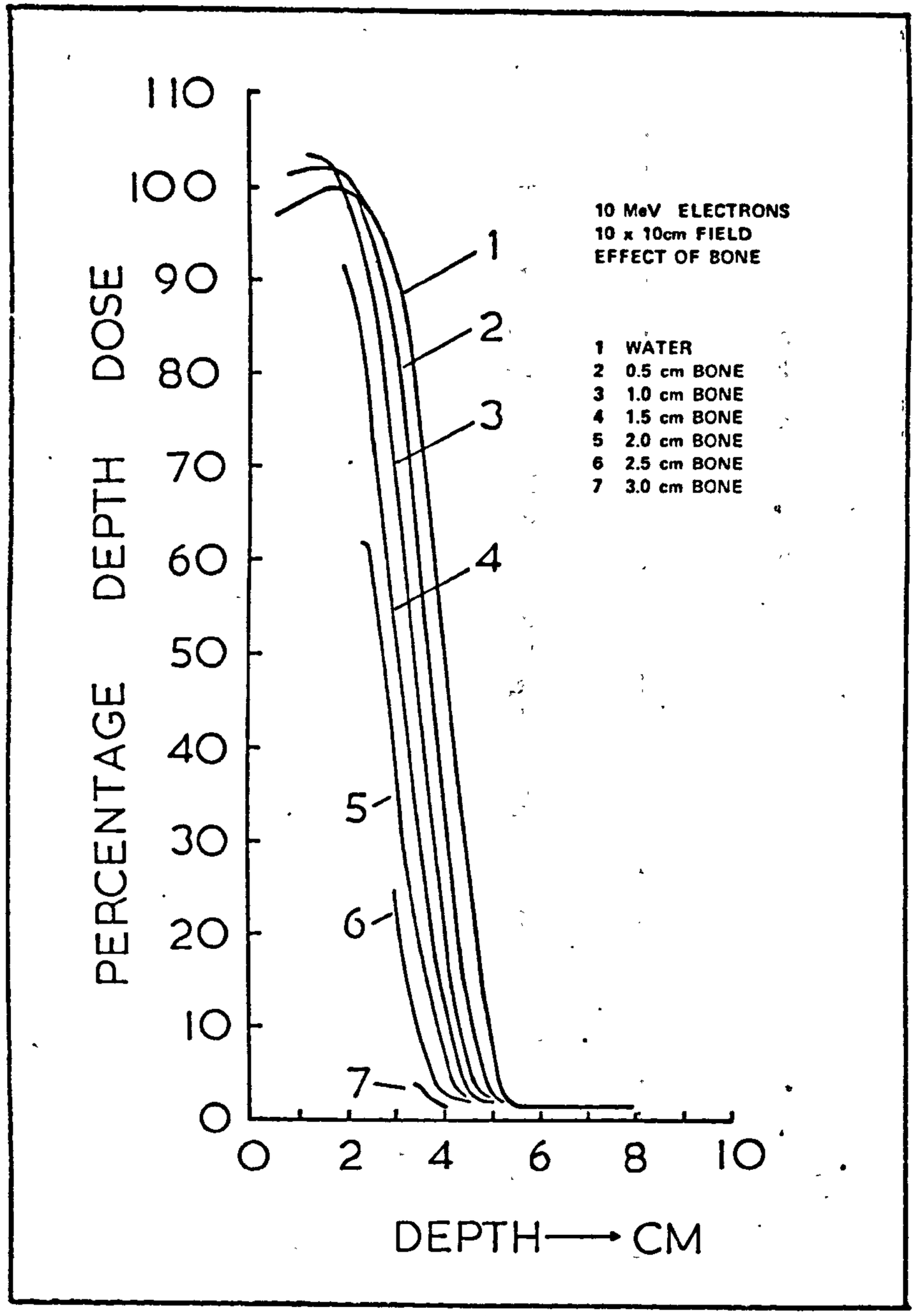

Figure 5.32 Central axis percentage depth dose curves in water with various thicknesses of overlying bone

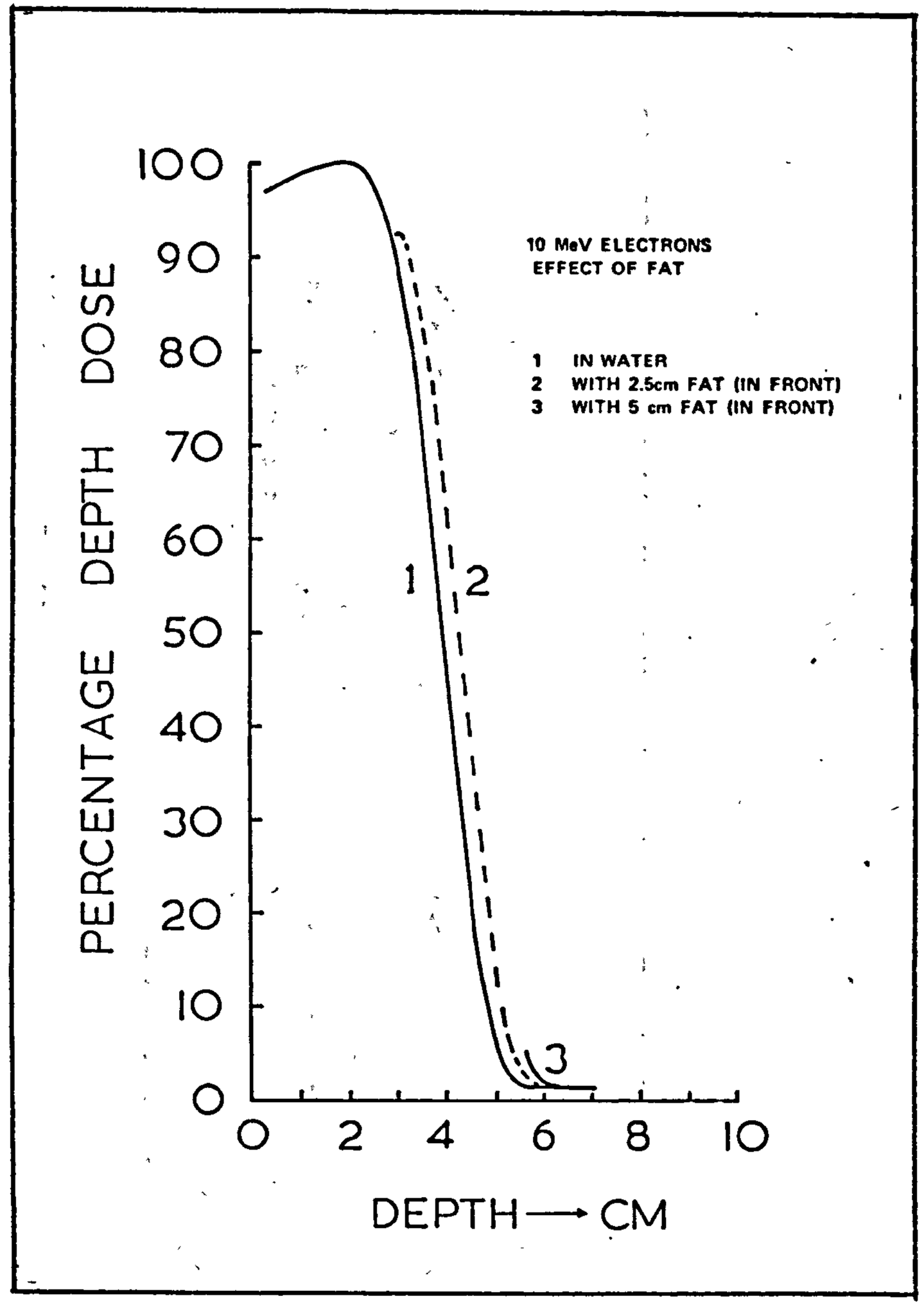

Figure 5.33 Central axis percentage depth dose curves in water with different thicknesses of overlying fat (FT/SF1)

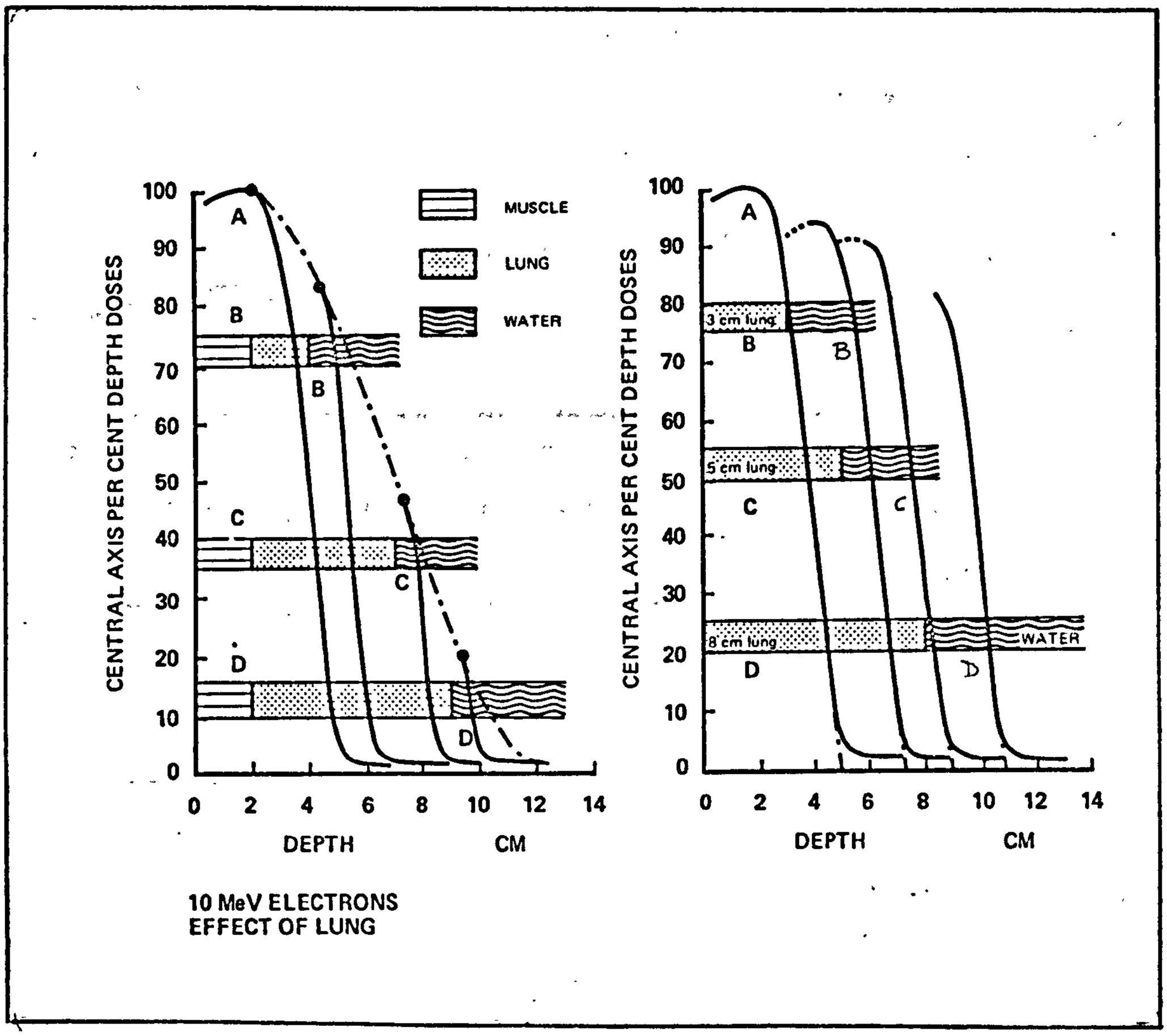

Figure 5.34 Effect of lung on the central axis depth doses from 10 MeV electrons

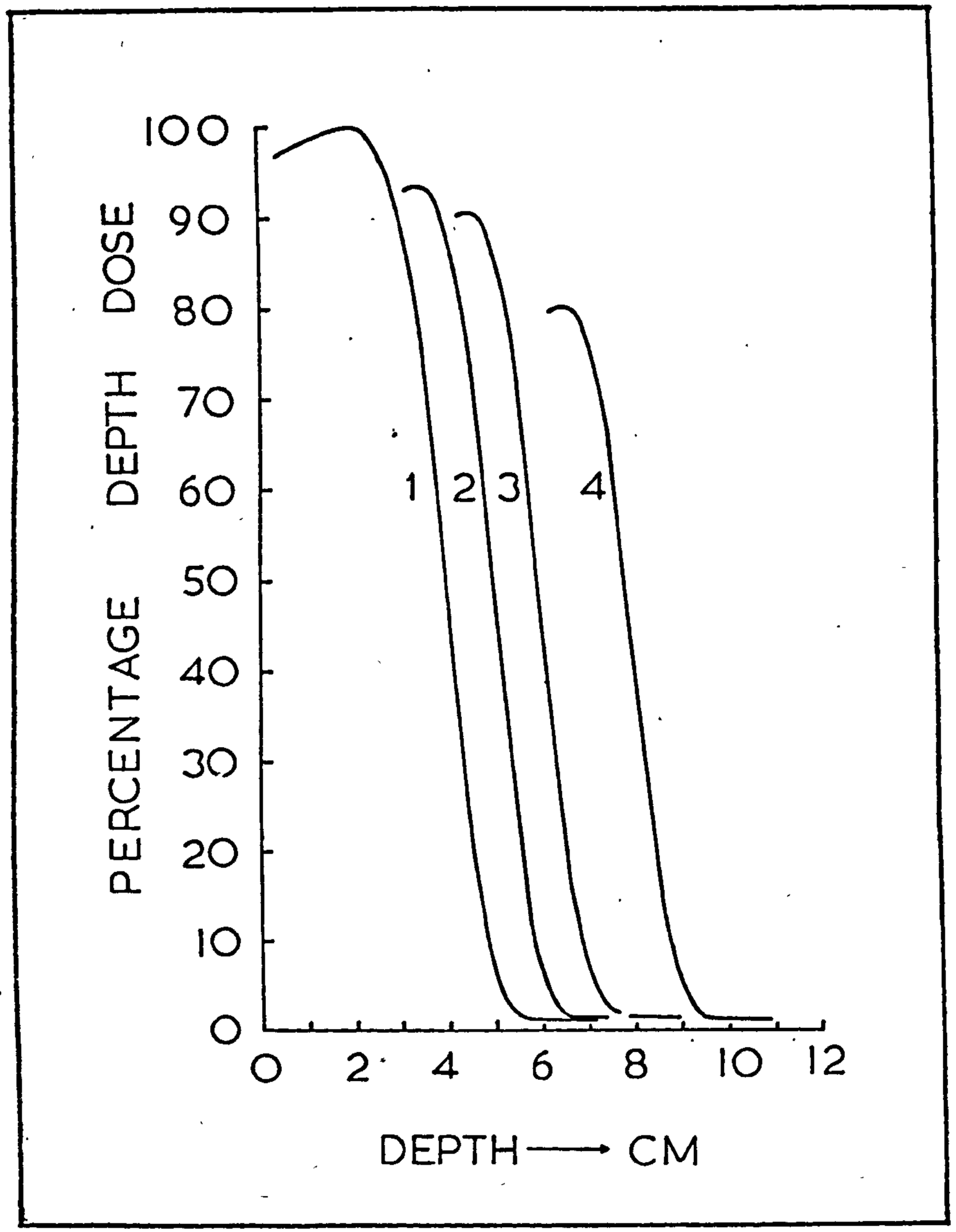

Figure 5.35 Central axis depth dose curves from 10 MeV electrons (10 cm x 10 cm)

1. In water
2. 2 cm MS/SR4 + 1 cm air + water
3. 2 cm MS/SR4 + 2 cm air + water
4. 2 cm MS/SR4 + 4 cm air + water

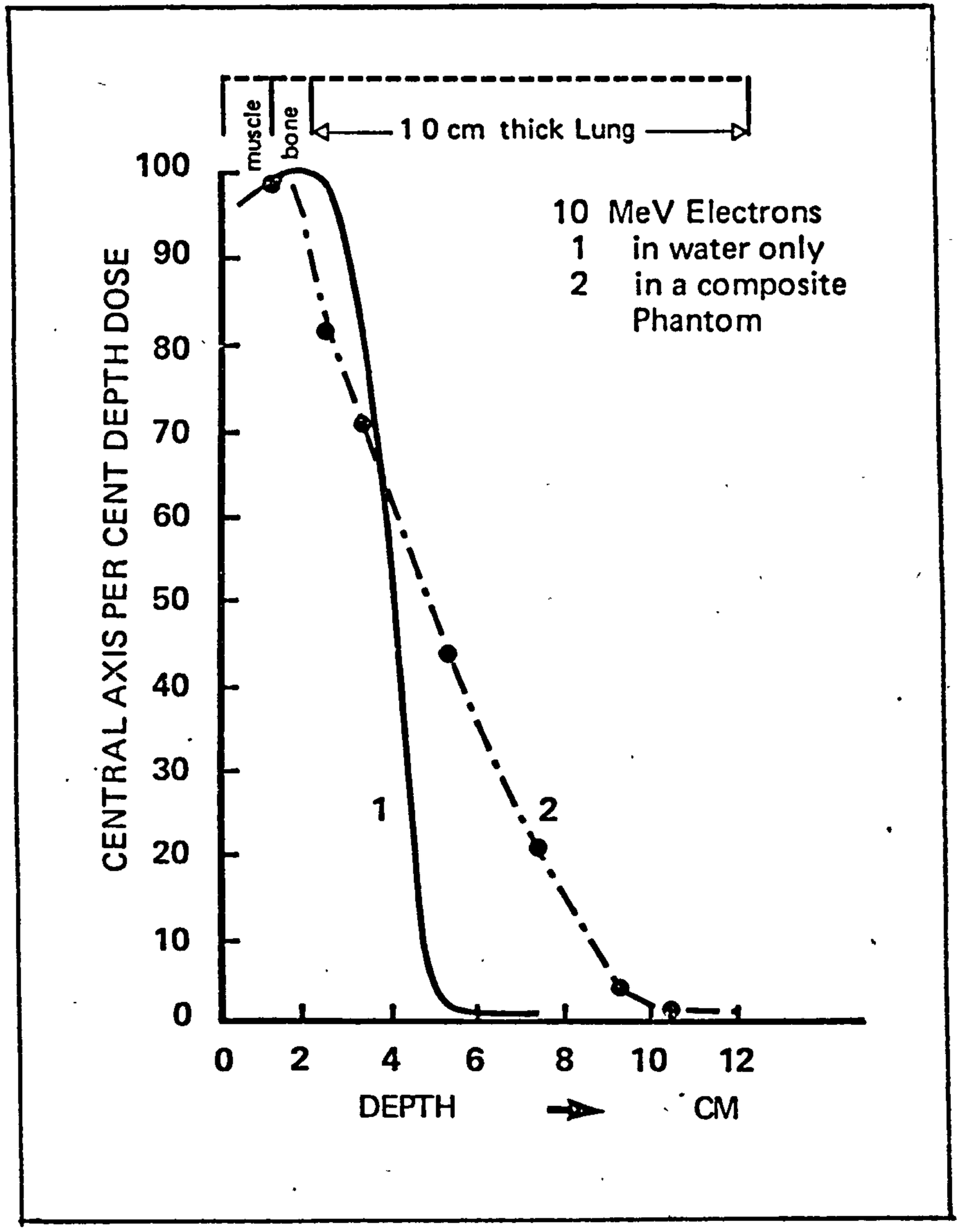

Figure 5.36 Electron depth doses in a composite phantom

5.4 DEPTH DOSE DISTRIBUTIONS OF A 70 MeV π^- MESON BEAM IN VARIOUS TISSUE SUBSTITUTES

(i) EQUIPMENT AND METHODS

The depth dose distributions of negative pions in various tissue substitutes were measured on the π 11 beam line of the proton synchrotron NIMROD (Rutherford High Energy Laboratory, U.K). NIMROD was used to accelerate protons to 7 GeV; a 6 x6x 10 cm copper target was placed in the proton beam and the negative pions produced were extracted at an angle 94^{o} , with an average momentum 160 MeV/c , corresponding to a kinetic energy of 70 MeV. Figure 5.37 illustrates the beam line used. (PERRY and HYNES, 1971).

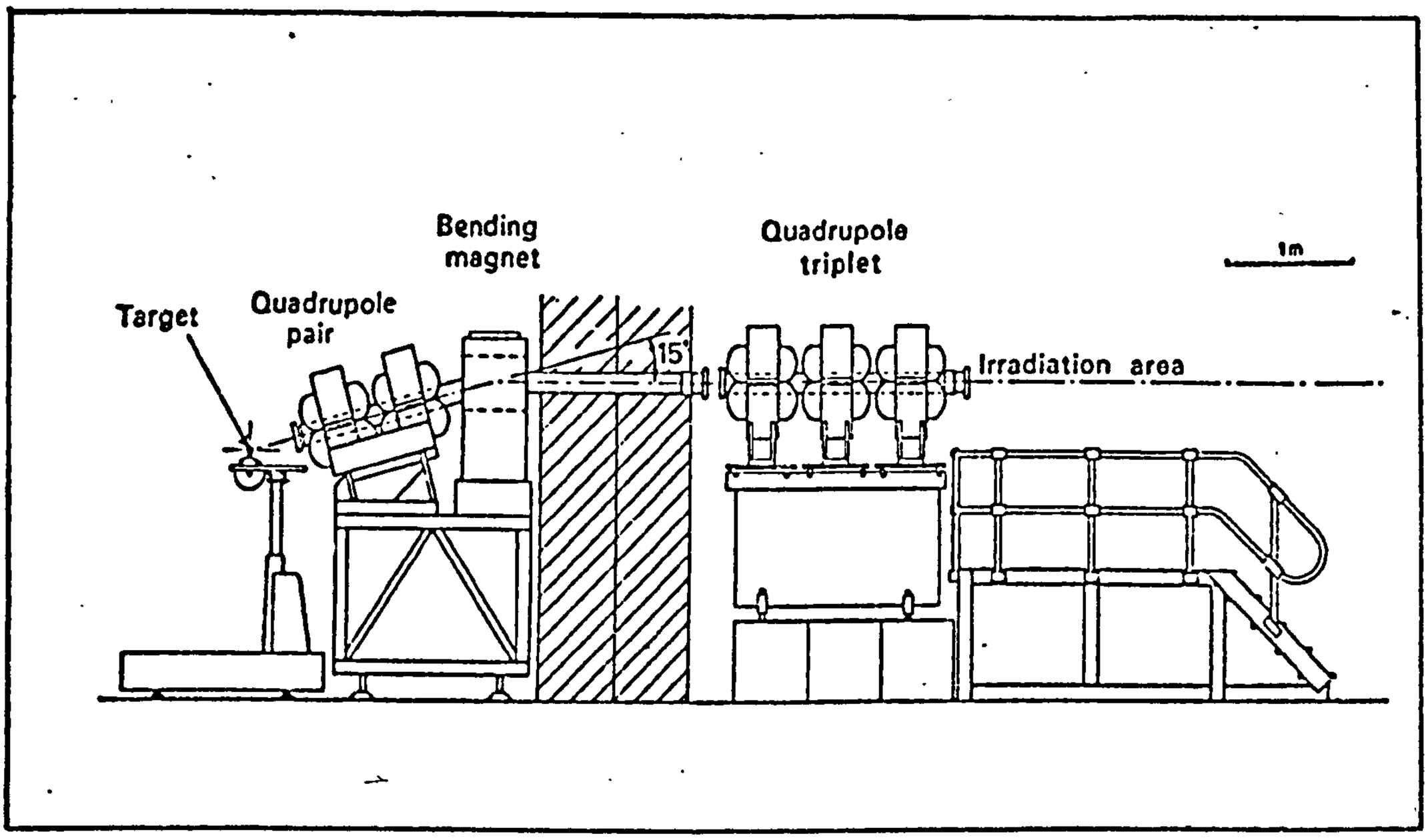

Figure 5.37 The π 11 beam line at the Rutherford Laboratory

Quadrupole pair : Initial collimation and focussing of the pion beam.

Quadrupole triplet : Final focussing on the irradiation position at 1 m from the last element of the triplet.

The 0.2 cm^3 air-filled cylindrical ionisation chamber (made of A-150 plastic) of the Rutherford Laboratory was used and its signal was fed into a Keithley 602 electrometer. Central axis measurements were carried out in various tissue substitutes, with at least two readings being taken at each depth. The average ratio $\left(\frac{TE}{TC}\right)_{AV.}$ where TE is the charge collected by the cylindrical ionisation chamber and TC is the charge collected simultaneously by the monitor transmission chamber, was plotted against depth in each material.

5.4(ii) MEASUREMENTS

Figure 5.38 shows the central axis depth dose curves from the 70 MeV pion beam in Perspex, in a muscle substitute (MS/SR4) and in water. Measurements were also carried out in a muscle equivalent liquid (MS/L1) and then repeated in a liquid which has approximately the same C,H,N,O contents as MS/L1 but includes no trace elements (MS/L1A). The effect of the trace elements was found to be insignificant, since the two sets of measurements were, within experimental error, the same.

The effect of hard bone, lung and an air gap placed in the plateau region were investigated and are shown in Figure 5.39, 5.40 and 5.41 respectively. Table 5-XII summarises the results.

By expressing the peak depth in g/cm^2 (i.e. by correcting for density), the difference in "equivalent thickness" between water and muscle was found to be less than 3%. When bone is present in the muscle phantom, however, the peak depth-equivalent thickness is larger than that in "muscle only" by about 6% for a 4 cm-thick hard

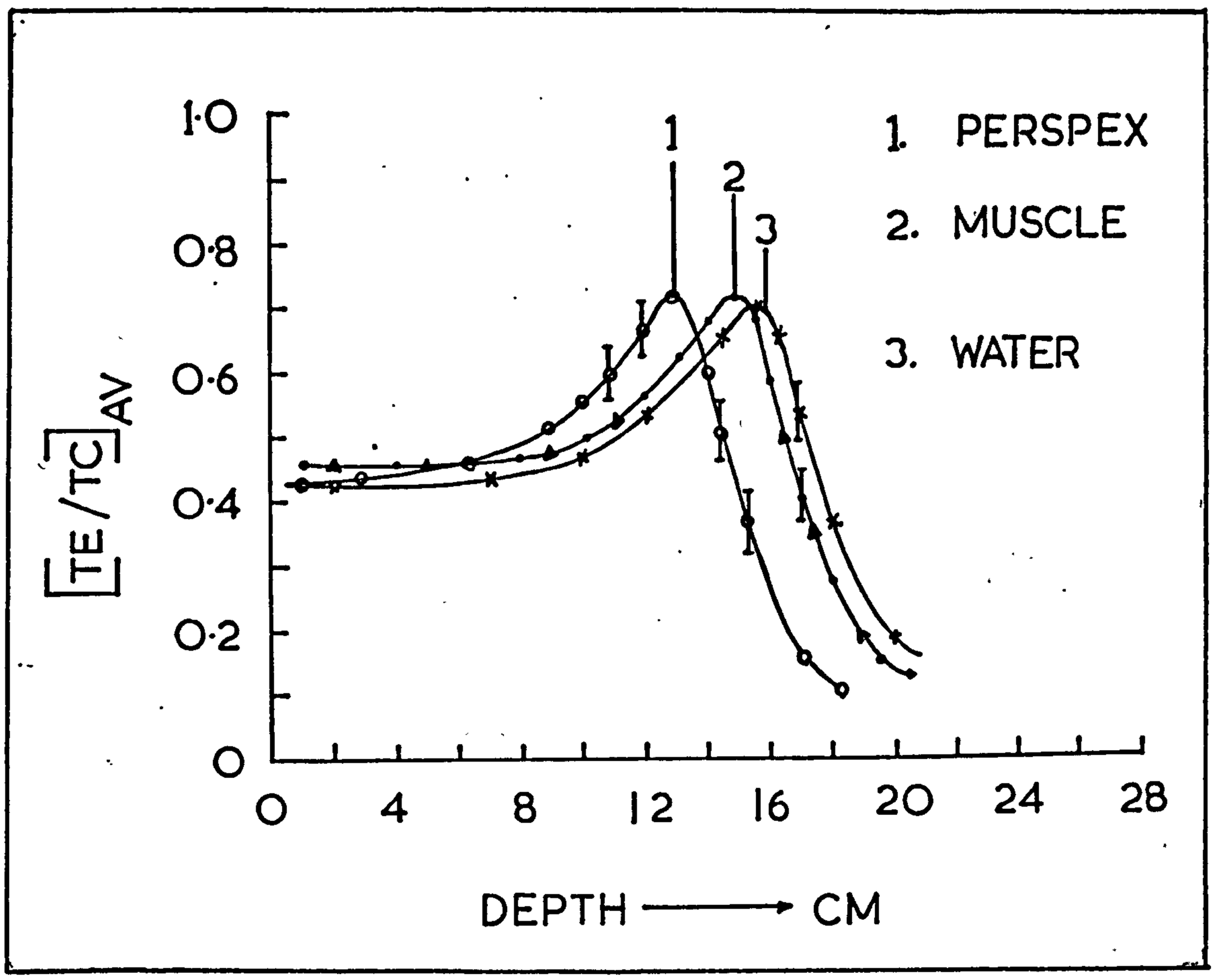

Figure 5.38 Central axis depth dose curves from 70 MeV negative pions in Perspex, muscle (MS/SR4 and MS/L1), and water

bone slab (HB/SR1) placed in the plateau. This is because bone with low hydrogen content, and hence lower electron density, is less effective than muscle in stopping pions on a gram for gram basis. However, the peak was found to be lower when bone was present. This could be due either to increased stopping of pions in bone (per cm of path) or increased scattering in bone.

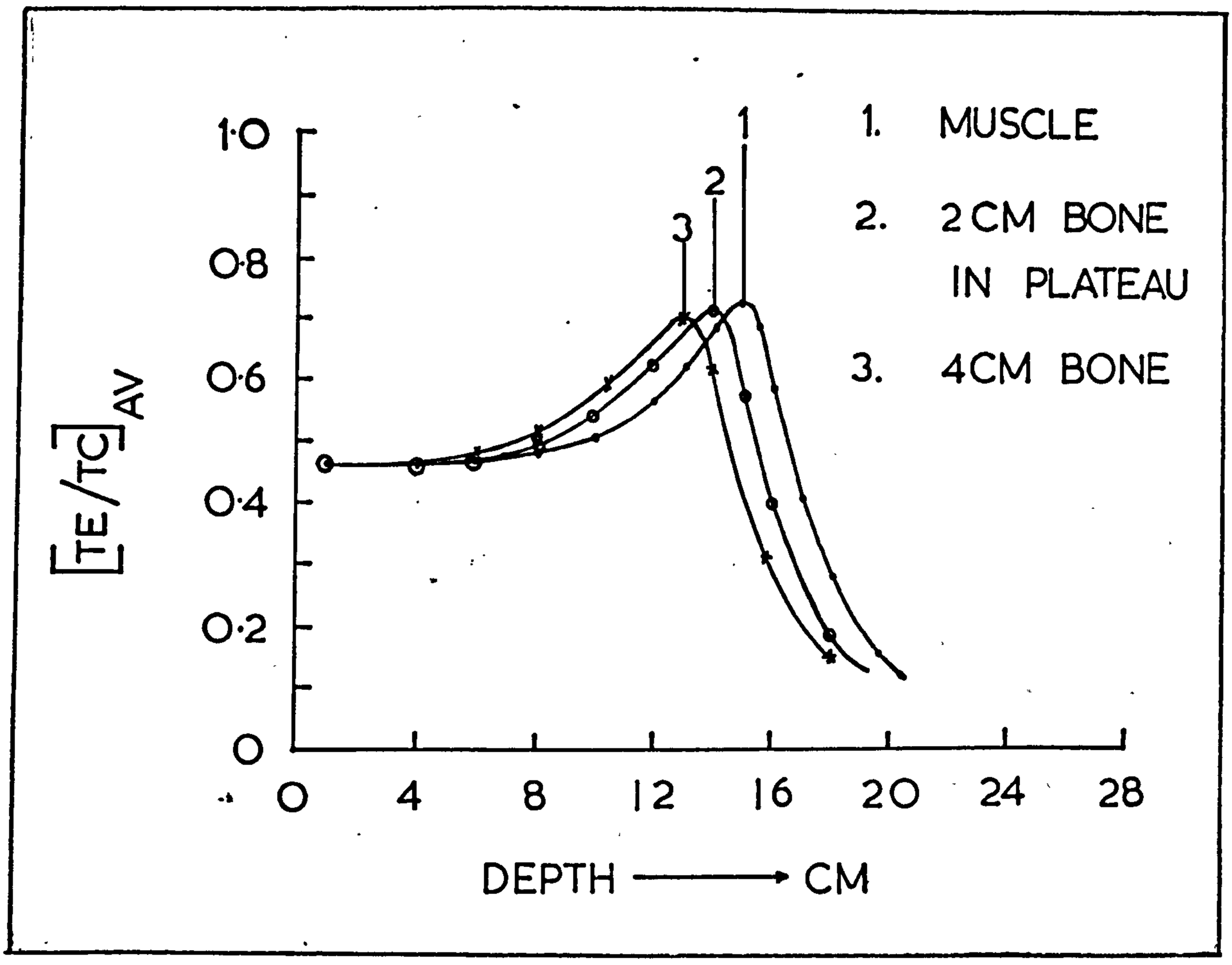

Figure 5.39 Effect of bone on the central axis depth doses of 70 MeV negative pions in muscle

In the case of lung and air gap, increased transmission and inverse square law effect result in an overall reduction of the peak height and the peak/entrance ratio. A density correction for lung would give the depth of the peak in muscle with less than 1% error. If the heterogeneity is in the pre-peak region, the effect is more pronounced. The corresponding shift of the peak position is given in Table 6-I, Chapter 6.

In summary, the peak/plateau ratio was found to be reduced:

a) by about 2% per cm of lung ,

b) by about 5% per cm of air gap ,

c) by 1.5-2.0% per cm of hard bone .

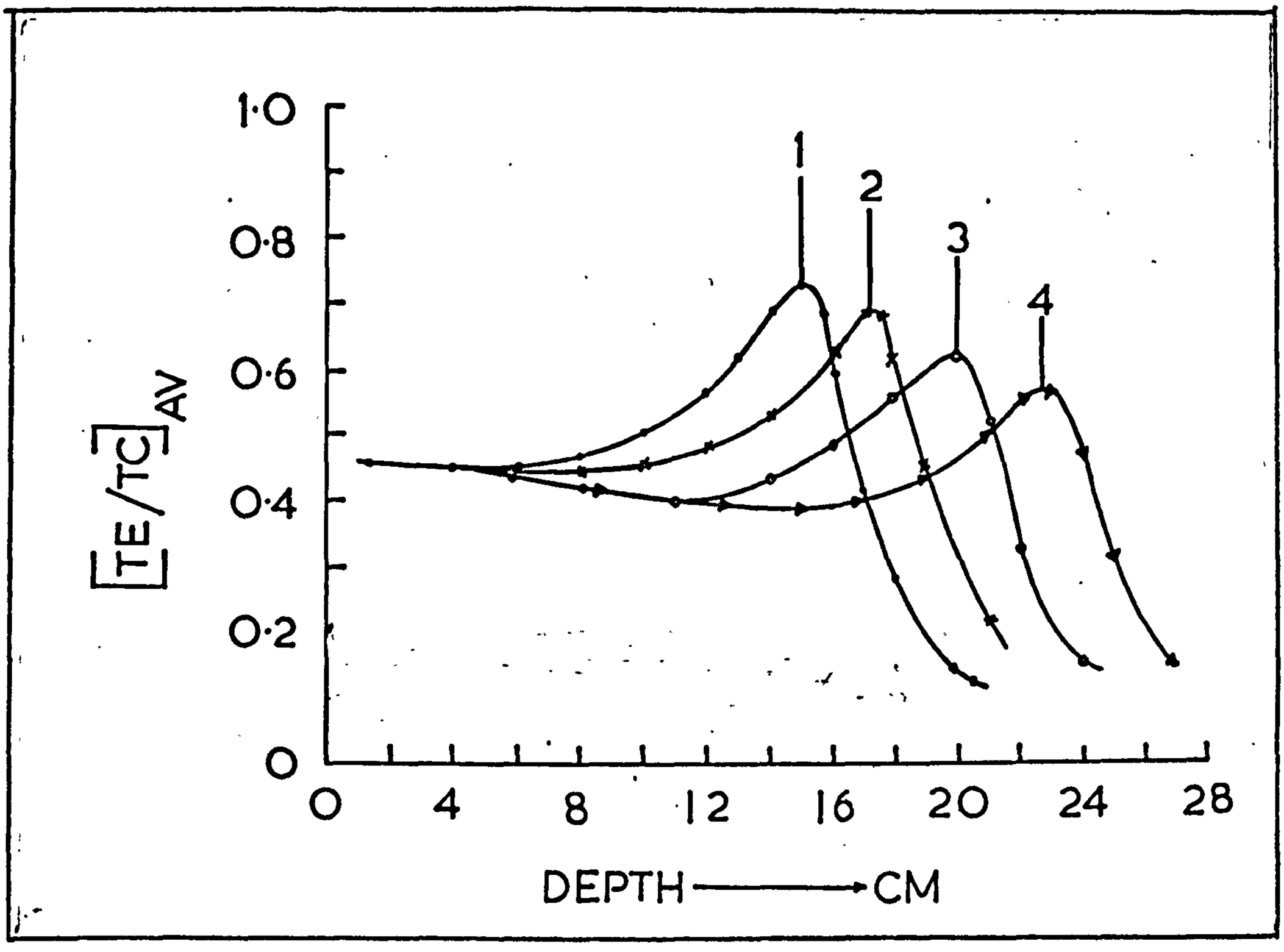

Figure 5.40 Effect of lung on the central axis depth doses of 70 MeV negative pions in muscle.

1) In muscle
2) 3 cm lung in plateau
3) 6 cm lung in plateau
4) 10 cm lung in plateau

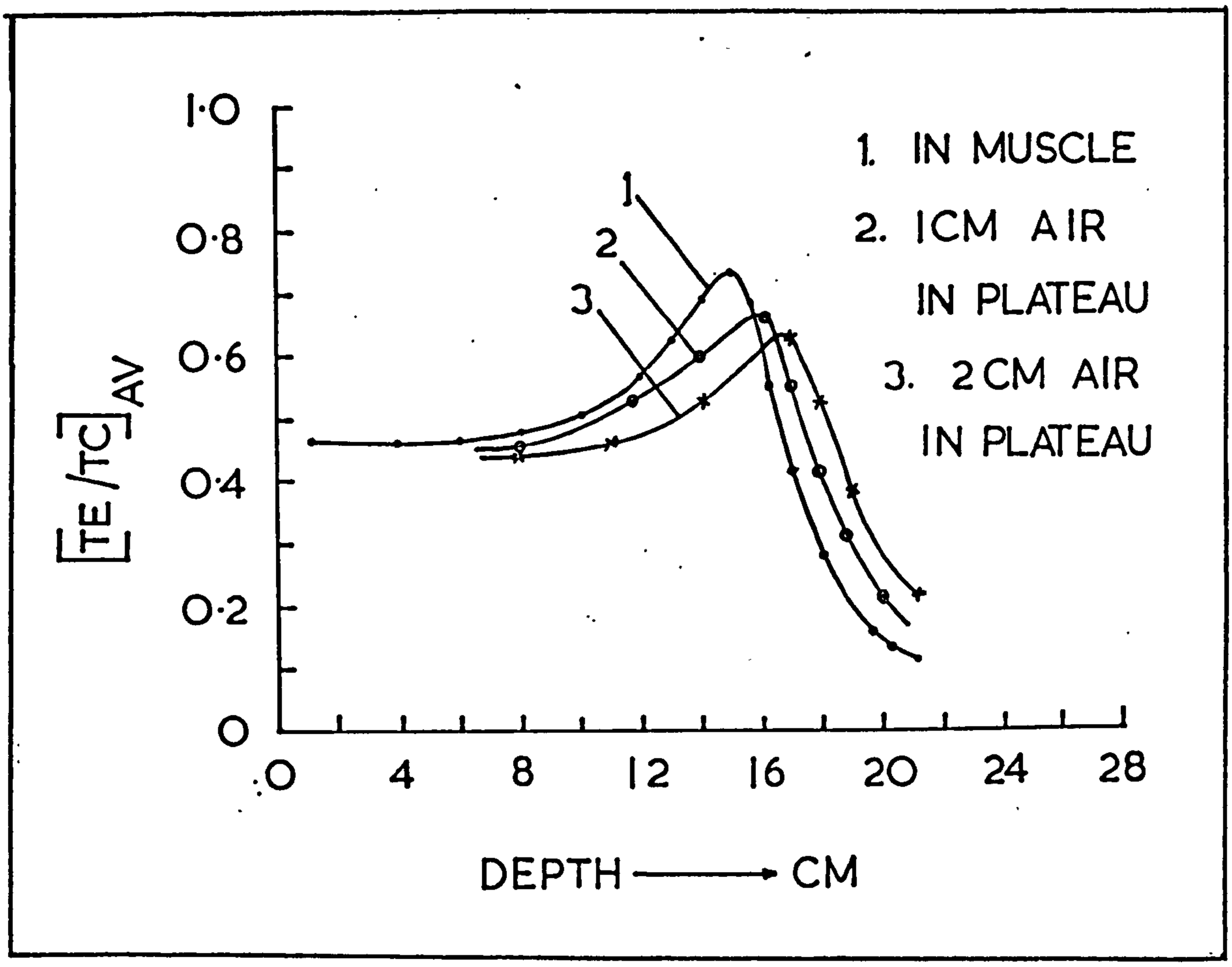

Figure 5.41 The effect of air spaces on the pion depth dose curves

The full width of the Bragg peak at the 80% level in MS/SR4, in the direction of the central axis of the beam was found to be 3.6 cm. A lateral scan of the pion beam at the depth of the peak, gave a beam profile with full width, at the 80% level, equal to 2.2 cm. Consequently, the volume enclosed by the 80% isodose surface, (assuming symmetry in the vertical and lateral directions), would be 3.6 cm x 2.2 cm x 2.2 cm. The volume given by ELLIS, et al., (1976) for the 80% dose contour of the same pion beam, is 4.0 cm x 2.3 cm x 2.3 cm.

TABLE 5-XII PHYSICAL DATA FOR 70 MeV NEGATIVE PIONS IN VARIOUS TISSUE SUBSTITUTES

Material	Peak depth		Peak height $(TE/TC)_{AV}$	Peak / Plateau	Full width at 80% level (cm)
	cm	g/cm^2			
Muscle	15.0	15.90	0.73	1.59	3.6
Perspex	13.0	15.50	0.71	1.55	3.2
Water	15.5	15.50	0.70	1.62	3.5
Muscle with:					
a) 4 cm hard bone in plateau	13.0	16.54	0.69	1.47	3.9
b) 6 cm lung in plateau	19.5	15.87	0.65	1.39	3.6
c) 2 cm air in plateau	16.8	15.90	0.67	1.44	3.2

* Relative density of lung used: 0.26

** Materials used: LN/SR4 for lung, MS/SR4 and MS/L1 for muscle, HB/SR1 for bone.

5.5 ENERGY LOSS BY ALPHA PARTICLES TRAVERSING VARIOUS LIQUID TISSUE SUBSTITUTES

The charged particles which contribute to the ionisation in the gas of ionisation chambers frequently used in neutron, proton and pion dosimetry, are mainly protons, pions, alpha particles and ions of carbon, nitrogen and oxygen. It is through the stopping of these particles that energy is deposited when heavy charged particles and neutrons interact with matter. A series of measurements using alpha particles emitted from an Americium-241 source was performed during this work, with the purpose of establishing the residual energy of these particles when they traverse known thicknesses of various liquids simulating different biological tissues. Such information can be used to determine the stopping powers of real tissues for alpha particles in the energy range from 1 MeV to 5 MeV. There are few published results of experimental measurements of the stopping power of liquids for alpha particles and these were restricted mainly to hydrocarbon liquids, ethanol, carbon tetrachloride and water (PALMER and SIMONS, 1959; PALMER, 1973 and 1978).

5.5(i) EXPERIMENTAL PROCEDURE AND MEASUREMENTS

An alpha particle source consisting of ^{241}Am deposited in a thin layer on a 0.317 cm diameter platinum disc, was positioned on top of a multihole collimator consisting of 26 holes of 0.35 mm diameter and 2.2 mm depth (see Figure 5.42). This collimator lay above a silicon detector (D) and could be moved vertically with the help of a micrometer system. As the detector was cemented in position in the base of the cell containing the liquid under investigation, the thickness of the liquid layer between the detector and the lower end of the collimator could be varied in increments of 1 μm. A more detailed description of the system used, which is the property of the City

University, London, was given by PALMER (1973).

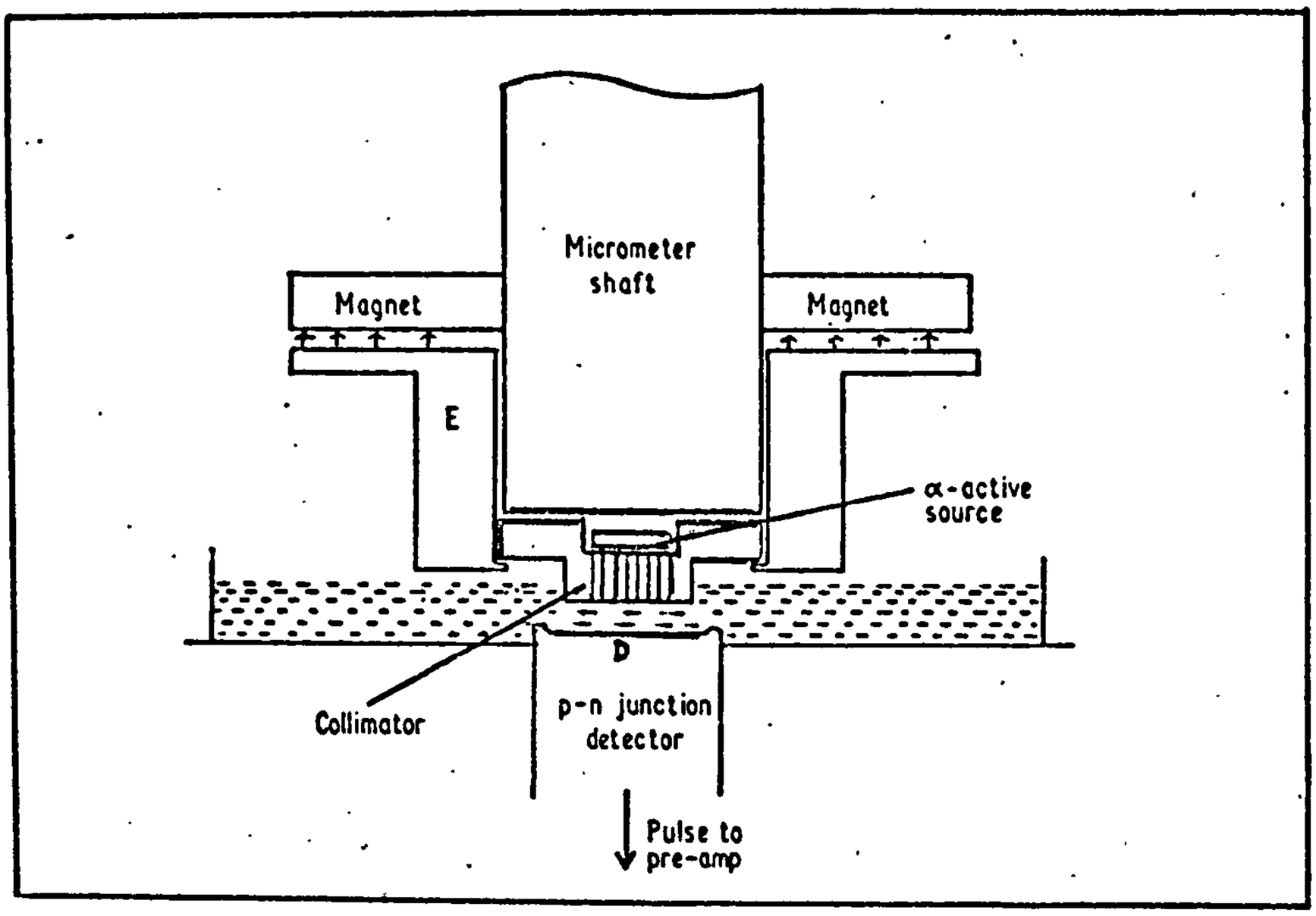

Figure 5.42 Apparatus used for the measurement of the energy loss by alpha particles traversing various liquids (PALMER, 1973)

The lower surface of the collimator was covered with a 1-2 μm-thick Melinex film, in order to prevent liquid from rising into the collimator holes by capillary action. The pulses produced in the detector by alpha particles traversing a liquid layer, were fed through a charge sensitive pre-amplifier to a calibrated 400 channel Laben pulse height analyser (PHA) and so their residual energy could be derived. Allowance was made for the initial energy loss of the particles in the air path in the collimator, in the Melinex film covering the collimator and in the window of the detector. The initial energy of the alpha particles was 5.48 MeV but their energy just before they entered the liquid was $E_a \simeq 5$ MeV (PALMER 1978). The channel number corresponding to the peak of the spectrum on the pulse height analyser indicated the residual energy of the particles and could be found within ± 2 channels. This meant an uncertainty in the measurement of the residual energy of ± 0.02 MeV.

With the liquid under investigation in the cell, the micrometer was first set as close to the "zero liquid path" position as practicable, and the residual energy of the alpha particles measured. Then the liquid path was increased in 2 μm increments, the residual energy being measured each time. A list of the liquid substitutes used and the energy loss ΔE_a in a 20 μm-thick layer of each, are given in Table 5-XIII.

An attempt to measure the same energy loss ΔE_a with 20 μm-thick sections of human fat, brain and muscle, for comparison purposes, failed. The real tissues were frozen with "carbon dioxide ice" and a microtome in a freezing cabinet was used to cut sections from the real tissues. All these sections had too many pinholes for the resulting spectrum on the pulse height analyser to have a clearly defined peak. An estimated position of a broad peak corresponded to the energy of the alpha particles passing through the pinholes rather than the solid material.

5.5(ii) RESULTS AND DISCUSSION

The energy loss ΔE_a suffered by the alpha particles in 20 μm-thick layer of each of the liquids used, is given in Table 5-XIII. In the last column, the value of ΔE_a, divided by the relative density of each liquid, i.e. normalised to "unit density material" is given. The maximum difference between any two of the normalised values of ΔE_a is 1.36% of the energy of the alpha particles just before they enter the liquid ($E_a \simeq 5$ MeV). However, if the measured values are compared, the most significant differences are between FAT and MUSCLE (8.2% of E_a), WATER and MUSCLE (2.5% of E_a) and TOTAL SKELETON and MUSCLE (15.32% of E_a).

TABLE 5-XIII ENERGY LOSS ΔE_a IN 20 μm OF SUBSTITUTE

TISSUE	SUBSTITUTE	EXPERIMENT ΔE_a(MeV)	IN UNIT DENSITY MATERIAL ΔE_a (MeV)
FAT	FT/L1	2.248	2.498
WATER	H_2O	2.535	2.535
MUSCLE	MS/L1	2.656	2.506
BLOOD	BL/L2	2.603	2.479
BRAIN	BRN/L6	2.566	2.467
TOTAL SOFT TISSUE	TST/L1	2.575	2.500
TOTAL SKELETON	TSK/L1	3.422	2.516

Measurements in two muscle substitutes, namely MS/L1 and MS/L1A, the first with and the second without trace elements, showed that the effect of trace elements is negligible. It appears that the difference in density and not in chemical composition among the various tissues is mostly responsible for their different effectiveness as far as stopping alpha particles from radioactive sources is concerned.

Using the same method and apparatus, PALMER (1978) measured the stopping powers of water and a muscle equivalent liquid (FRIGERIO 1972), for alpha particles of energies 0.5 MeV to 8 MeV and found similar results; the maximum difference between the stopping powers of water and "unit density muscle" was about 5% at 0.75 MeV. For measurements below 1.0 MeV, however, the data analysis may not have been accurate. At these low energies, the residual range is less than 10% of the total range and statistical fluctuations and noise affect the resolution of the system and reduce the accuracy.

Figure 5.43 shows the variation of the alpha particles' residual energy with thickness of liquid layer traversed, for four of the liquids used. By using the slopes of these curves, the values of the stopping powers given in Table 5-XIV were derived. (For the stopping power at 2 MeV, for example, the average of the slopes at 1.8, 2.0 and 2.2 MeV was considered).

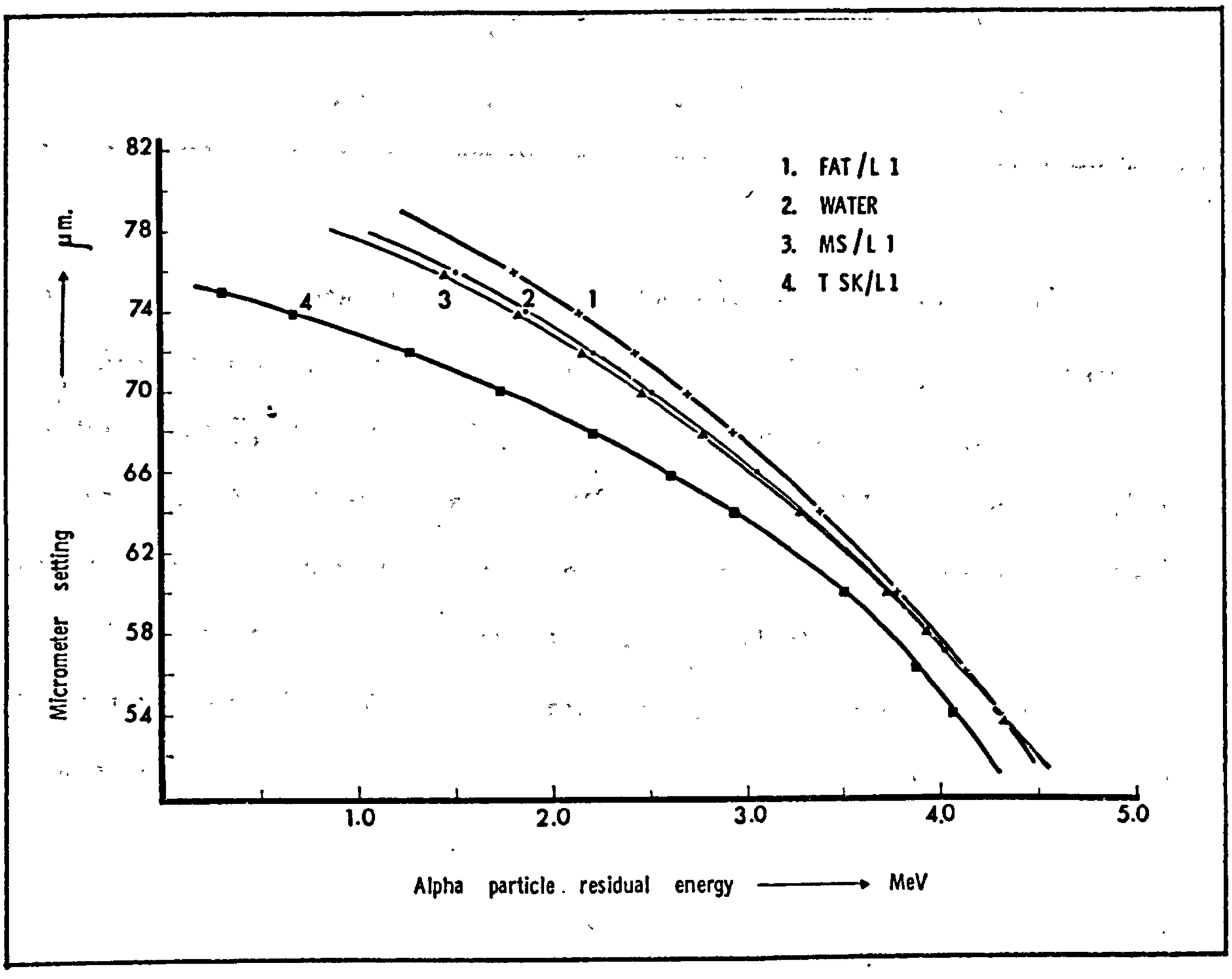

Figure 5.43 Relation of alpha particle residual energy with thickness of liquid traversed.

The stopping power values for water and MS/L1 are within ±.2% of those measured by PALMER (1978) but both sets are lower in general than calculated values given by OLDENBURG and BOOZ (1972) and by BARKAS and BERGER (1964). The difference between the calculated and measured stopping power of water for alpha particles of 4 MeV, for example, is 5%.

TABLE 5-XIV STOPPING POWERS OF VARIOUS TISSUE SUBSTITUTES FOR ALPHA PARTICLES OF 1-4 MeV

ENERGY MeV	STOPPING POWER (MeV/ μm)			
	FAT	WATER	MUSCLE	TOTAL SKELETON
1.0	0.193	0.218	0.230	0.296
2.0	0.151	0.169	0.179	0.230
3.0	0.115	0.128	0.137	0.175
4.0	0.086	0.103	0.108	0.136

Such measured data are sparse and because of the complexity of the interactions and processes involved (shell corrections, charge exchange etc), it is difficult to calculate them with acceptable accuracy. Now that suitable TISSUE EQUIVALENT liquids exist, further experimental measurements should be carried out using the most important of them, in order to establish their stopping power for alpha particles of energies encountered in neutron, proton and pion therapy.

CHAPTER 6

THE EFFECT OF TISSUE HETEROGENEITIES ON THE DOSE DISTRIBUTIONS IN RADIOTHERAPY

6.1 SOME GENERAL COMMENTS

The standard isodose curves and depth dose tables apply to beams of radiation entering a homogeneous unit density phantom. The presence of tissue heterogeneities, however, can alter the dose distribution. Body heterogeneities may be defined as those tissues whose interactions with radiation differ from that of muscle.

If a beam has passed through a heterogeneity, the absorbed dose at any point beyond it, is modified. Apart from that, the energy deposited at points within the heterogeneity itself, for a given exposure, is not the same as in muscle.

It is sufficient in practical dosimetry to take into account only the heterogeneities of lung, air spaces, bone tissue and fat.

In lung tissue, owing to its lower density and, therefore, lower absorption, there is greater transmission of radiation than in soft tissue of the same thickness. Although the amount of radiation scattered by the lung is smaller, for points beyond it, the increase in dose due to extra transmission is always greater than the loss in scattered radiation dose.

In the case of air cavities, there is a further effect to note; the removal of virtually all the absorbing material results in a loss of complete charged particle equilibrium for narrow beams. This means that, in spite of the increased transmission of radiation, the dose at a point just beyond an air cavity can be less than the dose at a corresponding point in a complete phantom. MASSEY (1962) found

that with 4 MeV X-rays, the loss of dose does not exceed 10% at the most, but unfortunately occurs just where the tumour may be. At 1 cm beyond the air cavity, however, the small increase due to extra transmission of radiation is observed.

If the heterogeneity in the irradiated tissue is bone, the depth dose at points lying in its "shadow" will be different from what it would have been, had the bone not been present. The change depends mainly on the thickness of the bone and the type and energy of the radiation beam. With X and gamma rays the dose at points behind the bone is reduced and this reduction is more pronounced in the case of soft X-rays. In the case of electrons, due to the strong dependence of scattering on the atomic number, there is increased scattering in bone relative to its mass and this results in a slightly elevated dose in bone and at points lying in the tissue close to the distal interface of the bone.With fast neutrons, the low hydrogen content of bone counterbalances its higher density and so the effect of the presence of bone on the depth doses beyond it, is greatly reduced.

A set of "isodose shift factors" for different types of radiation as well as lung correction factors for clinical use with 7.5 MeV neutrons and cobalt-60 gamma rays, derived from measurements during this study, will now be presented.

6.2 MEASURED ISODOSE SHIFT FACTORS FOR THE EFFECT OF AIR, LUNG, FAT AND BONE ON THE DOSE DISTRIBUTIONS, WITH VARIOUS RADIATION MODALITIES

It is usual in radiotherapy to estimate the dose at various points by first assuming that the body consists of homogeneous soft tissue and then to correct the dose distribution thus obtained, for the presence of heterogeneities.

When such corrections are carried out either manually or by means of a computer, the volume and composition of the heterogeneities must be known as accurately as possible. The accuracy with which this information is obtained, affects the overall accuracy of the isodose plan.

An empirical method of correcting for the effect of heterogeneities consists in merely displacing the isodose curves by a fraction of the thickness of the heterogeneity traversed by the beam, according to the rules given in Table 6-I. The values given in this Table were derived by comparing the depth dose curve in muscle substitute alone, to those obtained when part of the homogeneous substitute was replaced with various thicknesses of the heterogeneity. The displacement of the depth dose curve was divided by the thickness of the heterogeneity used, to give the corresponding isodose shift factor.

The muscle substitutes used for the measurements with fast neutrons, high energy protons and pions, were MS/SR4 and MS/L1. In the case of cobalt-60 gamma rays and electrons, water was used as the muscle substitute. The lung substitute (LN/SR4) used for the measurements with π^- mesons had a relative density of 0.26, whereas the lung sample used for all the other measurements had a relative density of 0.30. Most of the experimental depth dose data used for the

derivation of the isodose shift factors, have already been given in the previous chapter.

TABLE 6-I ISODOSE SHIFT FACTORS FOR VARIOUS TYPES OF RADIATION AND VARIOUS BODY HETEROGENEITIES

Type of radiation and energy	Heterogeneity	Position of point with respect to heterogeneity	Isodose shift (t=thickness of heterogeneity)	Direction of movement of isodose curve
Cobalt-60 gamma rays	Air	Behind	0.60 t	Distal
	Lung *	Behind d < 5 cm	0.35 t	Distal
		" d > 5 cm	0.45 t	Distal
	Fat	Behind	0.10 t	Distal
	Average skeleton	Behind	0.25 t	Proximal
	Cortical bone	Behind	0.40 t	Proximal
Neutrons $\bar{E}_n$ = 7.5 MeV	Air	Behind	0.75 t	Distal
	Lung **	Within (first half)	0.10 t	Proximal
		" (second ")	0.20 t	Distal
		Behind d < 5 cm	0.50 t	Distal
		" d > 5 cm	0.60 t	Distal
	Fat	Behind	no shift	-
	Cortical Bone	Behind	no shift	-
Electrons 10 MeV	Air	Behind	1.00 t	Distal
	Lung	Behind	0.70 t	Distal
	Fat	Behind	0.10 t	Distal
	Cortical Bone	Behind	0.60 t	Proximal
π - Mesons 70 Mev	Air	Behind	0.90 t	Distal
	Lung	Behind	0.75 t	Distal
	Fat	Behind	0.10 t	Distal
	Cortical Bone	Behind	0.50 t	Proximal
Protons 150 MeV	Air	Behind	0.90 t	Distal
	Lung	Behind	0.75 t	Distal
	Fat	Behind	0.10 t	Distal
	Total Skeleton	Behind	0.25 t	Proximal
	Cortical Bone	Behind	0.40 t	Proximal

* For points behind the lung, a single isodose shift factor of 0.4 t for Cobalt gamma rays would give the true doses with an error of the order of ± 2 percent.

** With 7.5 MeV neutrons, a single distal shift of 0.5 t, would give doses behind the lung within ± 2 percent.

When the effect of air spaces present in the phantom, on the dose distributionsfrom high energy protons, fast neutrons and cobalt-60 gamma rays was investigated, polypropylene tubes with 1 mm-thick walls and diameters of 1 cm to 4 cm were used, covering only part of the beam cross section. All the other experiments were made with the heterogeneity covering the entire cross section of the radiation beam.

SUNDBOM (1965), experimented with cobalt-60 gamma rays and suggested a 0.5t distal displacement of the isodose curves for lung (t=thickness of heterogeneity traversed). GREEN and STEWART (1965), suggested a 0.4t distal shift for lung and a 0.5t proximal shift for bone; the substitutes they used, however, were cork of unknown composition for lung and aluminium which is considerably denser than bone.

With the use of computers in treatment planning, it is possible to produce accurate isodose distributions provided that a set of correction factors is available for each type of heterogeneity and that the shape, location and density of the internal organs is accurately known; information about the shape and position of the internal organs is now easily obtained with computerised tomography scanners.

The lung correction factors for 7.5 MeV neutrons and cobalt-60 gamma rays measured during this work will be given in the next section.

6.3 LUNG CORRECTION FACTORS FOR USE IN COMPUTERISED ISODOSE PLANNING

It was not until the beginning of the past decade that computers have really been used to obtain dose distributions corrected for tissue heterogeneities. Today the problem can be approached by using either a set of measured correction factors or mathematical models.

If no correction is made, errors well in excess of ± 5% of the average tumour dose, considered as clinically acceptable, could result.

The new lung and muscle substitutes were used to measure lung correction factors and to investigate the effect of field size and position of the lung in the phantom on these correction factors in the cases of cobalt-60 gamma rays and 7.5 MeV neutrons.

Unlike cork and other materials used to approximate lung in the past, the porous nature and elemental composition of the lung substitute formulated and used in this work, are very close to those of real lung.

6.3(i) LUNG CORRECTION FACTORS FOR FAST NEUTRONS

The measurements for the derivation of the lung correction factors for fast neutrons were made in a 20 cm-cube phantom made of 1 cm and 2 cm-thick slabs of a solid muscle substitute (MS/SR4), using the neutron beam of the Medical Research Council cyclotron, at Hammersmith, London. The slabs of the solid lung substitute (LNG/SR4) used were flat and had lateral dimensions larger than the largest field size. Readings were taken at each depth with and without the presence of lung, first in the muscle in front of the lung, then within the lung itself and finally in the muscle behind the lung. The gamma ray component of the dose was subtracted from the total dose at each depth,

to give the neutron dose. At each point, the neutron dose with the lung present was divided by the neutron dose without the lung, to give the correction factor. Lung thicknesses from 1 cm to 10 cm were used and the measurements were repeated for three field sizes, namely 4.5 cm x 6 cm, 9.5 cm x 9.5 cm and 14 cm x 14 cm.

Figure 6.1 shows the central axis neutron depth dose curve in muscle for a 9.5 cm x 9.5 cm field, as well as the effect of 5 cm and 8 cm-thick lung on the depth doses.

The correction factors for the 9.5 cm x 9.5 cm field are given in Table 6-II and plotted for 3 cm, 5 cm and 8 cm-thick lung in Figure 6.2, where the field size effect for 8 cm-thick lung is also shown.

The neutron dose in the muscle tissue lying in front of the lung is reduced by 2-3 percent at the most; for the first few centimeters within the lung, the correction factor fell below 1.00, indicating that the neutron dose in lung can be lower than the neutron dose for the same point in muscle. For points deeper in lung, the increased transmission of the primary beam more than compensates for the reduced scattered radiation and the net result is an increase of the neutron dose with increasing depth in lung. The dose to a point lying in an 8 cm-thick lung, just 1 cm from the distal interface, would be larger than the dose at the same point in muscle, by about 25 percent. The correction factor continues to increase in the muscle behind the lung nearly linearly and towards the back of the phantom it tends to level off, possibly due to reduced backscatter at the end of the phantom. It is notable that at a point 10 cm behind an 8 cm-thick lung, the neutron dose could be as much as 100% larger than the dose that normal depth dose curves would indicate.

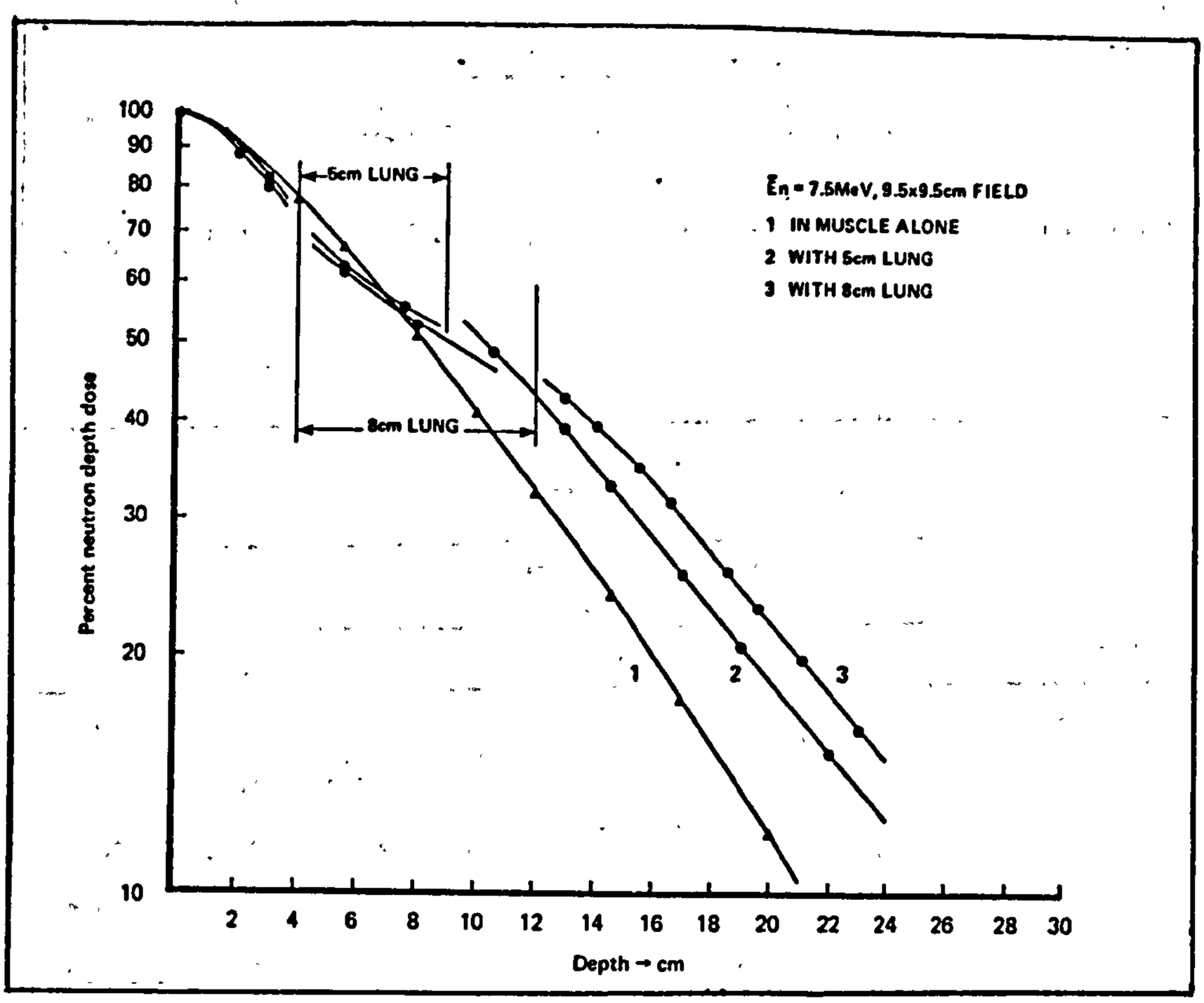

Figure 6.1 Effect of lung on the central axis neutron depth doses in muscle.

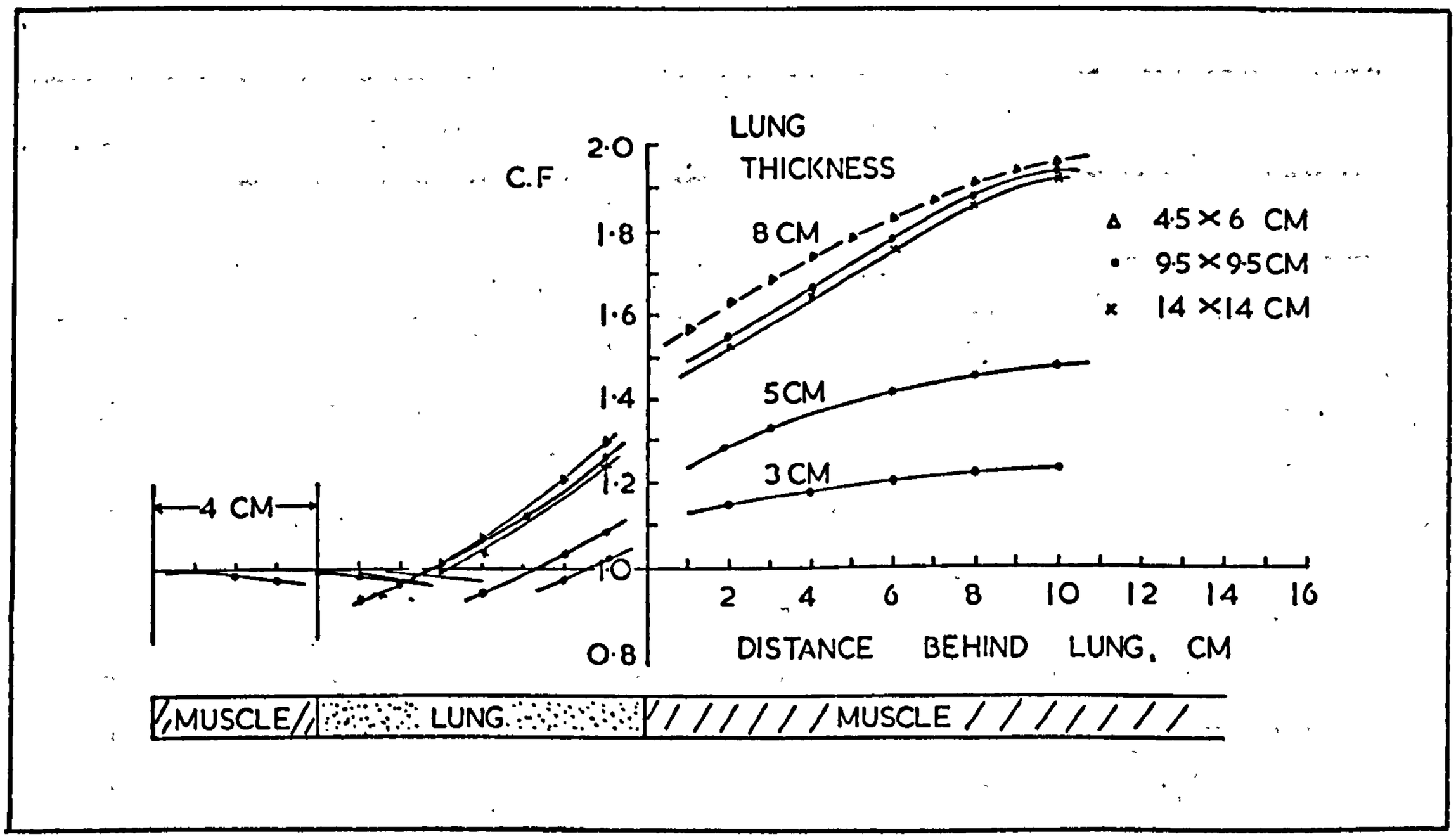

Figure 6.2 Lung correction factors for fast neutrons ($\bar{E}_n$ = 7.5 MeV, TSD = 120 cm) - Effect of field size and lung thicknes.

TABLE 6 - II

LUNG* CORRECTION FACTORS FOR FAST NEUTRONS

($\bar{E}_n$ = 7.5 MeV, 9.5cm x 9.5cm FIELD , T.S.D. = 120cm).

Thickness of lung traversed cm	Point in muscle tissue before the lung			Point within the lung								
	Distance from interface (cm)			Distance from first interface (cm)								
	1	2	3	1	2	3	4	5	6	7	8	9
1	0.991	0.993	0.995									
2	0.989	0.991	0.993	1.00								
3	0.987	0.989	0.991	0.980	1.024							
4	0.985	0.987	0.990	0.960	1.00	1.040						
5	0.982	0.985	0.989	0.940	0.980	1.035	1.080					
6	0.979	0.983	0.988	0.933	0.970	1.015	1.070	1.185				
7	0.976	0.931	0.987	0.924	0.960	1.00	1.050	1.115	1.185			
8	0.972	0.978	0.986	0.920	0.958	0.999	1.050	1.115	1.184	1.260		
9	0.968	0.975	0.985	0.918	0.944	0.980	1.025	1.100	1.180	1.260	1.330	
10	0.964	0.972	0.984	0.916	0.940	0.978	1.015	1.080	1.165	1.245	1.320	1.390

Thickness of lung traversed cm	Point in muscle tissue behind the lung									
	Distance from second interface (cm)									
	1	2	3	4	5	6	7	8	9	10
1	1.040	1.060	1.070	1.080	1.090	1.095	1.100	1.105	1.110	1.115
2	1.075	1.100	1.110	1.020	1.130	1.140	1.150	1.160	1.165	1.170
3	1.135	1.150	1.165	1.175	1.190	1.205	1.215	1.225	1.235	1.240
4	1.190	1.210	1.230	1.260	1.280	1.300	1.310	1.320	1.330	1.340
5	1.250	1.290	1.330	1.360	1.390	1.415	1.440	1.460	1.470	1.480
6	1.320	1.375	1.415	1.460	1.490	1.525	1.555	1.585	1.610	1.635
7	1.415	1.460	1.510	1.560	1.610	1.660	1.700	1.735	1.765	1.790
8	1.510	1.560	1.610	1.670	1.720	1.780	1.840	1.880	1.905	1.925
9	1.590	1.650	1.710	1.770	1.830	1.890	1.980	2.000	2.050	2.070
10	1.690	1.760	1.830	1.900	1.960	2.020	2.080	2.140	2.180	2.210

* relative density = 0.30

The gamma ray component of the total dose was found to be smaller in front of and within the lung, but it becomes larger than the corresponding dose in muscle just 1-2 cm behind the second interface.

It should be mentioned that the neutron and gamma ray doses were measured at points whose distance from the nearest interface was not less than 1 cm, because of the size of the detectors used, e.g. the 1 cm^3 spherical EG & G ionisation chamber. These curves, therefore, give no information about transition effects at interfaces in the phantom.

Table 6-III gives the correction factors for lung as a function of field size. For a given depth, the correction factor is larger for the smaller field size. If one applied the 9.5 cm x 9.5 cm correction factors for the other field sizes, the error would be about 3 percent near the interface, but not more than 1 percent at distances larger than 6 cm behind the lung.

TABLE 6-III VARIATION OF LUNG CORRECTION FACTORS WITH FIELD SIZE ($\bar{E}_n$ = 7.5 MeV)

Lung thickness cm	Field size cm x cm	Distance from interface point behind the lung			
		1 cm	4 cm	7 cm	10 cm
3	4.5 x 6.0	1.155	1.200	1.240	1.265
	9.5 x 9.5	1.135	1.175	1.215	1.240
	14.0 x 14.0	1.130	1.170	1.210	1.235
5	4.5 x 6.0	1.310	1.400	1.470	1.505
	9.5 x 9.5	1.250	1.360	1.440	1.480
	14.0 x 14.0	1.245	1.340	1.410	1.460
8	4.5 x 6.0	1.580	1.740	1.870	1.950
	9.5 x 9.5	1.510	1.670	1.840	1.925
	14.0 x 14.0	1.485	1.650	1.820	1.920

By applying the correction factors given in this section, neutron depth dose distributions with errors of less than $\pm$ 2 percent can be obtained.

6.3(ii) LUNG CORRECTION FACTORS FOR COBALT GAMMA-RAYS

BATHO (1964) used for the first time Tissue-Air Ratios (TARs) to calculate corrections for the effect of lung. The Tissue-Air Ratio (TAR), defined as the ratio of the dose to a small mass of tissue in the medium to the dose at the same point in air, is frequently used in the computation of dose distributions. The correction factor, as Batho suggested, can be calculated from the equation

$$CF = \left\{ \frac{TAR(A, d_2)}{TAR(A, d_1)} \right\}^{\rho_e - 1} \qquad (6.1)$$

where ρ_e is the electron density of the heterogeneity relative to soft tissue and d_1, d_2 are the distances from the point of interest to the two surfaces of the overlying heterogeneity. This method allowed only for the case of points lying behind the inhomogeneity and the above equation is valid only in the energy range where absorption and scattering of the photons is determined solely by the number of electrons per cm^3 of the medium, i.e. where the attenuation is due almost entirely to the Compton process. Batho assumed the average density of lung tissue to be 0.35 g cm^{-3} and calculated lung correction factors using equation (6.1).

YOUNG and GAYLORD (1970), carried out experiments with cobalt-60 radiation to test the validity of equation 6.1. They used aluminium, carbon, Perspex and air, and found that the calculated correction factors could be used with an error of about 3 percent.

SONTAG and CUNNINGHAM (1977), gave a generalized formula for this correction factor, that allowed for correction of the dose to points within the heterogeneity as well, and accounted for the differences in atomic number between the heterogeneity and the tissue-like material.

$$CF = \frac{TAR(A, d_1)^{\rho_a - \rho_b}}{TAR(A, d_2)^{1 - \rho_b}} \times \frac{\left(\mu_{en}/\rho\right)_a}{\left(\mu_{en}/\rho\right)_b} \qquad (6.2)$$

where ρ_a is the density of the material in which the point of interest lies at a depth d_1 and ρ_b is the density of the overlying material of thickness $(d_2 - d_1)$. They used cork for lung and aluminium for bone and found that the agreement between values measured within the aluminium and those predicted by the generalized formula was not quite as good, with differences of 4-5 percent being observed.

Figure 6.3 shows the correction factors obtained with a phantom consisting of 4 cm-thick muscle substitute (MS/SR4) followed by 3 cm, 5 cm or 8 cm of lung substitute (LNG/SR4) and this followed by a 30 cm x 30 cm x 40 cm tank full of water. Measurements were repeated with 2 cm of muscle in front of the lung, in order to see how the thickness of overlying tissue affects the correction factors. The two sets of correction factors were within 1 per cent of each other and it was concluded that the correction is independent of the thickness of the overlying tissue.

The dotted lines in Figure 6.3 show the values predicted by the Batho formula (equation 6.1); the maximum difference, for the 8 cm-thick lung, is 2 percent.

The lung correction factors derived in this way seem to vary linearly with depth; the fact that the phantom was rather extended behind the heterogeneity may be responsible for this, because no measurements were made near the exit of the phantom where the backscatter is gradually reduced; this reduced backscatter is probably responsible for the levelling off observed with the lung correction factors for neutrons.

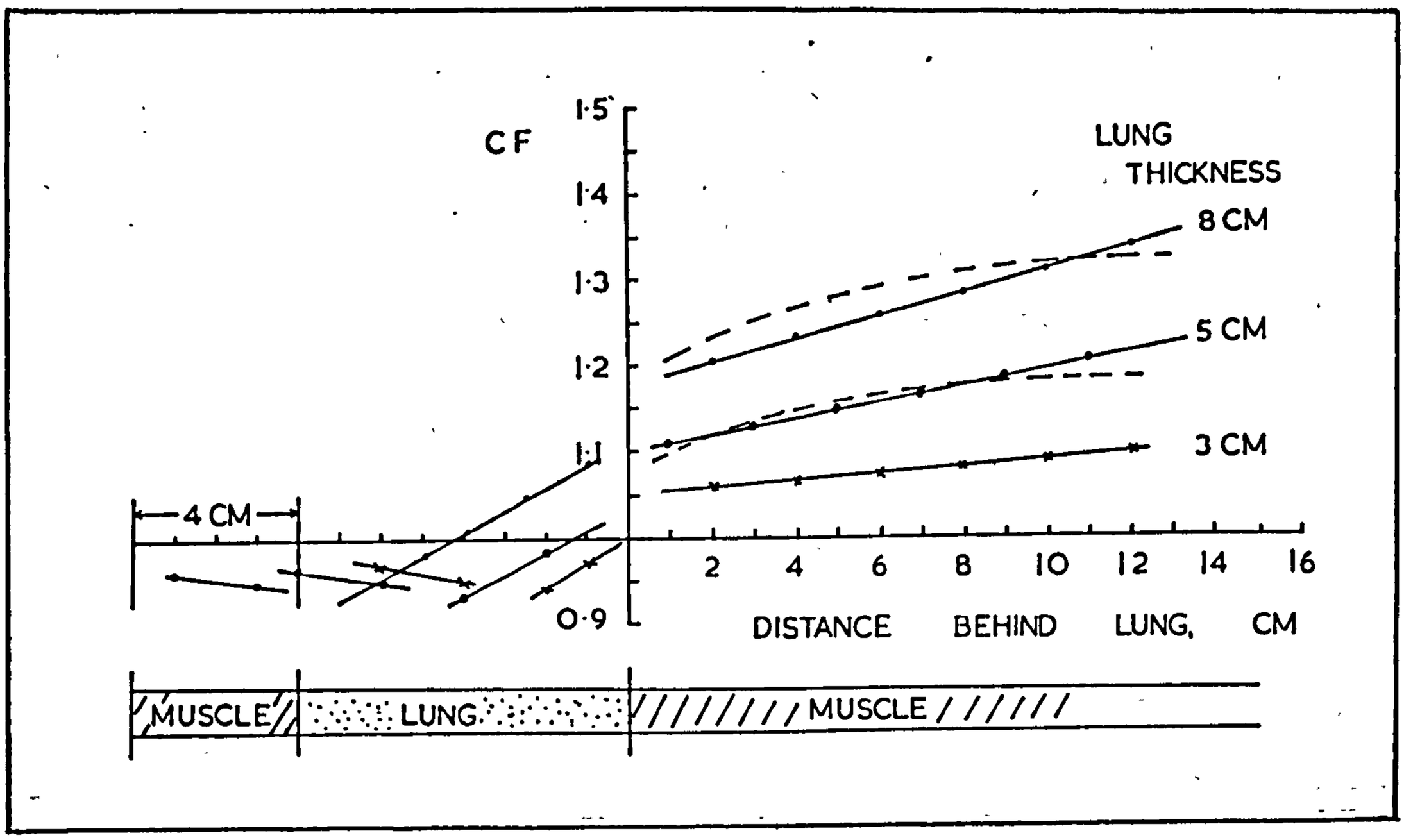

Figure 6.3 Lung correction factors for cobalt-60 gamma rays, (10 cm x 10 cm field, SSD = 75 cm). Dotted lines : values predicted from equation 6.1

The effect of field size on the lung correction factors was also investigated by repeating the measurements for three field sizes, namely 5 cm x 5 cm, 10 cm x 10 cm and 15 cm x 15 cm. Figure 6.4 shows the correction factors for the above three field sizes in the case of 8 cm-thick lung. Table 6-IV gives correction factor values for points behind 3 cm, 5 cm and 8 cm-thick lung, for the three field sizes. It can be seen that for a point lying 5 cm behind an 8 cm-thick lung, for example, the correction factor for the 5 cm x 5 cm field is about 3 percent larger than that of the 10 cm x 10 cm field, while the correction factor for the 15 cm x 15 cm field is about 2 percent lower.

A single set of correction factors for each thickness of lung traversed, based on an average field size could probably be used.

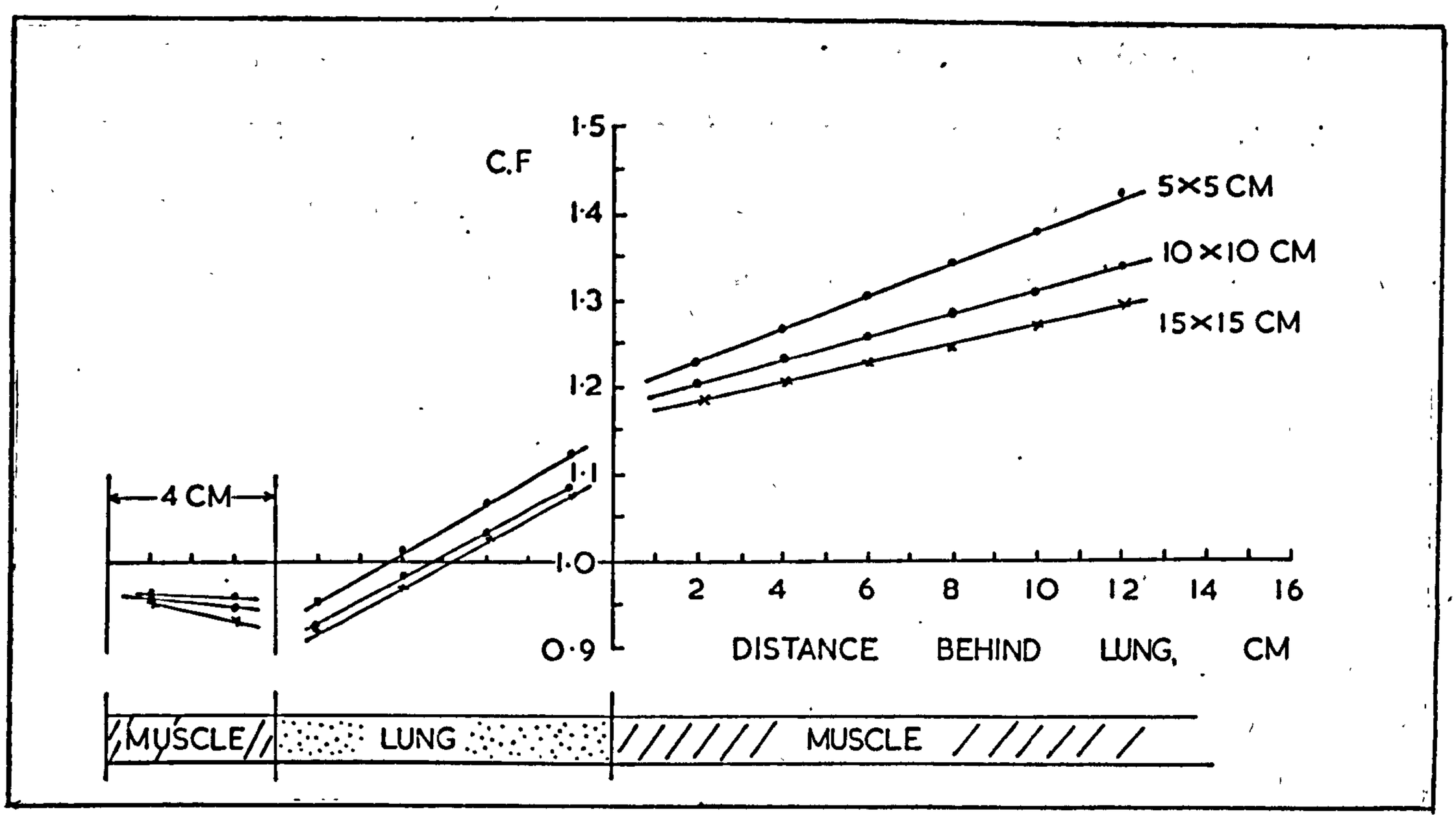

Figure 6.4 Effect of field size on the lung correction factors for cobalt-60 gamma rays (Lung thickness = 8 cm)

TABLE 6-IV LUNG CORRECTION FACTORS AS A FUNCTION OF LUNG THICKNESS, FIELD SIZE AND DISTANCE OF POINT FROM THE LUNG

Cobalt-60 radiation

Lung thickness cm	Field size (cm x cm)	Distance of point from lung		
		1 cm	5 cm	10 cm
3	5 x 5	1.064	1.089	1.104
	10 x 10	1.059	1.800	1.095
	15 x 15	1.055	1.074	1.087
5	5 x 5	1.125	1.160	1.210
	10 x 10	1.110	1.144	1.193
	15 x 15	1.095	1.128	1.175
8	5 x 5	1.209	1.285	1.380
	10 x 10	1.191	1.247	1.311
	15 x 15	1.180	1.218	1.273

Table 6-V gives the lung correction factors for cobalt-60 gamma rays, for points lying in the tissue in front of the lung, for points within the lung and finally in the soft tissue behind the lung. The use of such correction factors in computerised isodose planning would improve the accuracy of the dose distributions thus obtained.

TABLE 6 - V

CORRECTION FACTORS FOR LUNG*

(10 cm x 10 cm)

COBALT-60 GAMMA RAYS

Thickness of lung cm	Point in tissue before lung			Point within the lung								
	Distance from Interface(cm)			Distance from first interface (cm)								
	1	2	3	1	2	3	4	5	6	7	8	9
1	0.951	0.958	0.975									
2	0.951	0.958	0.972	0.955								
3	0.950	0.957	0.969	0.942	0.972							
4	0.950	0.957	0.966	0.935	0.965	0.994						
5	0.950	0.956	0.964	0.935	0.958	0.984	1.009					
6	0.949	0.955	0.962	0.931	0.957	0.983	1.009	1.035				
7	0.949	0.954	0.960	0.930	0.956	0.982	1.009	1.034	1.060			
8	0.948	0.953	0.959	0.929	0.955	0.982	1.008	1.034	1.059	1.087		
9	0.948	0.952	0.958	0.928	0.954	0.981	1.008	1.034	1.059	1.086	1.118	
10	0.947	0.951	0.957	0.927	0.953	0.980	1.007	1.033	1.059	1.086	1.118	1.145

Thickness of lung cm	Point in tissue behind the lung											
	Distance from second interface (cm)											
	1	2	3	4	5	6	7	8	9	10	11	12
1	1.014	1.015	1.019	1.023	1.025	1.027	1.030	1.033	1.035	1.040	1.043	1.045
2	1.030	1.035	1.039	1.043	1.046	1.050	1.053	1.056	1.060	1.064	1.068	1.072
3	1.059	1.061	1.063	1.065	1.068	1.072	1.076	1.080	1.084	1.089	1.094	1.098
4	1.082	1.090	1.098	1.105	1.112	1.118	1.125	1.132	1.139	1.146	1.152	1.160
5	1.110	1.118	1.128	1.139	1.148	1.158	1.168	1.177	1.187	1.196	1.207	1.215
6	1.140	1.150	1.161	1.173	1.185	1.195	1.206	1.216	1.227	1.238	1.250	1.262
7	1.164	1.177	1.190	1.204	1.216	1.229	1.242	1.255	1.268	1.281	1.294	1.307
8	1.191	1.205	1.221	1.234	1.247	1.258	1.270	1.285	1.300	1.311	1.325	1.340
9	1.235	1.250	1.265	1.280	1.295	1.308	1.320	1.335	1.350	1.364	1.378	1.392
10	1.278	1.293	1.308	1.323	1.337	1.351	1.366	1.381	1.395	1.410	1.425	1.440

* relative density = 0.30

CHAPTER 7

SOME APPLICATIONS OF THE NEW TISSUE SUBSTITUTES

Tissue substitutes are needed for several purposes in radiation dosimetry, radiotherapy, radiological protection and radiodiagnosis. For example, ionisation chambers, organ or body phantoms and radiographic test objects are some of the items that can be manufactured using the new substitutes. Some of these applications will be described here briefly.

7.1 MACROSCOPIC, MICROSCOPIC AND INTERFACE DOSIMETRY

The experimental work carried out during this study illustrates the usefulness of the new substitutes in both particulate and photon radiation dosimetry. Figures 7.1 ('a' and 'b') show samples of solid substitutes for lung, muscle and hard bone, while Figure 7.2 shows some liquid and gel tissue substitutes produced in this work.

Although non-conducting electrically, the new solid tissue substitutes can be used in the manufacture of ionisation chambers for use in particulate and photon radiation dosimetry, provided their electrodes are coated with a layer of graphite thin enough not to disturb the particle fluence (a few microns-thick).

The new substitutes can also facilitate interface dosimetry and microdosimetry. For example, small size thermoluminescent dosimeters (TLD chips or discs) can be placed very close to the tissue interface to measure the dose distribution in this region of interest. Nuclear emulsions can be sandwiched between slabs of solid tissue substitutes and exposed to particulate radiation beams in order to investigate the type and the yields of charged particles produced in tissue by these radiations. Similarly film dosemeters

(a)

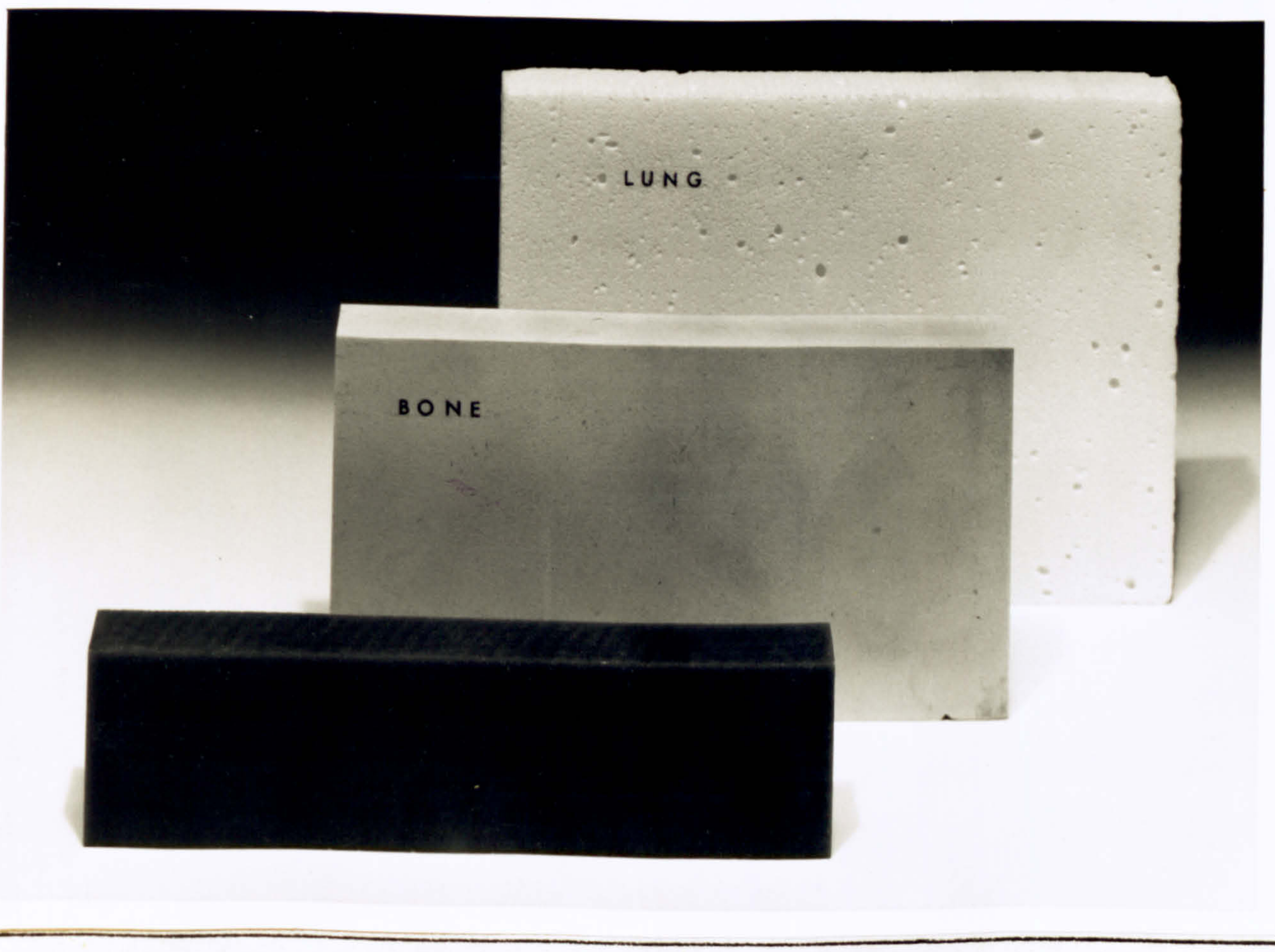

(b)

Figure 7.1 Some of the new solid tissue substitutes

Figure 7.2 Some new liquid, gel and solid tissue substitute materials

can be used in conjunction with central axis depth dose measurements to plot the isodose curves from radiation beams in various tissues like muscle, brain or bone. The use of the liquid tissue substitutes to measure the stopping powers of various tissues for alpha particles emitted from naturally radioactive substances is another application of the new materials.

Samples of lung and bone substitutes (LN/SR1 and HB/SR4) have been made for the Churchill Hospital Physics group (Oxford), at their request, in order to investigate the transmission and back scattering of 4 to 40 MeV electrons from these materials. Muscle and bone substitutes have also been used to study the yields of charged particles and the corresponding dose : LET distributions in the region of the peak of the 70 MeV pion beam of the Rutherford Laboratory, U.K. (PERRIS, et al., 1978).

7.2 RADIOGRAPHIC TEST OBJECTS

The new materials are also suitable for radiographic studies in diagnostic radiology. Lung phantoms, for example, can be used for the construction of realistic chest phantoms. If a number of lungs with the same shape, composition and density are manufactured, then different types of objects (e.g. calcifications, meshes etc) can be incorporated in each one of them for the purpose of testing imaging systems such as diagnostic X-ray machines and computerised tomography scanners. When the same test object is radiographed on different X-ray machines set to the same mAs and kVp, the amount of information obtained from the different radiographs can be compared.

A radiographic test object designed and manufactured for comparing resolution, detail and contrast on different imaging systems in an objective way, is shown in Figure 7.3. Various items have been embedded in the base material which is the epoxy system CB1.

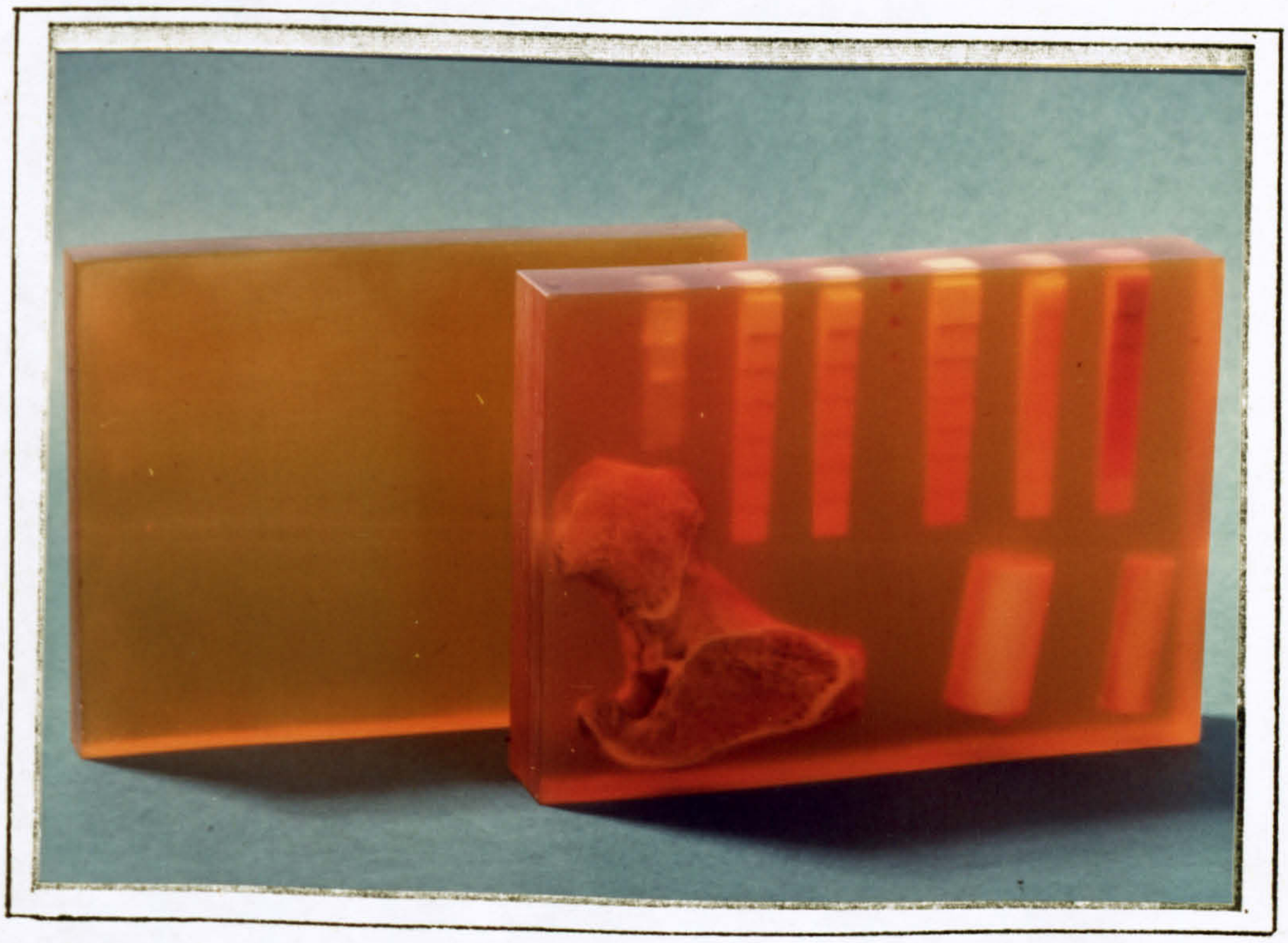

Figure 7.3 A radiographic test object
(dimensions : 15 cm x 20 cm x 3 cm)

These items include step wedges made of tissue substitutes ranging from fat to hard bone, aluminium oxide spheres ranging from 0.4mm to 4 mm diameter, a 1 cm-thick section of real bone and air spaces with fine wires of copper threaded through polyethylene tubes, the smallest diameter of the wires being 0.05 mm. The section of the head of the femur was impregnated with resin before being embedded so that, by excluding air, its trabecular structure could act as a test object for resolution and detail determinations.

Figure 7.4 shows radiographs of this test object taken with X rays, fast neutrons and with high energy protons. The techniques and methods used in proton scattering and end-of-range proton radiography have been described by WEST (1974) and STEWART and KOEHLER (1974). It is seen that the end-of-range proton radiograph (D) is the only one which provides information for both soft and skeletal tissues. It also shows bubbles of trapped air, not visualised on any of the other radiographs. The conventional X-ray radiograph (A) gives better detail of the structure of the real bone but the soft tissues are not visualised on it. On the neutrogram (B), apart from the air volumes, nothing else is visualised.

Another test object which was designed and manufactured at the request of the Diagnostic X-ray Department of St Bartholomew's Hospital, London, is shown in Figure 7.5. The requirement was to have a solid material which would be "invisible" on radiographs taken when a rack made of this material was immersed in water. The purpose was to study the changes observed on the radiographs when different concentrations of contrast media were used. As it was not feasible to formulate an elementally correct solid water substitute, the Basic Data method was employed and the substitute

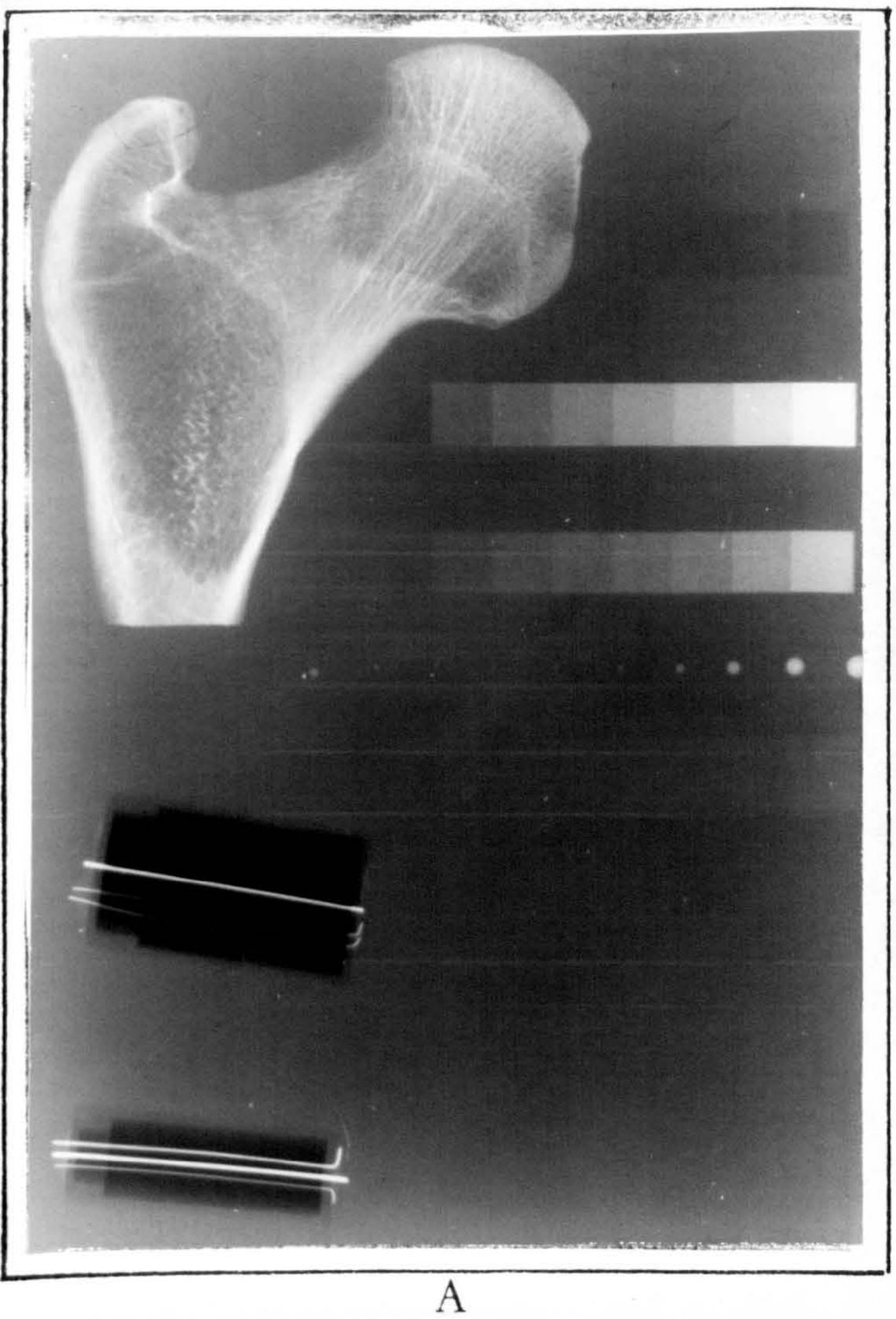

A

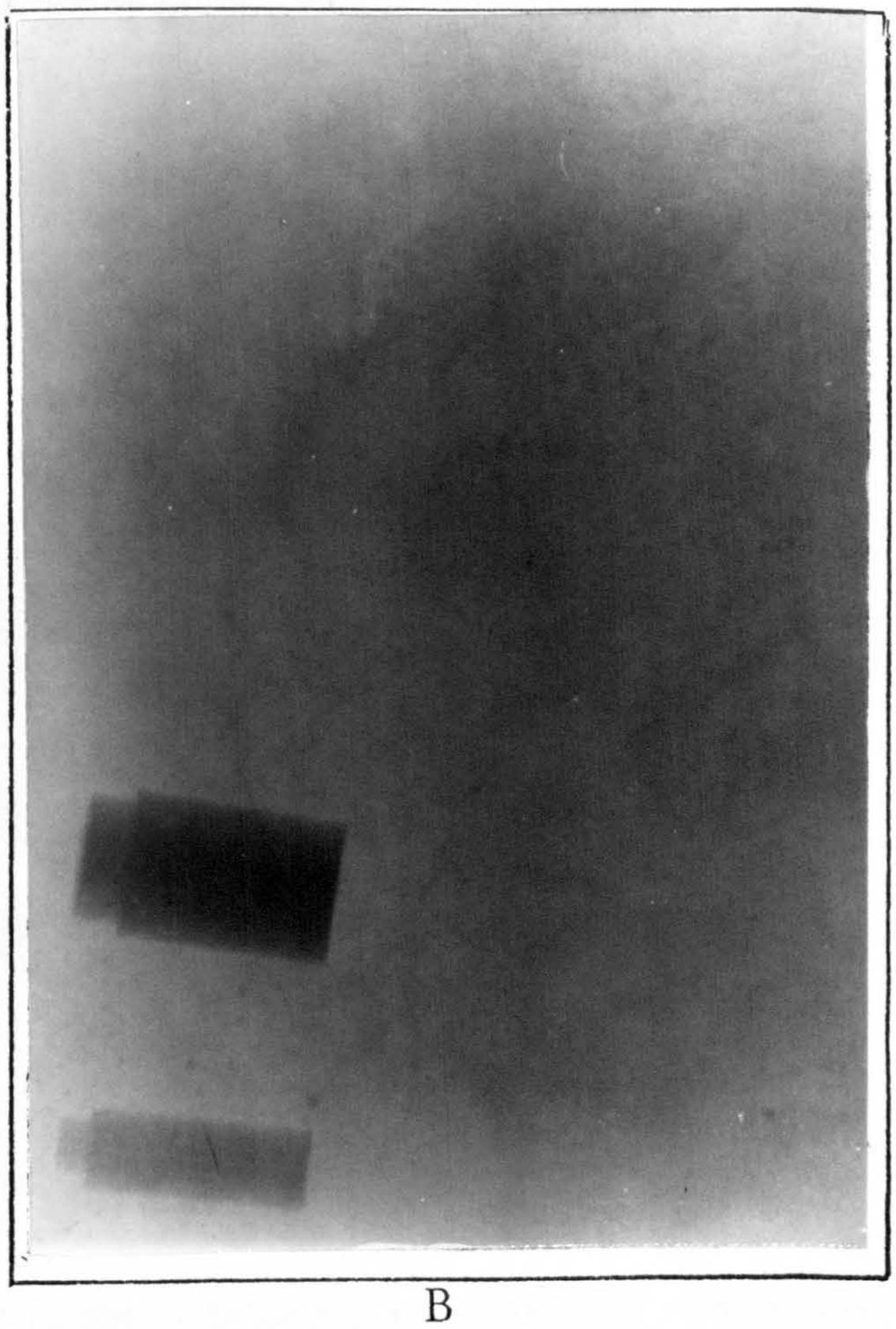

B

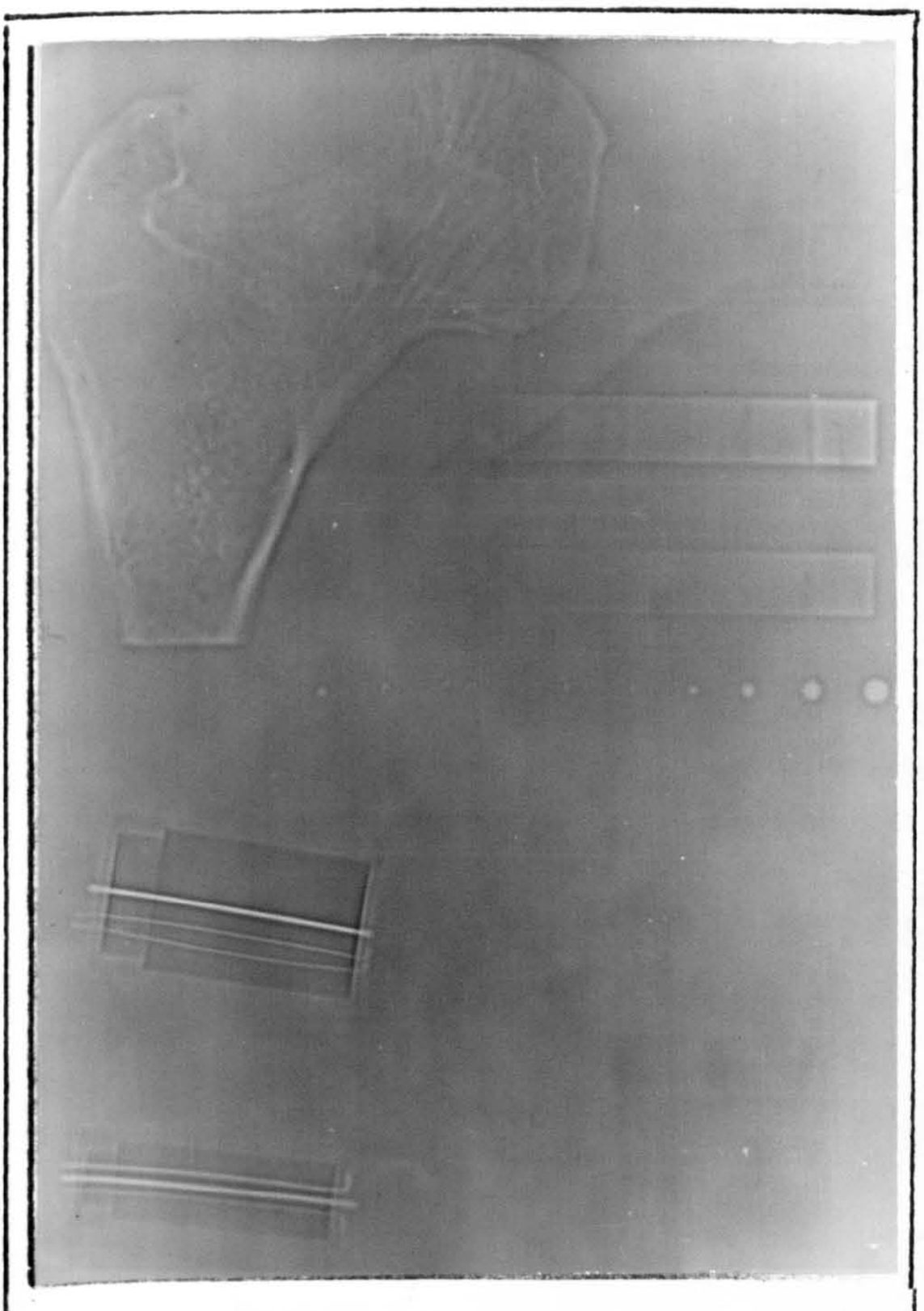

C

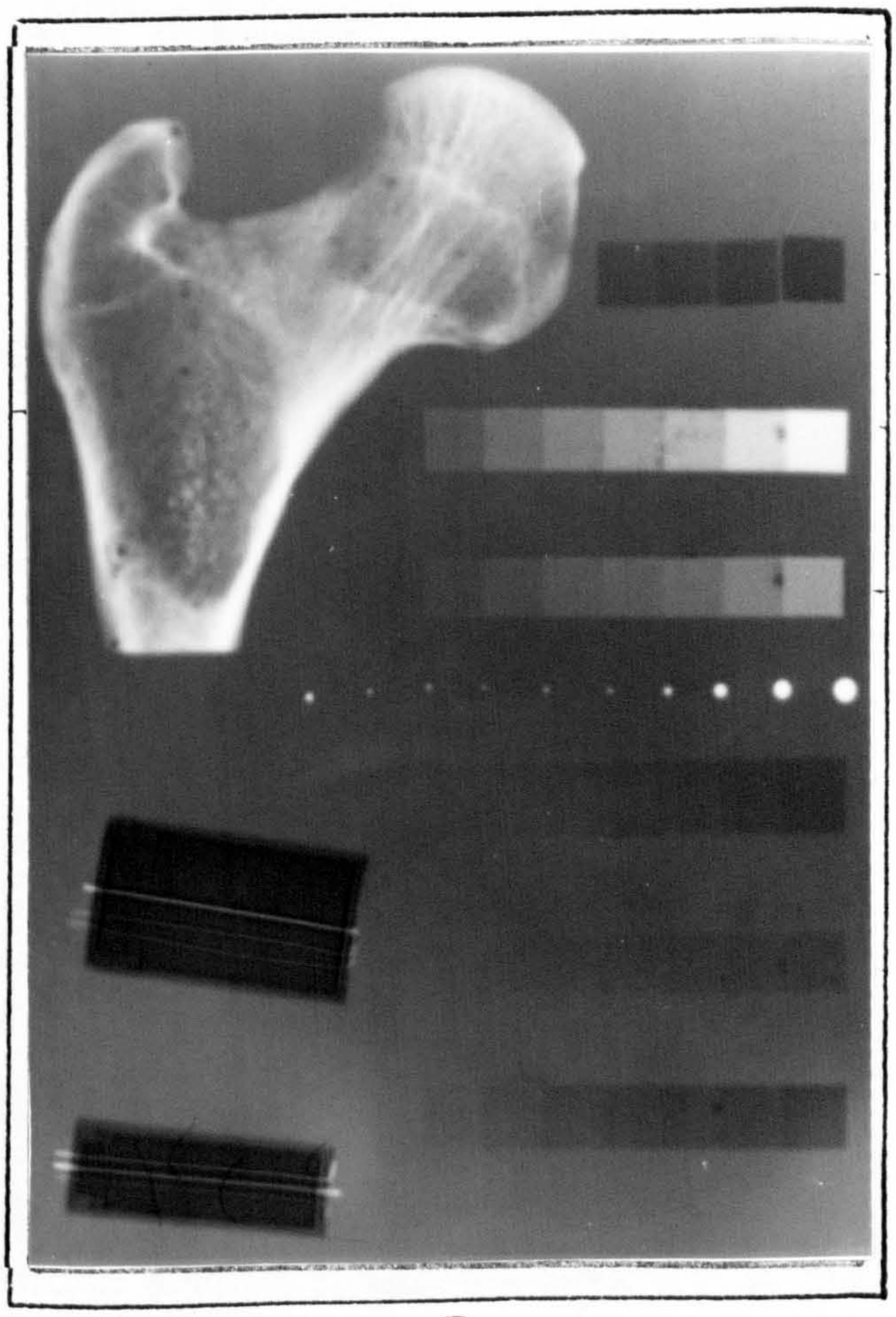

D

FT/SF1

HB/SF3

TSK/SF3

MS20

MS/SR1

AP/SF1

Figure 7.4 : Different radiographs of the same test object.

A: Conventional radiograph (60 kV_p X-rays, 20 mAs).

B: Neutrogram ($\bar{E}_n$ = 7.5 MeV).

C: Proton scattering radiograph (160 MeV protons, 3cm thick aluminium absorber).

D: End-of-range proton radiograph (160 MeV protons, 9.85cm thick perspex absorber).

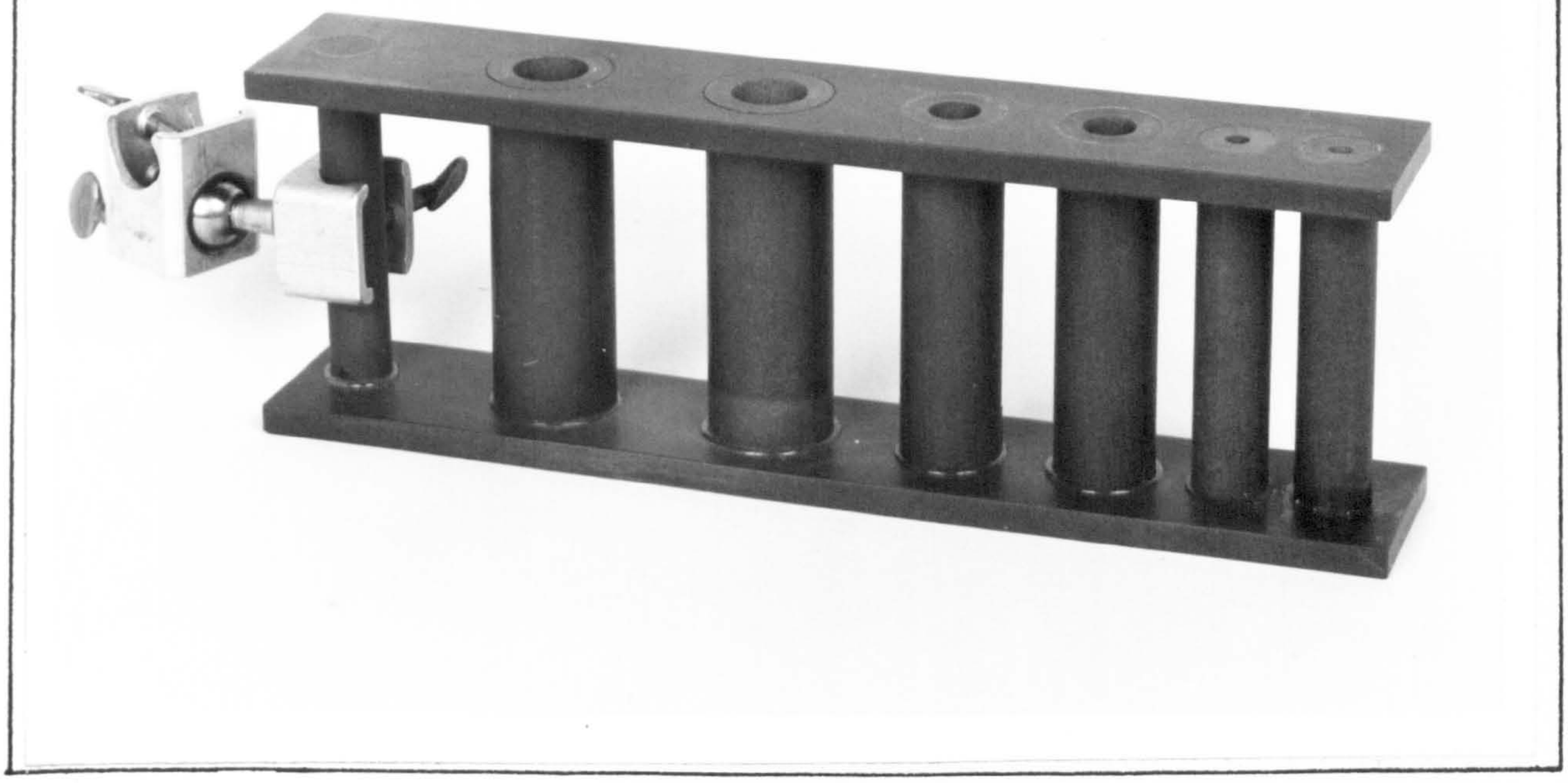

Figure 7.5 Object made of a solid water substitute

WT/SR1 was formulated and manufactured. Samples of this substitute were immersed in water and radiographed, but they were not visible on the radiographs. By using test tubes of different diameters the visualisation of dilated bile ducts filled with contrast media could be studied.

Radiographic test objects for CT scanners can also be manufactured using the new tissue substitutes, especially the liquids and gels. If epoxy resin based systems are to be used, then the powders added as fillers must be sieved to below 100 μm if the homogeneity required for this application is to be achieved. However, the solid substitutes produced by WHITE (1974), are better for this purpose because they are all class A (errors $< 5\%$) for photon energies below 0.1 MeV.

7.3 BODY PHANTOMS

The new tissue substitutes are suitable for the manufacture of organ and body phantoms for depth dose studies, for the assessment of the doses given to the irradiated areas of patients undergoing radiotherapy and for the comparison of different dosemeters. The manufacture of anatomically correct body phantoms (in slices) with the correct tissue substitutes, allows the dose distribution from the various fields used within the body to be accurately measured using dosemeters at different points in the phantom. Depending on the experimental requirements, the phantom employed could be either a complex reproduction of the human body or a simple homogeneous material.

An application that is currently being considered is the use of the gel substitutes for muscle as bolus material in both photon and particulate radiation therapy. These gel substitutes have low cost and when kept in sealed polythene bags can be used for several months.

The determination of the radiological hazard to patients who are administered radiopharmaceuticals, requires an assessment of the doses absorbed in various organs from a radioactive material deposited in another organ. For such applications, 2 mm-thick perspex sheets can be used to produce shell replicas of the various organs (kidneys, liver, thyroid, etc). These models can be filled with the appropriate liquid substitutes and placed in a man-sized shell phantom which in turn, is filled with "total soft tissue" liquid substitute. If a soluble radioactive material is mixed with one of the organ substitutes, then dosemeters placed at defined points within the phantom will permit the dose distribution to be plotted.

The addition of radionuclides in epoxy resin based substitutes during their manufacture and their subsequent use as counting standards is being investigated. If compartmented models are used, the effect of non-uniform distribution of radioactive materials on the counting efficiency of various detectors may be studied (for example, plutonium in lung substitutes).

CHAPTER 8

CONCLUSIONS AND SUGGESTED FUTURE WORK

The radiation physicist has a large number of tissue substitutes available for dosimetric studies. Some of the phantom materials used in the past, however, should not be used any longer because they have unknown composition and variable density and their radiation absorption and scattering characteristics probably differ from those of the real tissues by more than 20%. Pressdwood and paraffin wax, still used as muscle substitutes, sulphur and aluminium still used to represent bone, and sawdust, cork and sponge still used as lung substitutes are some typical examples of unacceptable materials.

The present study had two main aims. The first was to formulate new tissue substitutes with the same elemental composition and density as the corresponding real tissues. The second aim was to use these systems for dosimetric studies with those types of radiation which are used or are likely to be used for patient treatment, in order to establish their depth dose characteristics in various tissues and, in particular, to investigate the effect of tissue heterogeneities on the dose distributions in the patient's body.

A wide range of tissue substitutes in the liquid, gel and solid phases have been produced as a result of this work. Most of these materials are "TISSUE EQUIVALENT", particularly the liquid and gel substitutes. In the case of epoxy resin based substitutes, partial replacement of oxygen by carbon had to be accepted due to the fact that epoxy resins and polymers are rich in carbon and poor in oxygen. A similar problem exists when rubbers are

considered. Not only are rubbers poor in oxygen but they normally require high temperatures and pressures and elaborate equipment for their mixing. Until polymers or other base materials rich in oxygen are developed, no improvement is expected as far as this problem is concerned. However, this replacement of oxygen by carbon in the new tissue substitutes does not introduce significant errors when these materials are used with photons of energy above 0.1 MeV, high energy charged particles or fast neutrons.

The extensive series of measurements performed with cobalt-60 gamma rays, 7.5 MeV neutrons, 10 MeV electrons, 70 MeV pions and 150 MeV protons using a selection of the new tissue substitutes, resulted in the establishment of the depth dose characteristics of these radiations in muscle, brain, bone and water. The effect of tissue heterogeneities on the dose distributions was investigated and isodose shift factors for use in the planning of the treatment of patients undergoing radiotherapy, were derived. Detailed lung correction factors for cobalt-60 gamma rays and for neutrons of average energy $\bar{E}_n = 7.5$ MeV were also derived and these are readily available for computerised isodose planning.

The comparative information accumulated during the course of this study has added significantly to the sparse data on electron, negative pion, proton and neutron depth dose distributions in various tissues. The measurements performed on the 160 MeV proton beam of the Atomic Energy Research Establishment were a necessary pre-requisite for the proposed proton radiotherapy program using that proton beam facility. Experience has been gained in positioning the Bragg-peak "on target" and this problem, considered before as one of the main obstacles to the clinical use

of protons, is no longer a limiting factor. The collimator system of the above proton beam facility, however, should be improved so that scatter towards the patient is reduced.

It is hoped that a clinical study will be undertaken in the near future, to compare protons to megavoltage X-rays in the treatment of tumours for which it appears most likely that an improved dose distribution will be advantageous. Such a clinical trial should include enough cases to assure statistically significant results. The capacity to decrease the normal tissue dose relative to the tumour dose with proton treatment, should have merit in reducing the morbidity or in increasing local tumour control.

The usefulness of the measured isodose shift factors for all radiations and lung correction factors for photons and neutrons, over a wider energy range, should be established by further measurements. Measurements should also be performed very close to the tissue interfaces (distances 0-1 cm from interface) because the dose gradient in this region is more pronounced and it is in this region that the maximum errors in the estimation of dose usually occur.

It is hoped that this study will stimulate more interest in the use of tissue substitute materials and that the experimental results will contribute to improvements in clinical dosimetry.

APPENDIX 1

SYMBOLS, PHYSICAL CONSTANTS AND ELEMENTAL DATA USED IN THE STUDY

A (M)	Atomic weight (Molecular weight)
a_i	Fractional Electron content of the i^{th} element or compound
β	v/c
c	Velocity of light
CF	Correction factor
CT	Computerised tomography
δ	Density effect correction
e	Charge on electron (1.6×10^{-19} C)
Eeff	Effective energy
E_n	Neutron energy
$\bar{\Theta}^2$	Electron mean square scattering angle
$\Phi(E)$	Particle fluence
FWHM	Full Width at half maximum
K	Kerma
I	Mean excitation energy
ℓ	Path length
m_e	Rest mass of electron $\left(m_e c^2 = 0.510976 \text{ MeV}\right)$
m_i	Percentage by weight of the i^{th} compound in a mixture
$\left(\bar{\Theta}^2/\rho\ell\right)$	Mass angular scattering power
S/ρ	Mass stopping power
$\left(S/\rho\right)_{col}$	Collision mass stopping power
$\left(S/\rho\right)_{rad}$	Radiation mass stopping power
μ	'Narrow beam' linear attenuation coefficient
μ/ρ	Mass attenuation coefficient
μ_{en}/ρ	Mass energy absorption coefficient
μ_{tr}/ρ	Mass energy transfer coefficient
μ_τ/ρ	Photoelectric mass attenuation coefficient
N_A	Avogadro's number (6.02252×10^{26} kmol^{-1})
n_o	Electron density
p_e	Momentum of electron
π	Constant : 3.14159
π^-	Negative pions
r_e	Electron radius (2.81777×10^{-15} m)
ρ	Mass density

ρ_e	Electron density of a heterogeneity relative to soft tissue
σ_t	Total neutron cross section
SG	Relative density (specific gravity)
T	Kinetic energy of a particle
τ	Kinetic energy in units of $m_e c^2$
v	Velocity
W	The energy required to form an ion pair in the sensitive volume of a radiation detector
w/o	Percentage by weight
x	$\bar{Z}$-exponent
Z	Atomic number
z	Number of protons in a charged particle
$\langle Z/A \rangle$	Mean ratio Z/A for compound
$\bar{Z}(x)$	Effective atomic number
$\sum \frac{C_i}{Z}$	The term for shell corrections (equation 1.2)
Ω	Ohm
ω	Weight proportion

ELEMENTAL DATA

Z	ELEMENT		ATOMIC WT.	Z	ELEMENT		ATOMIC WT.
1	HYDROGEN	(H)	1.00797	37	RUBIDIUM	(RB)	85.47
2	HELIUM	(HE)	4.0026	38	STRONTIUM	(SR)	87.62
3	LITHIUM	(LI)	6.939	39	YTTRIUM	(Y)	88.905
4	BERYLLIUM	(BE)	9.0122	40	ZIRCONIUM	(ZR)	91.22
5	BORON	(B)	10.811	41	NIOBIUM	(NB)	92.906
6	CARBON	(C)	12.01115	42	MOLYBDENUM	(MO)	95.94
7	NITROGEN	(N)	14.0067	47	SILVER	(AG)	107.870
8	OXYGEN	(O)	15.9994	48	CADMIUM	(CD)	112.40
9	FLUORINE	(F)	18.9984	50	TIN	(SN)	118.69
10	NEON	(NE)	20.183	51	ANTIMONY	(SB)	121.75
11	SODIUM	(NA)	22.9898	52	TELLURIUM	(TE)	127.60
12	MAGNESIUM	(MG)	24.312	53	IODINE	(I)	126.9044
13	ALUMINIUM	(AL)	26.9815	55	CAESIUM	(CS)	132.905
14	SILICON	(SI)	28.086	56	BARIUM	(BA)	137.34
15	PHOSPHORUS	(P)	30.9738	57	LANTHANUM	(LA)	138.91
16	SULPHUR	(S)	32.064	58	CERIUM	(CE)	140.12
17	CHLORINE	(CL)	35.453	62	SAMARIUM	(SM)	150.35
18	ARGON	(AR)	39.948	63	EUROPIUM	(EU)	151.96
19	POTASSIUM	(K)	39.102	64	GADOLINIUM	(GD)	157.25
20	CALCIUM	(CA)	40.08	65	TERBIUM	(TB)	158.924
21	SCANDIUM	(SC)	44.958	67	HOLMIUM	(HO)	164.930
22	TITANIUM	(TI)	47.90	68	ERBIUM	(ER)	167.26
23	VANADIUM	(V)	50.942	69	THULIUM	(TM)	168.934
24	CHROMIUM	(CR)	51.996	70	YTTERBIUM	(YB)	173.04
25	MANGANESE	(MN)	54.9380	71	LUTETIUM	(LU)	174.97
26	IRON	(FE)	55.847	74	TUNGSTEN	(W)	183.85
27	COBALT	(CO)	58.9332	77	IRIDIUM	(IR)	192.2
28	NICKEL	(NI)	58.71	78	PLATINUM	(PT)	195.09
29	COPPER	(CU)	63.54	79	GOLD	(AU)	196.967
30	ZINC	(ZN)	65.37	80	MERCURY	(HG)	200.59
31	GALLIUM	(GA)	69.72	82	LEAD	(PB)	207.19
32	GERMANIUM	(GE)	72.59	83	BISMUTH	(BI)	208.980
33	ARSENIC	(AS)	74.9216	84	POLONIUM	(PO)	210)
34	SELENIUM	(SE)	78.96	88	RADIUM	(RA)	226)
35	BROMINE	(BR)	79.909	90	THORIUM	(TH)	232.038

AVOGADROS NUMBER : $6.02252 \times 10^{26} KMOL^{-1}$

APPENDIX 2

EXAMPLES OF FORMULATING TISSUE SUBSTITUTES USING THE "ELEMENTAL EQUIVALENCE" METHOD

The two examples included in this appendix, show the application of the Elemental Equivalence method in the formulation of the new tissue substitutes, as outlined in Chapter 2.

EXAMPLE 1

TISSUE : MUSCLE, relative density = 1.06.

Elemental composition (percentages by weight):

C (12.3); H (10.2); N (3.50); O (72.89); Na (0.08); Mg (0.02);
P (0.20); S (0.50); Cl (0.08); K (0.30); Ca (0.01)

STEP 1: Derive the number of moles of each element per kilogram of substitute.

C = 10.2415; H = 101.9000; N = 2.4986; O = 45.5625; Na = 0.0304;
Mg = 0.0080; P = 0.0646; S = 0.1562; Cl = 0.0220; K = 0.3900;
Ca = 0.200.

STEP 2 : Scan the compound library to find if there is a single compound with the above composition: no 'single component' muscle substitute was found.

STEP 3: Derive a set of compounds which will introduce the trace elements in a water-based substitute.

For 1 kg of substitute:

NaCl	: 0.0220 moles	=	1.288 g
$NaNO_3$	: 0.0044 moles	=	0.714 g
$KHSO_4$	: 0.1000 moles	=	13.617 g
$Mg(NO_3)_2.6H_2O$	: 0.0080 moles	=	2.051 g
$Ca(NO_3)_2$	: 0.0020 moles	=	0.328 g
H_3PO_4	: 0.0646 moles	=	6.270 g
	Total mass :		24.268 g

STEP 4 : Subtract the number of moles of C, H, N, O, etc., already introduced with the above compounds from the number of moles of each element derived in STEP 1.

What remains to be satisfied (for 1 kg of substitute), is:

C = 10.1415 moles; H = 100.80 moles; N = 2.4742 moles;

O = 44.7829 moles.

The formula of the remaining C, H, N, O can be written as:

$C_{10.1415}\ H_{100.8000}\ N_{2.4742}\ O_{44.7829}$

STEP 5 : The above formula can be written as the sum of two (or more) components with water being one of them:

$C_{10.1415}H_{100.80}N_{2.4742}O_{44.7829} = C_{10.1415}\ H_{11.2342}\ N_{2.4742}(H_2O)_{44.7829}$

If Urea $\left[NH_2CONH_2 = CH_2N_2(H_2O)\right]$ is used to satisfy the nitrogen requirement, then $\frac{2.4742}{2}$ = 1.2371 moles of Urea (74.23 g) will be needed. Consequently:

$C_{10.1415}H_{11.2342}N_{2.4742}(H_2O)_{44.7829} = 1.2371\ \underbrace{CH_2N_2(H_2O)}_{\text{Urea}} +$

$C_{8.9044}H_{8.760}(H_2O)_{43.5458}$

B

The C : H ratio in the first part of the component B is 1.016. Two compounds, namely, ethanediol = $C_2H_2(H_2O)_2$ and acetic acid $C_2(H_2O)_2$, with C : H ratios bracketing 1.016, are selected from the library.

Component B can now be written as:

$C_{8.9044}H_{8.760}(H_2O)_{43.5458} = 4.38\ \underbrace{\left[C_2H_2(H_2O)_2\right]}_{\text{Ethanediol}} + 0.0722\ \underbrace{\left[C_2(H_2O)_2\right]}_{\text{Acetic acid}} +$

$34.706(H_2O)$

water

But: 4.380 moles Ethanediol = 271.86 g (242 cm^3)

0.0722 moles Acetic acid = 4.34 g (4.0 cm^3)

34.706 moles Water = 625.30 g

Summary: The formulated MUSCLE EQUIVALENT liquid (MS/L1) will have the following constituents (percentages by weight):

MS/L1: Water(62.53); Traces(2.42); Urea(7.42); Ethanediol(27.19); Acetic acid(0.43)

Note: After the formula in Step 4 is derived and a decision is made on the compounds to be used, the calculation can proceed as follows:

STEP 6: Set up four simultaneous equations to satisfy the C, H, N, O requirements using Water(W) + Urea(U) + Ethanediol(E) + Acetic acid(A) $[H_2O + NH_2CONH_2 + C_2H_6O_2 + C_2H_4O_2]$.

for H: $2W + 4U + 6E + 4A = 100.8000$

for C: $0W + 1U + 2E + 2A = 10.1415$

for N: $0W + 2U + 0E + 0A = 2.4742$

for O: $1W + 1U + 2E + 2A = 44.7829$

The solution of the above system of equations gives exactly the same number of moles for the constituents of the substitute MS/L1, as the values derived with the previous method.

STEP 7: Apply equation 2.6 and derive the density of the formulated substitute, using the known density and percentage by weight of each component.

Calculated density of MS/L1 : 1.07 g/cm^3

EXAMPLE 2

TISSUE : ADIPOSE, relative density = 0.92

Elemental composition (percentages by weight):

C(64.00); H(12.00); N(0.80); O(22.90); Na(0.05); P(0.02);

S(0.07); Cl(0.12); K(0.03)

STEP 1 : Derive the number of moles of each element per kg of substitute:

C = 53.2844; H = 119.0476; N = 0.5711; O = 14.3146; Na=0.0221;

P = 0.0052; S = 0.0227; Cl = 0.0338; K = 0.0082

STEP 2 : Scan the compound library to find if there is a single compound with the above composition: no "single component" adipose substitute was found.

STEP 3 : Derive a set of compounds which will introduce the trace elements in an epoxy resin based solid substitute.

For 1 kg of substitute:

Na_2SO_4 : 0.0110 moles = 1.562 g

S : 0.0116 moles = 0.373 g

K_2HPO_4 : 0.0041 moles = 0.714 g

$CaHPO_4$: 0.0005 moles = 0.068 g

Total mass = 2.717 g

STEP 4 : From the initial number of moles per kilogramme, for each element, subtract the quantity introduced with the compounds for trace elements; remaining number of moles per kilogramme:

C = 53.2844; H = 119.043; N = 0.5711; O = 14.2522

STEP 5 : Decide on the type and quantity of epoxy resin to be used:

The low nitrogen and high hydrogen contentents make the epoxy resin CB3 the system of choice while at the same time it excludes the use of CB1, CB2 or CB4 because, due to their composition (see Appendix 5), less than 30% by weight of these should be used if the nitrogen content is not to be exceeded; such low percentage of base material, however, would certainly present viscosity problems.

The empirical formula of CB3, derived from its elemental composition is:

$$CB3 = \left[C_{6.1776} H_{11.2103} N_{0.1142} O_{0.750} Cl_{0.0253} \right]_n$$

In order to satisfy the 0.5711 moles of nitrogen, $\frac{0.5711}{0.1142} = 5.008$ moles of CB3 are needed, i.e. 500.08 g of CB3, a quantity in which an equal mass of any filler can be dispersed without any viscosity problems. Now subtract the quantity of C, H, N, O introduced with the base material (PART A), from the number of moles per kilogramme derived in Step 4. The following remain to be satisfied (PART B):

C = 22.39 moles; H = 62.98 moles; O = 10.50 moles

The C : H : O ratio here necessitates the use of compounds with high hydrogen and high oxygen content. Since no single compound was found with this C : H : O ratio, the compound library was rescanned for two compounds with high hydrogen and, at least one of them, with high oxygen content; the two compounds selected were Glucose (G) and Polyethylene (PE) but again, although it was possible to satisfy the hydrogen content exactly, this was not so for carbon and oxygen.

STEP 6 Set up two simultaneous equations and solve the system to find the quantities of G and PE which would give correct H and (C + O):

$$C_6H_{12}O_6 + (C_2H_4)_n \longrightarrow C_{22.39}H_{62.98}O_{10.50}$$

Glucose(G) Polyethylene(PE)

for H: $12\,G + 4\,PE = 62.98$

for(C+O): $(6\times12.01+6\times16.0)G + (2\times12.01)PE = 22.39\times12.01+10.5\times16.0$

The solution of these two equations give

G = 0.61 moles = 109.8 g Glucose

PE = 13.81 moles = 387.39 g Polyethylene

STEP 7: Find the quantity of phenolic microspheres (PMS) needed to adjust the relative density of the mixture to the required value of 0.92.

The application of equation 2.6 showed that the mixture 50.008 g (resin CB3 + PMS) + 38.739 g Glucose + 10.98 g Polyethylene would have a resultant density of 0.92 if the relative density of the component (resin CB3 +PMS) had a relative density of 0.84. Equation 2.6 applied to the mixture of epoxy system CB3 (relative density = 1.02) and PMS (relative density = 0.2), indicated that 5% by weight of PMS should be used, (i.e. 5g PMS in 95g of CB3). Consequently a total of 26.20 g of PMS was considered, their composition taken into account and the mass of each of the above components recalculated.

The final composition of the substitute, which is coded AP/SF1 is:

<u>For 1 kg of substitute:</u>

Epoxy system CB3 (499.00 g); Glucose (87.40 g); Polyethylene (384.72 g); PMS (26.20 g); Traces (2.717g).

APPENDIX 3

THE ELEMENTAL COMPOSITIONS AND RELATIVE DENSITIES OF THE REAL TISSUES AND THE NEW TISSUE SUBSTITUTES.

APPENDIX 3 : ELEMENTAL COMPOSITIONS AND RELATIVE DENSITIES OF THE REAL TISSUES AND THE NEW TISSUE SUBSTITUTES

TABLE I : ELEMENTAL COMPOSITIONS AND RELATIVE DENSITIES OF THE REAL TISSUES

REAL TISSUE	ELEMENTAL COMPOSITION (Percentages by weight)													RELATIVE DENSITY
	H	C	N	O	Na	Mg	P	S	Cl	K	Ca	Fe	I	
PRINCIPAL SOFT TISSUES														
ADIPOSE	12.00	64.00	0.80	22.90	0.05	-	0.02	0.07	0.12	0.03	-	-	-	0.92
BLOOD	10.00	9.82	2.91	76.40	0.18	-	0.03	0.18	0.27	0.16	0.01	0.05	-	1.06
MUSCLE (ICRU)	10.20	12.30	3.50	72.89	0.08	0.02	0.20	0.50	0.08	0.30	0.01	-	-	1.06
PRINCIPAL SKELETAL TISSUES														
CORTICAL BONE (ICRU)	6.40	27.80	2.70	41.00	-	0.20	7.00	0.20	-	-	14.70	-	-	1.50
CORTICAL BONE (SPIERS)	3.39	15.50	3.97	44.10	0.06	0.21	10.20	0.31	-	-	22.20	-	-	1.85
INNER BONE	8.66	40.31	2.58	40.35	0.08	0.06	2.30	0.46	-	0.23	4.97	-	-	1.12
RED MARROW	10.18	47.48	2.18	39.67	0.01	-	0.03	0.15	0.10	0.17	-	0.01	-	1.03
BODY ORGANS														
BRAIN	10.70	15.33	1.29	71.40	0.18	-	0.34	0.17	0.23	0.30	-	-	-	1.03
KIDNEY	10.30	12.90	2.74	73.24	0.20	0.01	0.16	-	0.24	0.19	0.01	0.01	-	1.05
LIVER	10.00	14.40	2.83	71.85	0.10	0.02	0.03	0.29	0.20	0.25	0.01	0.02	-	1.07
LUNG (ICRP)	9.90	12.30	2.80	74.00	0.18	0.01	0.08	0.22	0.26	0.19	0.01	0.04	-	0.26-1.05
THYROID	10.00	13.60	2.20	73.50	0.22	0.01	0.08	-	0.17	0.12	0.04	0.01	0.06	1.06
AVERAGE TISSUES														
AVERAGE BREAST														
(I) 25% FAT-75% MUSCLE	10.71	28.25	2.63	57.60	0.06	0.02	0.15	0.38	0.06	0.23	0.01	-	-	1.02
(II) 50% FAT-50% MUSCLE	11.20	44.20	1.75	42.30	0.04	0.01	0.10	0.25	0.04	0.15	-	-	-	0.99
(III) 75% FAT-25% MUSCLE	11.71	60.14	0.88	27.01	0.02	0.01	0.05	0.13	0.02	0.08	-	-	-	0.95
(IV) 50% FAT-50% WATER	11.70	38.04	-	50.26	-	-	-	-	-	-	-	-	-	0.96
TOTAL SOFT TISSUE	10.50	23.33	2.50	62.87	0.11	0.01	0.13	0.20	0.13	0.20	0.02	-	-	1.03
TOTAL SKELETON	7.00	22.70	3.90	48.60	0.30	0.10	7.00	0.20	0.10	0.20	9.90	-	-	1.40
TISSUE COMPONENTS														
FAT	12.21	76.08	-	11.71	-	-	-	-	-	-	-	-	-	0.92
PROTEIN	7.00	52.00	16.00	23.50	-	-	0.80		-	-	-	-	-	1.30-1.40
WATER	11.19	-	-	88.81	-	-	-	-	-	-	-	-	-	1.00

APPENDIX 3

TABLE II : ELEMENTAL COMPOSITIONS AND RELATIVE DENSITIES OF THE NEW TISSUE SUBSTITUTES

TISSUE SUBSTITUTE	ELEMENTAL COMPOSITION (Percentages by weight)													MEASURED RELATIVE DENSITY
	H	C	N	O	Na	Mg	P	S	Cl	K	Ca	Fe	I	
AP/SF1	11.96	75.50	0.80	11:11	0.05	-	0.01_5	0.07	0.45	0.03	0.02	-	-	0.92
AP/L1 (Ethoxyethanol)	11.18	53.31	-	35.50	-	-	-	-	-	-	-	-	-	0.93
AP/L2	12.18	29.29	0.80	58.81	0.05	0.00_2	0.86	-	0.12	0.03	0.00_2	-	-	0.90
BL/L1	10.00	9.81	2.91	74.56	0.18	0.00_2	-	0.20	0.27	0.14	0.00_4	-	-	1.07
BL/L2	10.01	9.82	2.91	74.57	0.18	0.00_2	-	0.20	0.27	0.14	0.00_4	-	-	1.06
MS/SR1	10.20	73.68	3.50	11.44	0.08	0.02	0.18	0.50	0.09	0.30	0.01	-	-	1.05
MS/SR2	10.20	70.54	3.50	14.62	0.08	0.02	0.18	0.50	0.10	0.30	0.01	-	-	1.07
MS/SR3	10.30	67.42	3.50	17.16	0.08	0.02	0.18	0.50	0.52	0.30	0.01	-	-	1.06
MS/SR4	9.50	70.38	3.48	15.55	0.08	0.02	0.18	0.50	0.12	0.30	0.01	-	-	1.06
MS/SR5	10.20	76.55	3.50	8.56	0.08	0.02	0.18	0.50	0.09	0.30	0.01	-	-	1.07
MS/G1	10.20	12.51	3.50	73.00	0.07	0.02	0.20	-	0.09	0.39	0.01	-	-	1.06
MS/G2	10.35	12.31	3.50	73.04	0.07	0.01_5	0.20	-	0.09	0.39	0.01	-	-	1.05
MS/L1	10.20	12.30	3.50	73.00	0.07	0.02	0.20	0.32	0.09	0.39	0.01	-	-	1.07
MS/L1 N.T	10.20	12.30	3.50	71.76	-	-	-	-	-	-	-	-	-	1.06

AP = Adipose BL = Blood (whole) MS = Muscle HB = Hard Bone (cortical) IB = Inner Bone RM = Red Marrow
BRN = Brain LN = Lung FT = Fat WT = Water TST = Total Soft Tissue TSK = Total Skeleton

cont....

TABLE II cont....

TISSUE SUBSTITUTE	ELEMENTAL COMPOSITION (Percentages by weight)													MEASURED RELATIVE DENSITY
	H	C	N	O	Na	Mg	P	S	Cl	K	Ca	Fe	I	
HB/SR1	3.79	32.82	3.97	26.46	0.06	0.21	10.20	0.32	0.08	-	21.81	-	-	1.75
HB/SR1 A	3.79	32.82	3.97	26.46	0.06	0.21	-	10.52	0.08	-	21.81	-	-	1.74
HB/SR2	4.33	32.46	2.53	30.03	0.06	0.21	10.00	0.32	0.07	-	19.99	-	-	1.66
HB/SF3	4.86	28.53	3.99	31.73	0.06	0.21	10.00	0.32	0.32	-	19.98	-	-	1.70
HB/SR4	4.45	29.09	3.88	31.93	0.06	0.21	10.00	0.32	0.06	-	19.99	-	-	1.67
HB/SR5	4.74	31.97	3.88	28.77	0.06	0.21	10.00	0.32	0.07	-	19.98	-	-	1.60
HB/SR6	3.78	32.76	1.43	31.37	0.06	0.21	9.99	0.32	0.08	-	19.99	-	-	1.76
HB/SR7	4.49	36.96	3.99	23.88	0.06	0.21	9.99	0.32	0.09	-	19.97	-	-	1.58
HB/SR8	4.32	34.57	3.99	25.19	0.06	0.21	9.06	0.32	0.08	-	22.20	-	-	1.64
HB/SR9	3.81	27.82	3.99	33.73	0.06	0.21	10.00	0.32	0.07	-	19.99	-	-	1.82
HB/POWDER 1	2.88	15.74	3.97	42.25	0.06	0.24	11.72	0.36	-	-	23.77	-	-	-
HB/POWDER 2	3.41	19.22	3.97	40.71	0.06	0.21	10.20	0.32	-	-	21.80	-	-	-
HB/PASTE 1	3.52	15.43	3.97	44.51	0.06	0.21	10.20	0.32	-	-	21.81	-	-	-
HB/G1	4.2	5.03	4.24	57.62	0.06	0.21	8.68	-	-	-	19.98	-	-	-
HB/SF1 (ICRU)	6.40	45.40	2.70	22.91	-	0.20	6.94	0.26	0.49	-	14.70	-	-	1.46
HB/G1 (ICRU)	6.37	13.77	2.70	54.98	0.24	-	6.01	-	-	14.34	-	-	-	-
IB/SR1	8.51	61.79	2.36	17.83	0.06	-	2.62	-	0.12	-	5.089	-	-	1.15
IB/G1	8.97	8.55	2.57	72.25	0.02	0.05	2.30	0.11	-	4.98	-	-	-	-
IB/L1	8.65	17.27	2.58	60.83	0.06	-	2.49	-	-	4.99	-	-	-	1.14

cont....

TABLE II cont....

TISSUE SUBSTITUTE	ELEMENTAL COMPOSITION (Percentages by weight)													MEASURED RELATIVE DENSITY
	H	C	N	O	Na	Mg	P	S	Cl	K	Ca	Fe	I	
RM/SF1	10.08	68.16	2.16	18.60	0.01	0.00_3	0.03	0.14	0.62	0.15	-	-	-	1.04
RM/SR2	10.16	76.72	1.97	10.69	0.01	0.00_3	0.03	0.14	0.10	0.15	-	-	-	1.03
RM/SF3	10.15	68.28	2.17	18.79	0.01	0.00_3	0.03	0.14	0.53	0.15	-	-	-	1.03
RM/SR4	10.08	73.57	2.16	13.77	0.01	0.00_3	0.03	0.14	0.11	0.15	-	-	-	1.03
RM/G1	10.20	9.38	2.36	78.18	0.08	-	0.03	0.15	0.17	0.17	-	-	-	1.07
RM/G2	10.18	47.48	2.36	39.93	0.08	-	0.03	0.15	0.17	0.17	-	-	-	-
RM/L1	11.15	47.47	2.22	39.81	0.08	-	0.03	0.15	0.17	0.17	-	-	-	-
RM/L2	10.18	20.69	2.22	66.58	0.08	-	0.03	0.15	0.17	0.17	-	-	-	1.05
RM/L3	10.17	12.77	2.22	74.49	0.08	-	0.03	0.15	0.17	0.17	-	-	-	1.04
BRN/SR1	10.65	72.30	1.28	14.67	0.18	0.01	0.36	-	0.06	0.30	0.01	-	-	1.01
BRN/SR2	10.69	72.33	1.28	14.59	0.18	0.01	0.36	-	0.06	0.30	0.01	-	-	1.04
BRN/SF3	10.73	71.02	1.12	15.50	0.18	0.01	0.36	-	0.63	0.30	0.01	-	-	1.03
BRN/SF4	10.70	70.96	1.12	15.55	0.18	0.01	0.36	-	0.63	0.30	0.01	-	-	1.00
BRN/L1	10.84	15.14	1.29	71.51	0.18	-	0.34	0.17	0.23	0.30	-	-	-	1.03
BRN/L2	10.95	15.19	1.29	71.35	0.18	-	0.34	0.17	0.23	0.30	-	-	-	1.02
BRN/L3	10.68	15.13	1.29	71.69	0.18	-	0.34	0.17	0.23	0.30	-	-	-	1.03
BRN/L4	10.68	15.13	1.29	71.69	0.18	-	0.34	0.17	0.23	0.30	-	-	-	1.04
BRN/L5	10.70	15.79	1.29	71.00	0.18	-	0.34	0.17	0.23	0.30	-	-	-	1.03
BRN/L6	10.68	15.14	1.29	71.67	0.18	-	0.34	0.17	0.23	0.30	-	-	-	1.04
BRN/L7	11.31	15.14	1.29	71.05	0.18	-	0.34	0.17	0.23	0.30	-	-	-	1.00

cont....

APPENDIX 3

TABLE II cont....

TISSUE SUBSTITUTE	ELEMENTAL COMPOSITION (Percentages by weight)													MEASURED RELATIVE DENSITY
	H	C	N	O	Na	Mg	P	S	Cl	K	Ca	Fe	I	
KD/L1	10.40	11.35	2.74	74.5	0.18	-	0.19	-	0.28	0.25	-	-	-	1.05
LV/L1	10.18	14.40	2.83	71.80	0.11	-	-	0.24	0.18	0.29	-	-	-	1.06
*LN/SR1	10.00	73.38	3.50	11.37	0.17	0.01	0.12	0.22	0.09	0.19	0.01	-	-	0.30
*LN/SF3	10.20	65.30	2.80	19.51	0.17	0.01	0.12	0.22	0.56	0.19	0.01	-	-	0.30
*LN/SR4	9.70	70.26	2.80	16.30	0.17	0.01	0.12	0.22	0.11	0.19	0.01	-	-	0.30
TH/L1	10.00	13.05	2.20	74.2	0.22	-	0.08	-	0.14	0.19	-	-	0.06	1.11
TH/L2	10.01	13.58	2.20	73.52	0.22	-	0.08	-	0.14	0.19	-	-	0.06	1.08
TH/L3	10.01	13.58	2.20	73.52	0.22	-	0.08	-	0.14	0.19	-	-	0.06	1.14

* Lung substitutes contain 0.5% silicon because the foaming agent used is a silicon product.

**The lung relative density can be adjusted from 0.26 to 1.06

cont....

APPENDIX 3

TABLE II cont....

TISSUE SUBSTITUTE	ELEMENTAL COMPOSITION (Percentages by weight)												MEASURED RELATIVE DENSITY
	H	C	N	O	Na	Mg	P	S	Cl	K	Ca	Fe I	
25% FAT - 75% MUSCLE													
AV. BR. I/SF3	10.23	67.84	2.65	17,96	0.05	0.01_5	0.15	0.37	0.63	0.29	0.01	- -	1.00
50% FAT - 50% MUSCLE													
AV. BR. II/SF2	11.10	72.53	1.73	13.44	0.03_5	0.01	0.10	0.25	0.62	0.19	0.00_3	- -	0.99
AV.BR.II/SF3	11.30	74.20	1.60	12.00	-	-	-	-	0.90	-	-	- -	1.02
50% FAT - 50% WATER													
AV. BR. */L1	11.19	38.55	-	50.26	-	-	-	-	-	-	-	- -	0.97
AV.BR. */L2	11.79	37.86	-	50.41	-	-	-	-	-	-	-	- -	0.96
AV.BR. */L3	11.79	37.81	-	50.39	-	-	-	-	-	-	-	- -	0.96
AV.BR. */L4	11.78	37.80	-	50.39	-	-	-	-	-	-	-	- -	0.93
75% FAT - 25 MUSCLE													
AV.BR. III/SF1	11.66	73.92	0.88	12.74	0.02	0.01	0.05	0.12	0.49	0.09	-	- -	0.95
T.S.T/L1	10.50	23.33	2.58	62.83	0.11	0.01	0.13	0.20	0.13	0.20	0.02	- -	1.05
T.S.T/L2	10.49	23.33	2.59	62.83	0.11	0.01	0.13	0.20	0.13	0.20	0.02	- -	1.02
T.S.T/L3	10.46	23.33	2.59	62.54	0.11	0.01	0.13	0.20	0.13	0.20	0.02	- -	1.04

cont....

TABLE II cont....

TISSUE SUBSTITUTE	ELEMENTAL COMPOSITION (Percentages by weight)													MEASURED RELATIVE DENSITY
	H	C	N	O	Na	Mg	P	S	Cl	K	Ca	Fe	I	
T.SK/SR1	6.45	46.42	2.81	26.40	0.31	0.12	7.02	0.16	0.10	0.15	10.02	-	-	1.39
T.SK/SF2	7.32	45.92	3.03	25.22	0.31	0.12	7.07	0.16	0.54	0.15	10.11	-	-	1.40
T.SK/SF3	7.16	45.50	3.08	26.12	0.31	0.12	7.02	0.16	0.47	0.15	10.03	-	-	1.36
T.SK/L1	7.45	4.64	2.94	66.93	0.32	-	7.00	-	0.13	10.15	-	-	-	1.36
T.SK/L2	7.17	13.93	2.94	57.96	0.32	-	7.00	-	0.13	10.15	-	-	-	1.40
T.SK/L3	7.27	2.47	3.00	69.63	0.32	-	7.00	-	0.13	0.14	10.02	-	-	1.34
T.SK/L4	7.15	8.41	3.00	63.81	0.32	-	7.00	-	0.13	0.15	10.02	-	-	1.36
FT/SF1	12.31	77.27	-	10.41	-	-	-	-	-	-	-	-	-	0.92
FT/SR2	12.41	76.00	-	11.73	-	-	-	-	-	-	-	-	-	0.92
FT/SR3	12.27	76.04	-	11.69	-	-	-	-	-	-	-	-	-	0.92
FT/L1	12.27	76.04	-	11.60	-	-	-	-	-	-	-	-	-	0.89
FT/L2	11.84	77.32	-	10.84	-	-	-	-	-	-	-	-	-	0.92
PR/S1	6.24	50.30	17.82	24.80	-	-	0.80	-	-	-	-	-	-	1.28
WT/SR1	8.09	67.22	2.40	19.84	-	-	-	-	-	-	-	-	-	1.00

T.SK = Total Skeleton FT = Fat PR = Protein WT = Water

APPENDIX 4

CONSTITUENTS, RELATIVE DENSITIES AND ELEMENTAL COMPOSITIONS OF SUBSTITUTES DEVELOPED IN THE PAST.

APPENDIX 4 : CONSTITUENTS, RELATIVE DENSITIES AND ELEMENTAL COMPOSITIONS OF SUBSTITUTES DEVELOPED IN THE PAST

TABLE I : CONSTITUENTS, RELATIVE DENSITIES AND REFERENCES

SUBSTITUTE	CONSTITUENTS (W%) or FORMULA (SYNONYMS, TRADE NAMES)	RELATIVE DENSITY	REFERENCE
ADIPOSE			
AP6	Epoxy CB4 (79.00); P M S (4 9 6.) ; Polyethylene (12.00); P.T.F.E. (4.04)	0.92	White, D.R., 1974
Polystyrene	$(C_8 H_8)_n$	1.05	Brydson, J.A., 1970
BONE			
Aluminium	Al (100)	2.70	Goodwin, P.N., 1960
Cameron wax	Paraffin wax (58); Calcium carbonate (42)	1.28	Cameron, J.R., 1965
Magnesium	Mg (100)	1.74	Laughlin, J.S., et al., 1965
Plaster of Paris	$Ca\ SO_4 \cdot 2H_2O$ (natural gypsum)	2.32	Spiers, F.W., 1946
P.T.F.E.	$(C_2 F_4)_n$ (Teflon)	2.10	Brydson, J.A., 1970
SB3	CB2 (32.51); Calcium carbonate (67.49)	1.84	White, D.R., 1974
Shonka plastic (B100)	Nylon (21.60); polyethylene (30.00); carbon (14.00); calcium fluoride (34.40)	1.45	Shonka, F.R., et al., 1958
Spiers liquid	Water (50); calcium bromide (50)	1.53	Spiers, F.W., and Chesters, M.S., 1962
Sulphur	S (100)	1.92-2.07	Markus, B., 1960
White's powder	Polyethylene (32.40); calcium sulphate (67.60)	1.72	White, D.R., 1976
Witt liquid	Water (38.46); dipotassium hydrogen orthophosphate (61.54)	1.68	Witt, R.M., and Cameron, J.R., 1975

cont....

TABLE I cont....

SUBSTITUTE	CONSTITUENTS (w/o) or FORMULA (SYNONYMS, TRADE NAMES)	RELATIVE DENSITY	REFERENCE
FAT			
Alderson Fat	Polyethylene/wax/antimony trioxide	0.91	Alderson S.W. et al., 1962
FT1	TPX(81.42); Lithium carbonate(18.58)	0.95	White, D.R., 1974
FT2	EVA-28(100)	0.92	White, D.R., 1974
LUNG			
Alderson lung	Epoxy system/phenolic microspheres/antimony trioxide	0.32	Alderson, S.W., et al., 1962
LN1	Polyurethane PU1 (85.73); Aluminium oxide (14.27)	0.30	White, D.R., 1974
Rogers adiprene	Adiprene(81.97); Moca(15.96); silicone(1.64); adipic acid(0.41);	0.26	Rogers, R.T., 1970
Shonka & McGinley lung	H_2O(68.5); NH_4OH(8.0); NaCl(1.0); Cellulose sponge $C_6H_{10}O_5$ (22.5)	0.15-0.30	Shonka, J.J., and McGinley, P.H., 1976
Stacey Latex	Latex/boron carbide/sulphur/ zinc oxide/other fillers	0.26	Stacey, A.J., 1972
MUSCLE			
Alderson muscle	Isocyanate rubber/phenolic microspheres/antimony trioxide	1.00	Alderson, S.W., et al., 1962
Bakelite	$(C_{43}H_{38}O_7)_n$ (phenol formaldehydes)	1.25	Christen, F.T., 1913
Bioplastic	Thermosetting polyester	1.20	Roderick, J.F., 1959
Frigerio gel	Water(59.3); Ammonium formate (18.0); Ethylene glycol(17.7); Agar(4.0); sodium carbonate(1.00)	1.12	Frigerio, N.A., 1962

cont...

APPENDIX 4

TABLE I cont....

SUBSTITUTE	CONSTITUENTS (w/.) or FORMULA (SYNONYMS, TRADE NAMES)	RELATIVE DENSITY	REFERENCE
MUSCLE cont'd			
Frigerio liquid	Water + misc. components	1.01-1.10	Frigerio, N.A., et al., 1972
Goodman liquid	Water(65.6); glycerol(26.8); urea(7.6)	1.07	Goodman, L.J., 1969
Harris wax	Paraffin wax(81); silicon dioxide(19)	0.98	Harris, J.H., et al., 1956
Lincolnshire bolus	Sucrose(87); magnesium carbonate(13)	1.06	Lindsay, D.D. and Stern, B.E., 1953
M3	Paraffin wax(76.92); magnesium oxide(22.35); calcium carbonate(0.72)	1.05	Markus, B., 1956
Mix D	Paraffin wax(60.8); Polyethylene(30.4); magnesium oxide(6.4); titanium dioxide(2.4)	0.99	Jones, D.E.A. and Raine, H.C., 1949
MS15	Epoxy CB3(58.63); PMS(3.24); polyeth(20.00); Al_2O_3(18.13)	1.00	White, D.R., et al., 1977
MS20	Epoxy CB2(58.58); PMS(4.81); polyeth(15.00); MgO(21.61)	1.00	White, D.R., et al., 1977
Paraffin wax	$C_{25}H_{52}$	0.93	Baumeister, L., 1923
Rossi liquid	Water(56.9); glycerol(28.4); urea(7.6); sucrose(7.1)	1.11	Rossi, H.H., and Failla, G., 1956
Shonka A-150	Polyethylene(45.14); nylon(35.22); carbon(16.06); calcium fluoride(3.58)	1.12	Shonka, F.R., et al., 1958
Siemens wax	Paraffin wax(82.64); magnesium oxide(17.36)	1.03	Ott, P., 1937
Spiers' powder	Rice(63); sodium bicarbonate(37)	1.06	Spiers, F.W., 1943
Temex.	Natural rubber/carbon/sulphur/titanium dioxide/zinc oxide/other fillers	1.01	Stacey, A.J., et al., 1961
Water	H_2O	1.00	Kienbock, R., 1906

APPENDIX 4

TABLE II : ELEMENTAL COMPOSITIONS OF SUBSTITUTES DEVELOPED IN THE PAST

SUBSTITUTE	ELEMENTAL COMPOSITION (Percentages by weight)
ADIPOSE	
AP6	H (8.36); C (69.14); N (2.36); O (16.94); F (3.07); Cl (0.14)
Polystyrene	H (7.74); C (92.26)
BONE	
Aluminium	Al (100)
Cameron wax	H (8.62); C (54.42); O (20.14); Ca (16.82)
Magnesium	Mg (100)
Plaster of Paris	H (2.34); O (55.76); S (18.62); Ca (23.28)
SB3	H (3.10); C (31.26); N (0.99); O (37.57); Cl (0.05); Ca (27.03)
Shonka plastic (B100)	H (6.51); C (54.24); N (2.26); O (2.59); F (16.74); Ca (17.66)
Spiers' liquid	H (5.60); O (44.41); Ca (10.03); Br (39.98)
Sulphur	S (100)
White's powder	H (4.66); C (27.74); O (31.78); S (15.92); Ca (19.90)
Witt liquid	H (4.70); O (56.80); P (10.90); K (27.90)
FAT	
Alderson fat	H (14.37); C (85.61); O (0.004); Sb (0.02)
FT1	H (11.70); Li (3.48); C (72.74); O (12.07)
FT2	H (12.31); C (77.28); O (10.41)

cont....

APPENDIX 4

TABLE II cont....

SUBSTITUTE	ELEMENTAL COMPOSITION (Percentages by weight)
LUNG	
Alderson	H (5.74); C (73.94); N (2.01); O (18.14); Sb (0.16)
LN1	H (6.00); C (51.44); N (4.29); O (30.72); Al (7.55)
Rogers' adiprene	H (13.95); C (40.89); N (8.79); O (30.79); Si (1.14); Cl (4.44)
Shonka & McGinley lung	H (10.21); C (10.00); N (3.20); O (75.60); Other (1.00)
Stacey latex	H (10.10); B (8.00); C (79.20); O (0.12); S (1.91); Zn (0.67)
MUSCLE	
Alderson muscle	H (8.87); C (66.81); N (3.10); O (21.13); Sb (0.08)
Bakelite	H (5.74); C (77.46); O (16.80)
Bioplastic	H (6.0); C (70.0); N (0.2); O (24.0)
Frigerio gel	H (10.0); C (12.0); N (4.0) O (73.3); Na (0.4); S (0.2); Cl (0.1)
Frigerio liquid	H(10.2); C(12.3); N(3.5); O(72.893); Na(0.07); Mg(0.02); P(0.20); S(0.32); Cl(0.08); K(0.39); Ca(0.01)
Goodman liquid	H (10.20); C (12.01); N (3.54); O (74.25)
Harris wax	H (12.04); C (68.96); O (10.12); Si (8.88)
Lincolnshire bolus	H (5.92); C (37.90); N (0.03); O (52.69); Mg (3.46)
M3	H (11.43); C (65.58); O (9.22); Mg (13.48); Ca (0.29)
Mix D	H (13.40); C (77.79); O (3.50); Mg (3.86); Ti (1.44)
MS15	H(9.75); C(63.16); N(0.94); O(16.02); Al(9.60); Cr(0.53)
MS20	H(8.12); C(58.35); N(1.78); O(18.64); Mg(13.03); Cl(0.09)

cont....

TABLE II cont....

SUBSTITUTE	ELEMENTAL COMPOSITION (Percentages by weight)
MUSCLE cont'd	
Paraffin wax	H (14.86); C (85.14)
Rossi liquid	H (9.82); C (15.62); N (3.54); O (71.01)
Shonka A-150	H (10.20); C (76.80); N (3.60); O (5.90); F (1.70); Ca (1.80)
Siemens wax	H (12.28); C (70.36); O (6.89); Mg (10.47)
Spiers' powder	H (4.36); C (33.29); O (52.22); Na (10.13)
Temex	H(9.60); C(87.00); N(0.06); O(0.47); S(1.53); Ti(0.33); Zn(0.45)
Water	H (11.19); O (88.81)

APPENDIX 5

COMPOSITION AND SUPPLIERS OF RESINS AND SOME SPECIAL AGENTS USED IN THIS WORK.

APPENDIX 5 : COMPOSITION OF THE RESINS AND SPECIAL AGENTS USED IN THIS WORK

TABLE I : COMPOSITION DATA

MATERIAL	CONSTITUENTS OR FORMULA ELEMENTAL COMPOSITION (Parts or percentages by weight bracketed)	RELATIVE DEMSITY
CB1	Araldide MY750 (100), Synolide 960 ≡ XD593 (60) H (8.906); C (72.162); N (5.625); O (13.155); Cl (0.150)	1.11
CB2	Araldide MY750 (100), Epoxide 7 (50), XD555 (31) H (9.535); C (71.253); N (3.031); O (16.030); Cl (0.150)	1.10
CB3	Epikote 871 ≡ EP588 (100), XD555 (10) H (11.300); C (74.200); N (1.600); Cl (0.900)	1.02
CB4	Araldide MY750 (100), XD716 (40) H (7.899); C (68.375); N (2.984); O (20.570) Cl (0.172)	1.15
PMS	H (7.877); C (78.228); O (13.895)	0.20
DC200/50 (surfactant)	H (8.270); C (33.10); O (20.92); Si (37.69)	1.00
DC1107 (foaming agent)	H (6.940); C (21.410); O (25.620); Si (45.980)	1,00
Gelatine (gelling agent)	H (7.00); C (50.00); N (18.00); O (25.00 ?); S (as impurity)	1.30
Agar-Agar (gelling agent)	H (2.59); C (31.09); O (49.74); S (16.58)	
Sodium Azide (bacteriostatic)	N (64.63); Na (35.37)	

APPENDIX 5

TABLE II : SUPPLIERS OF RESINS AND OTHER IMPORTANT COMPOUNDS

MATERIAL	SUPPLIER
Araldide MY750 XD555 XD716	Ciba-Geigy Ltd
Synolide 960	Cray Valley Products Ltd
Epoxide No.7	Proctor & Gamble Ltd
Epikote 871	Shell Chemicals (U,K) Ltd
PMS (BJO 0930)	Bakelite Xylonite Ltd
DC1107 DC200/50	Dow Corning Ltd

APPENDIX 6

A TABULATION OF THE COMPOUND LIBRARY

	NAME	FORMULA
1	ALUMINIUM ACETATE BASIC	$AL_2C_8H_{20}O_{13}$
2	ALUMINIUM AMMONIUM SULPHATE	$ALNS_2H_{28}O_{20}$
3	ALUMINIUM CHLORIDE ANHYDROUS	$ALCL_3$
4	ALUMINIUM FLUORIDE	ALF_3
5	ALUMINIUM NITRATE	$ALN_3H_{18}O_{18}$
6	ALUMINIUM NITRIDE	ALN
7	ALUMINIUM OXIDE	AL_2O_3
8	ALUMINIUM ORTHOPHOSPHATE	$ALPO_4$
9	ALUMINIUM SULPHATE	$AL_2S_3O_{12}$
10	AMMONIUM ACETATE	$NH_7C_2O_2$
11	AMMONIUM CARBONATE	$N_2H_8CO_3$
12	AMMONIUM CHLORIDE	NH_4CL
13	AMMONIUM CHROMATE	$N_2H_8CRO_4$
14	AMMONIUM HYDROGEN CARBONATE	NH_5CO_3
15	AMMONIUM HYDROGEN ORTHOPHOSPHATE	$N_2H_9PO_4$
16	AMMONIUM IODIDE	NH_4I
17	AMMONIUM NITRATE	$N_2H_4O_3$
18	AMMONIUM OXALATE	$N_2H_{10}C_2O_3$
19	AMMONIUM SULPHATE	$N_2H_8SO_4$
20	AMMONIUM HYDROGEN SULPHATE	NH_5SO_4
21	AMMONIUM SULPHIDE	N_2H_8S
22	AMMONIUM THIOCYANATE	N_2H_4CS
23	AMMONIUM THIOSULPHATE	$N_2H_8S_2O_3$
24	AMMONIUM DIHYDROGEN ORTHOPHOSPHATE	NH_6PO_4
25	BORIC ACID	H_3BO_3
26	CALCIUM ACETATE	$C_4H_6O_5CA$
27	CALCIUM CARBIDE	CAC_2
28	CALCIUM CARBONATE (ARGONITE)	$CACO_3$
29	CALCIUM CHLORATE	$CACL_2H_4O_8$
30	CALCIUM CHLORIDE	$CACL_2$
31	CALCIUM FLUORIDE	CAF_2
32	CALCIUM FORMATE	$CAH_2C_2O_4$
33	CALCIUM GLYCEROPHOSPHATE	$CAC_3H_7PO_6$
34	CALCIUM HYDROXIDE	CAO_2H_2
35	CALCIUM HYDROGEN ORTHOPHOSPHATE/	$CAHPO_4$
36	CALCIUM HYDROGEN ORTHOPHOSPHATE.	$CAHPO_4 \cdot 2H_2O$
37	CALCIUM DI-HYDROGEN ORTHOPOSPHATE	$CAH_6P_2O_8$
38	CALCIUM IODIDE	CAI_2
39	CALCIUM NITRATE	CAN_2O_6
40	CALCIUM ORTHOPHOSPHATE	$CA_3P_2O_8$
41	CALCIUM OXALATE	CAC_2O_4
42	CALCIUM OXIDE	CAO
43	CALCIUM PEROXIDE	CAO_2
44	CALCIUM STEARATE	$CAC_{36}H_{70}O_4$
45	CALCIUM SULPHATE	$CASO_4$
46	CALCIUM SULPHITE	CAS
47	CARBON	C
48	COBALT CHLORIDE	$COCL_2H_{12}O_6$
49	COBALT NITRATE	$CON_2H_{12}O_6$
50	CUBRIC ACETATE	$C_2H_6O_5CU$
51	CUPRIC CHLORIDE	$CUCL_2$
52	CUBRIC NITRATE TRIHYDRATE	$CUN_2H_6O_9$
53	CUBRIC OXIDE	CUO
54	CUBRIC SULPHATE	$CUSO_4$
55	FERRIC CHLORIDE	$FECL_3$

	NAME	FORMULA
56	FERRIC NITRATE HYDRATED	$FEN_3H_{18}O_{18}$
57	FERRIC OXIDE	FE_2O_3
58	FERRIC SULPHATE	$FE_2S_3O_{12}$
59	FERROUS CHLORIDE TETRA HYDRATE	$FECL_2H_8O_4$
60	FERROUS SULPHATE HEPTAHYDRATE	$FESH_{14}O_1$
61	MAGNESIUM	MG
62	MAGNESIUM ACETATE TETRAHYDRATE	$MGC_4H_{14}O_8$
63	MAGNESIUM CARBONATE	$MGCO_3$
64	MAGNESIUM CHLORIDE	$MGCL_2$
65	MAGNESIUM CHLORIDE HEXAHYDRATE	$MGCL_2H_{12}O_6$
66	MAGNESIUM FLUORIDE	MGF_2
67	MAGNESIUM HYDROXIDE	MGO_2H_2
68	MAGNESIUM IODATE	$MGIO_{10}H_8$
69	MAGNESIUM NITRATE HEXAHYDRATE	$MGN_2O_{12}H_{12}$
70	MAGNESIUM NITRIDE	MG_3N_2
71	MAGNESIUM OXIDE	MGO
72	MAGNESIUM SULPHATE	$MGSO_4$
73	MANGANESE	MN
74	MANGANESE FLUORIDE	MNF_2
75	MANGANESE DIOXIDE	MNO_2
76	MANGANESE SULPHATE	$MNSO_4$
77	PHOSPHORUS	P
78	POTASSIUM ACETATE	$C_2H_3O_3K$
79	POTASSIUM CARBONATE	K_2CO_3
80	POTASSIUM HYDROGEN CARBONATE	$KHCO_3$
81	POTASSIUM CHLORATE	$KCLO_3$
82	POTASSIUM PERCHLORATE	$KCLO_4$
83	POTASSIUM CHLORIDE	KCL
84	POTASSIUM CHROMATE	K_2CRO_4
85	POTASSIUM DICHROMATE	$K_2CR_2O_7$
86	POTASSIUM HYDROXIDE	KOH
87	POTASSIUM IODATE	KIO_3
88	POTASSIUM IODITE	KI
89	POTASSIUM NITRATE	KNO_3
90	POTASSIUM ORTHOPHOSPHATE	K_3PO_4
91	POTASSIUM DIHYDROGEN ORTHOPHOSPHATE	KH_3PO_4
92	DIPOTASSIUM HYDROGEN ORTHOPHOSPHATE	K_2HPO_4
93	POTASSIUM PERMANGANATE	$KMNO_4$
94	POTASSIUM SULPHATE	K_2SO_4
95	POTASSIUM HYDROGEN SULPHATE	$KHSO_4$
96	POTASSIUM THIOCYANATE	KCNS
97	SILICON DIOXIDE	SIO_2
98	SODIUM ACETATE	$NAC_2H_3O_2$
99	SODIUM CARBONATE	NA_2CO_3
100	SODIUM HYDROGEN CARBONATE	$NACHO_3$
101	SODIUM CHLORATE	$NACLO_3$
102	SODIUM CHLORIDE	NACL
103	SODIUM FLUORIDE	NAF
104	SODIUM HYDROXIDE	NAOH
105	SODIUM IODATE	$NAIO_3$
106	SODIUM IODIDE	NAI
107	SODIUM NITRATE	$NANO_3$
108	SODIUM ORTHOPHOSPHATE DODECAHYDRATE	$NA_3PH_{24}O_{16}$
109	SODIUM DIHYDROGEN ORTHOPHOSPHATE	NAH_2PO_4
110	DISODIUM HYDROGEN ORTHOPHOSPHATE	NA_2HPO_4

	NAME	FORMULA
111	DISODIUM HYDROGEN ORTHOPHOSPHATE	$NA_2HPO_4 \cdot 12H_2O$
112	SODIUM HYPOPHOSPHATE	$NA_2H_2P_2O_6$
113	SODIUM PEROXIDE	NA_2O_2
114	SODIUM SULPHATE	NA_2SO_4
115	SODIUM HYDROGEN SULPHATE	$NAHSO_4$
116	SODIUM THIOSULPHATE	$NA_2S_2O_3$
117	SULPHUR	S
118	TITANIUM DIOXIDE	TIO_2
119	ZINC CHLORIDE	$ZNCL_2$
120	ZINC SULPHATE HEPTAHYDRATE	$ZNSH_{14}O_1$
121	ZINC OXIDE	ZNO
122	ACETANILIDE	C_8H_9ON
123	ACETIC ANHYDRITE	$C_4H_6O_3$
124	ACETYLUREA	$C_3H_6N_2O_2$
125	ADIPIC ACID	$C_6H_{10}O_4$
126	ALDOL	$C_4H_8O_2$
127	P-AMINOBENZOIC ACID	$C_7H_7NO_2$
129	ANTHRACENE	$C_{14}H_{10}$
129	BENZANILIDE	$C_{13}H_1NO$
130	BENZOIC ACID	$C_7H_6O_2$
131	BENZOIC ACID SODIUM SALT	$C_7H_5O_2NA$
132	BORNEOL	$C_{10}H_{18}O$
133	P-TERT-BUTYLPHENOL	$C_{10}H_{14}O$
134	TERT.-BUTYLUREA	$C_5H_{12}N_2O$
135	CALCIUM FORMATE	$C_2H_2O_2CA$
136	CHLOROACETIC ACID SODIUM SALT	$C_2H_2O_2NACL$
137	5-CHLOROSALICYLIC ACID	$C_7H_5CLO_3$
138	CITRIC ACID	$C_6H_8O_7$
139	DL-CAMPHOR	$C_{10}H_{16}O$
140	DEXTRIN	$C_6H_{10}O_5$
141	3,5-DICHLOROSALICYLIC ACID	$C_7H_4CL_2O_3$
142	1,3-DICYCLOHEXYLUREA	$C_{13}H_{24}N_2O$
143	DIMETHYLGLYOXIME	$C_4H_8N_2O_2$
144	DIMETHYL TEREPTHALATE	$C_{10}H_{10}C_4$
145	DIPHENYLACETAMIDE	$C_{14}H_{13}ON$
146	DIPHENYLGLYOXIME	$C_{14}H_{12}N_2O_2$
147	1,1-DIPHENYL-2-THIOUREA	$C_{13}H_{12}N_2S$
148	D-(+)-GALACTOSE	$C_6H_{12}O_6$
149	GALLIC ACID	$C_7H_6O_5$
150	GLUCOSE (SOLUBLE)	$C_6H_{12}O_6$
151	HIPPURIC ACID	$C_9H_9NO_3$
152	P-HYDROXYBENZALDEHYDE	$C_7H_6O_2$
153	IMIDAZOL	$C_3H_4N_2$
154	B-D-LACTOSE	$C_{12}H_{22}O_1$
155	LINOLEIC ACID	$C_{18}H_{32}O_2$
156	MALEIC ACID	C_4H_4O
157	MENTHOL	$C_{10}H_{20}O$
158	METHYL-P-HYDROBENZOATE	$C_8H_8O_3$
159	METHYL LAURATE	$C_{13}H_{26}O_2$
160	METHYL METHACRYLATE	$C_5H_8O_2$
161	4-METHYL-2NITROANILINE	$C_7H_8O_2N_2$
162	METHYL SULPHONE	$C_2H_6O_2S$
163	MONOSTEARIN	$C_{15}H_{30}O_4$
164	2-NAPTHOL	$C_{10}H_8O$
165	OXALIC ACID	$C_2H_2O_4$

	NAME	FORMULA
166	PALMITIC ACID	$C_{16}H_{32}O_2$
167	PARAFFIN WAX	$C_{25}H_{52}$
168	PARAFORMALDEHYDE	CH_2O
169	P-PHENYLENEDIAMINE	$C_6H_8N_2$
170	PHTHALIC ACID	$C_8H_6O_4$
171	PTHALIC ANHYDRITE	$C_8H_4O_3$
172	PHTHALIMIDE	$C_8H_5NO_2$
173	PYROCATECHOL	$C_6H_6O_2$
174	PYROGALLOL	$C_6H_6O_3$
175	SALICYLIC ACID	$C_7H_6O_3$
176	SORBIC ACID	$C_6H_8O_2$
177	STARCH (SOLUBLE)	$C_6H_{10}O_5$
178	STEARIC ACID	$C_{18}H_{36}O_2$
179	SUCCINIC ACID	$C_4H_6O_4$
180	SUCCINIC ANHYDRITE	$C_4H_4O_3$
181	SUCROSE	$C_{12}H_{22}O_1$
182	SULFOACETIC ACID	$C_2H_4O_5S$
183	TARTARIC ACID	$C_4H_6O_6$
184	THIOCARBANILIDE	$C_{13}H_{12}N_2S$
185	THIOUREA	CH_4N_2S
186	TRICHLOROACETIC ACID SODIUM SALT	$C_2O_2CL_3NA$
187	UREA	CH_4ON_2
188	VINYL ACETATE	$C_4H_6O_2$
189	ACRYLICS	$C_5H_8O_2$
190	CELLULOSIC PLASTICS	$C_{20}H_{28}O_{14}$
191	ELVAX 220 (DU POND)	$C_{26}H_{50}O_3$
192	FLUORINATED POLYMERS - P.C.T.F.E.	C_2F_3CL
193	MELAMINE FORMALDEHYDES	$C_8H_6N_6O_3$
194	NYLONS - TYPE 6	C_6H_1NO
195	NYLONS - TYPE 6/6	$C_{12}H_{22}N_2O_2$
196	NYLONS - TYPE 6/10	$C_{16}H_{30}N_2O_2$
197	NYLONS - TYPE 11	C_1H_2NO
198	PHENOL FORMALDEHYDES	$C_{43}H_{38}O_7$
199	POLYACETALS	CH_2O
200	POLYCARBONATES	$C_{16}H_{14}O_3$
201	POLYOLEFINS - POLYETHYLENE	C_2H_4
202	POLYOLEFINS - POLYPROPYLENE	C_3H_6
203	POLYETHYLENE GLYCOL	$C_8H_{18}O_5$
204	POLYURETHANES - CAST ELASTOMER	$C_{37}H_{57}N_3O_8CL$
205	POLYURETHANES - RIGID CAST URETHANE	$C_{13}H_{20}NO_4$
206	POLYURETHANES - FLEXIBLE FOAM	$C_{52}H_{87}N_4O_{19}$
207	POLYURETHANES - RIGID FOAM	$C_{52}H_{55}N_6O_{1}CL$
208	UREA FORMALDEHYDES	$C_3H_4N_2O$
209	VINYLIDENE CHLORIDE POLYMERS	$C_2H_2CL_2$
210	POLYIMIDES	$C_{44}H_{20}N_4O_{10}$
211	POLYOLEFINS - TPX	C_6H_{12}
212	POLYSTYRENE	C_8H_8
213	PERSPEX	$C_5H_8O_2$
214	VINYL POLYMERS - PVC	C_2H_3CL
215	POLYVINYL ACETATE	$C_4H_6O_2$
216	POLYVINYL ALCOHOL	C_2H_4O
217	CB1A	
218	CB2	
219	CB3C	
220	CB4	

see appendix 5

	NAME	FORMULA
221	ACETIC ACID	$C_2H_4O_2$
222	ACETONITRILE	C_2H_3N
223	ACRYLIC ACID	$C_3H_3O_2$
224	ALLYL ALCOHOL	C_3H_6O
225	1-AMINO-2-PROPANOL	C_3H_9ON
226	ANILINE	C_6H_7N
227	ACETYLACETONE (2-4-PENTANEDIONE)	$C_5H_8O_2$
228	BENZALDEHYDE	C_7H_6O
229	1.3BUTANEDIOL	$C_4H_{10}O_2$
230	2-BUTANONE	C_4H_8O
231	2-BUTANOL	$C_4H_{10}O$
232	BUTYL ACETATE	$C_6H_{12}O_2$
233	BUTYL ALCOHOL	$C_4H_{10}O$
234	BUTYRALDEHYDE	C_4H_8O
235	ISO-BUTYRIC ACID	$C_4H_8O_2$
236	CARBON TETRACHLORIDE	CCl_4
237	CHLOROBENZENE	C_6H_5Cl
238	CYCLOHEXANOL	$C_6H_{12}O$
239	CYCLOHEXANONE	$C_6H_{10}O$
240	CYCLOPENTANONE	C_5H_8O
241	CYCLOHEXYL ACETATE	$C_8H_{14}O_2$
242	DIBUTYL PTHALATE	$C_{16}H_{22}O_4$
243	DICHLOROACETIC ACID	$C_2H_2O_2Cl_2$
244	1.2-DICHLOROPROPANE	$C_3H_6Cl_2$
245	DIETHYL CARBONATE	$C_5H_{10}O_5$
246	DIMETHYL SULFOXIDE	C_2H_6SO
247	DIMEHYL SULPHATE	$C_2H_6O_4S$
248	ETHANOL	C_2H_6O
249	ETHANEDIOL (ETHYLENE GLYCOL)	$C_2H_6O_2$
250	2-ETHOXYETHANOL	$C_4H_{10}O_2$
251	ETHYLENE DIACETATE	$C_6H_{10}O_4$
252	ETHYLENEDIAMINE	$C_2H_8N_2$
253	ETHYL OLEATE	$C_{20}H_{36}O_2$
254	GLYCEROL	$C_3H_8O_3$
255	GLYCEROL TRIOLEATE (TRIOLEIN)	$C_{58}H_{104}O_6$
255	1-HEPTANOL	$C_7H_{16}O$
257	HEXYL ALCOHOL	$C_6H_{14}O$
258	HEXYLAMINE	$C_6H_{15}N$
259	HYDRAZINE HYDRATE	N_2H_6O
260	HYDROCHLORIC ACID (5M SOLUTION)	HCL
261	HYDROGEN PEROXIDE (100 VOLUMES)	H_2O_2
262	IODOPROPANE (N-PROPYL IODIDE)	C_3H_7I
263	METHANOL	CH_4O
264	2-METHYL CYCLOHEXANOL	$C_7H_{14}O$
265	METHYL OLEATE	$C_{19}H_{36}O_2$
266	OLEYL ALCOHOL	$C_{18}H_{36}O$
267	ORTHOPHOSPHORIC ACID	H_3PO_4
268	1.5PENTANEDIOL	$C_5H_{12}O_2$
269	PENTANOL	$C_5H_{12}O$
270	PENTANONE	$C_5H_{10}O$
271	1.2PROPANEDIOL	$C_3H_8O_2$
272	1-PROPANOL	C_3H_8O
273	SULPHURIC ACID	H_2SO_4
274	TRIETHYLENE GLYCOL	$C_6H_{14}O_4$
275	WATER	H_2O

	NAME	FORMULA
276	AGAR-AGAR (GELLING AGENT)	$C_5H_8O_6S$
277	GELATINE (GELLING AGENT)	$C_{102}H_{15}O_{39}N_3$
278	DC1107 (FOAMING AGENT)	
279	DC200/50 (SURFACTANT)	
280	PHENOLIC MICROSPHERES (PMS)	see appendix 5
281	POTASSIUM AZIDE (BACTERIOSTATIC)	KN_3
282	SODIUM AZIDE (BACTERIOSTATIC)	NAN_3

REFERENCES

(1) ALDERSON, S.W., LANZL, L.H., ROLLINS, M., and SPIRA, J., 1962. An instrumented phantom system for analog computation of treatment plans. Am. J. Roentg., 87, 185-195.

(2) ARCHAMBEAU, J.O., BENNET, G.W., LEVINE, G.S., COWEN, R., and AKAMUMA, A., 1974. Proton Radiation Therapy. Radiology, 110, 445-457.

(3) AUXIER, J.A., SNYDER, W.S., and JONES, T.D., 1968. Neutron interactions and penetration in tissue. Radiation Dosimetry, Vol. I, Chapter 6. Attix, F.H., Roesch, W.C., and Tochilin, E. (Academic Press, New York).

(4) BARKAS, H.W., and BERGER, M.J., 1964. Tables of energy losses and ranges of heavy charged particles. National Aeronautics and Space Administration. (NASA SP-3013).

(5) BATHO, H.F., 1964. Lung corrections in cobalt-60 beam therapy. Journal of the Canadian Association of Radiologists, 15, 79-83.

(6) BAUMEISTER, L., 1923. Roentgen-ray measurements. Acta Radiologica, 2, 418-429.

(7) BERGER, M.J., and SELTZER, S.S., 1964. Tables of energy losses and ranges of electrons and positrons. National Research Council Report 1133, National Academy of Science.

(8) BERGER, M.J., et al., 1966. Additional stopping power and range tables for protons, mesons and electrons. National Aeronautics and Space Administration. NASA SP-3036 (Washington, D.C).

(9) BETHE, H.A., 1932. Bremsformel fur electronen relativisticher Geschwindigkeit. Z. Physik, 76, 293.

(10) BEWLEY, D.K., 1963. Pre-therapeutic experiments with the fast neutron beam from the M.R.C. cyclotron. II. Physical aspects of the fast neutron beam. Br.J. Radiol., 36, 81-88.

(11) BEWLEY, D.K., 1971. Physical characteristics of fast neutron beams. Europ. J. Cancer, Vol. 7, 99-104, (Pergamon Press).

(12) BEWLEY, D.K., 1975. Medical use of fast neutrons in radiotherapy and radiography. National Bureau of Standards, Special Publication 425, 527-532.

(13) BEWLEY, D.K., and PARNELL, C.J., 1969. The fast neutron beam from the M.R.C. cyclotron. Br. J. Radiol., 42, 281-288.

(14) BEWLEY, D.K., and PARNELL, C.J., 1978. Private communication.

(15) BIANCHI, M., HILL, C.K., BAARLI, J., and SULLIVAN, A.H., 1978. Effects of negative pions and neutrons on the growth of Vicia faba bean roots. Br. J. Radiol., 51, 127-131.

(16) BICHSEL, H., 1968. Charged particle interactions. Radiation Dosimetry, Vol. I, Chapter 4. Attix. F.H., Roesch, W.C., and Tochilin, E. (Academic Press, New York).

(17) BICHSEL, H., 1977. Stopping power data for neutron and pion dosimetry with ionisation chambers. Report for the Committee on Stopping Power for the ICRU. University of Washington, Internal Report 77.5.

(18) BOURLAND, P.D., and POWERS, D., 1971. Bragg-Rule Applicability to Stopping Cross Sections of Gases for a-Particles of Energy 0.3-2.0 MeV Physical Review B, Vol. 3, No.11 (June 1971) 3635-3641.

(19) BRAGG, W.H., and KLEEMAN, R., 1905. The alpha particles of radium and their loss of range in passing through various atoms and molecules. Phil. Mag. 10, 318.

(20) BRITISH JOURNAL OF RADIOLOGY, 1972. Central axis depth dose data for use in radiotherapy. Br.J. Radiol., Supplement 11.

(21) BROWNING, E., 1965. Toxicity and Metabolism of industrial solvents. Elsevier, New York.

(22) BRYDSON, J.A., 1970. 'Plastics Materials'. Second Edition (Iliffe Books, London).

(23) CAMERON, J.R., 1965. Factors affecting the measurement of bone-mineral content by the direct photon absorption technique. USAEC Progress Report, COO-1422-4.

(24) CHRISTEN, F.T., 1913. 'Messung und Dosierung der Roentgenstrahlen'. Published by Lucas, Gräfe & Sillen, Hamburg. Abstract in Archives of the Roentgen Ray, 18, 280, 1913.

(25) CONSTANTINOU, C., and WHITE, D.R., 1977. The simulation of different biological tissues in neutron dosimetry. Proceedings of the Third Symposium on Neutron Dosimetry in Biology and Medicine, 849-858. Euratom.

(26) DUTRANNOIS, J.R., HAMM, R.N., TURNER, J.E., and WRIGHT, H.A. 1972. Analysis of Energy Deposition in Water around the site of Capture of a Negative Pion by an Oxygen or Carbon Nucleus. Phys. Med. Biol., 17, No.6, 765-770.

(27) ELLIS, R.E., LINDOP, P.J., COGGLE, J.E., and FRASER, G., 1976. Radiobiological work using a negative pion beam at the Rutherford laboratory 1971-1976. Rutherford Laboratory Report RL-76-092

(28) ELLIS, R.E., and PERRY, D.R., 1972. Comparative dosimetry of 14 MeV electron, 14 MeV neutron and pi-meson beams. Br.J. Radiol., 45, 549-550.

(29) ELLIS, R.E., and READ, L.R., 1969. Recombination in ionisation chambers irradiated with pulsed electron beams. I: Plane parallel plate chamber. Phys. Med. Biol., 14, 293-304.

(30) FRIGERIO, N.A., 1962. Neutron penetration during neutron capture therapy. Phys. Med. Biol., 6, 541-549.

(31) FRIGERIO, N.A., COLEY, R.F., and SAMPSON, M.J., 1972. Depth Dose Determinations I. Tissue Equivalent Liquids for Standard Man and Muscle. Phys. Med. Biol., Vol. 17, No.6, 792-802.

(32) GOODMAN, L.J., 1969. A modified Tissue Equivalent Liquid. Health Physics Pergamon Press, 16, 763.

(33) GOODWIN, P.N., 1960. Calorimetric measurements of bone/tissue absorption ratios. Radiology, 75, 112-115.

(34) GREEN, D.G., and STEWART, J.G., 1965. Isodose curves in non-uniform phantoms. Br. J. Radiol., 38, 378-385.

(35) HARRIS, J.H., TUDDENHAM, W.J., STANTON, L., GLAUSER, F., and PENDERGRASS, E.P., 1956. The development of a chest phantom for use in radiologic dosimetry. Radiology, 67, 805-814.

(36) H.M.S.O. 1967. The Carcinogenic Substances Regulations. Her Majesty's Stationery Office, London.

(37) HOLDERNESS, A., and LAMBERT, J., 1977. A new certificate Chemistry, Fifth edition, p.113. Heinemann Educational Books, London.

(38) HUBBELL, J.H., 1969, Photon cross sections, attenuation coefficients, and energy absorption coefficients from 10 keV to 100 GeV. National Bureau of Standards, NSRDS-NBS 29.

(39) HUTCHINSON, E., 1964. Chemistry : The elements and their properties. Philadelphia : Saunders.

(40) INTERNATIONAL COMMISSION ON RADIOLOGICAL PROTECTION (ICRP). Publication 23, 1975. (Oxford : Pergamon Press).

(41) INTERNATIONAL COMMISSION ON RADIATION UNITS AND MEASUREMENTS, 1972. Radiation Dosimetry : Electrons with initial energies between 1 and 50 MeV. ICRU Report 21. (Washington D.C. 20014).

(42) INTERNATIONLA COMMISSION ON RADIATION UNITS AND MEASUREMENTS, 1977. Neutron dosimetry for Biology and Medicine. ICRU Report 26. (Washington D.C. 20014).

(43) JOHNS, H.E., and CUNNINGHAM, J.R., 1969. The Physics of Radiology. American Lectures Series. Charles C. Thomas - Publisher.

(44) JONES, D.E.A. and RAINE, H.C., 1949. (Letter). Br.J. Radiol., 22, 549-550.

(45) JONES, J.C., 1972. Electron beams : 2-30 MeV. In central axis depth dose data for use in radiotherapy. Br. J. Radiol., Supplement No.11, Section 9.

(46) JONES, T.D., 1974. Distributions for the design of dosimetric experiments in a tissue equivalent medium. Health Physics, 27, 87-96.

(47) KEMBER, N.F., SMITH, F.A. and PERRIS, A.G., 1975. An approach to microdosimetry in a π^- meson beam using nuclear emulsions. Phys. Med. Biol., 20, 918-925.

(48) KIENBOCK, R., 1906. On the quantimetric method. Archives of the Roentgen Ray 11, 17-20.

(49) KIM, Y.S., 1973. Density effect in dE/dx of fast charged particles traversing various biological materials. Rad. Res., 56, 21-27.

(50) KIM, Y.S., 1974. Human Tissues: Chemical Composition and Photon.Dosimetry Data. Radiation Research, 57, 38-45.

(51) KOEHLER, A.M., 1967. Dosimetry of proton beams using small silicon diodes. Radiation Research, Supplement 7, 53-63.

(52) KOEHLER, A.M., 1968. Proton Radiography. Science, 160, 303-304.

(53) KOEHLER, A.M., and PRESTON, W.M., 1972. Protons in Radiation therapy. Radiology 104, 191-195

(54) LAUGHLIN, J.S., LUNDY, A., PHILLIPS, R., CHU, F., and SATTAR, A., 1965. Electron beam treatment planning in inhomogeneous tissue. Radiology, 85, 524-531.

(55) LINDSAY, D.D., and STERN, B.E., 1953. A new tissue-like material for use as bolus. Radiology, 60, 355-362.

(56) LOVELL, S., and SHEN, H., 1976. A flow calorimetric method of determining electron beam energy. Phys. Med. Biol., 21, 198-208.

(57) MARKUS, B., 1956. Uber den Begriff der Gewebeäquivalenz und einige 'wasserähnliche' Phantomsubstanzen fur Quanten von 10 keV bis 100 MeV sowie schnelle Elektronen. Strahlentherapie, 101, 111-131.

(58) MARKUS, B., 1960. Ionisationsdosimetrie und Dosisverteilungen schneller Elektronen in Knochengewebe. Strahlentherapie, 113, 379-393.

(59) MASSEY, J.B., 1962. Dose distribution problems in megavoltage therapy. I. The problem of air spaces. Br.J. Radiol., Vol. 35, 736-738.

(60) McCULLOUGH, E.C., et al., 1976. Performance evaluation and quality assurance of computed tomography scanners, with illustrations from the EMI, ACTA and Delta scanners. Radiology, 120, 173-188.

(61) McGINLEY, P.H., and McLAREN, J.R., 1976. Neutron Dose in bone. Medical Physics, Vol. 3, No.3, 181-183.

(62) NATIONAL BUREAU OF STANDARDS, 1964. Physical aspects of irradiation. ICRU Report 10b, Handbook 85.

(63) NAYLOR, G.P., and WILLIAMS, P.C., 1972. Dose distribution and stability of radiotherapy electron beams from a linear accelerator. Br. J. Radiol., 45, 603-609.

(64) OLDENBURG, U., and BOOZ, J., 1972. Mass stopping power and pathlength of neutron produced recoils in tissue and tissue equivalent materials. I. Neutron energy ≤ 6 MeV. Commission of the European Communities, EUR 4786 e.

(65) ORCHARD, P.G., 1964. Decrement lines : A new presentation of data in cobalt-60 beam dosimetry. Br. J. Radiol., 37, 756-763.

(66) ORR, J.C., LAURIE, J., and WAKERLEY, S., 1964. A study of 4 MeV transverse data and associated methods of constructing isodose curves. Phys. Med. Biol., 9, 505-515.

(67) OTT, P., 1937. Zur Röntgenstrahlenbehandlung oberflächlich gelagerter Tumoren. Strahlentherapie, 59, 189-223.

(68) PAGES, L., BERTEL, E., JOFFRE, H., and SKLAVENITIS, L., 1970. Pertes d'energie, parcours et randement de freinage pour les electrons de 10 keV à 100 MeV dans les elements simples et quelqués composes cliniques. Report CEA-R-3942 (Centre d'Etudes Nucléaires de Saclay).

(69) PARNELL, C.J., BEWLEY, D.K., and FIELD, S.B., 1965. Physical aspects of the fast neutron beam from the Medical Research Council cyclotron. Proceedings XI International Congress of Radiology, p.907.

(70) PARNELL, C.J., 1971. Physical aspects of cyclotron produced radiation beams for radiobiology and radiotherapy. Ph.D. Thesis, London University.

(71) PALMER, R.B.J., 1973. The stopping power of organic liquids for alpha particles over the range 1-8 MeV. J. Phys. B : Atom. Melec. Phys. Vol. 6, 384-392.

(72) PALMER, R.B.J., 1978. Private communication.

(73) PALMER, R.B.J., and SIMONS, H.A.B., 1959. Range-Energy relations for a's in water and water vapour and $\frac{dE}{dx}$ for water and its vapour for a's at energies below 8.78 MeV Proceedings of the Physical Society, Vol. 74, p.585.

(74) PERRIS, A.G., SMITH, F.A., and PERRY, D.R., 1978. Charged particle emission from the capture of negative pions : Energy spectra, LET distributions and W-value. Phys. Med. Biol., 23, 217-234.

(75) PERRY, D.R., and HYNES, M.A., 1971. A pion beam for radiobiological and dosimetric studies using a proton synchrotron external target. Proceedings of International Conference on protection against accelerator and space radiations. CERN, 220-230.

(76) RAJU, M.R., and PHILLIPS, T.L., 1977. The potential for heavy particle radiation therapy. Los Alamos Scientific Laboratory Report LA-6588-MS.

(77) RAJU, M.R., and RICHMAN, C., 1972. Negative pion therapy : Physical and radiobiological aspects. Current Topics in Radiation Research, Quarterly 8, 159-233.

(78) RODERICK, J.F., 1959. Plastic roentgen ray phantoms. Am. J. Roentg., 81, 331-335.

(79) ROGERS, R.T., 1970. A phantom material to represent lung. Br. J. Radiol., 43, 441-444.

(80) ROSSI, H.H., and FAILLA, G., 1956. Tissue-Equivalent Ionization Chambers. Nucleonics, Vol. 14, No.2, 32-37.

(81) SHONKA, F.R., ROSE, J.E., and FAILLA, G., 1958. Conducting plastic equivalent to tissue, air and polystyrene. Progress in Nuclear Energy, Series 12, 1, 184-187. (Geneva Conference Paper).

(82) SHONKA, J.J., and McGINLEY, P.H., 1976. Preparation of Phantom Lung Material. P.M.B. 21, No.1, 150-153.

(83) SMATHERS, J.B., et al., 1975. Composition of A-150 Tissue Equivalent Plastic. Report on a project supported by Grant CA 12542 from the National Cancer Institute, USA.

(84) SONTAG, M.R., and CUNNINGHAM, J.R., 1977. Correction to absorbed dose calculations for tissue inhomogeneities. Medical Physics, 4, 431-436.

(85) SPIERS, F.W., 1943. Materials for depth dose measurements. Br. J. Radiol., 16, 90-97.

(86) SPIERS, F.W., 1946. Effective atomic number and energy absorption in tissues. Br. J. Radiol., 19, 52-63

(87) SPIERS, F.W., and CHESTERS, M.S., 1962. Theoretical and experimental dosimetry based on bone structure from: "some aspects of Internal Irradiation", (Pergamon Press, London).

(88) STACEY, A.J., 1972. The absorption and scattering of radiation in heterogeneous media. M. Phil. Thesis, University of London.

(89) STACEY, A.J., BEVAN, A.R., and DICKENS, C.W., 1961. A new phantom material employing depolymerised natural rubber. Br. J. Radiol., 34, 510-515.

(90) STEWARD, V.W., and KOEHLER, M.A., 1974. Proton Radiography in the Diagnosis of Breast Carcinoma. Radiology, 110, 217-221.

(91) STORM, E., and ISRAEL, H.I., 1970. Photon cross sections from 1 keV to 100 MeV for elements Z = 1 to Z = 100. Nuclear Data Tables, A7, 565-581.

(92) SUNDBOM, L., 1965. Dose planning for irradiation of thorax with cobalt-60 in fixed beam teletherapy. Acta Radiol. Ther. Phys. Biol., 3, 342-352.

(93) THE CHESTER BEATTY RESEARCH INSTITUTE, 1966. Precautions for laboratory workers who handle carcinogenic aromatic amines. (Reprints available from Hopkins & Williams Ltd., on request).

(94) THWAITES, D.I., and WATT, D.E. 1978. Stopping power ratios for neutrons and alpha particles in tissue equivalent media. Proceedings of the Third Symposium on Neutron Dosimetry in Biology and Medicine, 45-60.

(95) TURNER, J.E., 1964. Values of I and Iadj suggested by the subcommittee. In : Studies in penetration of charged particles in matter. National Academy of Science-National Research Council, Publication 1133 (Washington D.C).

(96) WEBER, J., and van den BERGE, D.J., 1969. The effective atomic number and the calculation of the composition of phantom materials. Br. J. Radiol., 42, 378-383.

(97) WEST, D., 1974. A general description of proton scattering radiography. Atomic Energy Research Establishment, AERE-R 7757.

(98) WHITE, D.R., 1974. The formulation of Substitute Materials with Predetermined Characteristics of Radiation Absorption and Scattering. Ph.D. Thesis, London University.

(99) WHITE, D.R., 1976. Tissue substitute materials. 4th International Conference on Medical Physics, Ottawa, July 25-30.

(100) WHITE, D.R., 1977. An analysis of the Z-dependence of photon and electron Interactions. Phys. Med. Biol., 22, 219-228.

(101) WHITE, D.R., 1977. Phantom materials for photons and electrons. The Hospital Physicist's Association, Scientific Report Series - 20.

(102) WHITE, D.R., and FITZGERALD, M., 1977. Calculated Attenuation and Energy Absorption Coefficients for ICRP Reference Man (1975) Organs and Tissues. Health Physics, 33, 73-81. (Pergamon Press).

(103) WHITE, D.R., MARTIN, R.J., and DARLISON, R., 1977. Epoxy resin based tissue substitutes. Br. J. Radiol., 50, 814-821.

(104) WHITE, D.R., and SPELLER, R., 1978. The measurement of effective photon energy and "Linearity" in computerised tomography. To be published.

(105) WHITEHEAD, C., 1974. A synchrocyclotron and its proton beam. Proceedings of the Royal Society of Medicine, Vol. 67, 29-31 (section of endocrinology, 1-3).

(106) WILSON, I.J., and WHITE, D.R., 1974. A theoretical and experimental evaluation of tissue substitute materials. Proceedings of Second Symposium on Neutron Dosimetry in Biology and Medicine (Nuherberg/Munchen).

(107) WITT, R.M., and CAMERON, J.R., 1975. Bone standards. USAEC Report COO-1422.

(108) WOODARD, H.Q., 1964. The composition of human Cortical Bone. Clinical Orthopaedics, No.37, 187-193.

(109) YOUNG, M.E.J., and GAYLORD, J.D., 1970. Experimental tests of corrections for tissue inhomogeneities in radiotherapy. Br. J. Radiol., 43, 349-355.